ORGANIC EXPANDER ACTION AT LEAD ELECTRODES

by

Philip John Mitchell

Supervisor: Professor N. A. Hampson

A Doctoral Thesis submitted in partial fulfilment

of the requirements for the award of

Doctor of Philosopy of the Loughborough University of Technology

August 1983

SYNOPSIS

The instrumentation for digitally driven electrochemical experiments has been developed. Software has been written for experimental control and high speed data aquisition. The digital control methods were successfully used in the study of the electrochemistry of the porous lead electrode (the lead-acid battery negative plate), over an extended temperature range. The effects of a number of commercially pertenent additives have been studied at reduced temperatures. These reaction enhancing materials (expanders) have been studied in detail on both planar and porous lead electrode in sulphuric acid in the range 1M to 5M.

Deductions concerning the energetics of the reactions have been made from experimental results. The modes of action of certain expanders are discussed.

It was concluded that on the plane lead surface solution phase expander materials modify the mechanism of the lead sulphate electrocrystallisation - the current limiting reaction. This was an effect on the solid state process although a solution Pb^{2+} process was identified (for the first time) in battery strength acid.

Electrode incorporated organic expander materials act by modifying pore geometies and reaction penetration depths. The current transients due to electrocrystallization in porous lead are very complex and require very sophisticated modelling techniques to provide a useful fit.

ACKNOWLEDGEMENTS

Many thanks are due to my Supervisor, Professor Noel Hampson for his guidance, encouragement and ability to provide answers when I believed answers did not exist.

I am grateful to Joseph Lucas Ltd. for financial support and to Dr. D. Brown, Mr. K. Burdon, Dr. A. Fleming and Mr. J. Smith of that Company, for advice and industrial support.

The technical assistance required throughout this research has been considerable and the help provided by the Department, in particular by Bert Bower, is very much appreciated.

The rest of the lads in 'the group' deserve more than just a mention (but that's all they're getting) for their valuable discussion (arguments) and friendship, to name names would require a further page.

To my Mother and Father .....

for my education, your love and encouragement

CONTENTS

C H A P T E R 1

NEGATIVE ELECTRODE FOR THE LEAD-ACID BATTERY

1.1 The battery as a whole

The lead acid storage battery is the most widely used electrochemical storage system in the world today. Its uses vary from miniature sealed units for domestic and portable equipment, to large, thousands of ampere-hour batteries in submarines and telephone exchanges. Lead-acid is also exclusively used for starting, lighting and ignition in motor-vehicles. Its use as a motive power source is now being investigated with renewed vigour since its 'new' competitors are suffering from various operational problems. Although the lead-acid power source was discovered over 120 years ago, continued research aimed at developing lightweight, low-cost, secondary electrochemical power sources has failed to produce a serious competitor for automotive or tractive purposes.

The basic reactions occurring during charge and discharge of a lead-acid cell are as follows.

Positive plate:

$$PbO_2 + 4H^+ + SO_4^{2-} + 2e^- \underset{\text{CHARGE}}{\overset{\text{DISCHARGE}}{\rightleftharpoons}} PbSO_4 + 2H_2O \qquad (1.1)$$

$E = +1.66V$

Negative plate:

$$Pb + SO_4^{2-} \underset{\text{CHARGE}}{\overset{\text{DISCHARGE}}{\rightleftharpoons}} PbSO_4 + 2e^- \qquad (1.2)$$

$E = -0.35V$

During discharge the negative plate operates as an anode, lead oxidising to lead sulphate, pushing electrons into the external circuit (negative current i.e. electron flow, hence the designation negative plate). At the positive plate PbO_2 is reduced to $PbSO_4$ and thus acts as an electron sink for the external circuit. The overall reaction can be reduced to:

$$PbO_2 + Pb + 2H_2SO_4 \underset{\text{CHARGE}}{\overset{\text{DISCHARGE}}{\rightleftharpoons}} 2PbSO_4 + 2H_2O \qquad (1.3)$$

$E = +2.01V$

This equation is the basis of the theory of double sulphation, which was first postulated in 1882 by Gladstone and Tribe[1] and has since been confirmed thermodynamically by Craig and Vinal.[2,3]

1.2 Pasted plate type electrodes

The electrodes of greatest interest to the battery manufacturer are the pasted plate type, the 'active material' of which has been pressed as a paste into the recesses of a lead alloy grid which provides rigidity and a means of extracting current. Specific paste mixtures and methods of pasting and forming are unique to a particular manufacturer. However a general procedure[4] will be outlined.

The paste is initially composed of lead monoxide and finely divided lead, (28% ±4 of free Pb), and mixed in 1 ton batches with sulphuric acid of S.G. 1.4 and water. This mixture forms mainly

$$(PbO)_3.PbSO_4 + H_2O + Pb$$

and some free PbO.

A rheological calibration is carried out, and the density is measured before pasting. The paste is rolled out as sheets and pressed into the grids, which are then dried in an oven and cured, or conditioned. The free lead is air oxidised and the water evaporates away. After conditioning, less than 4% Pb and 5% water remain. The material recrystallizes and cements, by corrosion, to the grid. The plates are packed, sealed and charged according to their respective polarities. Most batteries are charged in dilute acid (S.G. 1.080). The weak acid, in batteries to be used immediately, is removed and replaced with S.G. 1.280; similarly the acid in batteries to have a long shelf life is removed, and the plates are then dried with inert gas.

This procedure suggests that the only difference between the two types of active material (positive and negative) is in the polarity of the charge applied. However this is not the case, since, during the initial mixing, various so-called 'expander' materials are added to the negative paste. The nature of these materials and possible reasons for their inclusion are outlined below.

1.3 Reactions of Lead electrodes[6] and expander action

If the un-modified paste mix were reduced, the product would be a spongy, porous mass of lead. This is a highly ductile material which tends to coalesce and densify on charge/discharge cycling,[5] thus bringing about a loss in effective surface area, causing a rapid loss in capacity and the shrinking and falling away of active material from the grids. It is reported[7,8] that

the inclusion of 'expander' materials helps to suppress this deterioration. However, the precise nature of the beneficial effect of the expander has not yet been clearly defined. It is generally accepted that expanders modify crystal growth during cycling and initial formation,[9-11] so as to maintain the porous structure, in their absence this structure tends to collapse.[7]

Expanders are generally of an organic nature, and their necessity has been known from early times.[12] Richie[8] has comprehensively reviewed all the listed expanders up to 1947. Since the 1950's all the organic expanders have been based on wood and cellulosic materials, and there are very few instances of comprehensive investigations since pre-war years. One exception was the work at the Chloride Group Research Laboratories in the mid 1950's, when a thorough study was made under the direction of Barak.[13] Today, all the commercially used expanders are based on lignosulphonic acid, which is a complex material of uncertain structure.[14,15]

The discharge of the lead electrode represented by:

$$Pb \rightarrow Pb^{2+} + 2e^{-} \rightarrow PbSO_{4\downarrow}$$

initially involves the dissolution of solid lead to the divalent cation;[16,17] this is then followed by the formation of a non conducting (impedance $\simeq 10^{10}$ ohm.cm^{-1}) $PbSO_4$ surface film, which ultimately restricts the Pb^{2+} ion production. A parallel reaction to the dissolution-precipitation mechanism is one which takes place by direct attack of the sulphate anion upon the lead surface. This, however, requires a critical potential, negative of which the reaction cannot be initiated.

According to Archdale and Harrison,[17-20] during the discharge reaction a soluble lead solution species (complex) is formed. This was only identifiable in a small potential region negative of the previously mentioned critical potential for solid state formation of $PbSO_4$. Since that work the existance of this free dissolution region has been adequately confirmed.[21-26] The lead dissolution has also been postulated to involve a Pb(I) species either as a one electron step with disproportionation[27]

$$2Pb^{+} \rightleftharpoons Pb + Pb^{2+}$$

or with Pb(I) existing in a dimeric form[28] eventually producing Pb^{2+} and yielding electrons.

$$[Pb^{+}]_2 \rightleftharpoons 2Pb^{2+} + 2e^{-}$$

In addition, measurements on concentrated Pb(Hg)[19] which simulates solid Pb free of mechanical defects, showed that as the formation of $PbSO_4$ increased, the concentration of soluble Pb species decreased. This is indicative of passage of Pb into solution between $PbSO_4$ crystals and not through them. It has also been suggested that if $PbSO_4$ formation did not interfere then the reaction would simplify to a $2e^{-}$ reversible charge transfer reaction.[16,21] If a polished lead electrode is oxidised and then the formed sulphate reduced back, not all of the anodic charge is recovered.[29] This suggests that the $PbSO_4$ is being reduced from nucleation sites occurring in the substrate, and depending on what type of crystal growth is involved on spreading from the nucleation point, subsequent entrapment of $PbSO_4$ in the reduced mass may occur, hence depleting the active material available for oxidation in the next cycle.

The specific action of expander materials, when incorporated into the lead negative, is clear to the battery manufacturer. Without additive, discharge capacity is progressively reduced, especially under conditions which impose a high demand on the battery such as high rates and low temperatures.[32,33] This progressive depletion can be offset to a large extent by the incorporation of expander material.[10,11,34] However the mechanism by which the expander achieves this is ill-defined and compiled evidence from investigation suggests that the system is extremely convoluted.

Archdale and Harrison[20] suggest that adsorbed expander at lead surfaces hinders the diffusion of Pb^{2+} ions and delays the onset of solid phase passivation. Evidence for this is provided by Brennan and Hampson[30] but there is also an observed effect upon the solid state pathway for $PbSO_4$ production. Hampson and Lakeman[31] found that at ambient temperatures the incorporation of a lignosulphonate expander into lead negative paste increased the number of nucleation sites available for lead sulphate crystallisation during discharge. Properties and effects ascribed to Lignin derivatives are numerous. Sharpe[35,36] and others[11,20,30] suggest that the organic is adsorbed onto the lead surface in its course of action. Simon[37] takes this a stage further in suggesting that the lignins had to be first oxidised before adsorption would take place. Passivation[11,20] (complete coverage with $PbSO_4$) is said to be delayed by expanders by suppression of the solid state mechanism[30] for sulphate formation. That lignins are beneficial in the initial formation process,[9,10,31,38,39] is another widely supported view. Increasing the surface area, possibly by lowering

the surface energy of the lead, making the formation of smaller more loosely packed crystals were favourable.[40] Lignins are also thought to influence the morphology of the $PbSO_4$ deposit,[10,34,41] making the crystals smaller and a more open porous film which is easier to reduce.

CHAPTER 2

THEORETICAL PRINCIPLES

2.1 Charge transfer at the polarised electrode

For an electrode reaction, equilibrium is characterised by the Nernst equation,[42-44] which links the electrode potential to the bulk concentrations of the reactants. In the general case:

$$O + ne \underset{kb}{\overset{kf}{\rightleftharpoons}} R \qquad (2.1)$$

this equation is

$$E = E^{\ominus} + \frac{RT}{nF} \ln \frac{C_{ox}}{C_R}$$

where C_{ox} and C_R are the bulk concentrations and $E^{\ominus}$ is the standard potential. Any theory of electrode kinetics must predict this result for corresponding conditions. The theory must also explain the observed dependence of current on potential under varying conditions. In a situation where the current is controlled strictly by the interfacial dynamics, i.e. no mass transport, the current is related exponentially to the overpotential η ($\eta = E - E_{rev}$). That is $i = a \exp. (\eta/b)$ or as given by Tafel in 1905.[45]

$$\eta = a + b. \ln i \qquad (2.2)$$

A successful model of electrode kinetics must explain the frequent validity of this expression. If we consider the cathodic and anodic currents in equation (2.1) then:

$$i_c = nF\ k_f\ C_{ox} \text{ and} \qquad (2.3)$$

$$i_a = nF\ k_b\ C_R \qquad (2.4)$$

[From dimensions $\frac{-dc}{dt} \equiv \frac{I}{nF}$]

the net current being

$$i = i_c - i_a = nF\ (k_f\ C_{ox} - k_b\ C_R). \qquad (2.5)$$

It is clear from (2.2) that any species participating in a heterogeneous redox reaction will have its kinetic behaviour strongly influenced by the interfacial potential difference. It is possible to control the potential and to predict the way in which the kinetics depend on it.

Considering the process:

$$O^z + ne \underset{kb}{\overset{kf}{\rightleftharpoons}} R^{z'} \qquad (2.6)$$

where z and z' are the charges on ions O and R. If we assume that the rate constants kf and kb follow the Arrhenius expression and the principles of transition state theory[46-48] (see Appendix 1), then

$$k_f = \frac{k_B T}{h}\ e^{-\Delta\bar{G}_f^{\ddagger}/RT} \qquad (2.7)$$

and

$$k_b = \frac{k_B T}{h}\ e^{-\Delta\bar{G}_b^{\ddagger}/RT} \qquad (2.8)$$

where the activation free energies are written with a bar to signify their dependence on interfacial potential difference i.e. they are electrochemical free energies of activation and can be separated into chemical and electrical components (see Appendix 2).

$$\overline{\Delta G_f^{\ddagger}} = \Delta G_f^{\ddagger} + (\Delta G_f^{\ddagger})_e \qquad (2.9)$$

$$\overline{\Delta G_b^{\ddagger}} = \Delta G_b^{\ddagger} + (\Delta G_b^{\ddagger})_e \qquad (2.10)$$

The free energy surface can be viewed as the sum of a chemical free energy surface and an electrical free energy surface as in Figure 2.1.

Assuming that the chemical free energies of activation $\Delta G_f^{\ddagger}$ and $\Delta G_b^{\ddagger}$ do not change with potential, so that the effects of potential are wholly manifested within the electrical components, and that the electrical components of the activation energies are fixed fractions of the overall electrical free energy change, in going from O + ne to R we have

$$(\Delta G_f^{\ddagger})_e = \alpha(\Delta G^{\ominus})_e \quad \text{and} \qquad (2.11)$$

$$(\Delta G_b^{\ddagger})_e = -(1-\alpha)(\Delta G^{\ominus})_e \qquad (2.12)$$

The standard electrochemical free energy (per mole) of the state corresponding to species O^z plus n electrons on metal M (state I) is:

$$\overline{G}_I^{\ominus} = \overline{\mu}_O + n\overline{\mu}_e = \mu_O{}^{\ominus S} + zF\phi^S + n\mu_e{}^{oM} - nF\phi^M \qquad (2.13)$$

The equivalent free energy for species $R^{z'}$ (state II) is

$$\overline{G}_{II}^{\ominus} = \overline{\mu}_R = \mu_R{}^{\ominus S} + z'F\phi^S \qquad (2.14)$$

$(\Delta G^{\ominus})e$, is simply the difference between the electrical terms for states II and I -

$$\text{i.e.} \quad (\Delta G^{\ominus})e = (z' - z)F\phi^S + nF\phi^M = nF\ (\phi^M - \phi^S) \qquad (2.15)$$

Figure 2.1

Free energy surfaces showing the electrochemical free energy, $\overline{G}$, split into its components of chemical free energy, G, and electrical energy $(G)_e$.

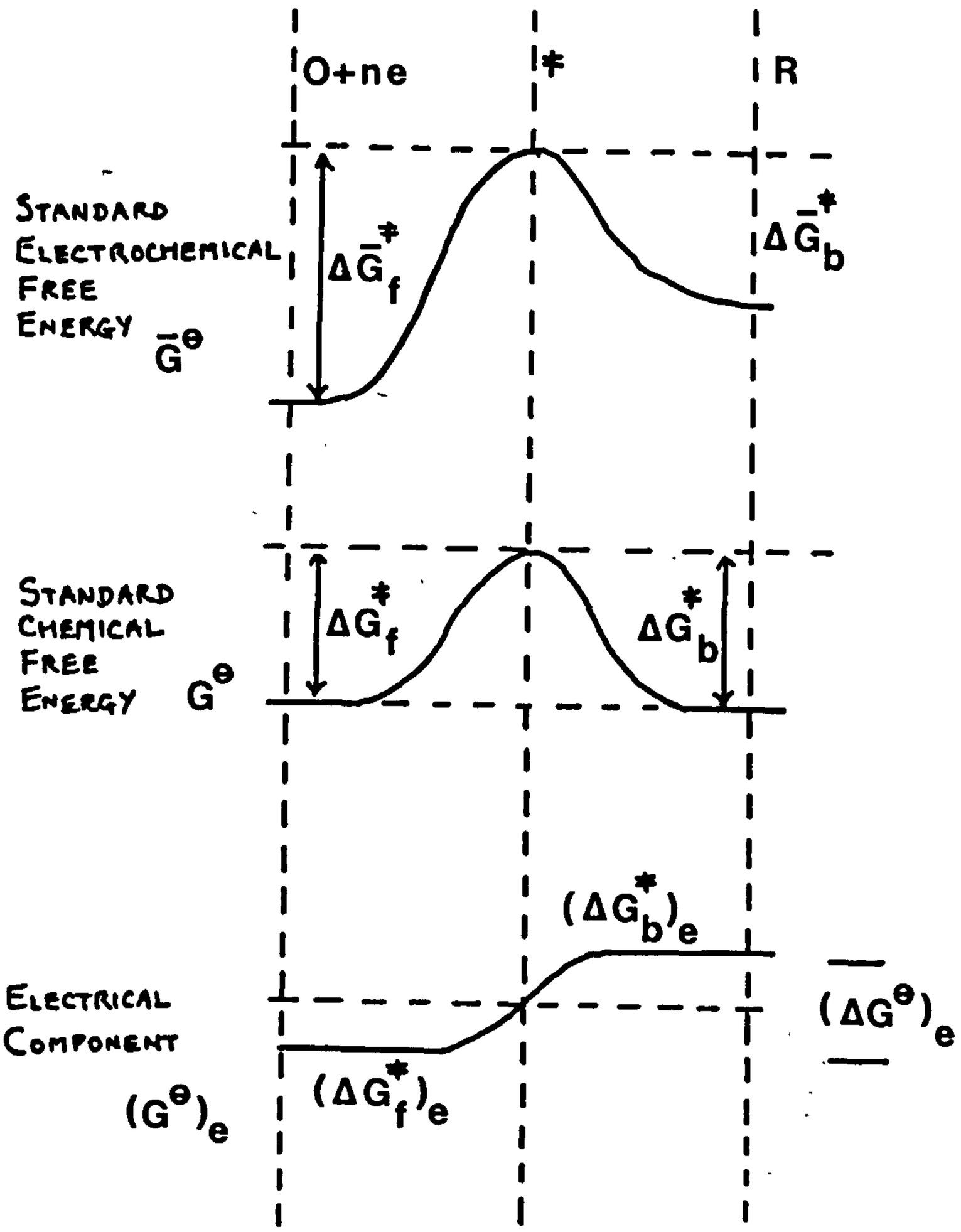
O+ne
*
R
STANDARD ELECTROCHEMICAL FREE ENERGY $\bar{G}^{\ominus}$
$\Delta\bar{G}_f^*$
$\Delta\bar{G}_b^*$
STANDARD CHEMICAL FREE ENERGY $G^{\ominus}$
ΔG_f^*
ΔG_b^*
ELECTRICAL COMPONENT
$(G^{\ominus})_e$
$(\Delta G_f^*)_e$
$(\Delta G_b^*)_e$
$(\Delta G^{\ominus})_e$
REACTION COORDINATE

Since the electrode potential E is related to the interfacial potential difference $\phi^M - \phi^S$ by a constant, k,

$$E = (\phi^M - \phi^S) + k \tag{2.16}$$

then

$$(\Delta G_f^{\ddagger})_e = \alpha nF(E - k) \tag{2.17}$$

and

$$(\Delta G_b^{\ddagger})_e = -(1 - \alpha)\, nF(E - k) \tag{2.18}$$

Substitution of (2.17) and (2.18) into (2.9) and (2.10) and then into (2.7) and (2.8) gives

$$k_f = \frac{k_B T}{h}\; e^{-\Delta G_f^{\ddagger}/RT}\; e^{\alpha nFk/RT}\; e^{-\alpha nFE/RT} \tag{2.19}$$

and

$$k_b = \frac{k_B T}{h}\; e^{-\Delta G_b^{\ddagger}/RT}\; e^{-(1-\alpha)nFk/RT}\; e^{(1-\alpha)nFE/RT} \tag{2.20}$$

All factors but the last exponential in both of these expressions are independent of potential and they can be collected into the constants k_f^o and k_b^o :

$$k_f = k_f^o\; e^{-\alpha nFE/RT} \quad \text{and} \tag{2.21}$$

$$k_b = k_b^o\; e^{(1-\alpha)nFE/RT} \tag{2.22}$$

Insertion of these relations into (2.5) yields the complete current-potential characteristic:

$$i = nF\left\{ k_f^o\, C_{ox}\, \exp.\, \left(\frac{-\alpha nF}{RT} \cdot E\right) - k_b^o\, C_R\, \exp.\, \left(\frac{(1-\alpha)\, nF}{RT} \cdot E\right)\right\} \tag{2.23}$$

At the reversible (i.e. equilibrium) potential, E_{rev} of the solution, the net rate of reaction (2.6) is zero, i.e. i = 0. Therefore $i = i_o = i_f = i_b$.

$$nFk_f^o\ C_{ox}\ \text{exp.}\ \left(\frac{-\alpha nF}{RT}\cdot E_{rev}\right) = nFk_b^o\ C_R\ \text{exp.}\ \left(\frac{(1-\alpha)\ nF}{RT}\cdot E_{rev}\right) \quad (2.24)$$

The overpotential η is measured with respect to the reversible potential

$$\eta = E - E_{rev} \quad (2.25)$$

Introducing (2.24) and (2.25) into (2.23) we obtain:

$$i = i_o \left\{ \text{exp.}\ \left(\frac{-\alpha nF}{RT}\cdot \eta\right) - \text{exp.}\ \left(\frac{(1-\alpha)\ nF}{RT}\cdot \eta\right) \right\} \quad (2.26)$$

The fractions α and $(1-\alpha)$, which were introduced in equations (2.11) and (2.12), are termed the transfer coefficient[49] and its compliment respectively.

Equation (2.26) can be simplified in one of the following ways:

(a) With an electrode approaching reversibility, when overpotential is very low ($\eta < \sim 0.02V$), the exponentials can be expanded using only two terms of the series $e^x = 1 + x$:

$$i = i_o \left(1 + \frac{-\alpha n\eta F}{RT}\right) - i_o \left(1 - \frac{(1-\alpha)n\eta F}{RT}\right) = i_o \frac{n\eta F}{RT} \quad (2.27)$$

Hence, in this case, net current is a linear function of overpotential.

(b) If the electrode is irreversible and the overpotential is high ($\eta > 0.05V$), the rate of the reverse reaction is negligible in comparison with that of the forward reaction (or vice versa).

Equation (2.26) becomes:

$$i = i_o\ \text{exp.}\ \left(\frac{-\alpha n\eta F}{RT}\right)$$

$$\ln i = \ln i_o + \frac{-\alpha n\eta F}{RT}$$

$$\eta = \frac{-RT}{-\alpha nF}\ \ln i_o + \frac{RT}{-\alpha nF}\ \ln i \quad (2.28)$$

Because i_o is a constant we can re-write this as:

$$\eta = a + b \ \ln i \qquad (2.2)$$

This in effect is equation (2.2), as predicted by Tafel. Plotting η against log i gives a straight line of gradient b and intercept a.

(c) If polarisation is large but only a limited range or current density is considered, the Tafel equation (2.2) becomes

$\eta = a + b\ i$ since $\log i \sim i$ for low values of i. Thus, over a limited range, overpotential varies linearly with current.

In numerous cases the reaction mechanisms, and hence a and b, may change as the current is increased. The number of electrons, n, involved in the reaction can be deduced from b, and the magnitude of the exchange current obtained by extrapolating the Tafel line to $\eta = 0$.

Returning to equations

$$(2.21) \quad k_f = k_f^o \ e^{-\alpha nFE/RT} \quad \text{and}$$

$$(2.22) \quad k_b = k_b^o \ e^{(1-\alpha)nFE/RT},$$

if we now consider the special case in which the interface is at equilibrium with a solution in which $C_{ox} = C_R$, and hence $E = E^{\ominus}_{rev}$ and $k_f C_{ox} = k_b C_R$, which implies that $k_f = k_b$. That is:

$$k_f^o \ e^{\frac{-\alpha nFE^{\ominus}_{rev}}{RT}} = k_b^o \ e^{\frac{(1-\alpha)nFE^{\ominus}_{rev}}{RT}} = k^{\ominus} \qquad (2.29)$$

where $k^{\ominus}$ is the standard state rate constant, which is the value of k_f and k_b at $E^{\ominus}_{rev}$. Using equation (2.29) to substitute for k_f^o and k_b^o in (2.21) and (2.22), we get,

$$k_f = k^{\circ} e^{-\frac{\alpha nF(E-E^{\circ}_{rev})}{RT}} \quad \text{and}$$

$$k_b = k^{\circ} e^{\frac{(1-\alpha)nF(E-E^{\circ}_{rev})}{RT}}$$

Insertion of these relations into (2.5) yields an equation similar to (2.23)

$$i = nFk^{\circ}\left\{ C_{ox} \exp.\ \left[\frac{-\alpha nF(E-E^{\circ}_{rev})}{RT}\right] - C_R \exp.\ \left[\frac{(1-\alpha)nF(E-E^{\circ}_{rev})}{RT}\right] \right\} \quad (2.30)$$

From the Nernst Equation

$$E_{rev} = E^{\circ}_{rev} + \frac{RT}{nF} \ln \frac{C_{ox}}{C_R}$$

exponentiating gives

$$e^{\frac{nF(E-E^{\circ}_{rev})}{RT}} = \frac{C_{ox}}{C_R} \quad (2.31)$$

From (2.30), at zero current, we have

$$nFk^{\circ} C_{ox} e^{-\frac{\alpha nF(E-E^{\circ}_{rev})}{RT}} = nFk^{\circ} C_R e^{\frac{(1-\alpha)nF(E-E^{\circ}_{rev})}{RT}} \quad (2.32)$$

Even though the net current is zero at equilibrium, we still have balanced faradaic activity i.e. the exchange current i_o, which is equal in magnitude to either i_c or i_a. If both sides of (2.31) are raised to the power, $-\alpha$, we obtain

$$e^{-\frac{\alpha nF(E-E^{\circ}_{rev})}{RT}} = \left(\frac{C_{ox}}{C_R}\right)^{-\alpha} \quad (2.33)$$

Substitution of (2.33) into

$$i_o = nFk^{\circ} C_{ox} e^{-\frac{\alpha nF(E-E^{\circ}_{rev})}{RT}} \quad \text{from (2.32)}$$

gives

$$i_o = nFk^{\circ} C_{ox}^{(1-\alpha)} C_R^{\alpha} \quad (2.34)$$

The exchange current is therefore proportional to k°, and can often be substituted for k° in kinetic equations. k° can be simply interpreted as a measure of the kinetic capacity of a redox couple. A system of large k° will achieve equilibrium quickly, whereas a smaller k° will take longer.

Thorough treatments are presented by Vetter and Bard and Faulkner.

2.2 Mass transport effects

When a species, which has been formed as a consequence of the electrode reactions, passes through the electrode/solution interface a perturbation of concentration occurs. The result is diffusion to or from the electrode to counter this disturbance. This however has the ultimate effect of hindering current flow. Hence the effect of mass transfer[51,52] as well as charge transfer has to be considered when trying to design a model of any electrode reaction.

If we consider an electrode process whose electron transfer kinetics and associated chemical reactions are very rapid compared to the mass transfer effect, then the rate of reaction is governed by the mobility of the electroactive species.

From the relation between reaction rate and faradaic current:

$$\frac{-dc}{dt} = \frac{i}{nF} \quad \left(\frac{\text{mol.}}{s} \equiv \frac{C.s^{-1}}{C.\text{mol.}^{-1}}\right)$$

Since electrode reactions are heterogeneous some treatments include the electrode area A i.e.

$$\text{Rate } (\text{mol.s}^{-1}.\text{cm.}^{-2}) = \frac{i}{nFA}$$

If the velocity of mass transfer is given by V_{mt} then

$$\frac{-dc}{dt} = V_{mt} = \frac{i}{nF} \qquad (2.35)$$

There are three modes of mass transfer:

(1) migration - movement of a charged species through a gradient of electrical potential.

(2) diffusion - movement of a species (charged or uncharged) through a gradient of chemical potential.

(3) convection - hydrodynamic transport due to natural or forced convection.

Mass transfer to an electrode is governed by the Nernst-Planck equation, which can be written for one dimensional mass transfer along the x-axis as:

$$J_j(x) = -D_j \frac{\partial C_j(x)}{\partial x} - \frac{n_j F}{RT} D_j C_j \frac{\partial \phi(x)}{\partial x} + C_j v(x) \qquad (2.36)$$

where $J_j(x)$ is the flux of species j ($mol.s^{-1}\ cm^{-2}$) at distance x from the surface, D_j is the diffusion coefficient ($cm^2\ s^{-1}$), $\partial C_j(x)/\partial x$ is the concentration gradient at x, $\partial \phi(x)/\partial x$ is the potential gradient, n_j and C_j are the charge and concentration of species j respectively, and v(x) is the velocity ($cm.s^{-1}$) with which a volume element in solution moves along the axis. The three terms on the right-hand side are the contributions of diffusion, migration and convection to the flux respectively.

If we consider a section of solution where, for a species j at two points in the solution, r and s, $\bar{\mu}_j$ (r) $\neq \bar{\mu}_j$ (s). This gradient of electrochemical potential can arise because of difference in activity of j at r and s, or because of differences of ϕ at r and s (see Appendix 2). In general, a flux of species j will arise to bridge this difference of $\bar{\mu}_j$.

The flux J is proportional to the gradient, ∇, of $\bar{\mu}_j$.

Hence,

$$J_j \propto \nabla \bar{\mu}_j \tag{2.37}$$

For one-dimensional mass transfer $\nabla = j(\partial/\partial x)$, and for three-dimensional mass transfer

$$\nabla = j \frac{\partial}{\partial x} + \frac{\partial}{\partial y} + \frac{\partial}{\partial z} \tag{2.38}$$

If we add the constant of proportionality to (2.37) we obtain:

$$J_j = - \left(\frac{C_j D_j}{RT}\right) \nabla \bar{\mu}_j \tag{2.39}$$

For one-dimensional mass transfer:

$$J_j = - \left(\frac{C_j D_j}{RT}\right) \frac{\partial \bar{\mu}_j}{\partial x} \tag{2.40}$$

If, in addition to this $\bar{\mu}$ gradient, the solution is moving from s with a velocity v, an additional term is added, giving

$$J_j = - \left(\frac{C_j D_j}{RT}\right) \nabla \bar{\mu}_j + C_j v \tag{2.41}$$

In one dimension:

$$J_j = - \left(\frac{C_j D_j}{RT}\right) \frac{\partial \bar{\mu}_j}{\partial x} + C_j v(x) \tag{2.42}$$

If activity is reduced to concentration we obtain the Nernst-Planck equation (2.36), which can be written in three dimensions as:

$$J_j = -D_j \nabla C_j - \frac{n_j F}{RT} D_j C_j \nabla \phi + C_j v \tag{2.43}$$

Ignoring convective mass transfer (unstirred solution with no density gradients) we can drop the last term in equations (2.36) and (2.43). From equation (2.36) we have:

$$J_j(x) = -D_j \frac{\partial C_j(x)}{\partial x} - \frac{n_j F}{RT} D_j C_j \frac{\partial \phi(x)}{\partial x} \qquad (2.44)$$

If species j is charged, then the flux J_j is equivalent to a current density. Considering a one-dimensional mass flow system of cross-sectional area A, then J is equal to $-i_j/n_jFA$, (from (2.35)), where i_j is the current component at any value of x arising from a flow of species j.

$$-J_j = \frac{i_j}{n_jFA} = \frac{i_{d,j}}{n_jFA} + \frac{i_{m,j}}{n_jFA} \qquad (2.45)$$

Hence,

$$\frac{i_{d,j}}{n_jFA} = D_j \frac{\partial Cj}{\partial x} \qquad (2.46)$$

and

$$\frac{i_{m,j}}{n_jFA} = \frac{n_jFD_j}{RT} C_j \frac{\partial \phi}{\partial x} \qquad (2.47)$$

$i_{d,j}$ and $i_{m,j}$ are diffusion and migration currents of species j respectively. The factor $|n_j|FD_j/RT$ is the ionic mobility u_j (see Appendix 3). Hence:

$$\frac{i_{m,j}}{|n_j|FA} = u_j C_j \frac{\partial \phi}{\partial x} \qquad (2.48)$$

At any location in solution the total current i is made up of the sum of all species i.e.

$$i = \Sigma_j i_j \qquad (2.49)$$

Migration and diffusion currents can be summarised as:

$$i = nFD \left(\frac{\partial C}{\partial x}\right) \quad \text{and} \qquad (2.50)$$

$$i = nFu\, C \left(\frac{\partial \phi}{\partial x}\right) \qquad (2.51)$$

Having ignored convective transport, in the derivation of equations (2.50) and (2.51), we must return to it since it is very important in its applications to electrochemical kinetic analysis techniques, in particular the rotating disc system.

The law of conservation of mass can be expressed in a differential form as

$$\frac{\partial \rho}{\partial t} = -\nabla.(\rho v) \qquad (2.52)$$

where v is the mass-average velocity of a fluid, defined as

$$v = \frac{1}{\rho} \Sigma\ C_j\ M_j\ v_j \qquad (2.53)$$

where $C_j\ v_j$ is the molar flux of species j, M_j is the molecular weight and ρ is the density of the medium.

When density is constant in space and time equation (2.52) reduces to

$$\nabla.v = 0 \qquad (2.54)$$

A material balance can be produced for the component j

$$\frac{\partial C_j}{\partial t} = -\nabla.J_j + R_j \qquad (2.55)$$

Accumulation/ Depletion	net input	Production (non-electrode reactions)

where for a volume element the net input is given by the net amount of material brought in on the various faces of the element. The differences in fluxes accounts for accumulation or depletion. The production term R_j involves homogeneous chemical reactions in the bulk but not electrode reactions, thus R_j is frequently zero in electrochemical systems.

If the contribution of ionic migration to the total flux is neglected (in practice this can only be justified for the reaction of a minor species in a solution containing excess supporting electrolyte; but this treatment is invariably applied to most systems) the Nernst-Plank equation becomes

$$J_j = -D_j \nabla C_j + vC_j \qquad (2.56)$$

If this is substituted into the material balance equation (2.55) we arrive at

$$\frac{\partial C_j}{\partial t} + v.\nabla C_j = D_j \nabla^2 C_j \qquad (2.57)$$

which is known as the equation of convective diffusion.

Frequently, due to the small value of the diffusion coefficient, the concentrations differ significantly from their bulk values only in a thin region near the electrode. In this region fluid velocity is small and diffusion is of primary importance to the transport process. Far away from the electrode convective transport dominates. This thin layer or Nernst diffusion layer concentration profile is shown in Figure 2.2.

Under forced convection conditions such as the rotating disc system the diffusion, or static layer, still exists. However the position of boundary between the diffusion layer and the bulk solution is not easy to define. This is because the hydrodynamic equations for the system have to be solved in order to deduce the convective velocity normal and near to the electrode. The solution to the hydrodynamic problem is soluble for the case of the rotating disc electrode. The exact flow pattern of electrolyte to a rotating disc was first established

Figure 2.2

The diffusion layer concentration profile.

Figure 2.3

The mass-transport fluxes, at the rotating disc electrode, resolved into three components of a cylindrical polar system.

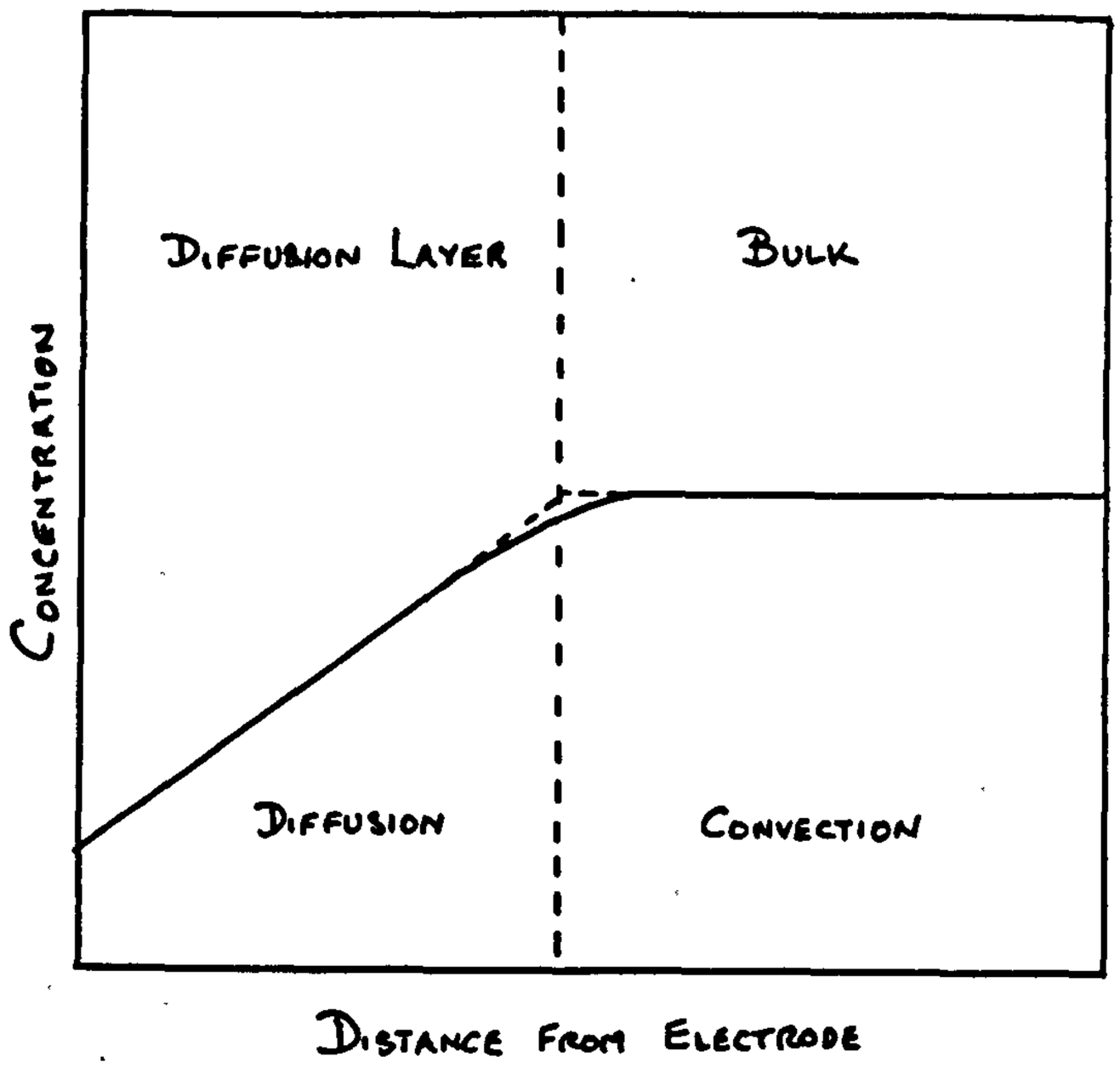
Diffusion Layer
Bulk
Concentration
Diffusion
Convection
Distance From Electrode

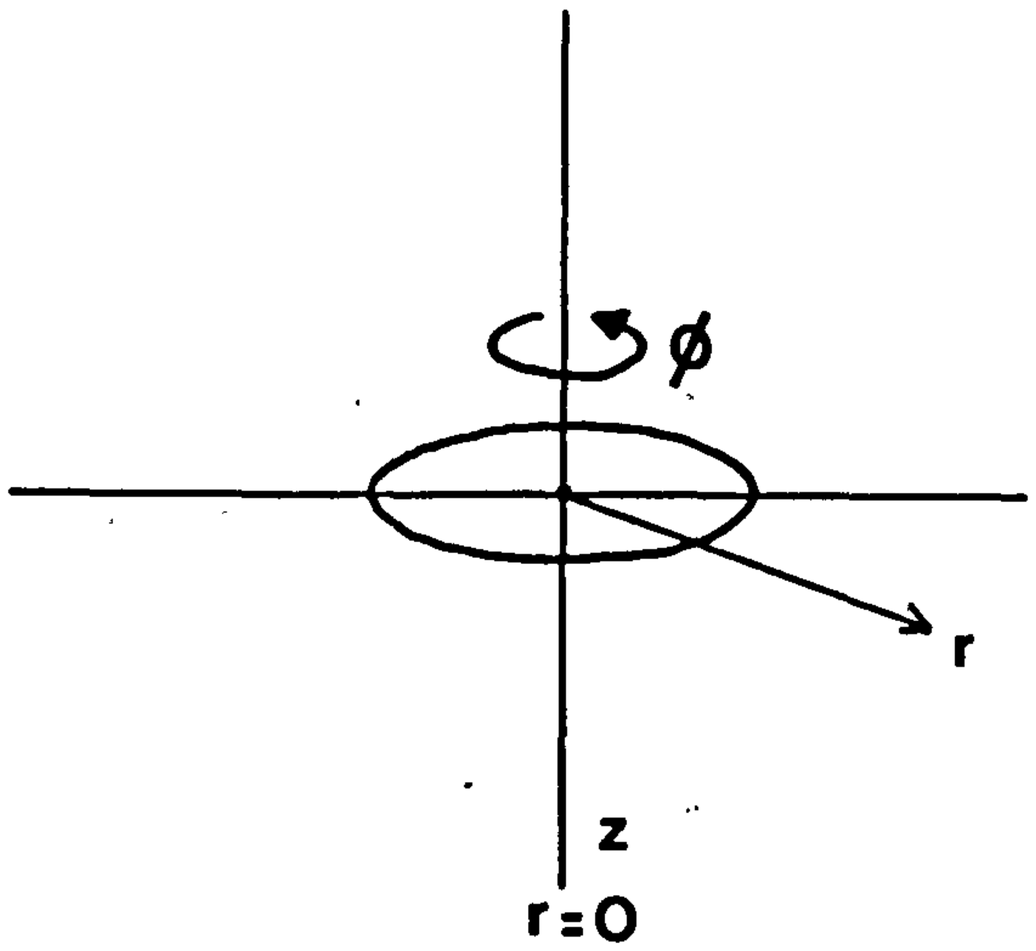
ϕ
r
z
r=0

by Von Karman[53] in 1921 and improved by Cochran[54] in 1934. Von Karman calculated the mass balance for the system and the resulting equation of continuity with all contributing fluxes resolved into three components of a cylindrical polar system. These are shown in Figure 2.3. The electrode can be considered to be a simple cylinder rotating about its axis. The spinning motion induces radial fluid flow close to the surface and the solution is flung out centrifugally. This solution is replaced from below by a stream flowing towards the electrode. The pertinent feature of Von Karman's results is that the velocity normal to the disc is dependent on z only not r. Levich[55] used this fact as a basis for the calculation of transport to the R.D.E. On the electrode surface the solution is rotating with the electrode and lack of normal convection close to the electrode, leads to this region being called the stagnant layer. If a steady state is assumed i.e. the amount of material leaving a volume element in the diffusion layer (by diffusion) is equivalent to the amount of material entering (by convection) then since concentration is independent of the radial co-ordinate r, and polar angle θ, the equation of convective diffusion (2.57), in one plane normal to the electrode, is reduced to

$$\frac{\partial C_j}{\partial t} = D_j \frac{\partial^2 C_j}{\partial z^2} - V_z \cdot \frac{\partial C_j}{\partial z} \qquad (2.58)$$

at steady state $\frac{\partial C_j}{\partial t} = 0$

therefore

$$V_z \frac{\partial C_j}{\partial z} = D_j \frac{\partial^2 C_j}{\partial z^2} \qquad (2.59)$$

If this equation is integrated with the boundary conditions that as $z \to \infty$ then $c \to c_\infty$ we arrive at

$$\left(\frac{\partial C_j}{\partial z}\right)_{z=0} = \frac{C_\infty - C_o}{\delta_D} \qquad (2.60)$$

where $\delta_D = 0.643\ \Omega^{-\frac{1}{2}}\ \nu.^{1/6}\ D_j^{1/3}$ (2.61)

and Ω is rotation speed in Hz. δ_D is the effective thickness of the diffusion (stagnant) layer. Modern texts which cover Von Karman's derivation and the integration of equation (2.59) are references 55 and 56.

If equation (2.60) is substituted into Fick's first law for planar diffusion (first term in 2.44)

$$J_j = -D_j \frac{\partial C_j}{\partial z}$$

we arrive at

$$J_j = -D_j . \frac{C_\infty - C_o}{\delta_D} \qquad (2.62)$$

and similarly from equation (2.50)

$$i = zFD_j \left(\frac{\partial C_j}{\partial z}\right)$$

we get

$$i = zFD_j \left(\frac{C_\infty - C_o}{\delta_D}\right) \qquad (2.63)$$

If we then substitute this into the equation for a general charge transfer reaction (2.5)

$$i = i_c - i_a = zF\ (k_f\ C_{ox} - k_b\ C_R)$$

we arrive at

$$i\,[1-k_f\,\delta_{ox}/D_{ox} + k\delta_R/D_R] = zF\,[k_f\,C_{ox} - k_b\,C_R] \qquad (2.64)$$

The right hand side is the current in absence of diffusion and is given by i_∞.

If (2.61) is introduced into (2.64) we get

$$i^{-1} = i_\infty^{-1} + \frac{0.643\,\nu^{1/6}\,(k_b D_R^{-2/3} - k_f\,D_{ox}^{-2/3})\,\Omega^{-\frac{1}{2}}}{zF(k_f\,C_{ox} - k_b\,C_R)} \qquad (2.65)$$

Thus a plot of i^{-1} versus $\Omega^{-\frac{1}{2}}$ will be linear with slope;

$$\frac{\partial i^{-1}}{\partial \Omega^{-\frac{1}{2}}} = \frac{0.643\,\nu^{1/6}\,(k_b D_R^{-2/3} - k_f\,D_{ox}^{-2/3})}{zF(k_f\,C_{ox} - k_b C_R)} \qquad (2.66)$$

and intercept

$$i^{-1} \text{ at } \Omega=0 = i_\infty^{-1}$$

When the reaction is reversible $i_\infty^{-1} \to 0$ and i^{-1} versus $\Omega^{-\frac{1}{2}}$ passes through the origin.

If the reaction is not limited by diffusion then i becomes independent of Ω.

Newman's book[52] provides an excellent treatment of current distribution and mass transfer in electrochemical systems albeit written in the chemical engineering vein. Levich[55] provides a comprehensive review of hydrodynamic phenomena. Treatments dedicated to electrochemistry include references 50, 51 and 44. A good introduction to methods of solving mass transfer problems is given in reference 57.

2.3 Investigation via perturbation

Having considered the effects of overpotential and the transport of electroactive species as two discrete entities, we must now unite them to produce a system which we can interpret as a working model. The kinetics of heterogeneous reactions are normally determined by a sequence of steps involving both solution transport and charge transfer at the interface.

Over the last twenty-five years, the necessity to extract information from 'fast' electrochemical reactions has been realised. Hence the development of relaxation or transient techniques[58] which are capable of defining the effects of mass-transport and charge transfer at very short times. All of these methods require that the reaction be disturbed from equilibrium or its steady state by applying a perturbing impulse to the system. It is then allowed to relax to a new equilibrium or steady state and the (transient) response as a function of time is recorded. Numerous methods of perturbation are employed all ultimately yielding kinetic information but differing in the method of aquisition and treatment of data.

(i) Potential step method

With the instantaneous application of a potential step a time dependent curve i(t) is obtained from which the rate constants of the various processes of the electrode reaction can be determined. Experimentally, to establish this constant potential and instantaneous jump, considerable operational amplifier control circuitry is usually employed[57,58] (potentiostat and function generator).

Thus considering the equation relating reaction rate to the concentration profile of a species in solution

$$v = D \frac{\partial^2 C}{\partial x^2}$$

and rate of change of concentration with time $v = \frac{\partial C}{\partial t}$ we arrive at Fick's second law

$$\frac{\partial C}{\partial t} = D.\frac{\partial^2 C}{\partial x^2} \qquad (2.67)$$

We must solve this linear diffusion equation to calculate the diffusion limited current and concentration profile.

Boundary conditions:

$$C_o\ (x,o) = C_{o,\ BULK} \qquad (2.68)$$

$$C_o\ (x,t) = C_{o,\ BULK} \qquad (2.69)$$

$$x \to \infty$$

$$C_o\ (o,t) = o \qquad \text{for } t > o \qquad (2.70)$$

Equation (2.70) expresses the surface condition after the imposition of the potential step.

After Laplace transformation of (2.67) and applying (2.68) and (2.69) yields

$$\overline{C}_o\ (x,s) = \frac{C_{o,BULK}}{s} + A(s)\ e^{-\sqrt{s/D_o}x} \qquad (2.71)$$

By applying (2.70) the function A(s) can be evaluated and inversion of $\overline{C}_o\ (x,s)$ will give the concentration profile of species 0. Transforming (2.70) gives

$$\overline{C}_o\ (o,s) = o \qquad (2.72)$$

implying

$$\bar{C}_o\ (x,s) = \frac{C_{o,BULK}}{s} - \frac{C_{o,BULK}}{s}\ e^{-\sqrt{s/D_o}x} \qquad (2.73)$$

From equation (2.46) we can see that

$$-J_o\ (o,t) = \frac{i(t)}{zFA} = D_o \left[\frac{\partial C_o(x,t)}{\partial x}\right]_{x=o} \qquad (2.74)$$

which is transformed to

$$\frac{i(s)}{zFA} = D_o \left[\frac{\partial \bar{C}_o(x,s)}{\partial x}\right]_{x=o} \qquad (2.75)$$

The derivative in (2.75) can be evaluated from (2.73) giving

$$i(s) = \frac{zFA\ D_o^{\frac{1}{2}}\ C_{o,BULK}}{s^{\frac{1}{2}}} \qquad (2.76)$$

inverting we get

$$i(t) = \frac{zFA\ D_o^{\frac{1}{2}}\ C_{o,BULK}}{\pi^{\frac{1}{2}}\ t^{\frac{1}{2}}} \qquad (2.77)$$

This is the Cottrell equation showing the effect of depleting the electroactive species near the surface to be characterised by a $^1/t^{\frac{1}{2}}$ function, i.e. $i \propto {}^1/t^{\frac{1}{2}}$. This would suggest at t=o, or very close to this, the current should tend to infinity (even neglecting double layer capacitance). In fact at t=o the current corresponding to a Faradaic response can never assume an infinite value because of rate control by the charge transfer reaction which will limit the current. Thus to understand the current time curve it is necessary to study the interaction of diffusion and charge-transfer rate control.

Considering the simple reaction

$$O + ne \rightleftharpoons R$$

From Ficks second law

$$\frac{\partial C_o}{\partial t} = D_o \frac{\partial^2 C_o}{\partial x^2} \quad \text{and} \quad \frac{\partial C_R}{\partial t} = D_R \frac{\partial^2 C_R}{\partial x^2}$$

and equation (2.26).

$$i = i_o \left\{ \exp \left[\frac{-\alpha nF}{RT} \eta \right] - \exp \left[\frac{(1-\alpha)nF}{RT} \eta \right] \right\}$$

as an expression for charge-transfer current density. With the following boundary conditions for C(x,t)

$$C_o(x,o) = C_{o,BULK} \qquad C_R(x,o) = C_{R,BULK}$$

$$C_o(\infty,t) = C_{o,BULK} \qquad C_R(\infty,t) = C_{R,BULK}$$

$$i = -nF\, D_o \left[\frac{\partial C_o}{\partial x} \right]_{x=o} = + nF\, D_R \left[\frac{\partial C_R}{\partial x} \right]_{x=o}$$

From this we arrive at the time-function of the current density with charge-transfer and diffusion control. Equations (2.78) A, B + C

$$i = i(o) \cdot \exp(\lambda^2 t) \cdot \operatorname{erfc}(\lambda\sqrt{t}) \quad A$$

[where $\operatorname{erfc}(x) = 1 - \operatorname{erf}(x) = 1 - \frac{2}{\sqrt{\pi}} \int_o^x \exp(-u^2)\, du.$]

and $\lambda = \frac{i_o}{nF} \cdot \left\{ \frac{1}{C_{R,BULK}\sqrt{D_R}} \cdot \exp \left[\frac{\alpha nF}{RT} \eta \right] + \frac{1}{C_{o,BULK}\sqrt{D_o}} \right.$

$$\cdot \exp\left(\frac{-(1-\alpha)nF}{RT}\,\eta\right)\Bigg\} \quad B$$

$$\text{with } i(o) = i_o \quad \exp\left(\frac{\alpha nF}{RT}\,\eta\right) - \exp\left(\frac{-(1-\alpha)nF}{RT}\,\eta\right)\Bigg\} \quad C$$

The current density $i(t,\eta)$ which is dependent on t and $\eta = E - E_{rev}$, is thus determined by the exchange current density i_o, the transfer coefficient α, the equilibrium concentrations $C_{o,BULK}$ and $C_{R,BULK}$ and the diffusion coefficients D_o and D_R.

At t=o the above equations reduce to

$$i(o) = i_o \cdot \left\{ \exp\left(\frac{\alpha nF}{RT}\,\eta\right) - \exp\left(\frac{(1-\alpha)nF}{RT}\,\eta\right) \right\}$$

Thus, only pure charge-transfer exists at time t=o. At short times an approximate expression for the current density can be obtained from equations (2.63)

$$i = i(o)\left(1 - \frac{2}{\sqrt{\pi}} \cdot \lambda\sqrt{t}\right) \qquad (2.79)$$

this indicates that the current is a linear function of $\sqrt{t}$ at short times. For longer periods we approximate to

$$i = i(o)\,\frac{1}{\sqrt{\pi} \cdot \lambda \cdot \sqrt{t}} \qquad (2.80)$$

a $1/\sqrt{t}$ dependence.

(ii) Linear Potential Sweep (and Cyclic Voltammetry)

Linear potential sweep methods enable a rapid scan of the 'electrochemical spectrum' in the three dimensional E.i.t. realm. Continued sweeping of the potential back and forth between two electrochemical states is known as cyclic voltammetry. In potential sweep methods, the electrode potential is varied linearly with time so that we have

$$E_v(t) = E - \nu t \qquad (2.81)$$

where E is the initial potential and ν the sweep rate. See Figure 2.4.

If the response of the electron transfer reaction

$$O + ne \rightleftharpoons R$$

is first considered. It is clear that at very slow sweep rates the current overpotential characteristic is that of steady state measurements. If ν is increased, however, a peak appears in the i-E curve. This peak is due to the effect of mass transfer and progressive depletion of the electroactive species at the electrode.

With the assumption that the rate of electron transfer is so high as not to limit Nernstian equilibrium at the interphase then the diffusion equations (2.82)

$$\frac{\partial C_o(x,t)}{\partial t} = D_o \frac{\partial^2 C_o(x,t)}{\partial x^2} \quad \text{and} \quad \frac{\partial C_R(x,t)}{\partial t} = D_R \frac{\partial^2 C_R(x,t)}{\partial x^2}$$

$$C_o(x,o) = C_{o,BULK} \qquad C_R(x,o) = 0$$

$$C_o(x,t) = C_{o,BULK} \qquad C_R(x,t) = C_{R,BULK}$$

$$x \to \infty \qquad x \to \infty$$

Figure 2.4

Typical potential profile and current response for a linear potential sweep.

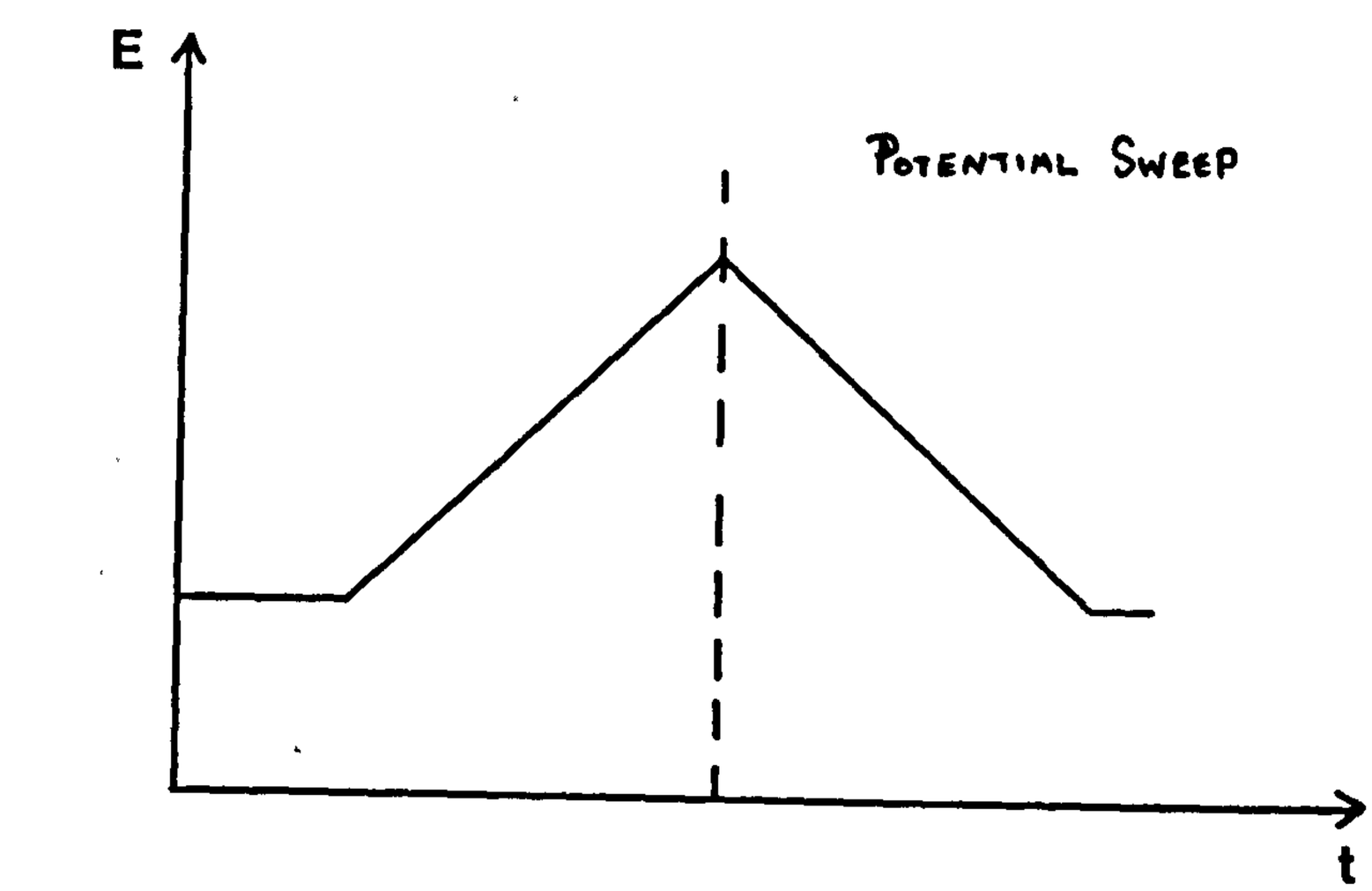
E
POTENTIAL SWEEP
t

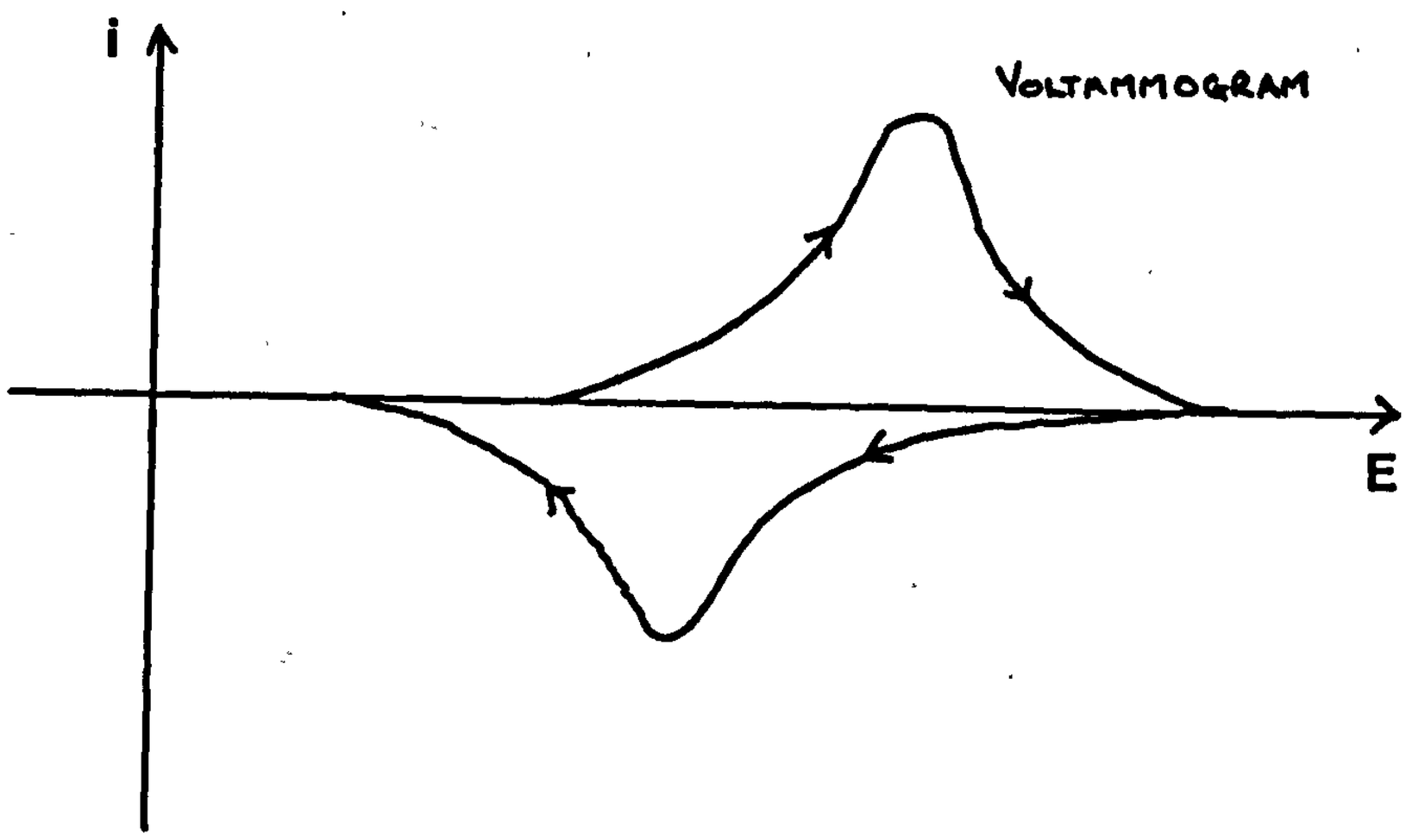
i
VOLTAMMOGRAM
E

$$\frac{i(t)}{zFA} = D\left[\frac{\partial C_o(x,t)}{\partial x}\right]_{x=o} = D\left[\frac{\partial C_R(x,t)}{\partial x}\right]_{x=o}$$

still apply.

However the Nernst equation changes to

$$\frac{C_o(o,t)}{C_R(o,t)} = \exp\left[\frac{nF}{RT}(E - \nu t - E^{\ominus})\right] \qquad (2.83)$$

indicating that the ratio C_o/C_R is now a function of time. This cannot be transformed in the Laplace plane directly due to this time dependence. However this equation which specifies the boundary conditions can be written as

$$\frac{C_o(o,t)}{C_R(o,t)} = \theta\, c^{-\sigma t} = \theta\, S(t) \qquad (2.84)$$

where $\theta = \exp[(nF/RT)(E - E^{\ominus})]$ and $\sigma = (nF/RT)\,\nu$.

At this point without entering into the mathematical treatment it will suffice to state that the diffusion equations of (2.82) can be transformed, individually for both species, combined and inverted via the convolution theorem. The boundary conditions of (2.84) are applied resulting in an integral equation dependent on $C_{o,BULK}$ and D_o. This can be reduced to give an expression for the current i as a function of ν, and ultimately an expression for peak current is obtained

$$i_p = 0.4463\, nFA\, C_{o,BULK} \left(\frac{nF}{RT}\right)^{\frac{1}{2}} \nu^{\frac{1}{2}} D_o^{\frac{1}{2}} \qquad (2.85)$$

or at 25^oC for A in cm^2, D in $cm^2\ sec^{-1}$, C in $mol\ cm^{-3}$ and V in sec^{-1} giving i_p in amps we have

$$i_p = (2.69 \times 10^5)\, n^{3/2}\, A\, D_o^{1/2}\, \nu^{1/2} C_{o,BULK} \qquad (2.86)$$

The peak potential is independent of sweep rate and is related to half wave potential by

$$E_p = E_{1/2} - \frac{0.029}{n} \text{ volts.}$$

If however the Nernstian condition of reversibility is not satisfied due to the effect of charge transfer limitation then a similar treatment can be pursued with different boundary conditions. Yielding

$$i_p = (3.01 \times 10^5) n\, (\alpha\, n_\alpha)^{1/2}\, D_o^{1/2}\, C_{o,BULK}\, \nu^{1/2} \qquad (2.87)$$

where n_α is the number of electrons transferred up to and including the rate determining step.

Useful reviews of transient techniques are provided by references 51, 57 and 58.

2.4 Electrocrystallization

The electrode surface has so far been regarded as a two dimensional charge transfer site and only in this respect considered to affect the reaction kinetics. It has also been assumed that the rates, i.e. current flow, are controlled partly or wholly by mass transport of electroactive species. However; a further surface process is known to exist, in a large number of charge transfer reactions, which causes complete independence of rate and hydrodynamic phenomena. This is usually a function of the concentration and distribution of new species at the electrode surface, which can ultimately result in the creation of a new phase. This phase may be non-conducting or of sufficient

area to restrict mass transfer. Hence, we have the situation where the kinetics are rate limited by an additional variable.

Most of the early studies of electrolytic crystal growth were centred on the deposition of metal on like metal. The mechanism of growth was assumed to be similar to that of deposition from the gas phase. However the formation of a crystal from its vapour is in principle far simpler than the electrochemical case since solvent is absent and uncharged atoms are deposited. The gas deposition principle suggests that growth can develop from either two dimensional nuclei in a layer by layer pattern or by a screw dislocation mechanism in which atoms diffuse to the growing edges adding to the rotating spiral. Extrapolation of the work of Kossel-Stranski[59] (1927) to the electrochemical system was made by Erdey-Gruz and Volmer[60] in 1931 but the postulates that processes could be controlled by surface diffusion were delayed until the existance of dislocations was introduced by Burton, Cabrera and Frank[61] in 1949 into the concept of crystal growth. The expected growth spirals were observed by Steinberg[62] in crystals grown electrolytically. Vermilyea[63] applied electrode kinetics to surface processes and derived an expression relating current at the interface to a model of spiral growth.

Since these early advances, mechanisms for electrocrystallization have been established and elaborated upon. These mechanisms are still points of active interest and vigorous dispute. Rather than quote these mechanisms and models exhaustively attention is drawn to two good reviews which should provide access to all of the pertenent material. See Bockris and Razumney[64] and Harrison and Thirsk.[65]

Since the oxidation of lead electrodes in sulphuric acid to produce solid $PbSO_4$ is known to produce a characteristic rising transient[64] in response to a potential step then the nucleation and growth model is primarily considered.

A brief consideration of the thermodynamics of nucleation is presented in Appendix 4.

(i) Two-dimensional nucleation and growth (Response to a potential step)

The current obtained from a single nucleus can be derived from simple geometric arguments as follows:

$$i = nFkS \tag{2.88}$$

where S is the area over which material is deposited, and k is the rate constant. We can extend this to:

$$nFkS = \frac{\rho}{M} \; nF \; \left(\frac{dV}{dr}\right) \; \left(\frac{dr}{dt}\right) \tag{2.89}$$

V is the volume, M the molecular weight, and ρ the density of the deposit. As S and dV/dr are known functions of the geometry, then integration of equation (2.89) gives r as a function of t, and consequently gives $i_{(t)}$. As an example, if we consider deposition around the edge of a cylinder, $S = 2\pi rh$. Hence,

$$i = nF2\pi hk^2 \frac{M}{\rho} t \tag{2.90}$$

where h is the height of the nucleus. When N_o nuclei are initially formed equation (2.90) becomes:

$$i = nFN_o2\pi hk^2 \frac{M}{\rho} t \tag{2.91}$$

The expression for progressive nucleation can be calculated given that the number of nuclei at any time is:

$$N = N_o \ (1 - (\exp \ - At)) \qquad (2.92)$$

where A is a nucleation rate constant. For small values of A, equation (2.92) can be approximated to:

$$N = N_o \ At \qquad (2.93)$$

differentiating for the rate of change gives $\frac{dN}{dt} = N_oA$. Nucleation and growth occur simultaneously and the resulting current given by:

$$i = \int_o^t i \ (u) \ \left(\frac{dN}{dt}\right)_{t = t-u} du \qquad (2.94)$$

where u is the age of the nucleus.

If i(u) in equation (2.94) is represented by equation (2.90) with t replaced by u, and dN/dt by N_o (1 - (exp -At)), or by the approximation to this N_oAt (2.93), and if we absorb N_o into the definition of A, i as a function of t can be estimated. The result for the two-dimensional model i.e. growth in cylinders is:

$$i = \frac{nF\pi MhAk^2t^2}{\rho} \qquad (2.95)$$

Similar equations for other geometries are listed by Harrison and Thirsk.[65]

These equations predict that the current is infinitesimal with time, which is obviously unacceptable, as restrictions occur due to overlap of growth areas.

If the Avrami theory[67] is adapted it can be shown that if random overlap of nuclei occurs then the fraction of surface covered by growth centres, γ, is related to the fraction that

would be covered in the absence of overlap, γ_{ext}, by

$$d\gamma/d\gamma_{ext} = 1 - \gamma \tag{2.96}$$

with

$$\gamma_{ext} = N_o \pi r^2 \tag{2.97}$$

for instantaneous nucleation or

$$\gamma_{ext} = \pi \int_o^t r(u)^2 \, (dN/dt)_{t-u} \, du \tag{2.98}$$

for progressive nucleation.

Substituting for r with r = Mkt/ρ from (2.89) gives

$$\gamma_{ext} = \pi N_o M^2 K^2 t^2/\rho^2 \qquad \text{instantaneous} \tag{2.99}$$

$$\gamma_{ext} = \pi N_o A M^2 K^2 t^3/3\rho^2 \qquad \text{progressive} \tag{2.100}$$

If we integrate (2.96) to give γ in terms of γ_{ext} we have

$$\gamma = 1 - \exp(-\gamma_{ext}) \tag{2.101}$$

combining with (2.99) and (2.100) gives

$$\gamma = 1 - \exp(-\pi N_o M^2 K^2 t^2/\rho^2) \qquad \text{instantaneous} \tag{2.102}$$

and $$\gamma = 1 - \exp(-\pi N_o A M^2 K^2 t^3/3\rho^2) \qquad \text{progressive} \tag{2.103}$$

The volume per unit area of total surface is V = γh if we introduce (2.88) and (2.89) we can get the expressions for the transients

$$i = (2\pi FnMN_o K^2 ht/\rho) \exp(-\pi M^2 N_o K^2 t^2/\rho^2) \qquad \text{instantaneous} \tag{2.104}$$

$$i = (nF\pi MN_o A K^2 ht^2/\rho) \exp(-\pi M^2 N_o K^2 A t^3/3\rho^2) \qquad \text{progressive} \tag{2.105}$$

Comparison of these two equations with (2.91) and (2.95) show the effect of overlap accounted for by the exponential terms in time. As $t \to o$, then (2.104) → (2.91) and (2.105) → (2.95).

If we plot these two commonly occurring expressions (2.104) and (2.105) as dimensionless quantities we have the profiles shown in Figure 2.5.

These curves can be represented by the equations

$$\frac{i}{i_m} = \frac{t}{t_m} \exp \left[- \tfrac{1}{2} \left(\frac{t^2 - t^2_m}{t^2_m} \right) \right] \qquad (2.106)$$

and

$$\frac{i}{i_m} = \left(\frac{t}{t_m} \right)^2 \exp \left[- \frac{2}{3} \left(\frac{t^3 - t^3_m}{t^3_m} \right) \right] \qquad (2.107)$$

respectively. The experimental i-t plots should have a similar shape.

(2.104) and (2.105) can also be reduced to

$$i = \alpha_1 t \exp \beta_1 t^2 \qquad (2.108)$$

and

$$i = \alpha_2 t^2 \exp \beta_2 t^3 \qquad (2.109)$$

These have single maxima given by $di/dt = 0$ (i_m, t_m) at which

$$\alpha_1 = \frac{t_m}{i_m} e^{0.5}$$

$$\beta_1 = \frac{1}{2 t_m^2}$$

Figure 2.5

Reduced time plots for two-dimensional crystal growth with either instantaneous or progressive nucleation.

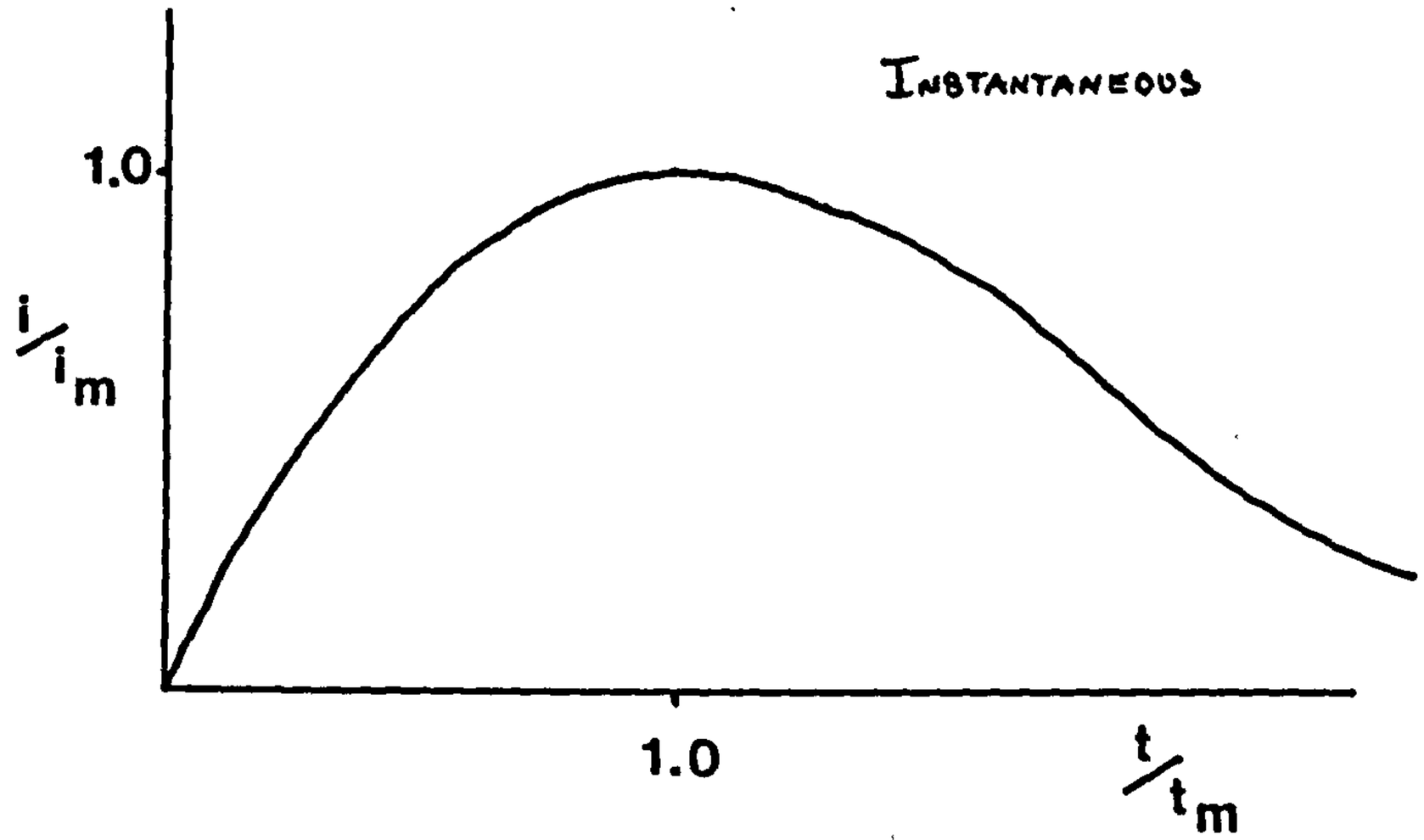
INSTANTANEOUS
1.0
i/im
1.0
t/tm

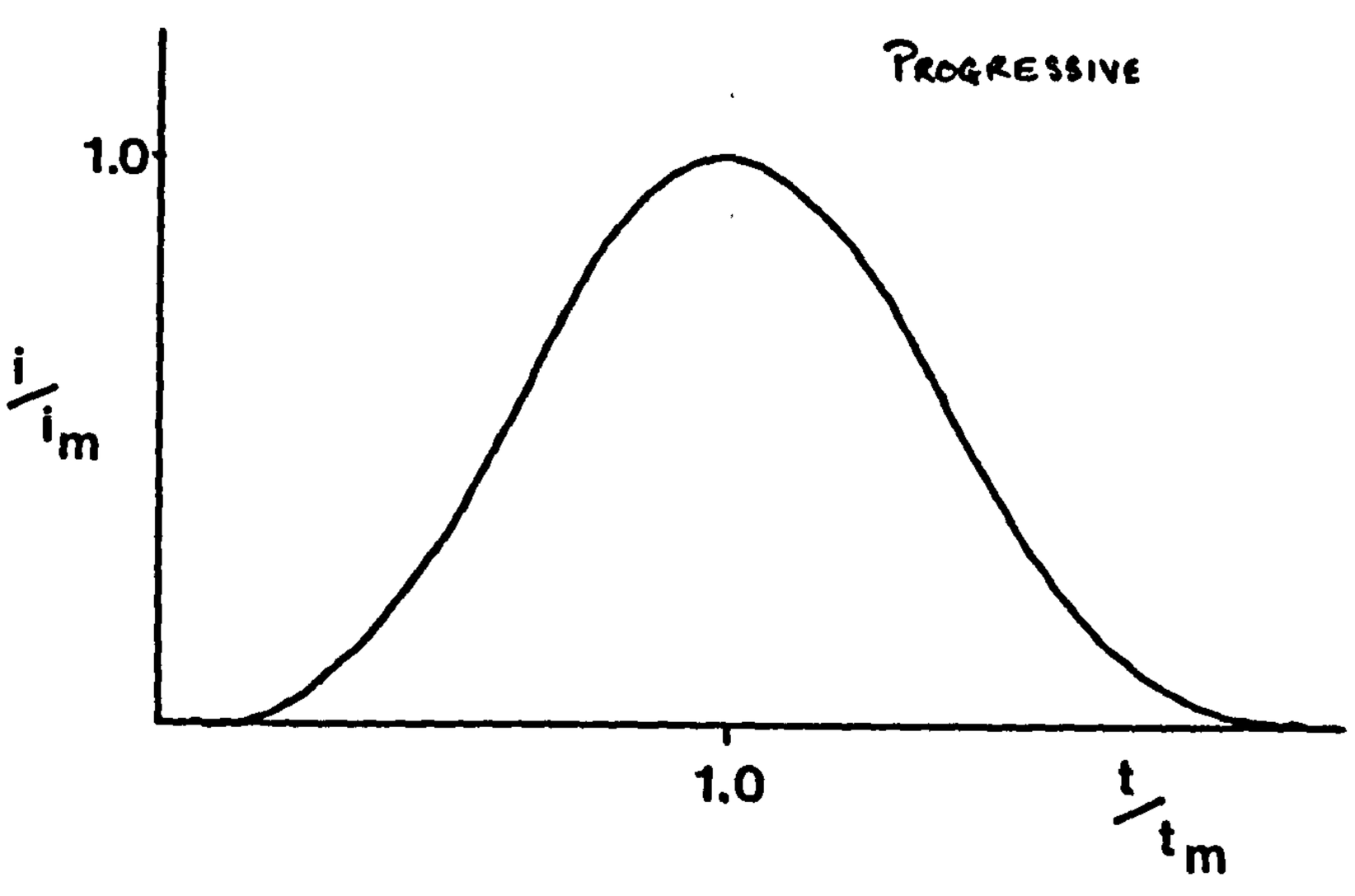
PROGRESSIVE
1.0
i/im
1.0
t/tm

$$\alpha_2 = \frac{i_m}{tm^2} \; e^{0.67}$$

$$\beta_2 = \frac{2}{3t_m{}^3}$$

If these expressions are fitted to experimental current responses we can, from reduced time plot fitting ($^{i}/_{i_m}$, $^{t}/_{t_m}$), determine the type of surface process taking place.

A unified crystal growth theory does not exist, but a set of complementary theories has been developed, each dealing with a certain aspect of the growth process. The theory presented so far in this section represents a system where nucleation is induced under potentiostatic conditions, by a potential change, and growth is not restricted by diffusion of active material to the growth site. Consequently, transport to and from the electrode plays little or no role in determining the kinetics of the overall reaction.

Although growth in two dimensions describes the fundamental process occurring when forming a new phase, it is known that many polycrystal films are formed by a process loosely described as three-dimensional nucleation and growth. The arguments used to derive the two dimensional equations can be extended to layer by layer growth[68,69] which ultimately results in a three-dimensional deposit. Expanding the theory of successive monolayer growth however does not result in an adequate theoretical model for 3D growth, despite the fact that the physical boundaries to the problem are well known. (A model of growth of cones is the most common approximation.) The major drawback in any attempt has been the establishment of a volume transformation which would

account for inter-crystal collisions in the appropriate way. Fletcher and Matthews[70(a)] have recently described an attempt at solving volume transforms for a number of types of nucleation and growth in what they term a 2½D system. The 2½D nucleation and growth is so called because crystal growth from an electrode surface extends only into one-half of the third dimension as growth into the substrate is forbidden. A key feature of this new model was the assumption that crystals grow in a shape preserving way and the rates of lateral and vertical growth were inter-related. The rate determining step was taken to be the spreading of the base of the crystal at the electrode surface. Evaluation of the model by investigation of i-η-t response and application to a physical system (Pb - $PbSO_4$)[70(b & c)] however, shows the real situation to be much more complex than that suggested by the theory.

The model gives a good approximation at short times but becomes increasingly inaccurate as reaction proceeds and subsequently fails to describe the highly developed, and idiosyncratic behaviours of intercrystal collisions in individual systems. Further development of this approach will be interesting to note.

(ii) <u>Adspecies model</u>

The applicability of theories involving the surface diffusion of adspecies in the exchange reaction between lead and lead sulphate is unlikely on energetic grounds. A consideration of the theories concerning adspecies will indicate why this is so. However before proceeding further, it should be noted that in order to avoid repetition the treatment of electron transfer in this section is sparse and is presented more fully in Section 2.5.

The main features of the 'adatom' model of Kossel and Stranski are shown in Figure 2.6(a). The initial step in the deposition process is the passing of an ion in solution across the electrified interface.

Considering the addition of metal ions from solution onto an electrode of the same metal. The metal is pictured to be a lattice of ions held together by a sea of electrons. Any ion which approaches the electrode from solution is surrounded by a hydration sheath, if passage through the double layer is to take place then the ion must distort its hydration sheath or become dehydrated to some extent. Not only must the ion divest itself of water but in order to form an adspecies it must accept an electron. If the energy profile of an 'ion' located as an adspecies on the metal surface is compared with that of the hydrated ion in solution the characteristic W-shaped overlap forming an energy barrier between the two is observed (see Figure 2.7). Electron transfer discharge condition is attained when the paths of the two energy distance curves overlap (see Section 2.5).

Bockris and co-workers[71,72] investigated the possible mechanisms for ion transfer from solution to the metal surface. Enthalpies of activation for transfer to different sites were calculated, that to a planar site being found to be significantly less than that to other sites (i.e. edges and kinks etc.). These enthalpy differences were due to the degree of displacement of the hydration sheath which has to take place at different sites (see Figure 26(b)). The greater the displacement the higher the energy barrier to discharge, at that site. Although the final state may be more energetically favourable, because of greater

Figure 2.6

(a) The adatom model of Kossel and Stranski showing the incorporation of a species from solution to, ultimately, a surface detect.

(b) Varying degrees of displacement of the hydration sheath with ion position on the metal surface.

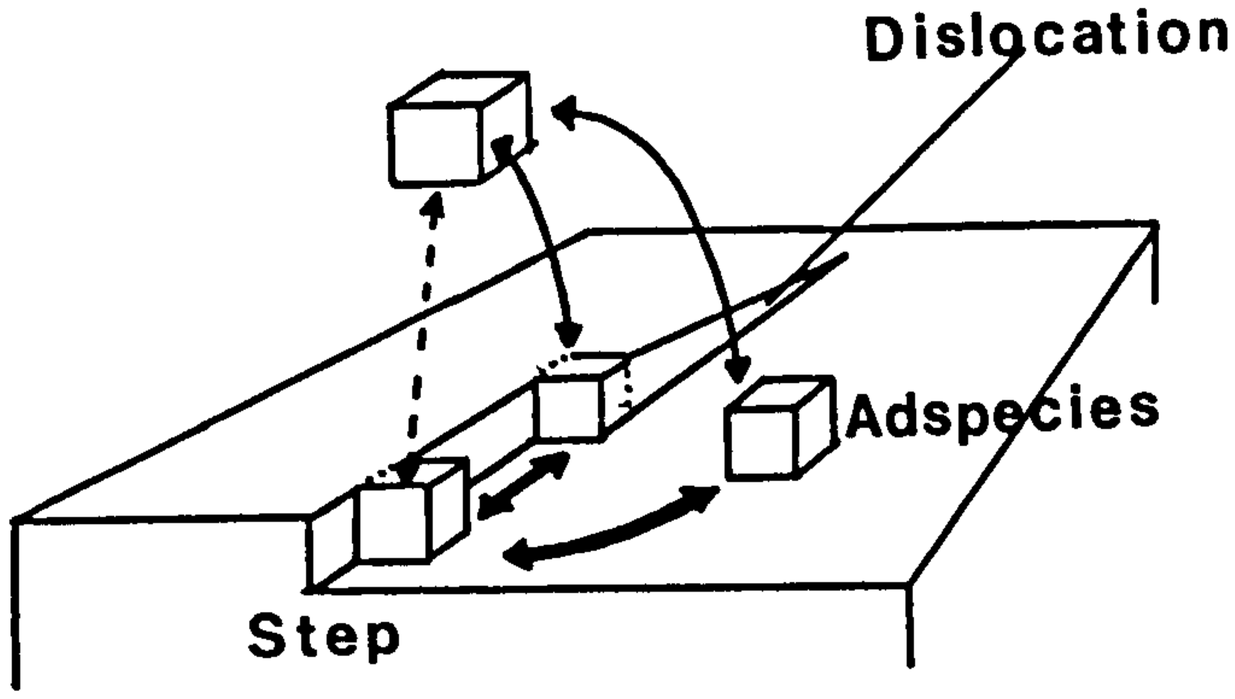
Dislocation
Adspecies
Step

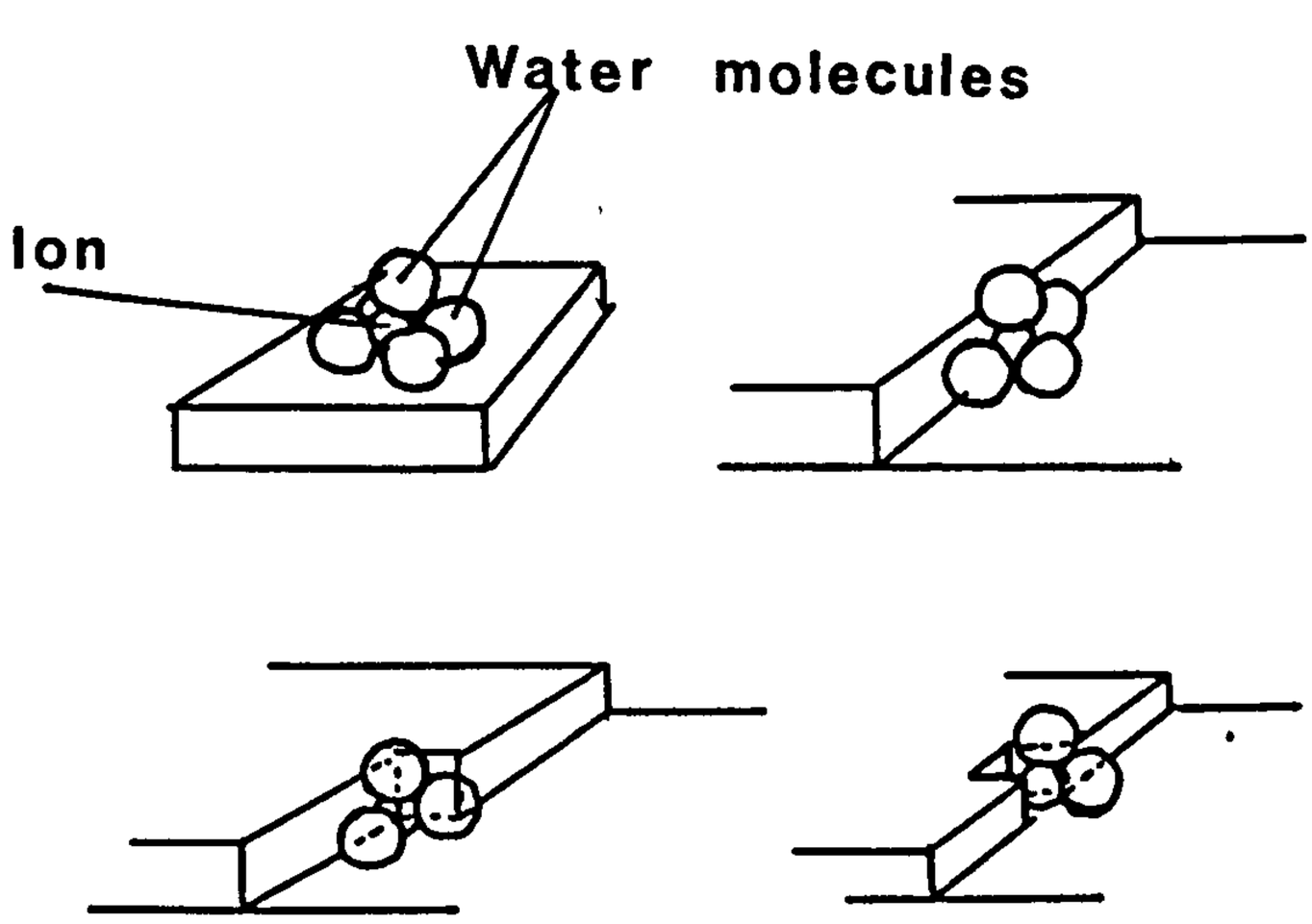
Water molecules
Ion

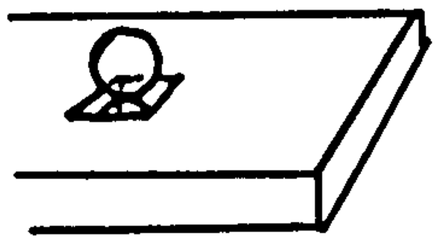

Figure 2.7

Energy profile of an 'ion' located as an adspecies on the metal surface superimposed on the energy profile of the hydrated ion in solution.

Figure 2.8

Passivation by the production of an insoluble film on the metal surface.

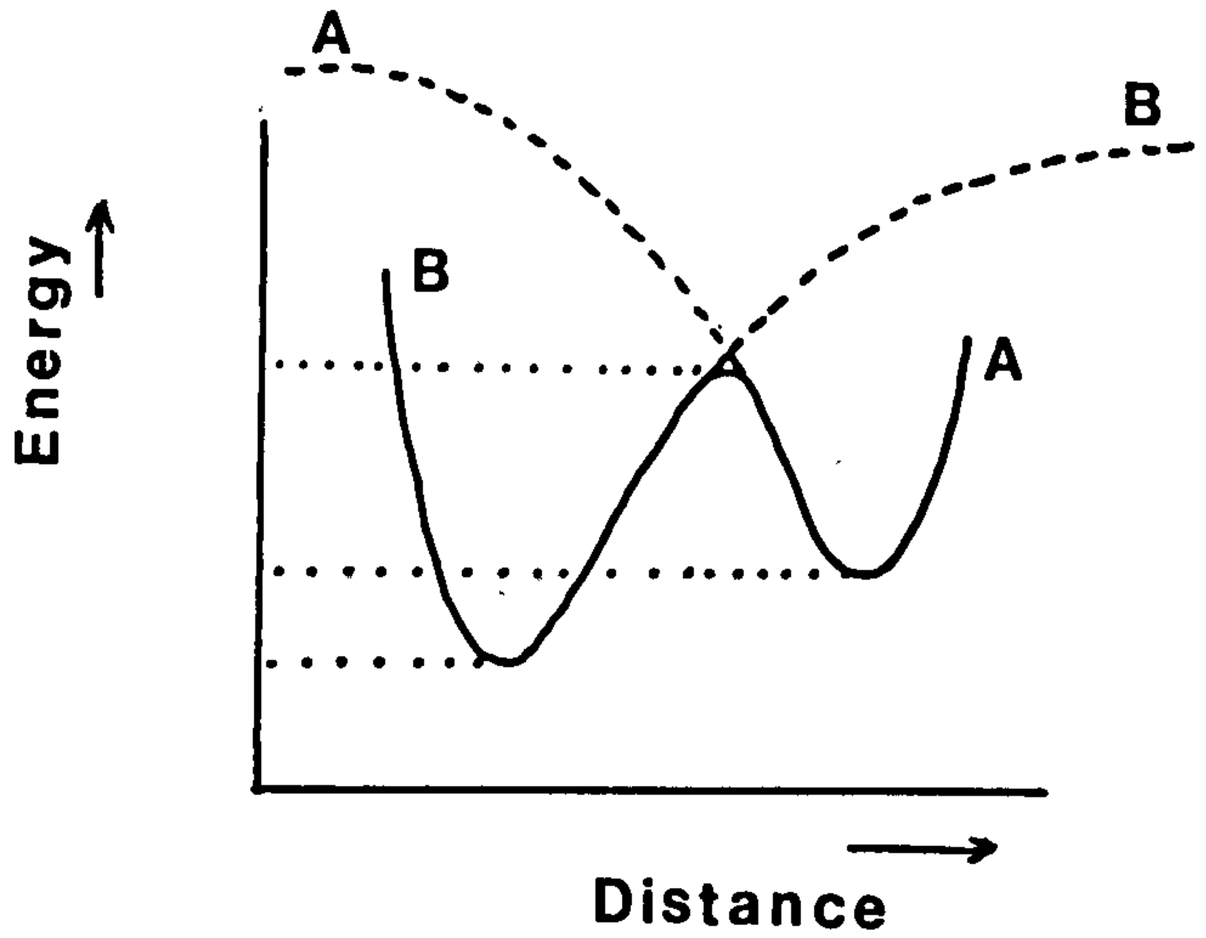

A: POTENTIAL ENERGY FOR HYDRATED ION.

B: POTENTIAL ENERGY FOR AN ADSORBED SPECIES ON THE SURFACE, AFTER CHARGE TRANSFER.

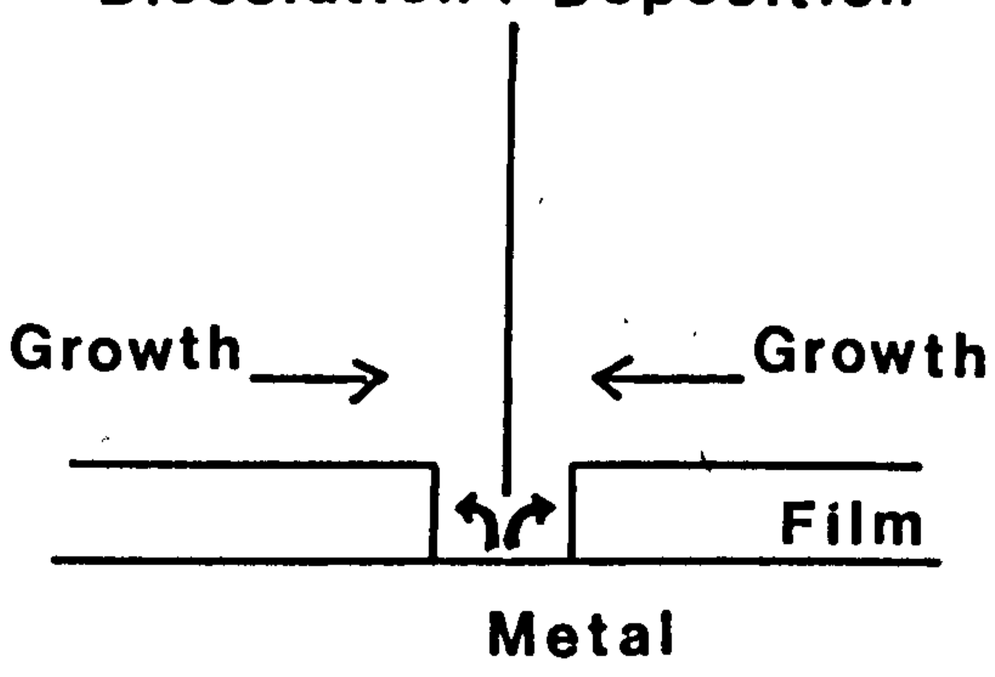

co-ordination, at kinks and edges; this does not influence the barrier height. The discussions of Fleischmann and Thirsk[73] and of Mott and Watts-Tobin[74] are lacking in this respect since they assume that the rates of charge transfer to be greater at defect sites or the same at all sites, respectively.

The fact that the adspecies retains some of its hydration sheath after passing to the electrode surface implies that the adspecies must retain some degree of ionic character. Hence we have the adion rather than a neutral adatom. Calculated enthalpies of activation[71,75] again show that the more stable species is the one in which charge is retained after 'charge transfer'. The adsorbed ion and associated electron can be assumed to form a dipole at the surface. These results can be used to support this argument in reverse, that is; if the adspecies is charged it is likely to retain some degree of hydration.

At this stage energy considerations leave the partially hydrated adion isolated on the surface. However to be incorporated into the lattice it must move to a surface step where it can lose further water and then to a kink site as an addition to the growing layer. The addition at this kink site of further adions eventually causes embodiment of the initial adion into the lattice, loss of all its water and removal of its charge. The surface diffusional process is a two dimensional random walk allowing the adion to migrate, from a given position to an adjacent similar position, by moving over and in contact with two of its three nearest neighbours in the surface. In this process, a bond with one of the three neighbours will be broken and a new bond, in the adjacent hollow, will be formed with another atom. The adion motion is unaffected

by the electric field since it is normal to the electrode surface.

The adion concentration at the surface is determined by the rate of incorporation into the lattice and the rates of formation of adions and removal back out into solution.

It can be seen why this theory is restrictive when applied to the formation of a lead sulphate surface on lead. Since SO_4^{2-} is a negatively charged ion with a complete valence shell it is unlikely to share charge with a metalic surface and form an adion species and therefore the nucleation of a new phase is required.

(iii) Passivation

Many mechanisms have been proposed to explain passivation,[77] however only one, due to Müller,[76] will be outlined.

Passivation by the production of an insoluble film on the metal surface can be represented by:

$$M + X^- \rightarrow MX + ne$$

dramatically in figure 2.8. The spreading of the film takes the form of 'nucleation and growth', until only a small fraction of the initial area remains uncovered. The area available for dissolution reducing until the reaction is limited by solution resistance in the remaining pores.

The pore solution resistance can be given by

$$R_p = \delta/\kappa\ A_o\ (1-\theta) \qquad (2.110)$$

where κ is the specific conductivity of the solution

A_o is total surface area

θ is degree of coverage at time t

and δ the thickness of the film.

If the bulk solution resistance is R_o then the current flowing through the pores at potential E is

$$i = E/(R_p + R_o) \qquad (2.111)$$

combining (2.110) and (2.111) gives

$$i = E\kappa A_o(1-\theta)/[\delta + R_o\kappa A_o(1-\theta)] \qquad (2.112)$$

To relate the change in current to the change in θ with time we can write from Faraday's law i.e. $w = MIt/nF$

$$i = (nF\rho\delta A_o/M)(d\theta/dt)$$

$$i = k_o(d\theta/dt) \qquad (2.113)$$

In linear potential sweep experiments (or cyclic voltammetry) the potential is a function of time

$$E = E_i + \nu t$$

where E_i is the initial potential

and ν is the sweep rate.

Thus combining (2.112) and (2.113)

$$\frac{d\theta}{dt} = (\kappa A_o/k_o)(1-\theta)(E_i + \nu t)/[\delta + R_o\kappa A_o(1-\theta)] \qquad (2.114)$$

Maximum current occurs when $\frac{d^2\theta}{dt^2} = 0$ (2.115)

Differentiating (2.114) and substituting into (2.115) gives:

$$\frac{d\theta_m}{dt} = [\delta(1-\theta_m)\ \nu + R_o\kappa A_o\ (1-\theta_m)^2\ \nu]/\delta(E_i + \nu t_m) \qquad (2.116)$$

Substituting E_m for $E_i + \nu t_m$ in (2.116) and solving for E_m in (2.112).

Putting (2.112) into (2.115) gives a solution for $\frac{d\theta_m}{dt}$ which is then substituted into (2.113) to give a solution for i_m^2. Ultimately yielding an expression for the maximum current

$$i_m = (nF\rho\kappa/M)^{\frac{1}{2}} A_o(1-\theta_m) \nu^{\frac{1}{2}} \qquad (2.117)$$

The potential where the current maximum occurs can be found by substitution into (2.112)

$$E_m = (nF\rho\kappa/M)^{\frac{1}{2}}[(\delta/\kappa) + R_o A_o (1-\theta_m)] \nu^{\frac{1}{2}} \qquad (2.118)$$

From (2.117) and (2.118) it can be seen that if θ_m is independent of sweep rate, then both peak current and peak potential vary linearly with $\nu^{\frac{1}{2}}$.

2.5 The electrode-electrolyte interphase

The basic techniques and underlying theory of the methods of investigation employed in this research, have been presented in the preceding sections of this chapter. However, what has not been discussed is the microscopic events occurring at the electrode-electrolyte interphase upon which all the calculation is based. Reference is made to good treatments of this subject, whilst presenting a brief outline.

(i) Interphase structure

If we consider a metal electrode which when in contact with an electrolyte can have its potential shifted about the equilibrium potential without any electrochemical reaction taking place, then we have an ideal polarizable electrode. Useful for investigating interphase phenomena without reaction interference. Such a system

($Hg/KCl_{aq}(IM)$) was used by Grahame[78] in an early investigation of the structure of the 'double layer'. If the Hg/KCl system is considered then it can be seen that an accumulation of one of the ion species K^+ or Cl^- will occur at the electrode interphase depending on which way the potential is shifted about equilibrium. This accumulation alters the distribution of ions at the electrode and as a consequence alters the potential profile near the electrode. These two factors, concentration and potential, according to previous derivations, affect the rate of reaction. This implies an adulteration of the results of the same derivations.

Models for the interphase have developed through the years. Helmholtz originally proposed charge separation at electrodes, so that the model consisted of two sheets of charge, of opposite polarity, separated by a distance of molecular dimensions, the structure is equivalent to a parallel plate capacitor. This is where the name 'double-layer' arises. Although the charge on the electrode is confined to the surface the same is not necessarily true of the solution. A finite thickness of charge carriers would essentially arise because of the competition between chemical/electrical attraction, which pulls the species towards the electrode and solvation along with random thermal motions which resist these forces. Thus a diffuse layer, as proposed by Gouy-Chapman,[79,80] is established.

Figure 2.9 shows charge distribution and potential change in the double layer according to Helmholtz and according to Gouy-Chapman.

Stern[81] adapted the two models above to try to improve the theoretical values obtained for C_D (double layer capacitance), which were substantially higher than those obtained by experiment.

Figure 2.9

Charge distribution and potential profile through the double layer according to the Helmhotz and Gouy-Chapman models.

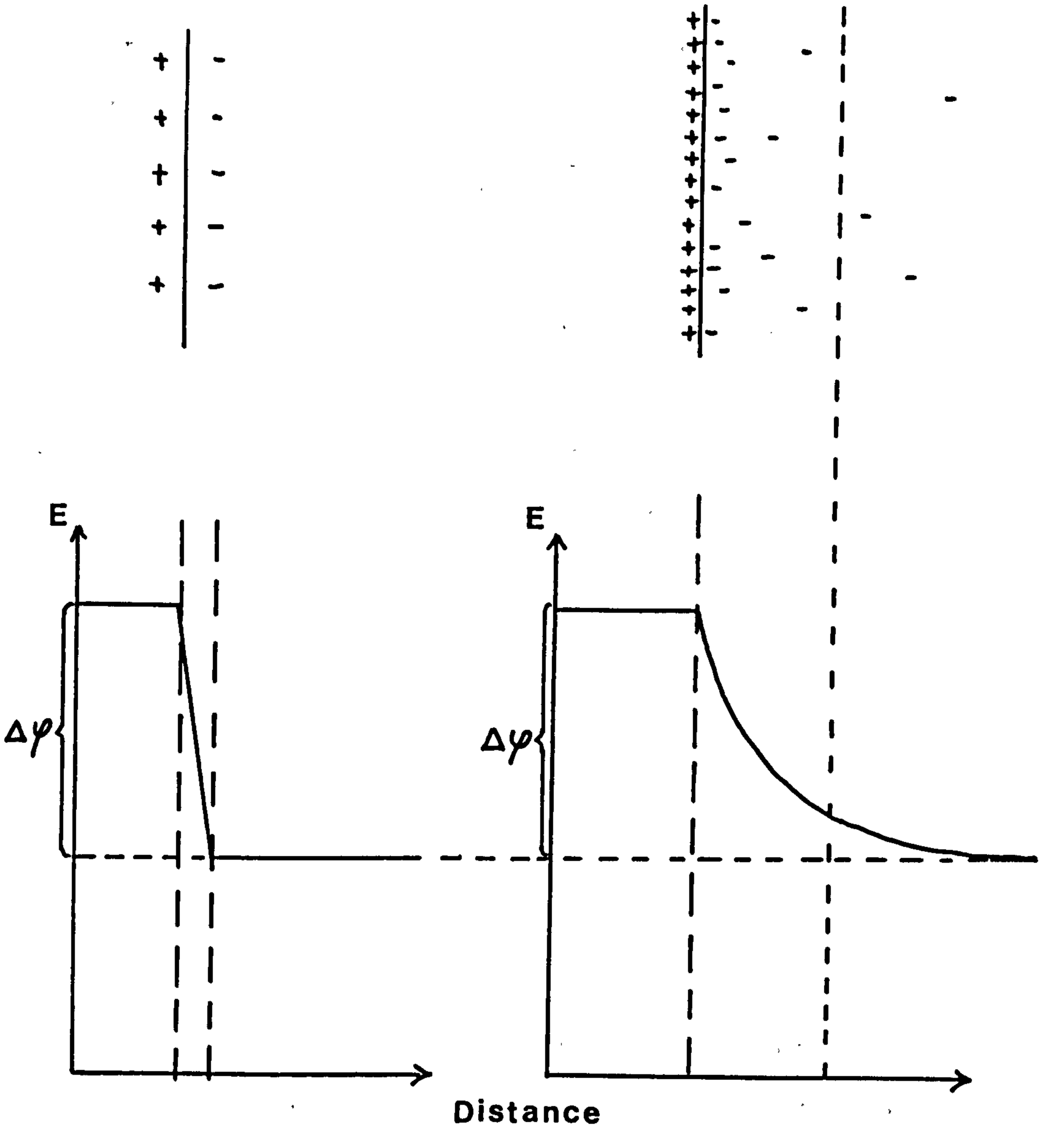
E
Δφ
E
Δφ
Distance
Helmholtz
Gouy & Chapman

He postulated that the double layer consisted of a Helmholtz layer of fixed ions producing a region of high field and low dielectric constant; beyond which there is an ionic atmosphere or diffuse layer in which the electrostatic and thermal motions are balanced. According to Grahame the capacitance of the Helmholtz compact double layer is in series with diffuse layer, so that:

$$\frac{1}{C_D} = \frac{1}{C_c} + \frac{1}{C_d} \qquad (2.104)$$

C_D is the total capacitance of the Stern double layer.

The potential gradient in the entire double layer has a large component due to the compact layer and a smaller conbribution from the diffuse layer, which is called the zeta potential (see Figure 2.10).

Stern also takes into consideration the orientation and specific adsorption of dipole molecules and ions, which leads to a change in the potential profile of the compact layer (see Figure 2.11).

Effect on reaction rates

Such deviations, in potential and concentration at the interphase, from those of the bulk electrode and electrolyte give rise to a number of apparent anomalies. The basic concepts have been described by Frumkin[82] and the observed effect is sometimes called the Frumkin effect.

The potential change through the double layer can affect the electrode kinetics.

Figure 2.10

Potential profile through the double layer according to the Stern model.

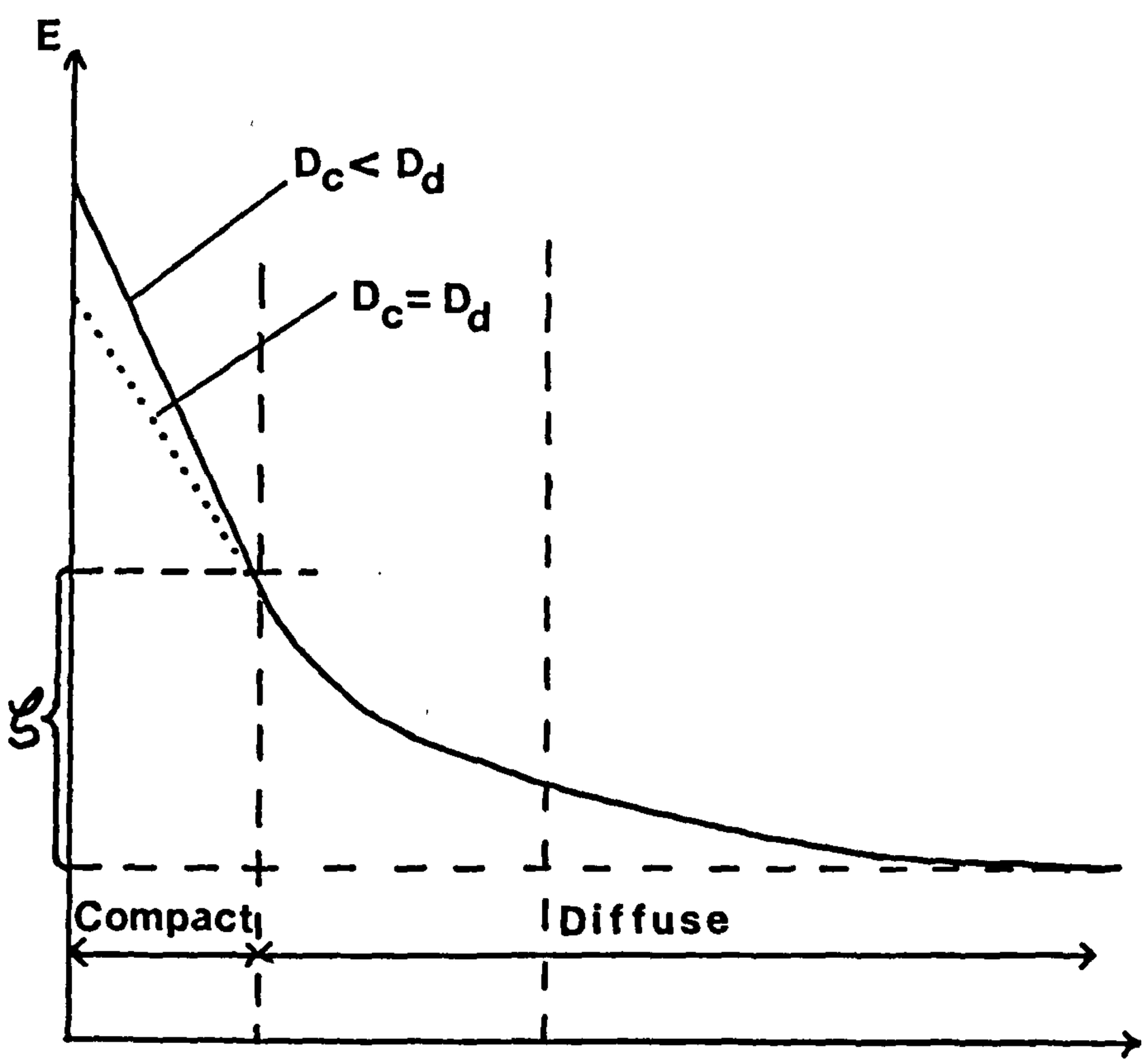

Stern Model

D IS THE DIELECTRIC CONSTANT OF THE COMPACT 'c' AND DIFFUSE 'd' LAYERS.

Figure 2.11

Modified charge distribution and potential profile for the Stern model with dipole adsorption and orientation.

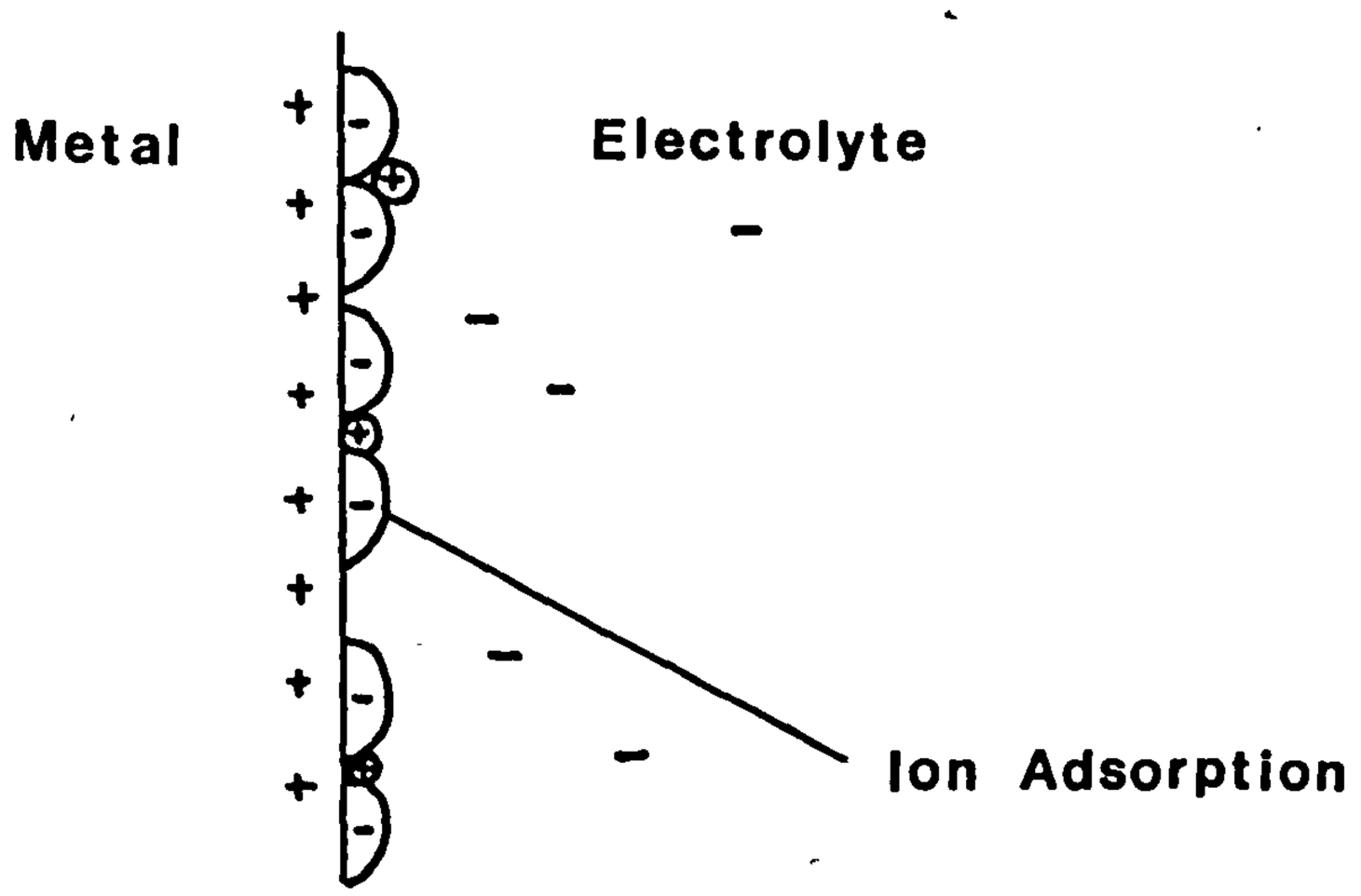

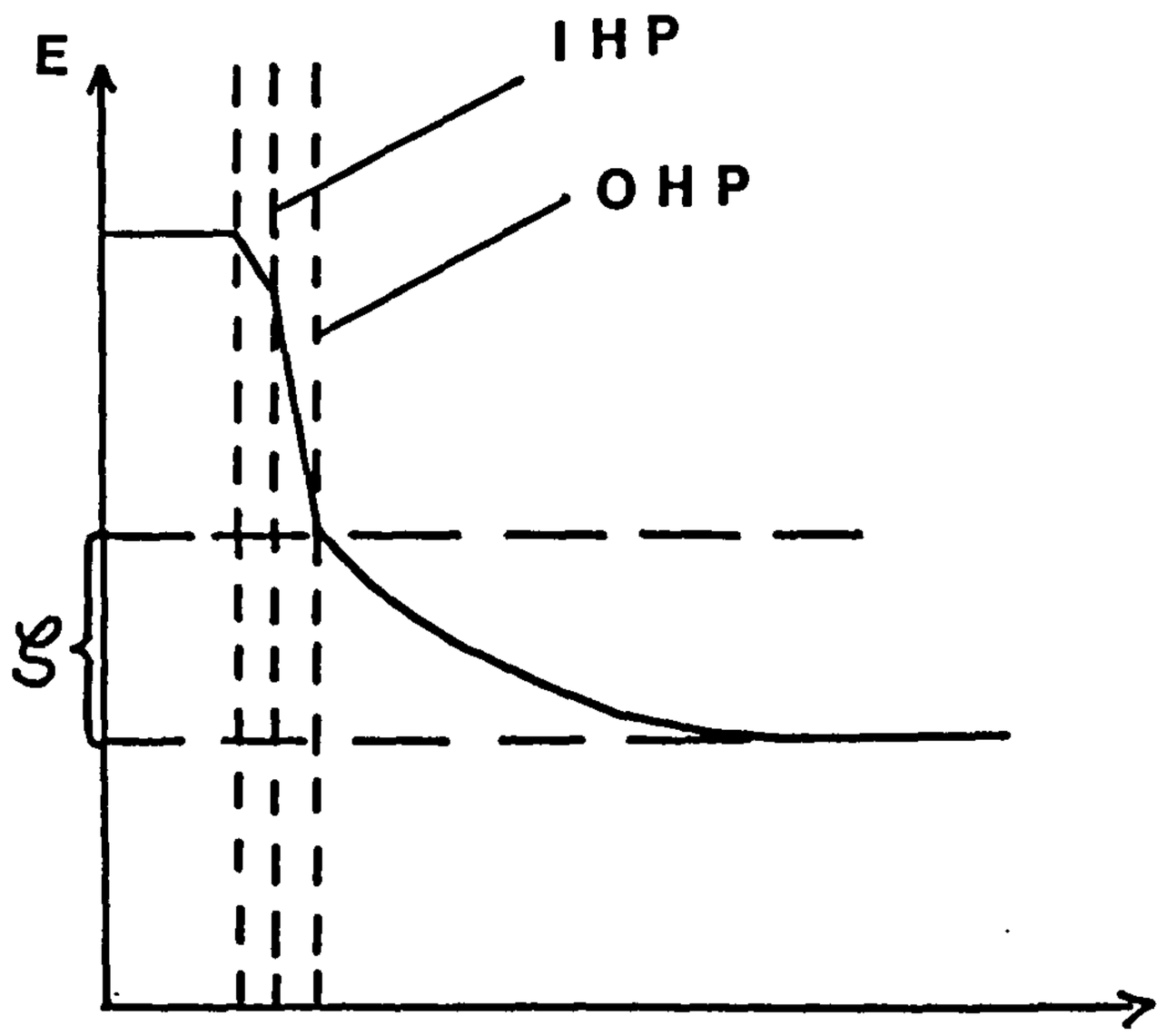

IHP Inner Helmholtz Plane

OHP Outer " "

Considering $O^z + ne \rightleftharpoons R^z$: the concentration of O^z within the double layer at the distance of the tightly bound Helmholtz layer will be different to that outside the diffuse layer, which in previous calculations has been used as C_{ox} the concentration at the electrode surface.

In order to relate the concentration within the double layer to the bulk concentration we can use a statistical mechanical approach proposed by Gouy-Chapman.[79,80] The solution in the diffuse layer is sub-divided into laminae parallel to the electrode surface. The laminae are in thermal equilibrium, but not ionic equilibrium, the ions also vary in energy due to the change in potential through the diffuse layer. The laminae can be regarded as different energy states whose number concentrations can be related by a Boltzmann factor. If we use a laminae in the bulk as a reference with ion population N_i^o, then the population in any other laminae is given by:

$$N_i = N_i^o \exp \frac{-n_i\ e\phi}{k_B T} \qquad (2.105)$$

where ϕ is the potential w.r.t. the bulk

e is the charge on the electron

k_B is the Boltzmann constant

T is the absolute temperature

and n_i is the (signed) number of units of electronic charge

Thus

$$C_{ox}(D) = C_{ox}\ C^{-n_i F\phi_D/RT} \qquad (2.106)$$

and from the rate equation (2.32)

$$\frac{i}{nF} = k^{\ominus} C_{ox} e^{-(\alpha nF/RT)(E-E^{\ominus})}$$

applying the correction for $C_{ox(D)}$ gives

$$\frac{i}{nF} = k_t^{\ominus} C_{ox} e^{-F\phi_D/RT} e^{-(\alpha nF/RT)(E-\phi_D-E^{\ominus})} \qquad (2.107)$$

rearranging

$$\frac{i}{nF} = k_t^{\ominus} e^{(\alpha n-n_i)F\phi_D/RT} C_{ox} e^{-\alpha nF(E-E^{\ominus})/RT} \qquad (2.108)$$

where $k_t^{\ominus}$ is the true rate constant.

The relationship between $k^{\ominus}$ and $k_t^{\ominus}$ is given by

$$k^{\ominus} = k_t^{\ominus} \exp\left(\frac{(\alpha n-n_i)F\phi_D}{RT}\right) \qquad (2.109)$$

This allows the calculation of the true rate constant from the apparent one.

In a similar way we can substitute $k_t^{\ominus}$ into equation (2.34)

$$i_{o_t} = nF\, k_t^{\ominus} C_{ox}^{(1-\alpha)} C_R^{\alpha}$$

producing

$$i_o = i_{o_t} \exp\left(\frac{(\alpha n-n_i)\, F\phi_D}{RT}\right) \qquad (2.110)$$

giving the true exchange current.

A more rigorous derivation can be based on the approach adopted previously via transition state theory.

Correction of the apparent rate constants to find the true values for $k_t^{\ominus}$ or i_{ot} are dependent on obtaining a value for ϕ_D

for the given experimental conditions. This has to be done mathematically based on a model similar to that of the laminae structure.

(ii) Electron movement

The kinetics of charge transfer were covered in 2.1 with almost complete disregard for the movement of electrons, without which there would be no charge transfer, a short note on the mechanism of electron shift is necessary to complete the picture.

If homogeneous electron transfer[83,84] is considered initially, principles drawn from the model can be later applied to heterogenic electrode reactions.

In the classical system the electron transfer mechanism is treated with reference to activated complex theory (Appendix 1) and the use of potential energy profiles. Figure 2.12 shows an electron transfer process by the classical treatment.

The rate constant for the electron-transfer step is given by

$$k_e = \kappa \frac{k_B T}{h} e^{-\Delta G^{\ddagger}/RT} \qquad (2.111)$$

where $\Delta G^{\ddagger}$ is the free energy of activation and κ the transmission coefficient. The transfer of the electron is so fast (10^{-16} s) that the system must obey Frank-Condon restrictions.[85,86] Thus the only possible place for transfer to occur is at the intersection point of the two curves. As a consequence the inner vibrational co-ordinates of the molecules and the outer hydration sheath must adjust to some nonequilibrium configuration prior to electron transfer.[87-90] The energy required to reorganise the system is given by $\Delta G^{\ddagger}$. Although a suitable configuration of

Figure 2.12

Potential energy variation with nuclear position to provide an intersection point, of the energies of the initial and final electron configurations, which will facilitate electron transfer.

Figure 2.13

Three-dimensional representation of electron transfer showing both the classical and quantal pathways.

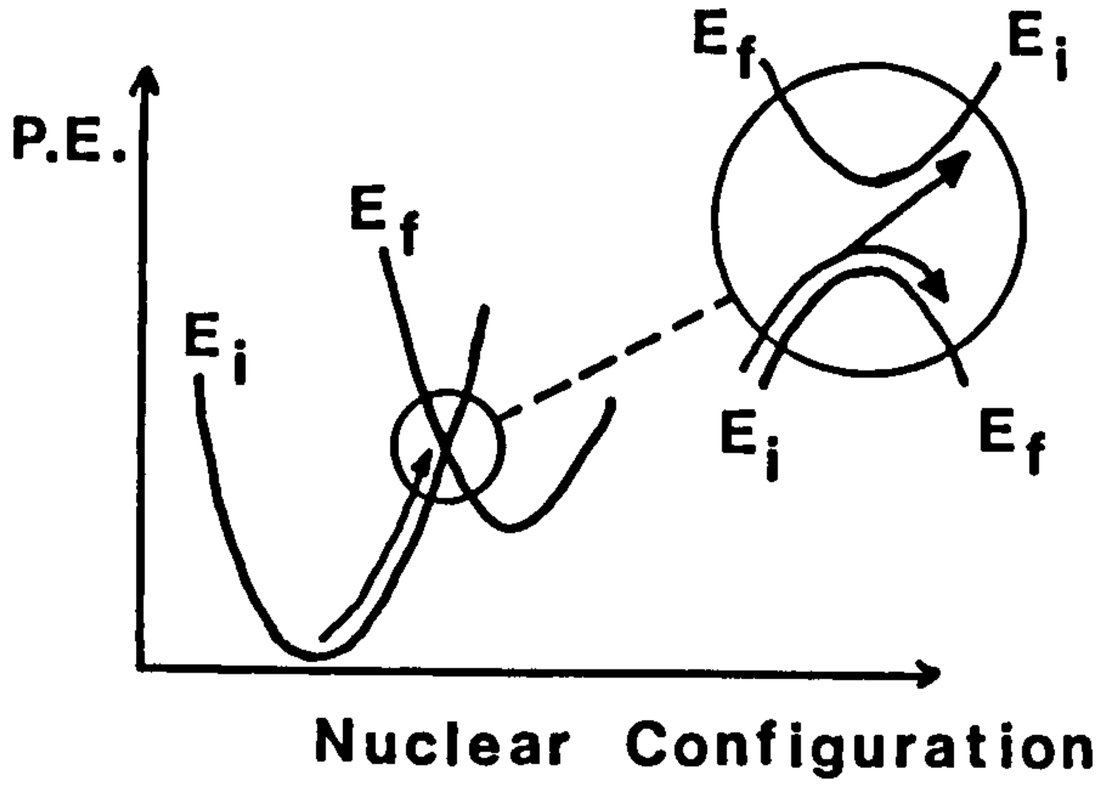

Minimum Potential Energy Profile
For initial 'i' and Final 'f'
States in Electron Transfer.

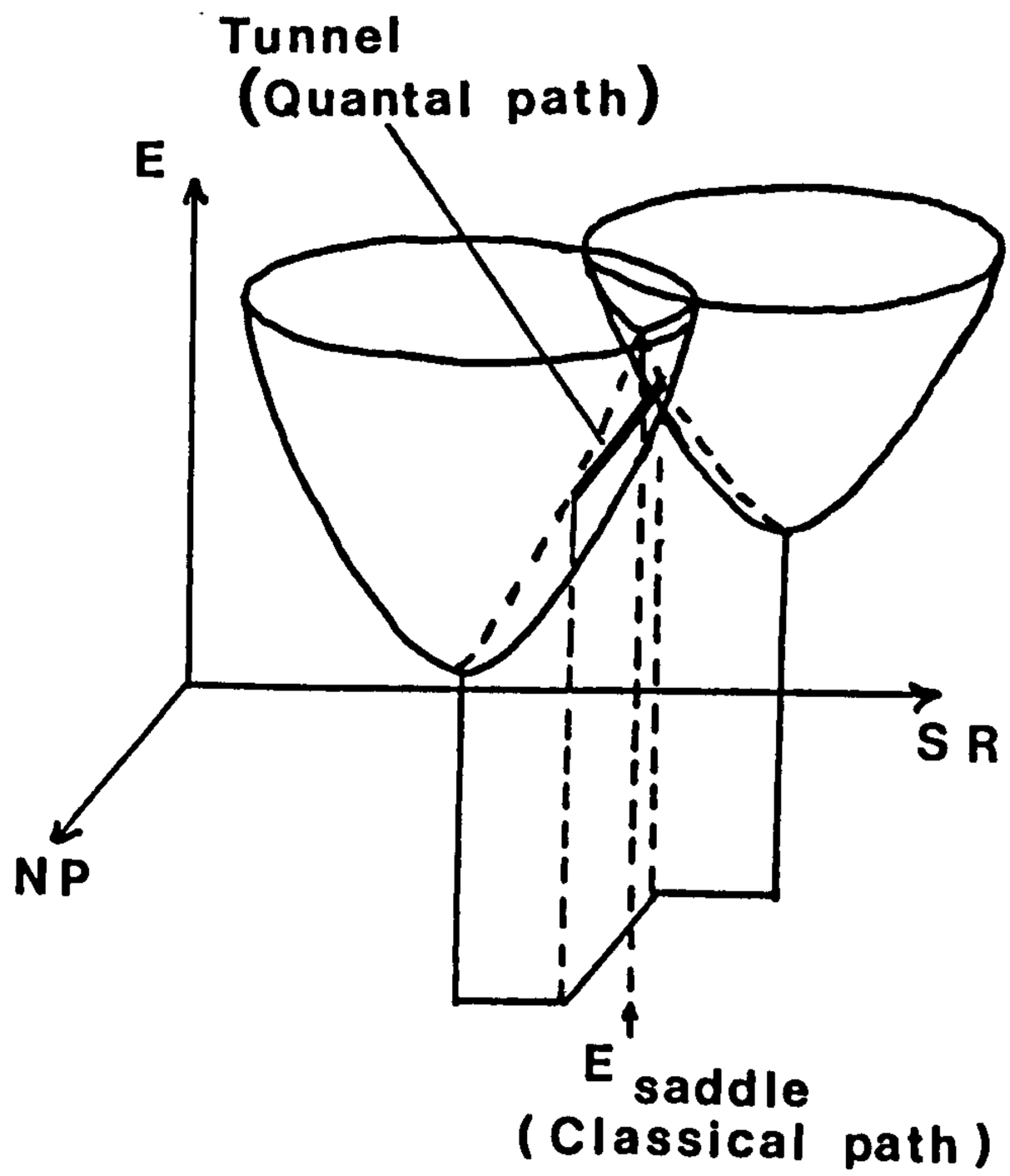

nuclei and hydration sheath may be achieved electron transfer is then dependent on further factors being favourable.

If electronic interaction occurs the degeneracy of systems at the intersection is removed and two new surfaces are formed as in Figure 2.12. The separation of the two surfaces is dependent on the magnitude of the interaction energy. The greater the interaction energy the more likely the reactants will progress to products rather than following the original zero-order curve and return without undergoing reaction. The probability factor which takes into account this effect is the transmission coefficient κ. When the transmission coefficient is unity the reaction is adiabatic, when it is less than unity the reaction is nonadiabatic.[83] Quantum mechanics show that the probability of electron transfer is proportional to the square of the interaction energy. Therefore the transmission coefficient provides a useful link between classical and quantum mechanical treatments.

The Born-Oppenheimer approximation[85] can be used to split the wavefunctions for the total system to derive Schrodinger equations for the electron and heavy nucleus.[56]

$$H\Psi = E\Psi \tag{2.112}$$

$$\Psi \simeq \psi_e\,(x_e)\;\psi_n\,(x_n) \tag{2.113}$$

giving:

$$H_e\psi_e = E_e\psi_e \quad \text{electron} \tag{2.114}$$

$$H_n\psi_n = E_\Sigma\psi_n \quad \text{nuclei} \tag{2.115}$$

where E_Σ is the total energy for the system.

A potential energy surface for the homogeneous reaction can be traced by plotting the eigen value of the fixed nuclei Hamiltonian in (2.115), given by:

$$H_n = -\tfrac{1}{2}\,\Sigma_i\,\nabla_i^2 + \sum_{i>j}\frac{1}{x_{ij}} + \sum_{K>L}\frac{Z_K Z_K}{x_{KL}} - \text{Attractive terms nucleus/electron}$$

at the nuclear configuration represented by point n, for the state ψ_n. i and j refer to electrons and K and L nuclei, Z is the charge on the nuclei. Ideally the surface of potential energy that is produced should have as many co-ordinates as there are vibration planes, plus one. However it is assumed that of all the possible pathways the one which follows the line of minimum potential energy is the most important. This allows the projection of a profile as in Figure 2.12. Since the form of the classical surface is dependent on nuclear positions and solvent reorganisation if these two factors are represented each by a co-ordinate which sums all of their possible vibrations we arrive at a three dimensional representation of the system as a Figure 2.13.

Figure 2.12 represents the 'reorganisation' restriction to electron transfer, based on the nuclear positions and total system energy. When the system reaches the intersection point or saddle then the electron interaction energy can be represented again in barrier fashion as E_e the solution for H_e in equation (2.114). Figure 2.14 shows the changes in E_e as E_Σ changes as in Figure 2.12. It can be seen that at the saddle point, E_e for reactants and products are isoenergetic it is at this point where electron transfer takes place. Although there is a W shaped profile at this point the quantum behaviour of the electron permits it to avoid climbing the barrier but rather to leak or tunnel through

Figure 2.14

Changes in electron energy with nuclear configuration for homogeneous electron transfer. Tunneling takes place when the energy of the electron in the initial and final states is equal.

Figure 2.15

Changes in electron energy as the ion orientates itself relative to the metal surface. Tunneling occurs when the electron energy on the ion equals that of the Fermi level of the metal.

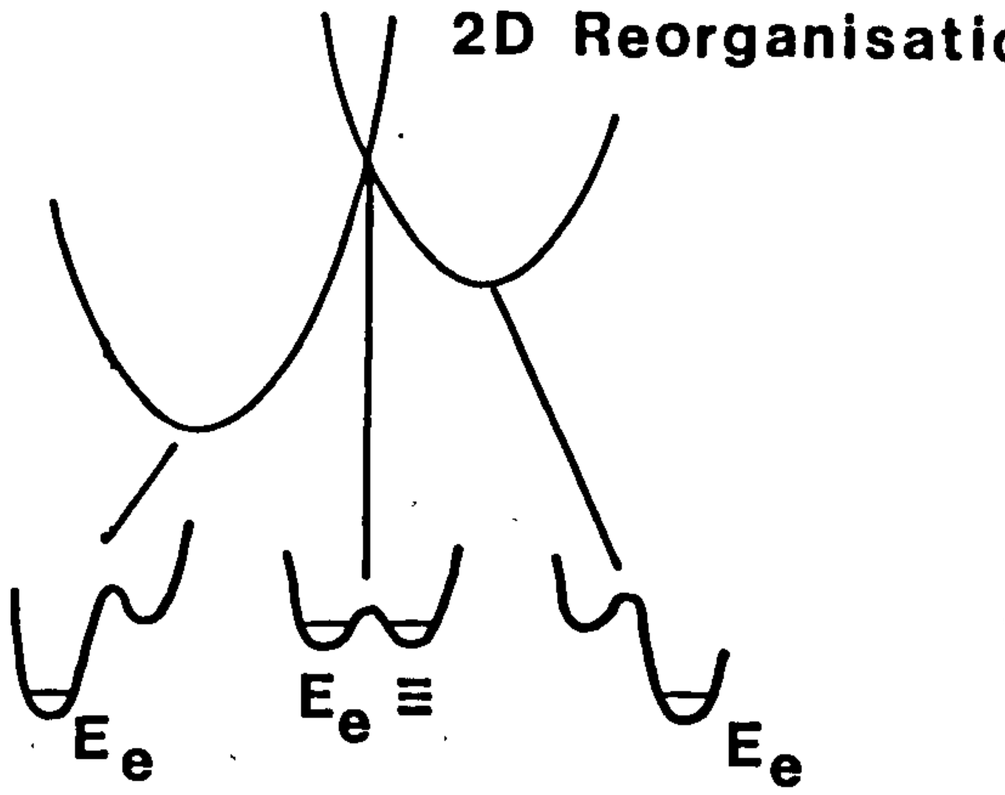
2D Reorganisation
E_e
$E_e \equiv$
E_e

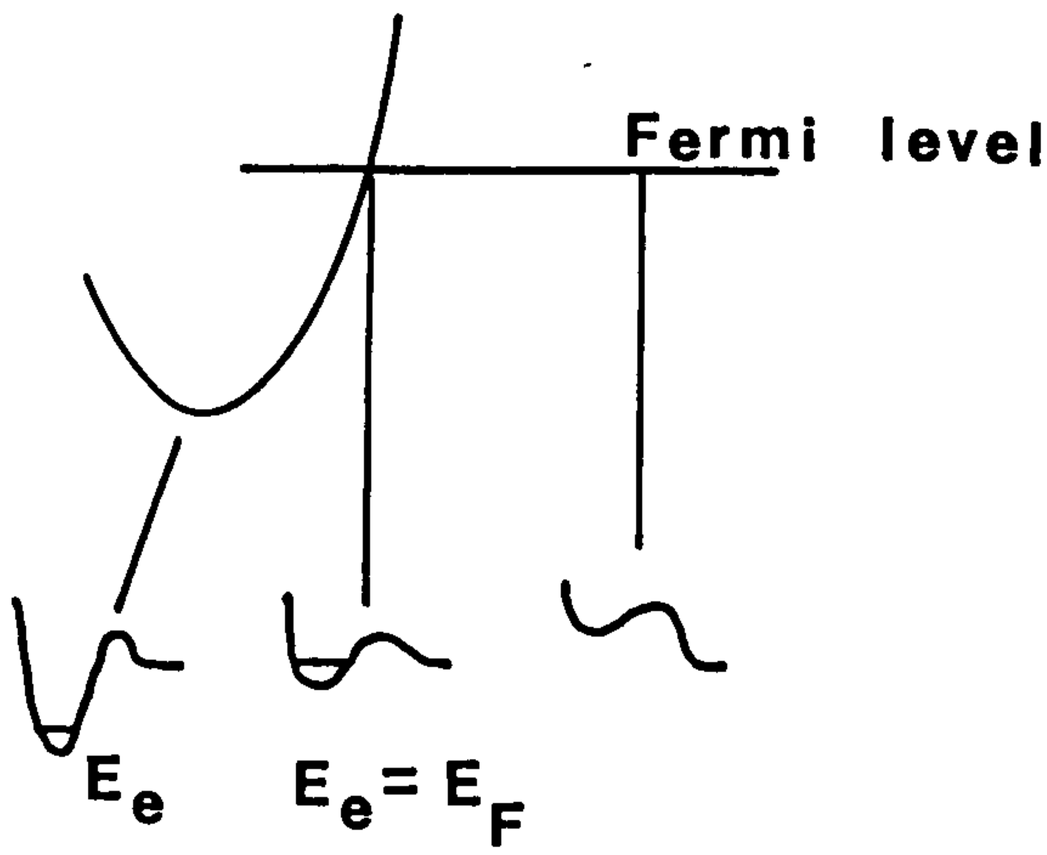
Fermi level
E_e
$E_e = E_F$

it.[91] This is because there is a finite probability, as described by the square of the wavefunction, of finding the electron on either side of the barrier. Again the electron energy on either side of the barrier must be equal.

If the features of the homogeneous system are applied to an electrode transfer it is noticed that all the reorganisation of the system can only take place in solution, as the metal is a fixed state. Electron transfer takes place when the reorganisation pushes the electron energy to the energy of the Fermi level. This is the boundary between the full and empty states of the metal and is constant. Thus Figure 2.15 shows the effect that the metal electrode has on E_e when E_Σ varies due to solvent and nuclear reorganisation. Quantum mechanical tunneling can again occur when $E_e = E_{Fermi}$.

C H A P T E R 3

THE INFLUENCE OF POROSITY ON 'LEAD ACID' ELECTROCHEMISTRY

3.1 Introduction

The electrochemistry as applicable to ideal electrode systems was presented in Chapter 2. The theory was derived mainly from work on mercury analgam electrodes or solid electrodes whose pre-treatment produced as ideal a surface as possible. Commercially useful electrodes do not present ideal surfaces for reaction. They are, usually, rough and fissured with large numbers of crystal planes in contact with the electrolyte and of surface which cannot be readily geometrically defined. In many cases electrodes are manufactured so as to intentionally produce a large surface of reactive material. These are loosely defined as porous systems, of which the negative electrode of the lead-acid battery is an example. The process of manufacture of the pasted type of electrode is outlined in Chapter 1, as is the basic electrochemistry of the $Pb/PbSO_4$ system.

The porous system convolutes the electrochemistry of the lead/sulphuric acid reaction and an interpretation of the processes which occur inside the pores is extremely difficult. Because of the large surface area[92,93] of porous lead the current density in a battery plate is low (10^{-5} - 10^{-6} A cm^{-2}) and hence the over-potential is small. However, because of restrictions to mass-transport and the formation of an insulating salt which causes ohmic effects, the current distribution becomes non-uniform.

Numerous factors affect the mass-transport and $PbSO_4$ formation some of the most important of which are, rate of discharge, amounts of active material, temperature and the previous history of the electrode; which implies anything from initial charging to hitting it with a hammer.

In order to perform a theoretical analysis of such a system, which is dependent on so many variables, it is necessary to establish a model which will account for the general features of the electrode without going into exact geometric detail. (Which would be extremely difficult with the structure shown in the S.E.M.'s of Ref. 40 .)

There are two main approaches to dealing with porous electrodes, the discrete pore model and the macrohomogeneous treatment. Both have been reviewed by a number of authors.[94-97]

3.2 The Pore model

de Levie[94] has treated the porous electrode using circuit networks applied to straight pores, perpendicular to the external face of the electrode. Figure 3.1 shows the 2D representation of the pore. This is shown as a network in Figure 3.2, only one side of the pore is considered since it is symmetrical down the length.

The change of potential with distance is equivalent to the iR drop:

$$\text{hence} \qquad \frac{dE}{dx} + iR = 0 \qquad (3.1)$$

and the change in current flowing to the pore wall with x is equal to the potential change through impedance Z

Figure 3.1

2D Representation of ideal pores.

Figure 3.2

Network of a pore as in Figure 3.1. (Only one side of the pore shown.)

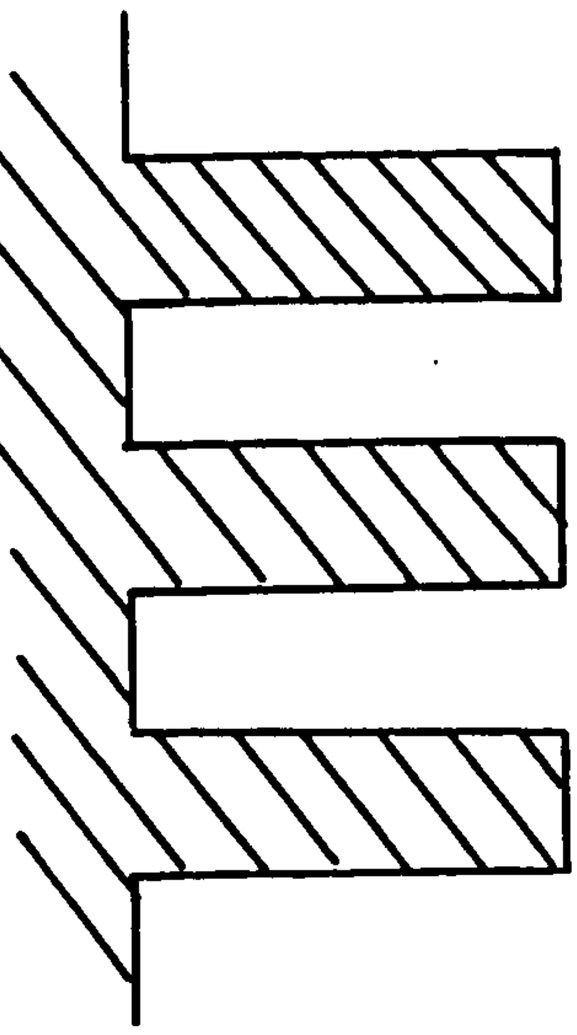

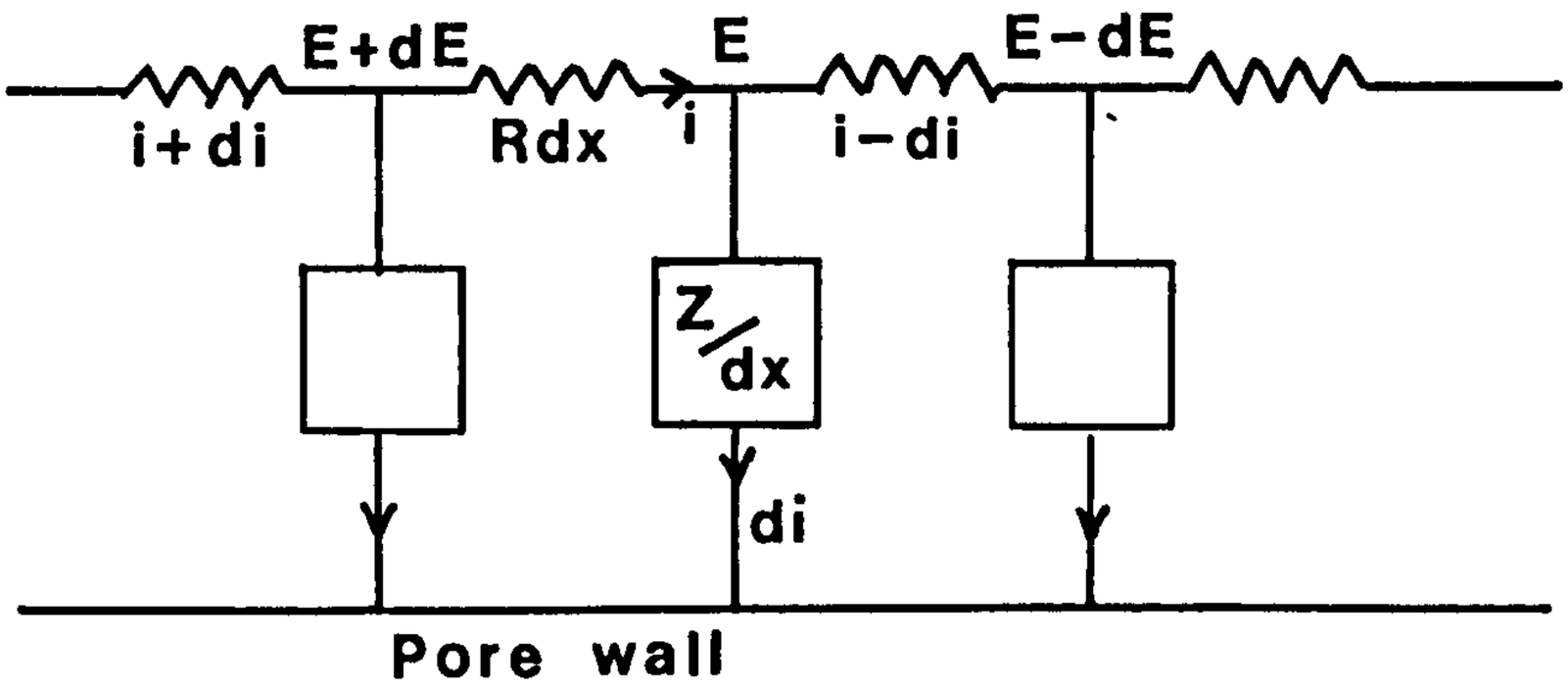
E+dE
E
E-dE
i+di
Rdx
i
i-di
Z/dx
di
Pore wall

$$\frac{di}{dx} + \frac{E}{Z} = 0 \qquad (3.2)$$

If R and Z are independent of x differentiating 3.1 and 3.2 gives

$$\frac{d^2E}{dx^2} - \frac{R.E}{Z} = 0 \qquad (3.3)$$

and

$$\frac{d^2i}{dx^2} - \frac{R.i}{Z} = 0 \qquad (3.4)$$

These latter two equations can be applied only if the electrode reaction produces no change in either electrolyte resistance throughout the pore or the impedance to current transfer at the pore wall. Therefore the porous lead electrode presents a problem since $PbSO_4$ is produced on discharge which is a very good insulator. For this type of case two further equations can be derived

$$\frac{d^2E}{dx^2} - \frac{d\ln R}{dx} \cdot \frac{dE}{dx} - \frac{R.E}{Z} = 0 \qquad (3.5)$$

and

$$\frac{d^2i}{dx^2} - \frac{d\ln Z}{dx} \cdot \frac{di}{dx} - \frac{R.i}{Z} = 0 \qquad (3.6)$$

Taking the simplest case using equations (3.1-3.4) the potential drop down the pore to a distance x into the pore from the surface (x=o) is given by

$$E_x = E_{x=o} \cosh (\rho x - \rho l)/\cosh \rho l \qquad (3.7)$$

where l is the pore length and ρ has the form

$$\rho = (R/Z)^{\frac{1}{2}} \qquad (3.8)$$

where R is the electrolyte resistance within the pore and Z the charge transfer impedance. The penetration depth is defined as being ρ^{-1} which has the dimensions of length.

The current at the mouth of the pore is given by

$$i_{x=o} = -R^{-1} \left(\frac{dE}{dx}\right)_{x=o} = \frac{\rho . E_{x=o} \tanh \rho L}{R} \qquad (3.9)$$

the pore resistance can be represented by

$$\frac{\text{Potential at } x=o}{\text{Current at } x=o} = \frac{E_{x=o}}{i_{x=o}} = (RZ)^{\frac{1}{2}} \operatorname{cotanh} \rho . L \qquad (3.10)$$

hence the current is inversely proportional to $(RZ)^{\frac{1}{2}}$. In contrast the current at a flat electrode is inversely proportional to Z.

Thus de Levie makes it clear that the electrochemistry, as represented by the charge transfer impedance Z, and the solution resistance R are inextricably bound together. Austin[98] has taken this work one stage further in that the electrode may also be diffusion as well as resistance controlled. This can be estimated by the magnitude of a dimensionless constant given by

$$\Omega = rD_n FC_{x=o} \cdot \alpha \frac{n.F}{RT} \qquad (3.11)$$

where r is the resitivity, D the diffusion coefficient and $C_{x=o}$ the electrolyte concentration at the surface. Electrode processes are resistance-controlled for $\Omega > 5$ and diffusion controlled for $\Omega < 0.5$. Bode[7] has calculated a value for a charged lead acid battery assuming $\alpha = 0.5$, r = 1.2 ohm.cm, $D \simeq 1.5 \times 10^{-9}$ m^2 s^{-1} and $C_{x=o}$ = 5M. Ω was found to be 0.7 indicating that reactions in porous lead are strongly affected by acid diffusion, in agreement with Burbank et al.[99]

Unlike a planar electrode where kinetics are described by equation (2.26), the porous electrode only follows the expected current potential relationship at polarizations of a few millivolts. When the overpotential is increased the Tafel slope for a cylindrical pore is twice that of the planar electrode. de Levie shows, through the treatment of Daniel-Bek[100] and an extension of the work of Austin and Lerner,[101] that similar Tafel slopes for either diffusion-limited or charge transfer limited operation of porous electrodes are obtained theoretically i.e. twice those of planar.

Another concept arising from pore modeling is the penetration depth (equation 3.8) $1/\rho$, which defines the distance to which a reaction can penetrate a porous electrode. This depth however varies with the mechanism of current control. The optimum thickness for the electrode is defined by $1/\rho$ since electrodes which are thicker than the penetration depth have excess material for reaction, whilst electrodes thinner than $1/\rho$ behave as planar electrodes of large surface.

Because of the complexity of industrially produced porous electrodes[102] the derivations from non-steady state systems must be treated with a degree of caution. However to produce any model at all the simplified approach[103] must be taken in order to reduce the mathematics to a tolerable level.

3.3 The Macrohomogeneous Model

This macroscopic treatment disregards the geometric detail of the porous system and bases its derivation on average quantities. An introduction to average quantities and their use in equating for representation of porous systems of multiple variables is

presented by Newman et al.[104,105] Averaging is throughout a volume element within the electrode. Porosity is represented by the volume fraction of electrolyte within the total element. The element also has volume fractions for the different solid phases which may be present. Two potentials are defined ϕ_1 and ϕ_2, for the solid matrix and pore electrolyte respectively, associated with which are two current densities i_1 and i_2. These current densities refer to the geometric electrode area. The flux N_j and concentration C_j of species j are referenced to the geometric area and the volume element respectively.

Within the matrix Ohm's Law gives

$$i_1 = -\sigma \nabla \phi_1 \tag{3.12}$$

where σ is the conductivity of the matrix.

The flux of species j is given by

$$J_j = -D_j \nabla C_j - n_j F u_j C_j \nabla \phi_2 + C_j v \tag{3.13}$$

which yields a current density in the pores of

$$i_2 = F \Sigma_j n_j J_j \tag{3.14}$$

If the electrode reaction is represented by

$$\Sigma_j s_j M_j \rightarrow ne^- \tag{3.15}$$

(i.e. s atoms of M yields n electrons on oxidation; hence s is the stoichiometry coefficient.)

The mass balance is given by

$$\frac{\partial C_j}{\partial t} = -\nabla . J_j + \frac{s_j}{nF} \nabla i_1 \tag{3.16}$$

The electrode kinetics can be represented by an equation of the Butler-Volmer type

$$\nabla i_1 = i_o \left\{ \exp \left(-\frac{\alpha n F}{RT} (\phi_1 - \phi_2) \right) - \exp \left(\frac{(1-\alpha) n F}{RT} (\phi_1 - \phi_2) \right) \right\} \quad (3.17)$$

Equations (3.12 - 3.17) along with the condition of electroneutrality

$$\Sigma_j \, n_j \, C_j = 0 \quad (3.18)$$

and hence the conservation of charge

$$\nabla . i_1 + \nabla \, i_2 = 0 \quad (3.19)$$

are sufficient to describe the porous electrode system. They can be applied in various forms to a one-dimensional system (i.e. the variables of the system are dependent only on depth and not lateral position) to yield models for specific electrodes under varying conditions. Further adaptations of the theory have allowed its extension to models of electrodes which are structurally transformed during operation.[106-109]

3.4 Applications to the lead-acid cell

Specific applications of the macrohomogeneous model have been made by Micka and Rousar who derived partial differential equations to describe the transport of mass and charge through the porous lead electrode.[110] They have also derived equations for the positive plate[111] and extended the system to the lead-acid cell as a whole.[112] These analyses indicate that the capacity of a conventional lead-acid battery is always limited by the positive

plate, PbO_2. They therefore recommended a reduction in the amount of lead in the negative plate, to increase overall energy density, and suggested that this could be achieved by increasing lead porosity. However Micka and Rousar neglected electrolyte concentration gradients between the plates and assumed mixing by convection. Mixing is unlikely; due to separator interference. Turner[113] investigated further and considered inter-plate concentration gradients. He showed that mass-transport determined cell capacity at high discharge rates and suggested moderate improvements could be achieved by, optimal matching of plate porosities and areas and increasing the acid concentration.

Simonsson has studied in detail the discharge behaviour of the positive plate. This treatment is applicable to porous lead, after adjustment of specific parameters, and shows how fruitful the macrohomogeneous model can be. Initially[114] the current distribution within the porous electrode was calculated from the relationship between current density and electrode potential as a function of the electrolyte concentration. The structure changes due to $PbSO_4$ formation were considered to affect the reaction[115] i.e. laying down of an insulating film and pore plugging. Computational methods were employed to solve numerically the pseudo-steady state equations, showing that at high current densities the discharge capacity is limited by both structural and mass-transport effects. Low rate discharge was also considered.[116] It was found that the current distribution at low rates becomes non-uniform because of changes in electrode porosity and electrolyte concentration. It was suggested that the degree of discharge was dependent on the initial porosity (Percentage voids).

Simonsson has summarised his own work[117] and presented experimental investigations of PbO_2 discharge behaviour.

Porous lead electrodes in sulphuric acid have been recently received, in some detail, by Hampson and Lakeman.[118]

CHAPTER 4

ELECTROCHEMICAL INVESTIGATION BY DIGITAL METHODS

4.1 Introduction

Despite the essentially analogue nature of electrochemical instrumentation, computers (and microprocessors) must become the most effective means of data acquisition and analysis.[119] It seems probable that, in the near future, digital electrochemical instrumentation will be manufactured to allow compatability with data processing equipment. It was with this in mind that a project to develop a microprocessor based control and data acquisition system was undertaken in parallel with the investigations into lead acid negative active material.

The basic microcomputer, which was acquired in mid-1980, was a prototype for a new series of microcomputer which were to be built specifically for laboratory or shop floor work. The supplier was a small electronic instrumentation firm, Kemitron Ltd., who had been purpose building electrochemical instrumentation for the electrochemistry laboratory at Loughborough for a number of years. The prototype was developed and modified over a period of eighteen months, whilst work on interfacing to electrochemical systems was in progress. Ultimately the machine became equivalent to what is marketed today.[120]

4.2 Selective Review

The very extensive literature on digital techniques in chemistry is almost exclusively confined to the analytical

journals and predominantly concerns specific developments and applications. Perone and Jones[121] and Dessy et al[122] have reviewed the field up to the early 1970's. Betteridge and Goad[123] have presented a short history and account of the developments to 1980.

Breiter,[124] in the mid-1960's, was possibly the first to analyse an electrochemical system direct, gathering voltammetric data via an analogue to digital (A to D) interface. This data, however, had to pass through a sequence of preparative stages before it could be put into the computer. The A to D converter supplied a punched paper tape output which was then transferred to magnetic tape to facilitate reading by the G.E. 225 computer. Hence,the operator was necessary as an intermediary in the proceedings and the system could not be termed 'on-line'. With an on-line system (experiment to computer, signal link) the computer can perform a control function as well as a passive data logging role. The computer can record the results of a predetermined sequence of events or operate in a 'feed-back' mode taking account of the response of the experimental system and act upon this response. Osteryoung in reference 119 presents an introduction to on-line computers in electrochemistry.

A great deal of the early work was before the advent of microprocessors and was based on mini-computers. Harrison[125,126] has developed a fully integrated system of experimentation and first-stage data processing using a DEC PDP-8 mini-computer, with subsequent transfer of data to a mainframe computer for further mathematical analysis. His work is summarised in a series of papers, entitled 'Automation of electrode kinetic

measurement', the references to which will be found in reference 126.

The rapid progress of digital technology has brought the microprocessor to the fore and has opened up a relatively low cost approach to digital techniques for control and data handling in the laboratory. Although it is somewhat limited in throughput and number crunching ability, as opposed to large computers, the microprocessor is more than adequate for many applications of instrumental control. Cohen and Heinmann[127] have described a microprocessor based unit for the control of a standard laboratory potentiostat. The unit was capable of reading data at predetermined times and carrying out some preliminary manipulation.

Brown[128] has given a detailed description of the hardware interfacing and software used to adapt the Apple II+ microcomputer into a powerful experimental machine. Gray and Workman[129] have followed a similar approach to Brown in adapting a readily available microcomputer, the TRS 80 to perform the task of experimental control for voltammetry and coulometry. Hampson and Willars[130] have used a potential-scanning potentiostat to record polarization curves automatically. When used in conjunction with the Solartron 1170 frequency response analyser,electrode impedance could be measured automatically. The potentiostat could also generate perturbing waveforms but could not record or store digitally; presenting only a paper tape print-out. The approach of Hampson and Willars has been extended considerably in the work presented here. A microcomputer based system for general electrochemical applications has been developed capable of executing a range of relaxation experiments. The data is

collected and held digitally and the observed behaviour treated mathematically and may be tested against kinetic models. The results can be tabulated or presented graphically.

4.3 Microcomputer Architecture and Function

Whatever type of arrangement of microcomputer is used for laboratory work it always has a number of fixed parameters specific to that particular machine. These parameters are dependent on the individual components from which the machine is manufactured and define its suitability for bench-top use.

How robust the microcomputer needs to be depends entirely upon the job it is required to do. In the electrochemistry laboratory however, the main cause for concern is most likely to be the atmosphere. Since most commercially available micro-computers have a forced ventilation system the interaction of atmospheric undesirables with contacts, components and data storage material etc. is unavoidable. There appears to be no machine specifically designed to combat this, therefore choice is immaterial in this respect. The original microcomputer in our laboratory is three years old; and has not suffered from air-borne corrosion or spoiling to our knowledge.

The main function of the bench-top machine is to control and monitor the progress of electrochemical experiments, the more clerical tasks such as hard copy tabulation and graphical representation is left to another device. The microcomputer cannot be considered as a whole but must be broken down into blocks of components each with its specific task.[131] The central processing unit (CPU) is usually a single integrated

circuit requiring a minimum of external circuitry to function. It organises the sequence and type of operation that is to occur for any given instruction from the controlling software. The speed at which it does this is governed by an external clock derived from a quartz oscillator. The CPU's power is usually crudely categorised as a function of its data path width or the number of binary digits which are transferred and operated on in parallel within the processor. Eight-bit CPUs, as are contained on many microprocessor integrated circuits, are more than adequate for use in bench-top machines. Our laboratory machines contain the Z80A[132] eight-bit CPU running at 4MHz with a typical instruction cycle time of 1.5 μ s.

Since most eight-bit CPUs run at clock frequencies between 1 and 5MHz speed is not a major consideration. However a thorough examination of the CPU's instruction set[131] may well reveal information pertinent to the suitability of the micro-computer as a whole for bench-top work.

The main pieces of the instruction set which are important are those commands dealing with the input and output of data between the processor and the outside world and also the processor's ability to handle interupt sequences which are hard-wired to the microcomputer from external devices. The Z80A is excellent in the former mode since it can input and output data through any of 255 ports (eight-bit data paths) in block format on a single instruction. In the latter the Z80A can be set up under software control to respond in any of three modes to any number of nested interupts, servicing them in a pre-determined order or priority.

Most CPUs require a small amount of external (again on integrated circuit) read/write or random access memory (RAM) to perform a useful but inflexible function.[133] This RAM is expanded in many cases to a size capable of holding a large control program with enough residual memory for storage and handling of thousands of data elements. The maximum size to which the memory is expandable and the ease with which it can be expanded is again determined by the CPU. Nearly all eight-bit CPUs have the ability to address, or access 64 thousand (actually $65,536 \equiv 2^{16}$) memory locations of a size equivalent to their data path width i.e. eight-bits. However it is not always the case that a standard machine is supplied with the maximum amount of addressable memory more may have to be added at a later date or this may not be possible at all. Memory capacities of 32K and 48K are suitable for many applications, however if the control software is particularly long and a large amount of data storage is required in a short space of time 64K may prove to be necessary. The amounts of memory available to the user as a fraction of the actual memory is also dependent on the operating system of the machine, this again is determined by the CPU and is discussed later.

Although the CPU and RAM alone is a functional system it cannot be termed a microcomputer without associated input/output modules for communication with an operator. These are provided in the form of integrated circuits which have the ability to convert the internal data of the CPU and RAM from its binary parallel arrangement into a train of pulses which are serially transmitted to a decoding video device providing a readable display. Similarly the individual keystrokes as received from

a teletype or keyboard device are assembled into parallel data for internal manipulation.

Storage of data and software is achieved by use of either magnetic cassette tape or more usually and reliably on magnetic 'floppy' disc. The floppy disc system has the distinct advantages of, carrying capacity, in some cases up to 1 Mega byte, and speed of read/write access, typically 30 μ s per byte. Floppy disc units are usually provided in pairs for ease of transfer of information from one disc to another. Our laboratory machines alow us to save up to 256K bytes per disc. For storage of huge amounts of data at a single access point 'hard' disc units are available. These enable tens of mega bytes to be held for immediate access by the CPU, the major factor which far outweighs the convenience gained by their use with a bench-top unit is the cost, which can easily double the price of a standard twin floppy disc microcomputer.

Each microcomputer has a means of directing the activities of the individual components described previously and managing the software files produced either for experimental control or by data acquisition. This ability is provided by a complex program which is either stored within the machine on non-volatile (memory retained without electrical power) read only memory or is collected, as soon as the machine is switched on, from floppy disc storage. Some of the machines which are currently available as accounting or hobbyist computers have this operating system contained as part of the memory map. The operating system in this case includes a single programming language, usually BASIC, which is entered immediately on start-up. This compulsory BASIC interpreter is always present and consumes a large portion of the addressable memory available to the CPU. Other more

flexible systems collect the operating system from disc under the direction of a very small read only memory component. The advantage of a disc based system is immediately apparent in that any programming language can be adopted provided that the software is available. Our laboratory machines all run the tried and tested CP/M[134,135] disc operating system which supports a vast suite of interpretive or compiler based languages (e.g. BASIC, FORTRAN, PASCAL and assembler/machine code facilities).

4.4 Analogue Interfacing

The digital to analogue converter (D to A) converts a digital code to an analogue potential that is proportional to the number which is represented by the code. There are three specifications of the D to A which are of particular interest to an electrochemist, these are resolution, accuracy and settling time (roughly equivalent to circuit risetime in a purely analogue device).

Resolution is specified by the number of possible output voltage levels and is usually defined as the number of bits of binary information that the converter will handle. For example an 8-bit device has a resolution of 2^8-1 distinguishable output voltage levels. Accuracy is the deviation of the analogue output from that represented by the digital pattern. It is usually expressed as a fraction of least significant bit (LSB). Typically this is ±½LSB, meaning that for an eight-bit converter the error will never exceed

$$V_{max}/(2^8-1) \times 2$$

where V_{max} is the full scale of the analogue output ($V_{max}/(2^8-1)$ ≡ 1 LSB). Settling time becomes increasingly important when a theoretically instantaneous change in voltage level is required for perturbation of the electrochemical system, as in potential step relaxation experiments. When the response time of the electrochemical system to a potential step is quite fast then the delay in attaining the final potential can cause serious abberations in the current response. Settling times usually are dependent on the resolution of the D - A integrated circuit used. With eight-bit resolution settling time is usually between 800 n s and 1.25 μ s, 12-bit is considerably slower between 2 and 2.5 μ s.

Analogue to digital conversion is undertaken by an integrated circuit which accepts an analogue signal and produces a corresponding digital code. The binary value of the code represents the magnitude of the analogue input at the time of conversion. There are two primary sources of error pertinent to electrochemical measurement, quantization and conversion error. A quantization error exists in any system that converts a continuous analogue signal into a discrete digital representation. An A to D has only a fixed number of ditial levels to represent a contiuum of input signals. For example if the converter is eight-bit resolution then it has 2^8-1 ≡ 255 levels to represent an analogue value between 0 and V_{max} (maximum voltage input) and 'rounding' errors must occur in this case. The quantization can be reduced, but never eliminated, by increasing the number of bits the converter can handle e.g. 12 or 16-bit. Conversion error is a timing problem due to the delay encountered on generating the digital code. In the time

elapsed between reading the analogue input and producing digital output the input signal may have changed to a slightly different value than that reflected by the output code. Typical conversion times are 10 μ s for an eight-bit device and 25 μ s for a 12-bit device. To avoid recording misleading data the highest frequency component of the analogue input should be considerably larger than the conversion time.

4.5 Chronological Development

The microcomputer systems (5 machines) that are in use in the laboratory at present (performing different tasks) are all based on the design developed from the machine purchased in mid-1980. Structural modifications were made to the original microcomputer, with all subsequent machines constructed the same, to alow easy access to the internal communications bus and logic facilities. The final design of microcomputer which was ultimately adopted by the manufacturer is shown in Figure 4.1, the technical specification is presented in Table 4.1. Analogue interfaces were designed and developed by Kemitron Ltd. to specifications which were established as the project progressed.

It was the application of the analogue interfaces and development of suitable controlling software for the same, which was the main consumer of time. This proved conclusively that the total expenditure is by no means contained in the initial outlay for hardware, but large capital costs are hidden in man-hours of development.

Figure 4.1

Schematic diagram of Kemitron K3000 typically fitted for laboratory use.

OSC - Crystal oscillator

ROM - Non volatile, Read Only Memory

RAM - Read/Write, Random Access Memory

MC - Memory Control

ALU - Arithmetic and Logic Unit

DAC - Digital to Analogue Converter

ADC - Analogue to Digital Converter

PPI - Programmable Peripheral Interface

TD - Transient Digitizer

VDU - Visual Display Unit

Front view, showing disc drives, serial communications links, memory and CPU boards; which are exposed for easy access.

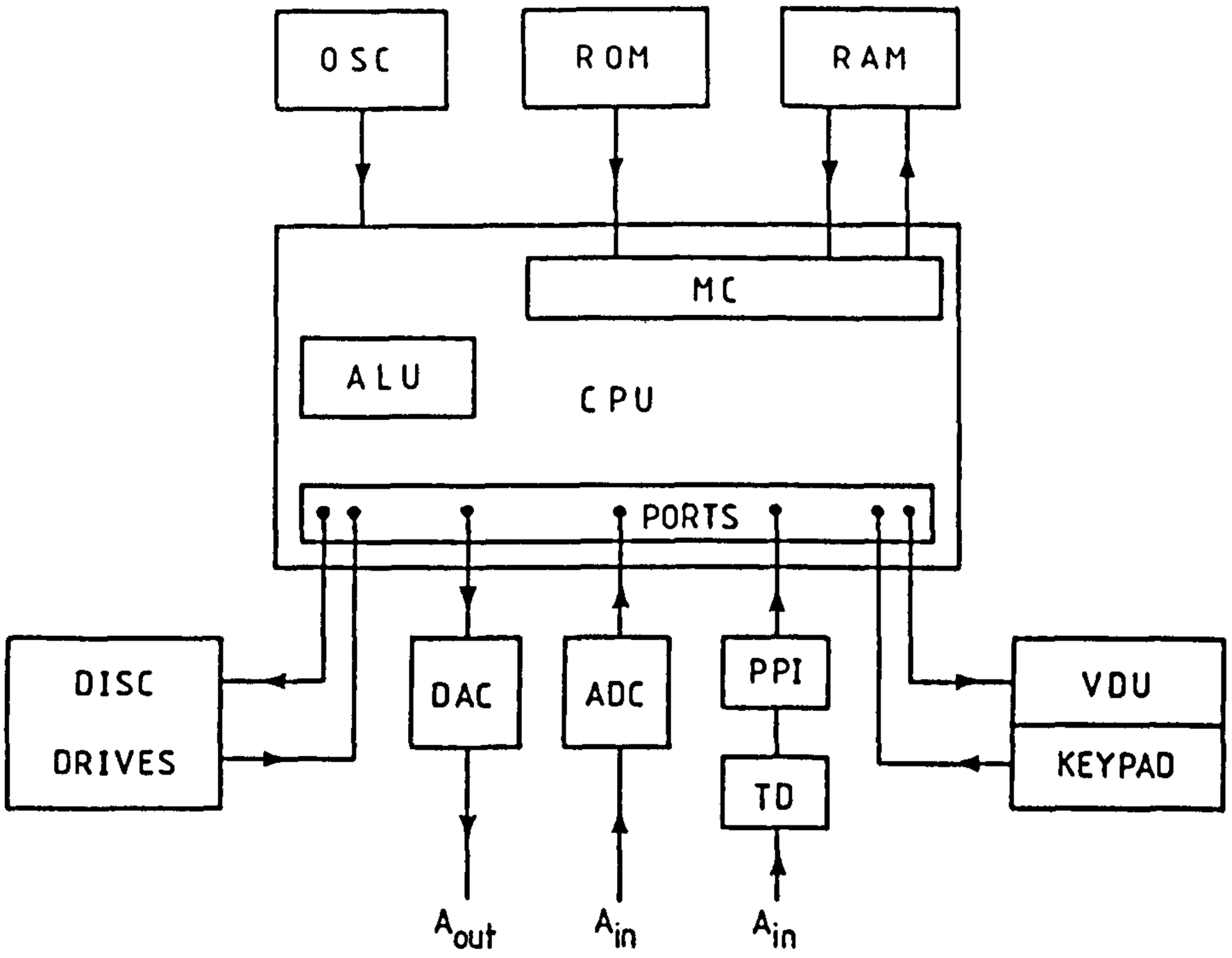
OSC
ROM
RAM
MC
ALU
CPU
PORTS
DISC
DRIVES
DAC
ADC
PPI
TD
VDU
KEYPAD
A_{out}
A_{in}
A_{in}

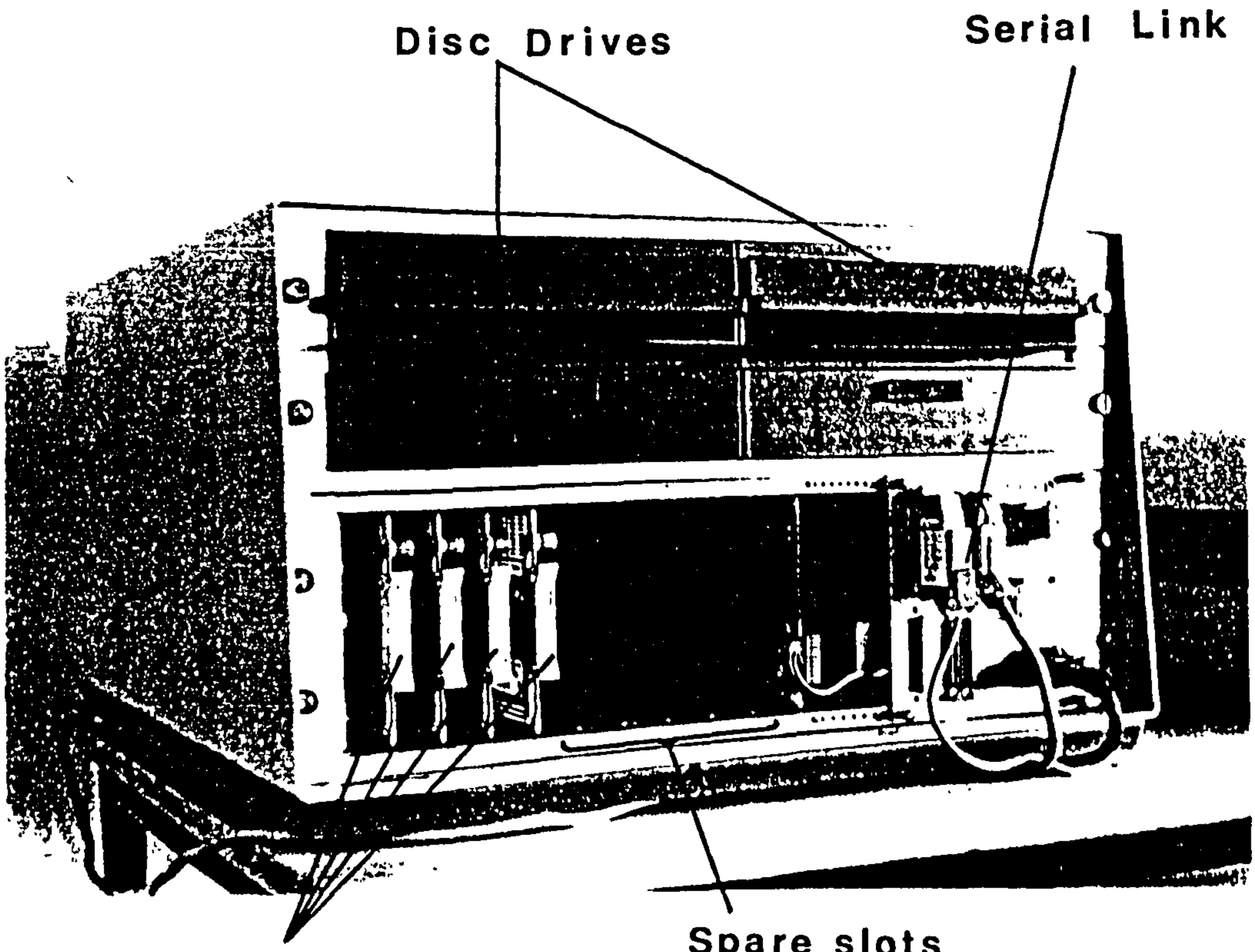
Disc Drives
Serial Link
RAM & CPU
Spare slots

TABLE 4.1

TECHNICAL SPECIFICATION

PROCESSOR

- Z80A 4 Megahertz

MEMORY

- 64K Dynamic RAM
- 150 nSec Access time
- No wait states
- 2K boot strap EPROM

PORTS

- Two programmable RS232 ports
- 15 Baud rates from 50 to 19200
- Single centronics port (P10)

Options

- Unlimited additional serial or parallel ports

DISK STORAGE

- Dual 8" double sided double density
- 1 Megabyte per disk
- S/W selectable single density mode
- IBM 3740 -FM and IBM system 34 MFM
- Soft sectored diskettes

DISK CONTROLLER

- Controls up to 4 drives
- Double or single sided/density

INPUT/OUTPUT

- Dual parallel port (P10)
- Fully programmable Input or Output
- Interrupt driven if required

Options

- Full range of Input/Output modules
- Digital - from 8 isolated outputs to 24 isolated inputs
- Analogue - from twin 12-bit A/D and D/A to 24 channel 12-bit A/D
- Programmable Input/Output ports

COUNTER/CLOCK

- Four channel counter/timer (CTC)
- Fully programmable
- Up/down count, Zero count timeout
- Interrup structure
- Used as counter, time or clock

BUS STRUCTURE

- 43 Way direct edge connector
- Full termination and de-coupling
- 12 slot mother board
- Slot independent boards

SYSTEMS SOFTWARE

- CPM 2.2 Operating system
- System boot routine

GENERAL SOFTWARE

Options

- Full range of CPM software
- BASIC, FORTRAN, Z80 Assembler, Process Control BASIC Etc.

POWER

- 240 V,50 Hertz
- Suppressed on input

PHYSICAL SIZE

- Overall
- Width - 49.53 cm
- Height - 30.48 cm
- Depth - 40.64 cm

Although a digital potentiostat is feasible in design and has been constructed elsewhere,[136] a simple analogue device will perform the task more accurately and cheaply. Since analogue potentiostats were readily available, and indispensable for the type of experiments we wished to perform, the process of interfacing the microcomputer as both a perturbing source and recording device was undertaken.

The original interfacing was to a simple operational amplifier design potentiostat as shown in Figure 4.2. A reference voltage is derived from a stabilised supply through a series of pre-set resistances [S1] this is split by the potential divider [D] and fed through a unity gain buffer [Op-amp 6]. External reference potentials can be added at this point [E & F] through another buffer [Op-amp 7]. By means of a switch [S2] the feed back to operational amplifier 8 can be altered for potentiostatic or galvanostatic control. Under potentiostatic control the potential from the reference electrode is followed by a high input impedance F.E.T. input buffer which draws, theoretically, zero current [Op-amp 4]. The potential from this buffer provides the feed back to the monitoring amplifier [Op-amp 8] which by means of a current booster [9] drives current through the counter electrode to the cell. The working electrode is earthed. Operational amplifiers 1 and 2 monitor the current flow through the cell as a voltage drop across the variable resistance R_S. Thus E as a function of i is presented at the output of op-amp 2 [J] the inverse is provided by op-amp 3 [I]. Communication between the microcomputer and potentiostat, and ultimately the cell, is via the inputs at E and F and the output at J .

Figure 4.2

Circuit of potentiostat which was subsequently interfaced to the microcomputer.

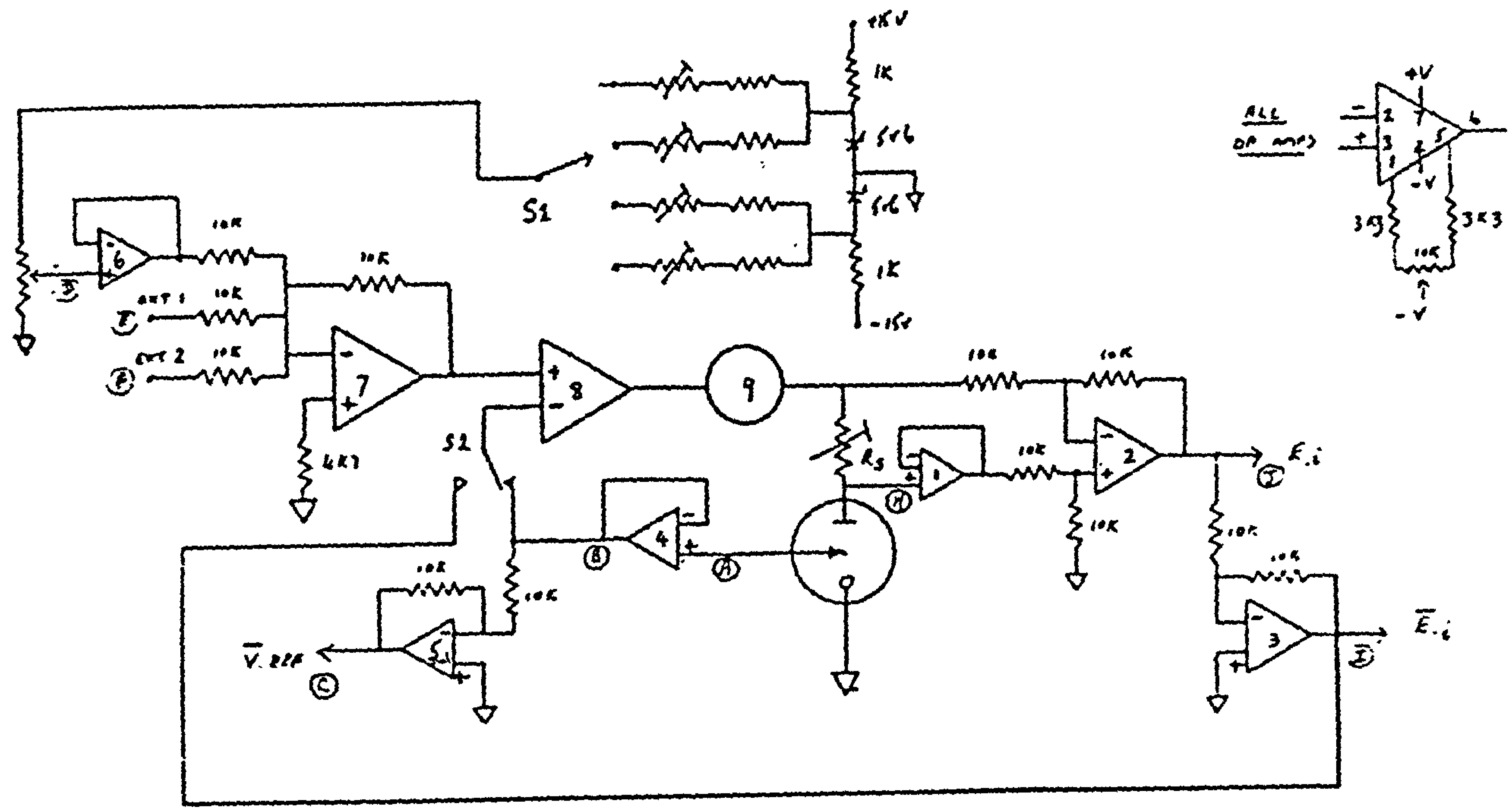
ALL OP AMPS
+V
-V
3K3
10K
S1
S2
1K
10K
4K7
EXT 1
EXT 2
R_S
E.i
V. REF

The perturbing signal from the microcomputer was originally provided by the use of an eight-bit resolution (1 in 255) ZN428[137] integrated circuit with a full scale output span of 2.55 V. The interfacing circuitry is given in Figure 4.3. The output potential was restricted to increments of 10 mV because of integrated circuit resolution. Therefore the microcomputer could be used to provide potential steps between ±10 and ±2550 mV in 10 mV to a good degree of accuracy. If, however, the microcomputer was required to generate a rising and falling potential ramp for use in linear sweep voltammetry a voltage staircase effect was produced. The outgoing signal was far from a pure analogue ramp, due to the significant potential jump at each bit change. The effect of the potential staircase on the current response of various cells was investigated. It was found that at slow sweep rates or with systems with fast response times the effect was quite pronounced, revealing itself as a train of current relaxation transients superimposed on the main current profile. Other than providing substantial smoothing circuitry, which detracts from the accuracy of the technique, the only way to reduce staircase effects was found to be by use of a converter I.C. of higher resolution. The next stage was to adopt a twelve-bit digital to analogue converter. The increase in resolution for a similar full scale output (2.048 V) was to 1 in 4096 providing an increment of 0.5 mV. The current 'jitter' was still discernable with the smaller potential increments (Figure 4.4) but markedly improved. A further increase in resolution was achieved by compressing the output signal, by means of an electronic attenuator, from the 2.048 V maximum to the required sweep range.

Figure 4.3

8-bit digital to analogue circuit employing the ZN428 I.C.

Figure 4.5

8-bit analogue to digital circuit employing the ZN427E I.C.

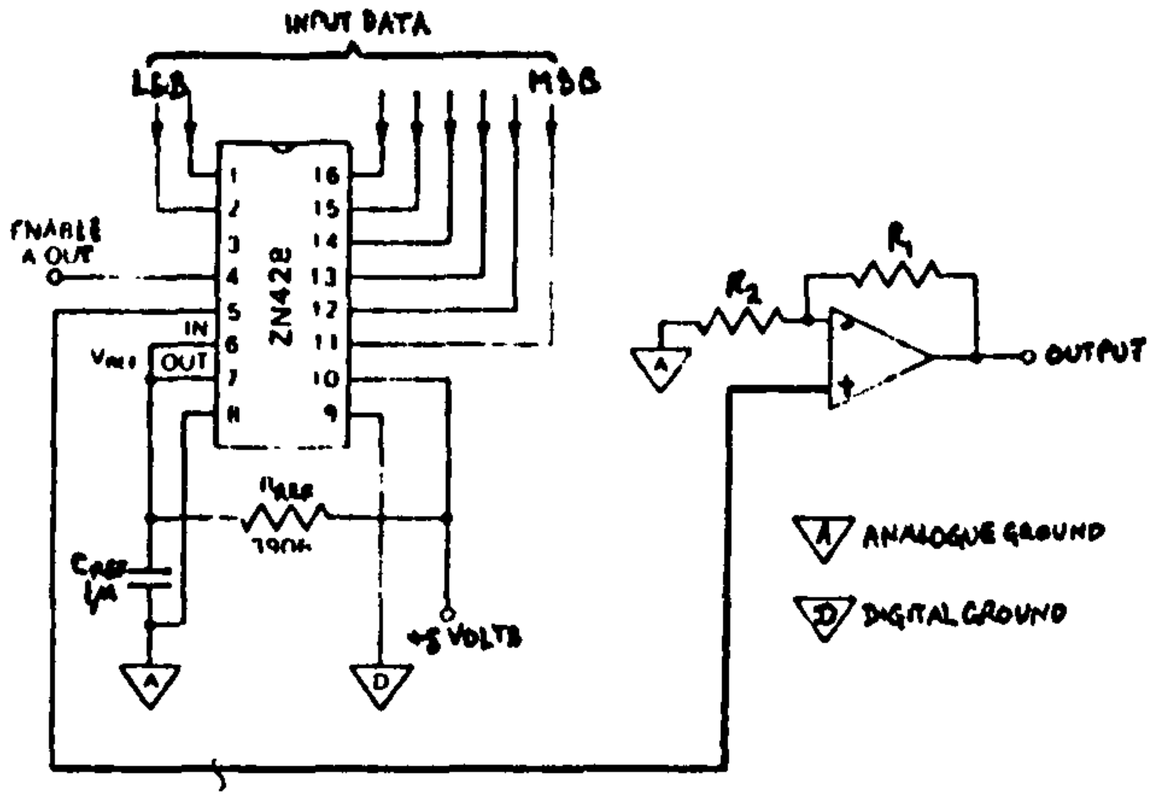

Unipolar operation - Basic Circuit

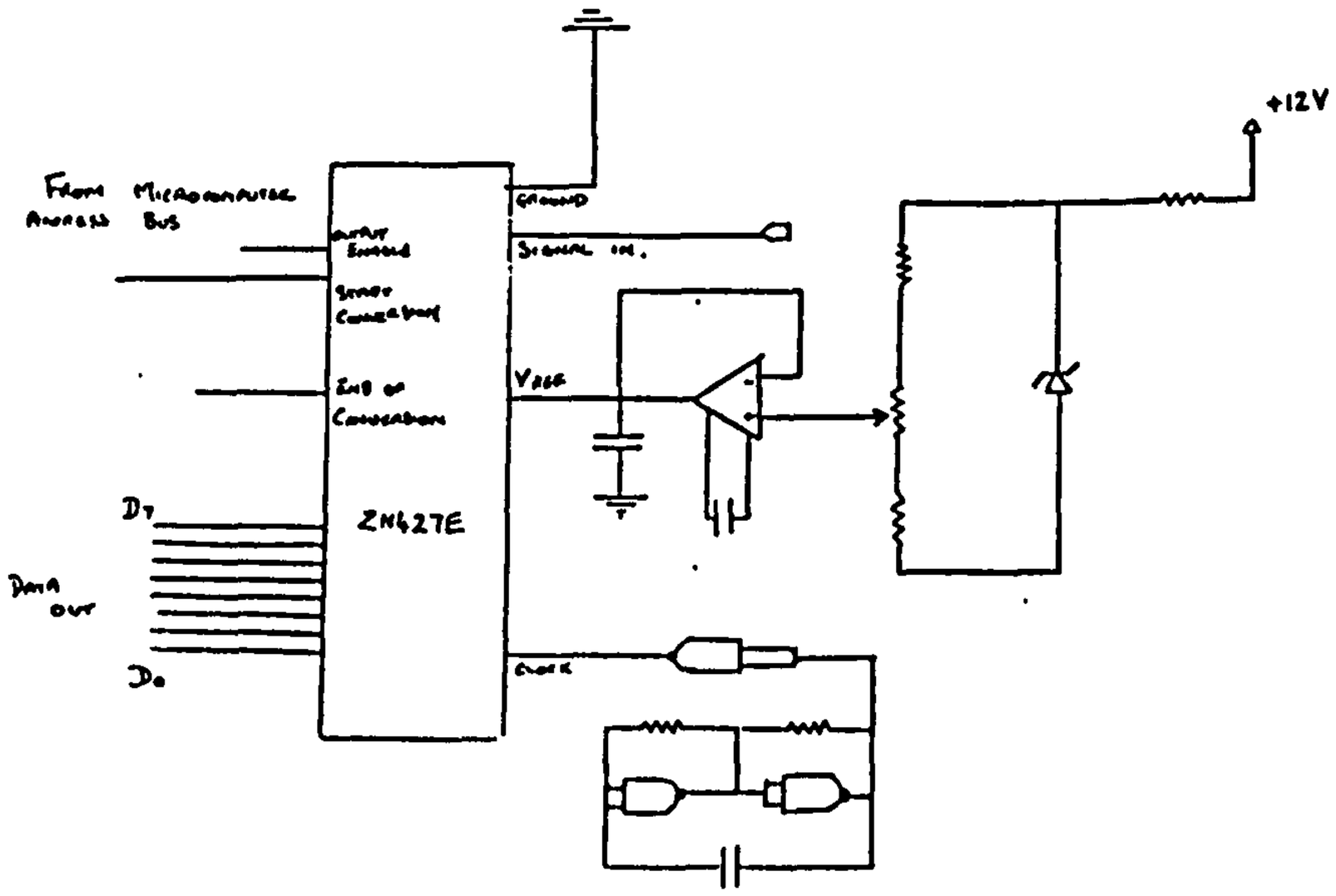

Figure 4.4

The response of a zinc electrode to 8- and 12-bit digital to analogue sweeping potentials.

NOTE Electrodes are modified to avoid superimposition of the current responses.

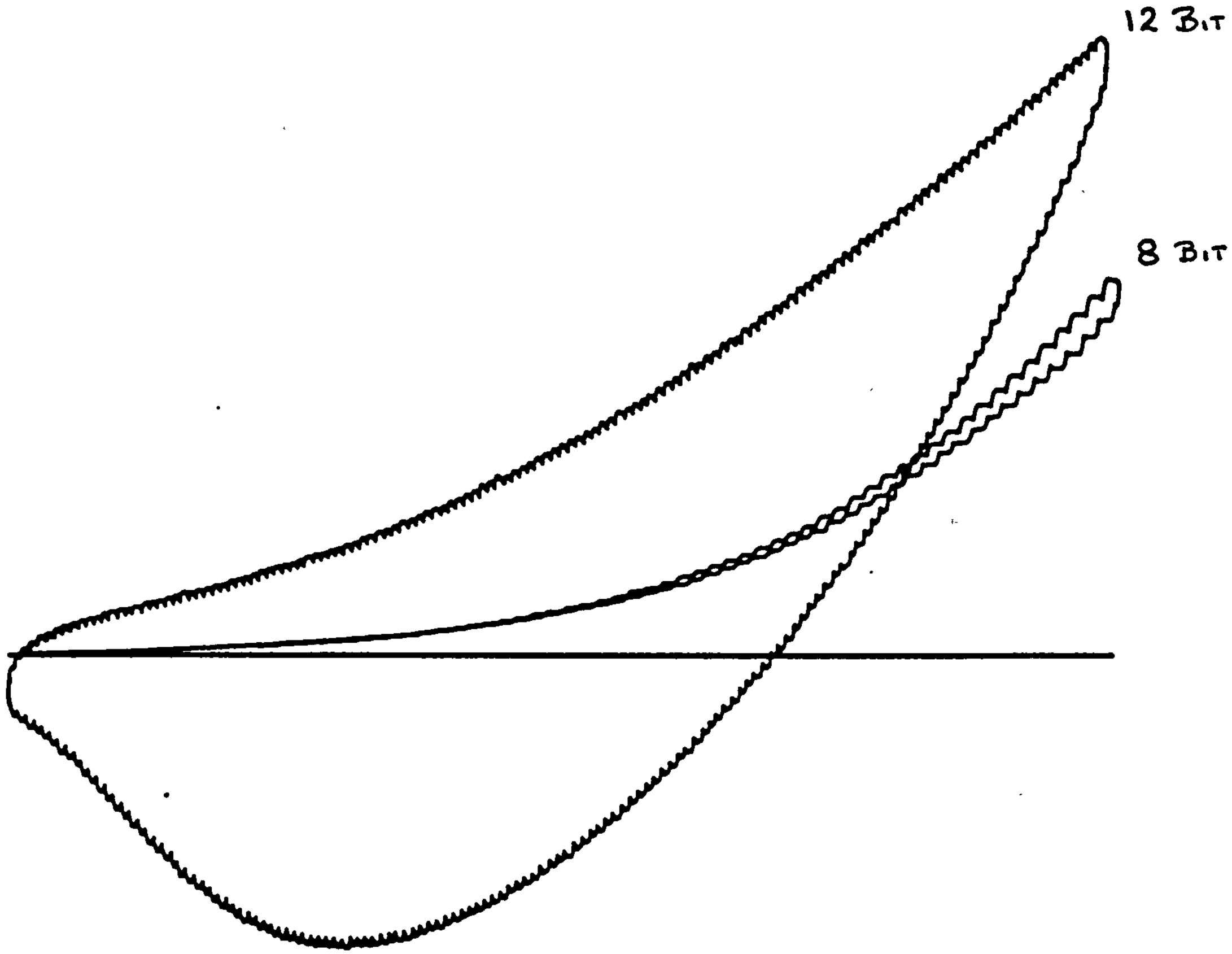
12 Bit
8 Bit

A Fylde FE-254-GA D.C. pre-amplifier was used for this purpose allowing attenuation factors of 2 or 5. This is a high precision instrument of input impedance >2 MΩ, accuracy ±0.1% and bandwidth D.C. to 400 KHz. Thus, for example, a linear sweep experiment required a 300 mV excursion and return from the reference potential. Without attenuation the potential increment would be 0.5 mV in 600 steps, with attenuation of 2 the output potential was expanded to 600 mV and hence a potential increment of 0.25 mV in 1200 steps was produced, similarly for an attenuation of 5, an output of 1500 mV provided 3000 steps of 0.1 mV. The twelve-bit integrated circuit was an AD7542[138] which had a settling time for the analogue voltage output of 2.0 μ s. A slightly faster settling time, 1.25 μ sec, was available from the original ZN428 eight-bit converter. When these times are compared with analogue circuit equivalent rise times of $\simeq$ 10 n s, the digital system is quite inferior. This has to be considered when using digital equipment to perturb an electrochemical system which responds very rapidly, or when recording data at very short times.

The output E_i at J in Figure 4.2 was linked to signal in of the ZN427E A to D converter[139] (Figure 4.5). Both E_i and signal in are referenced to earth. It was found at a later date that the direct interfacing of potentiostats which did not have a buffered current monitoring stage (i.e. the sensing resistance output was directly across the resistor and floating) to the ZN427E, one side of which was earthed, was impossible without distorting the potential E_i. Therefore a high input impedance, 20MΩ high accuracy differential D.C. amplifier was used to interface the two. This provided the added advantage of being

able to expand the signal level to the maximum input level of the converter chip. Hence as the whole input window is filled the accuracy is increased. A differential amplifier Fylde FE-255-DA, bandwidth D.C. to 100 KHz, was therefore retained for use with all potentiostats. The circuit design used in the microcomputer application comprised two I/Cs each for 2.55 V either side of zero. The ZN427E can be used in bi-polar mode, however; this gives only 1.25 V either side and a resolution of 1 in 128 if working with only one sense of current. The conversion inevitably takes time, in this case 10 μ s hence if the signal is fluctuating rapidly an error could be introduced in this period. The fastest rate at which the input, to the C.P.U. from the converter I.C., can be changed, is 100 KHz. (The C.P.U. has no influence on this rate since its operating speed allows data to be taken from the converter faster than it can be presented.) This establishes the upper limit on operating speed. Usually it is known when the signal frequency is likely to be too large for the recording instrument. However due to the discrete sampling nature of a digital system it is necessary to ensure that 'aliasing' does not occur. This effect arises when the sampling rate is too slow to correctly define the features of the signal,but the resultant record can appear, when the data is fitted back together, coherent. In some cases a low-pass filter can be fitted to limit the high frequency content of the signal.

An obvious drawback of digital devices is the quantization effect due to the fixed number of levels used to represent a continuum. Unfortunately the only way to reduce this error is to change the converter chip and inrease the number of levels.

This was done after the initial investigations with the ZN427E which proved the resolution of one in two hundred and fifty-five to be inadequate for many purposes. A twelve-bit converter was used to test its suitability, this was found to be significantly better and has since been adopted as standard on Kemitron boards (ADA-4). Figure 4.6 illustrates the quantization effect produced by the original eight-bit converter. The linear sweep voltammogram of $Pb/PbSO_4$ shows each recorded point and illustrates the jumping effect between two least significant bits whilst the signal level remained constant. The twelve-bit converter, AD574J,[140] had a resolution of 1 in 2^{12} i.e. 1 in 4096, a sixteen-fold increase in resolution. Its mode of operation and incorporation in a circuit is similar to that of the eight-bit in Figure 4.5. Unfortunately there had to be a trade off of speed for resolution since the conversion time of the AD574J was 25 μs (compared to 10 μs for ZN427E). A quicker eight-bit conversion, 16 μs, could be implemented on the same chip if required. These conversion times allowed maximum operating frequencies of 40 KHz and 62.5 KHz respectively. It was soon realised that the maximum operating frequencies could not possibly be attained if a high level language was to be used, particularly if the program was run interpretively (for programming convenience) under BASIC-80 rather than compiled as with FORTRAN. In order to achieve maximum operating speed machine code routines to extract the converted data and place it in memory were written. These were run as subroutines which could be called as needed. The approximate maximum operating rate with interpreted basic was found to be 40 Hz, this was adequate for steady state or slow

Figure 4.6

Cyclic voltammogram of $Pb/PbSO_4$ showing the quantization effect on the recorded signal by an 8-bit analogue to digital converter.

NOTE Perturbing signal was produced by a purely analogue device.

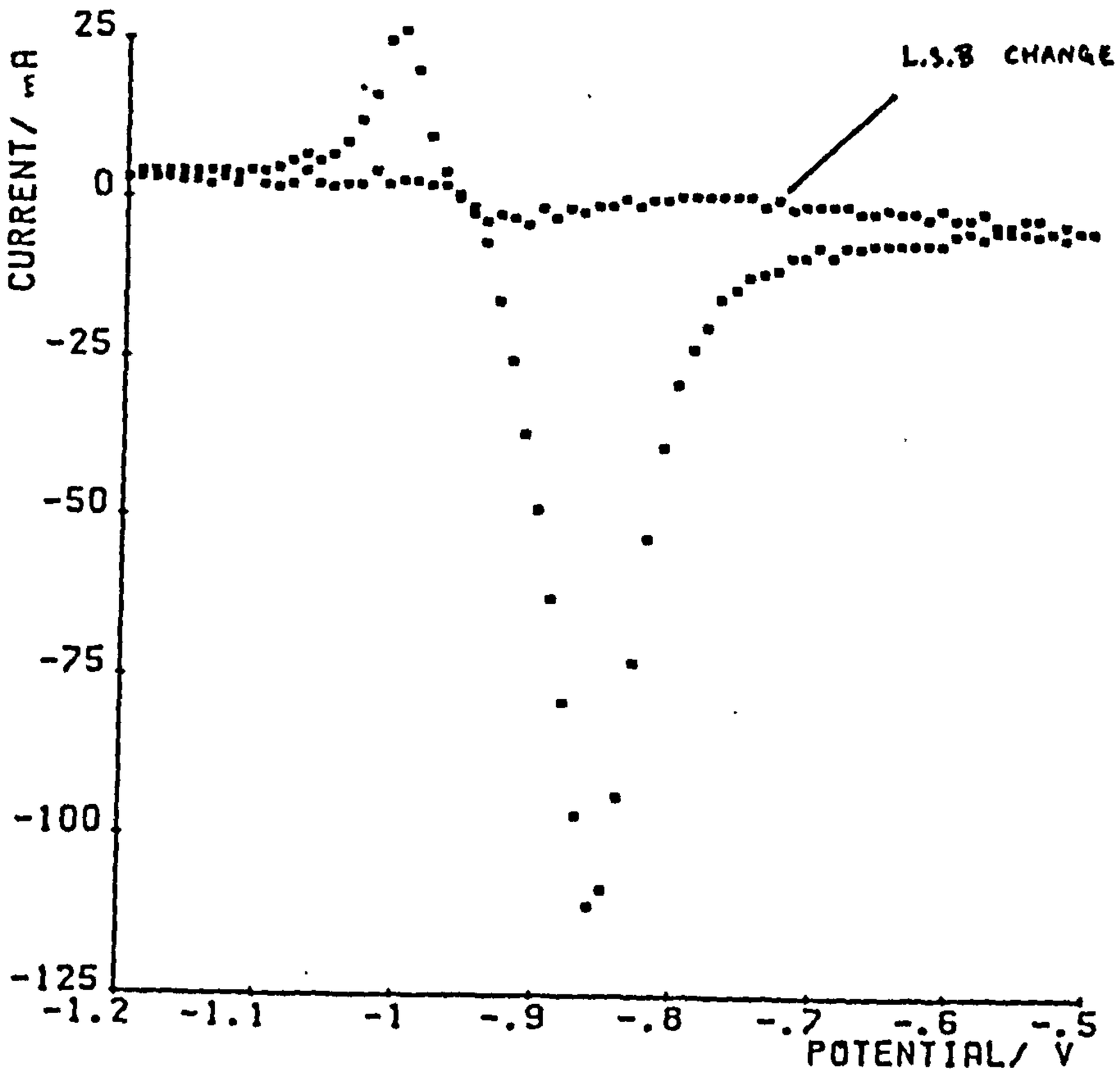
25
0
-25
-50
-75
-100
-125
CURRENT/ mA
L.S.B CHANGE
-1.2
-1.1
-1
-.9
-.8
-.7
-.6
-.5
POTENTIAL/ V

linear sweep (< 10 mV s^{-1}, one data point per 0.25 mV) work. For linear sweeps at greater speeds or for recording fast electrochemical response to a potential step the machine code routines with suitable timing had to be used.

Irrespective of the way the data was acquired (BASIC or machine code) the C.P.U. would place it in storage memory for subsequent examination and analysis.

Timing problems associated with the settling time of the D to A and conversion time of the A to D were easily compensated for in the controlling software.

Although it was desirable at this stage to extend the system's data recording ability to allow very fast capture, for general laboratory use, further improvement of the microcomputer's analogue interface was impractical due to the cost of high speed, high resolution, integrated circuits. (As more designs appear on the market the cost is now rapidly falling.) However, the availability in the laboratory of a fast transient digitiser inspired the development of an interface to allow extraction and processing of data recorded by this instrument. The transient recorder was a Datalab DL-905 with a recording frequency of 5 MHz, i.e. one sample per 0.2 μ.s, and storage capacity of 1024 samples. The resolution of this machine was only eight-bit, but twelve-bit conversion at this speed was not available at the time of manufacture, 1979. Although it is now possible to purchase a recorder with this capability the price is in excess of £5000. It was decided to link the recorder and microcomputer by a parallel data path eight-bits wide. This meant that data could be taken direct from the memory of one machine to the memory of the other. The transfer was facilitated via an 8255N[141] programmable

peripheral interface chip, which not only provided the data transfer port but also the mutual timing and control lines necessary for coherent transfer (see Figure 4.7). The transfer software routine was written in machine code which gave the added advantage of a transfer time of less than a second, the data was also written onto magnetic floppy disc in this time so that control was returned to the operator almost immediately after recording. This allowed another run to be initiated within a few seconds.

If required, the microcomputer would reset the transient recorder to log any number of subsequent batches of data whilst writing the previous batch to disc. When recording data at a speed in excess of 0.1 MHz an analogue perturbing signal had to be used, with a synchronising output to trigger the transient recorder. The Datalab 900 series of transient recorders all have similar eight-bit parallel TTL compatible data output boards which along with control lines terminate at a 24-way Amphenol connector. Consequently it was not difficult to modify the software to enable the use of other 900 series recorders with the microcomputer. Both DL-901 and DL-922 recorders were found to operate through this interface. The DL-922 has a sampling frequency of 20 MHz or 50 n s per point.

Descriptions have been given of the use of microcomputers for potential step and linear sweep methods. These techniques do not usually require feedback (see Section 4.2) from the electrochemical system in order to adjust the perturbing influence to enable useful data to be collected. However a technique which does require such control is the rotating disc. A microcomputer system has recently been developed, at Loughborough, by McNeil,[142] for such work. The system will not be described in detail[143] but

Figure 4.7

The INS8255 programmable peripheral interface as an integral part of the microcomputer system.

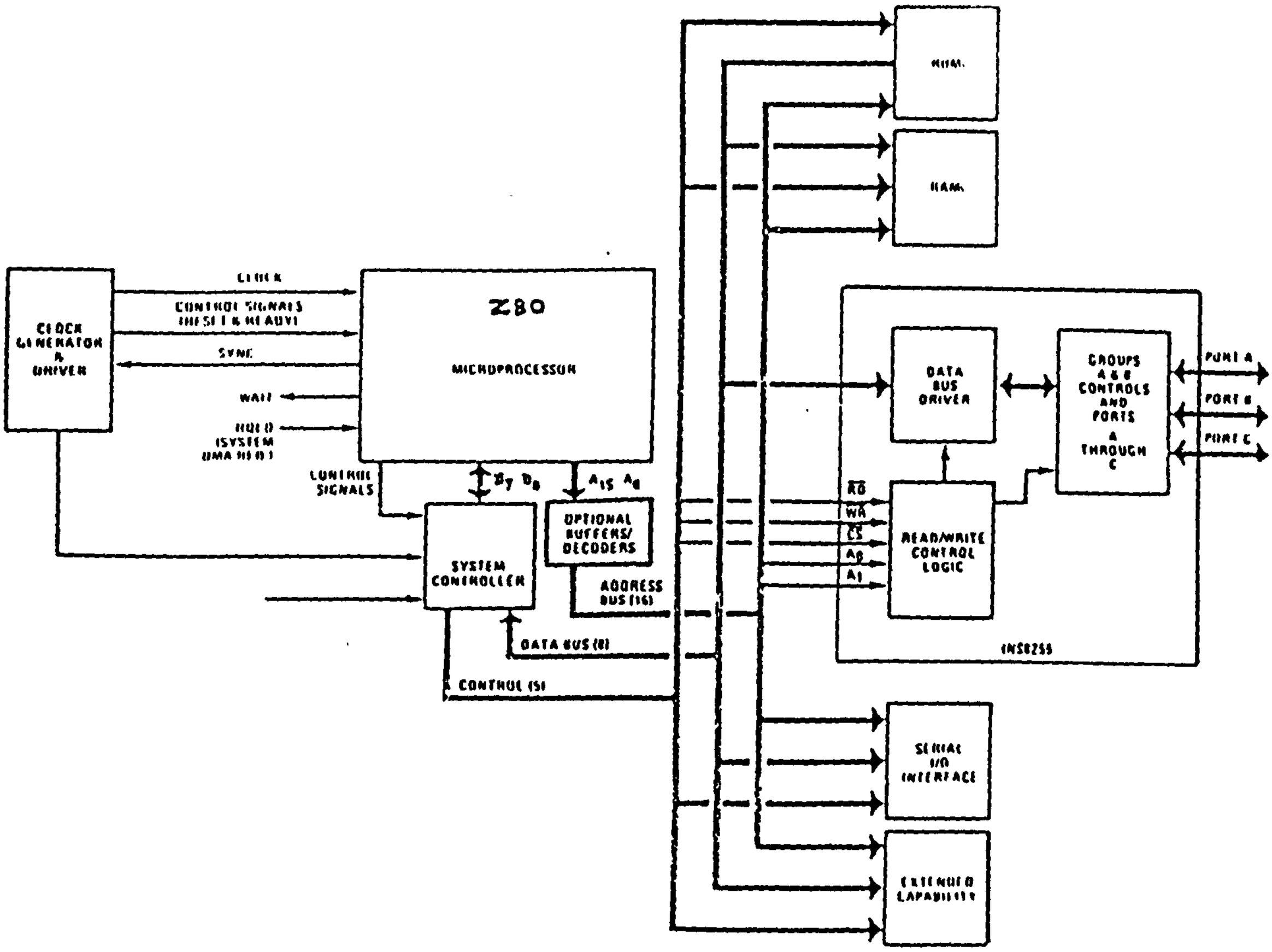

PORT

A ⟹ CONTROL

MICROCOMPUTER B ⟺ CONTROL DL 905

C ⟸ DATA

a brief outline is included to illustrate the ease of use of closed loop or feedback control. The analogue interfacting system was essentially as used in the potential step and linear sweep work. The actual configuration was; 12-bit A to D for polarization level, 12-bit D to A for current monitoring and 8-bit D to A for rotating disc motor control.

The algorithm illustrates the feedback mode most clearly and is presented here for ease of reference.

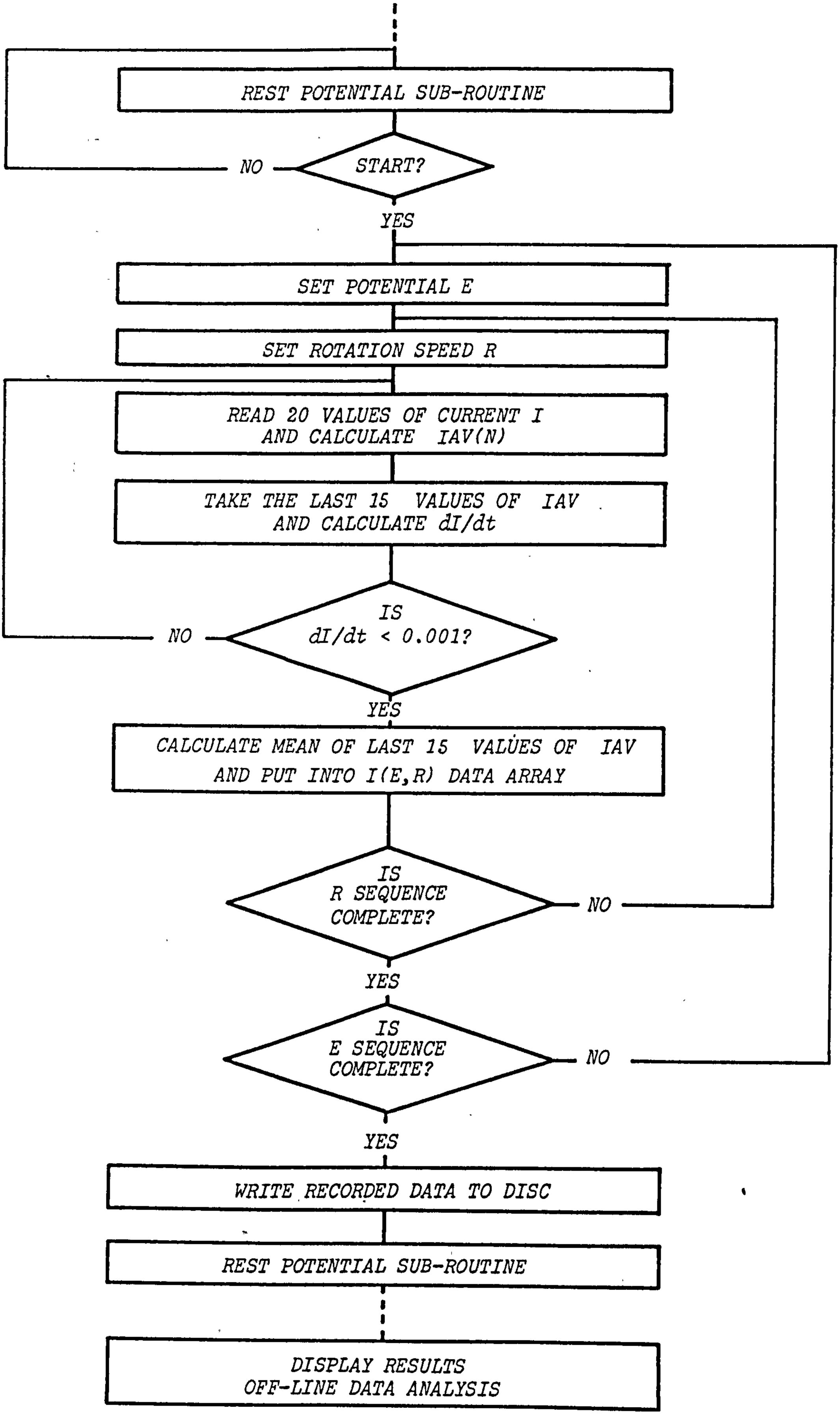
REST POTENTIAL SUB-ROUTINE
START?
NO
YES
SET POTENTIAL E
SET ROTATION SPEED R
READ 20 VALUES OF CURRENT I
AND CALCULATE IAV(N)
TAKE THE LAST 15 VALUES OF IAV
AND CALCULATE dI/dt
IS
dI/dt < 0.001?
NO
YES
CALCULATE MEAN OF LAST 15 VALUES OF IAV
AND PUT INTO I(E,R) DATA ARRAY
IS
R SEQUENCE
COMPLETE?
NO
YES
IS
E SEQUENCE
COMPLETE?
NO
YES
WRITE RECORDED DATA TO DISC
REST POTENTIAL SUB-ROUTINE
DISPLAY RESULTS
OFF-LINE DATA ANALYSIS

Values of E and R (potential and rotation speeds at that potential) are input to the microcomputer, typically six speeds per potential. The computer then enters a subroutine which adjusts the working electrode potential, to seek minimum current and establish a rest potential. When instructed to execute the experiment the potential is set and the electrode rotated. The current is continuously monitored and the rate of change of this current with time is calculated. The monitoring procedure is sustained until $di/dt < 0.001$ at which point the next speed is selected; and so on until the speed regime for that potential is completed. The microcomputer then moves to the next potential.

4.6 Conclusions

The microcomputer system as illustrated in this chapter has proved its ability to perform a useful and diverse function within the laboratory.[102,142,149,150] The work which is presented in the following chapters was carried out with the aid of the microcomputer system for either experimental control, data retrieval or both.

There are many advantages to be gained by adopting microcomputer 'assistance' a few are given here:

(i) Experimental data can be obtained both accurately and rapidly. Digital timing circuitry permits logging of data at software variable rates with very high precision.

(ii) The type of experiment to be performed is readily changed, as the form of perturbation and recording can be easily altered within the software.

(iii) Mathematical operation upon required data is immediately available. The data can subsequently be presented in a format which is easily assimilable by the experimenter.

(iv) Large amounts of data can be gathered, analysed and stored in a relatively short time.

(v) The experimenter is freed, to a certain extent, for higher tasks (such as going to watch cricket or for a pint).

It appears that as micromputers are rapidly becoming widely employed for interfacing, directly or indirectly, to experimental systems, there are a number of people who misguidedly believe that attaching a 'micro' will solve all the problems associated with that system. This is definitely not the case. Development of suitable interfacing hardware and the time consumed by software composition cannot be disregarded. I am of the opinion that, for electrochemical systems in particular, the microcomputer's tasks should be limited to data capture, experimental monitoring and feedback, for which the microcomputer has proved invaluable in our laboratory. However; the signals as supplied by digital to analogue integrated circuits, at the present state of the art, are not of sufficient analogue purity nor of high enough transition speed to replace the traditional analogue function generator. Perhaps the way forward in this respect is the use of a pre-programmable analogue function generator, which accepts digital information, allowing parameters to be set. This would then, after a short period, execute the required function whilst constantly informing the microcomputer (the timing and recording device) of its status.

Finally this type of system cannot be expected to operate without some intervention, since "electrode kinetics", as is neatly expressed by Dr. O. R. Brown, "is a branch of science in which experimental work is particularly subject to the influence of unintended artefacts".

C H A P T E R 5

THE ELECTRODE ENVIRONMENT

5.1 Cells

Electrolytic cells were made from borosilicate glass and conformed to the same pattern. The cell was designed for incubation in a liquid medium for low temperature studies and studies up to ambient temperature. Figure 5.1 shows the three compartment cell used which is free of joints or taps. Liquid seal taps were replaced by forming a ground glass seat between the reference electrode and the reference electrode compartment (C). The cell was also fitted with facilities for gassing the electrolyte solution via a porous glass frit (seen behind the working electrode compartment (B)).

A luggin capillary extended from the reference compartment (C) into the working compartment (B) to provide a luggin/working electrode gap of approximately 1 mm. The counter electrode compartment (A) was separated from the working compartment by a porous glass frit.

5.1.1 Forming Cell

The cell for galvanostatic charging of porous electrodes was also constructed of borosilicate glass. Figure 5.2 shows the design. The working electrode was inverted, to allow gas escape, and placed in position C held securely by a large neoprene bung. The counter electrode is shown in position B. A reference electrode could also be incorporated if required in position B.

Figure 5.1

Three compartment cell.

A - Counter

B - Working

C - Reference

D - Luggin Capillary

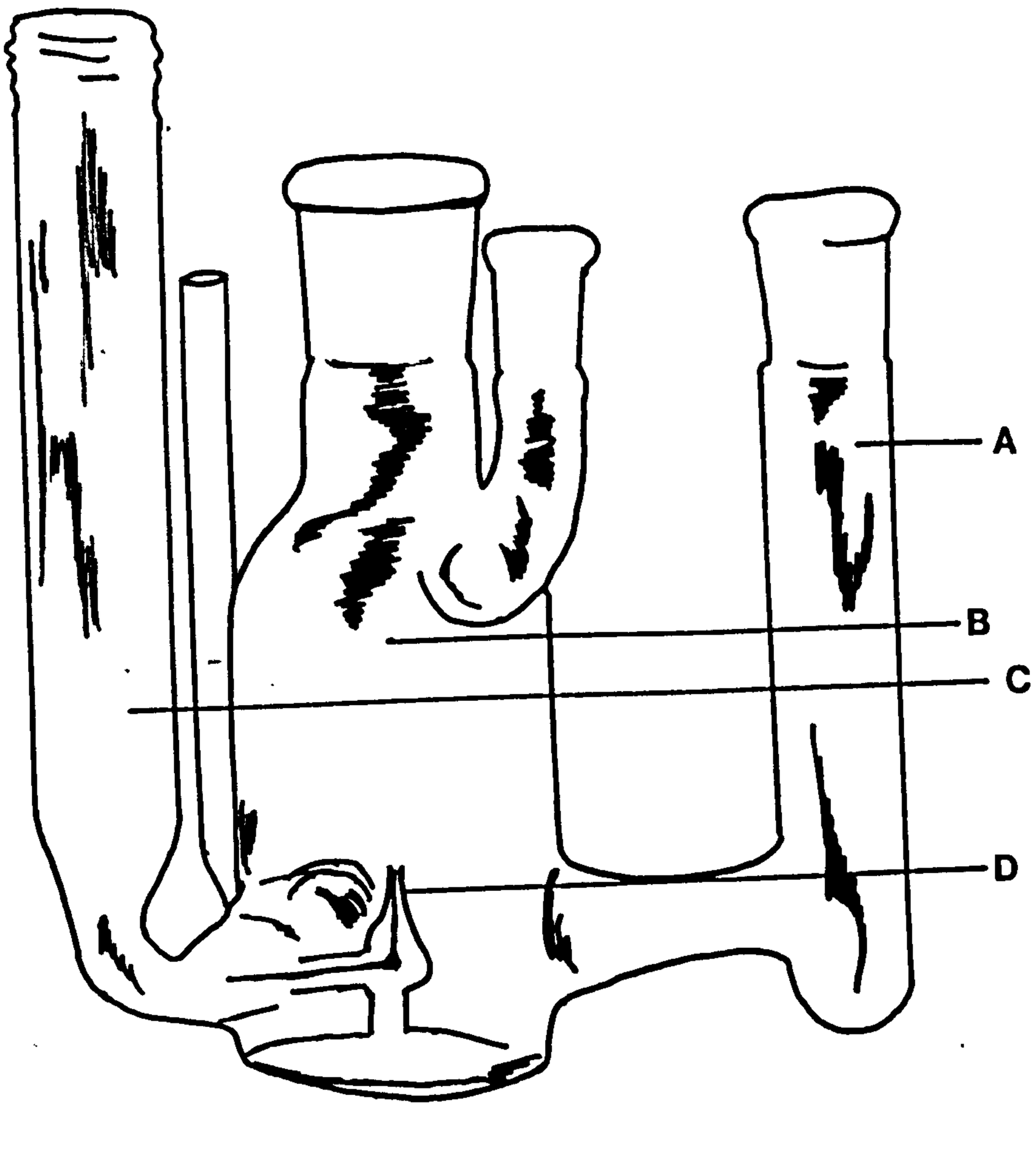
A
B
C
D

Figure 5.2

Formation cell.

A - Provision for reference electrode

B - Counter electrode

C - Working electrode

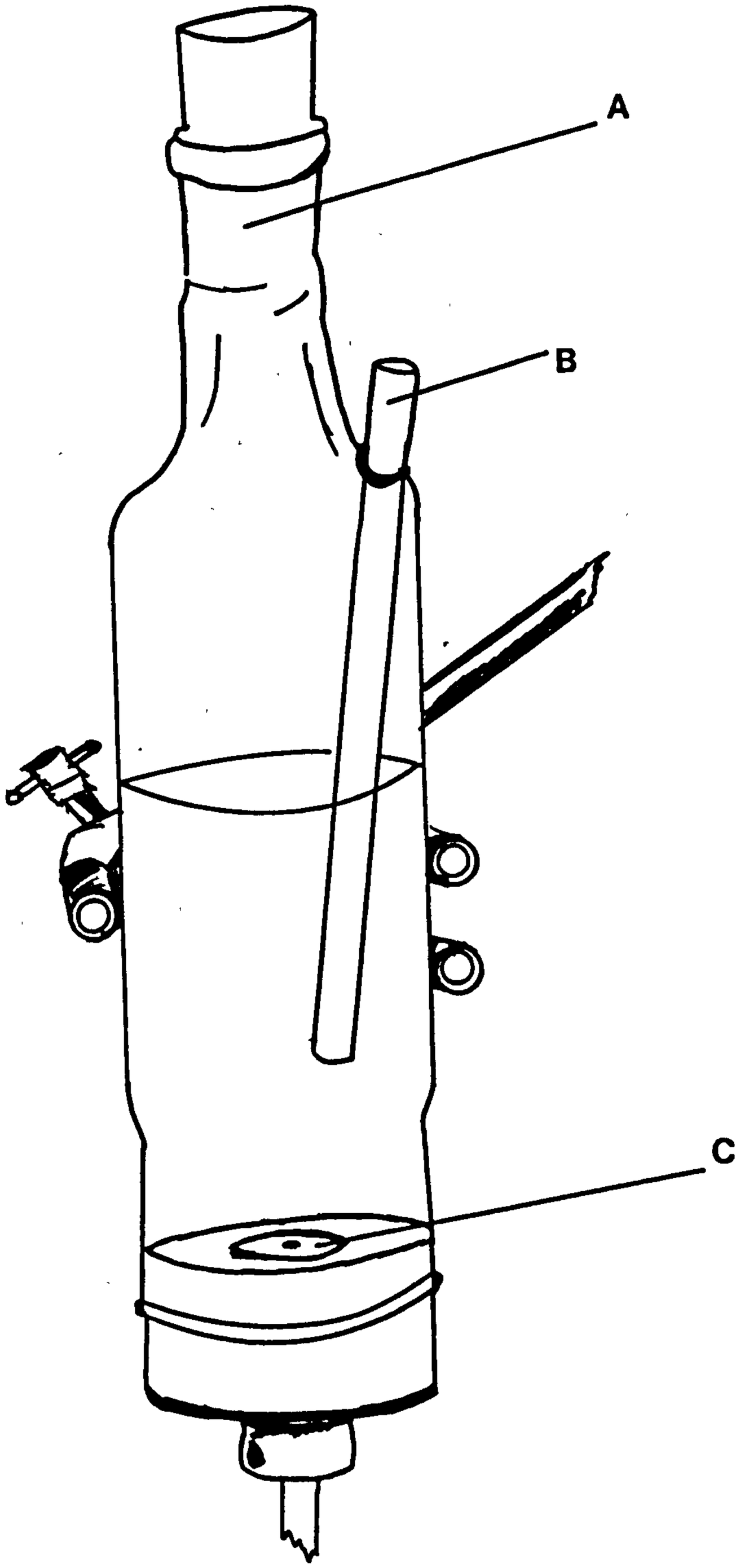
A
B
C

5.1.2 Cell Cleaning

Cells were cleaned by steeping in a 50:50 H_2SO_4/HNO_3 mix for 48 hours. These were then thoroughly washed with tridistilled water and soaked for 24 hours before use.

5.2 Thermostatic Bath

With the use of the thermostatic bath the electrode/electrolyte system could be maintained at any temperature between $+30^{o}C$ and $-50^{o}C$ $\pm 1^{o}C$. The bath was fabricated from polypropylene insulated with polystyrene and filled with methanol. It could be raised and lowered, to allow immersion and removal of the cell, by means of a laboratory jack. The temperature control system comprised a Townson and Mercer refrigeration unit working in opposition to ethylene glycol heated (1 Kw) externally in a tank and pumped through glass coils immersed in the methanol. This system provided excellent stability, (Figure 5.3).

5.3 Electrodes

5.3.1 Working Electrodes

Planar electrodes were made from 99.999% (Koch-Light) lead set in a Teflon shroud. This was then attached to the electrode assembly via a Teflon holder, (Figure 5.4). The electrode holder was attached to the shaft of the rotating disc system by either a grub screw or a thread in the centre of the holder. Contact between rotating disc system shaft and the lead was made by a mild steel spring. A mercury pool provided electrode contact between the rotating electrode and the potentiostat external

Figure 5.3

Schematic diagram of temperature control system.

Figure 5.4

Working electrode construction. The lead rod at A can be recessed to make provision for a porous electrode slug .

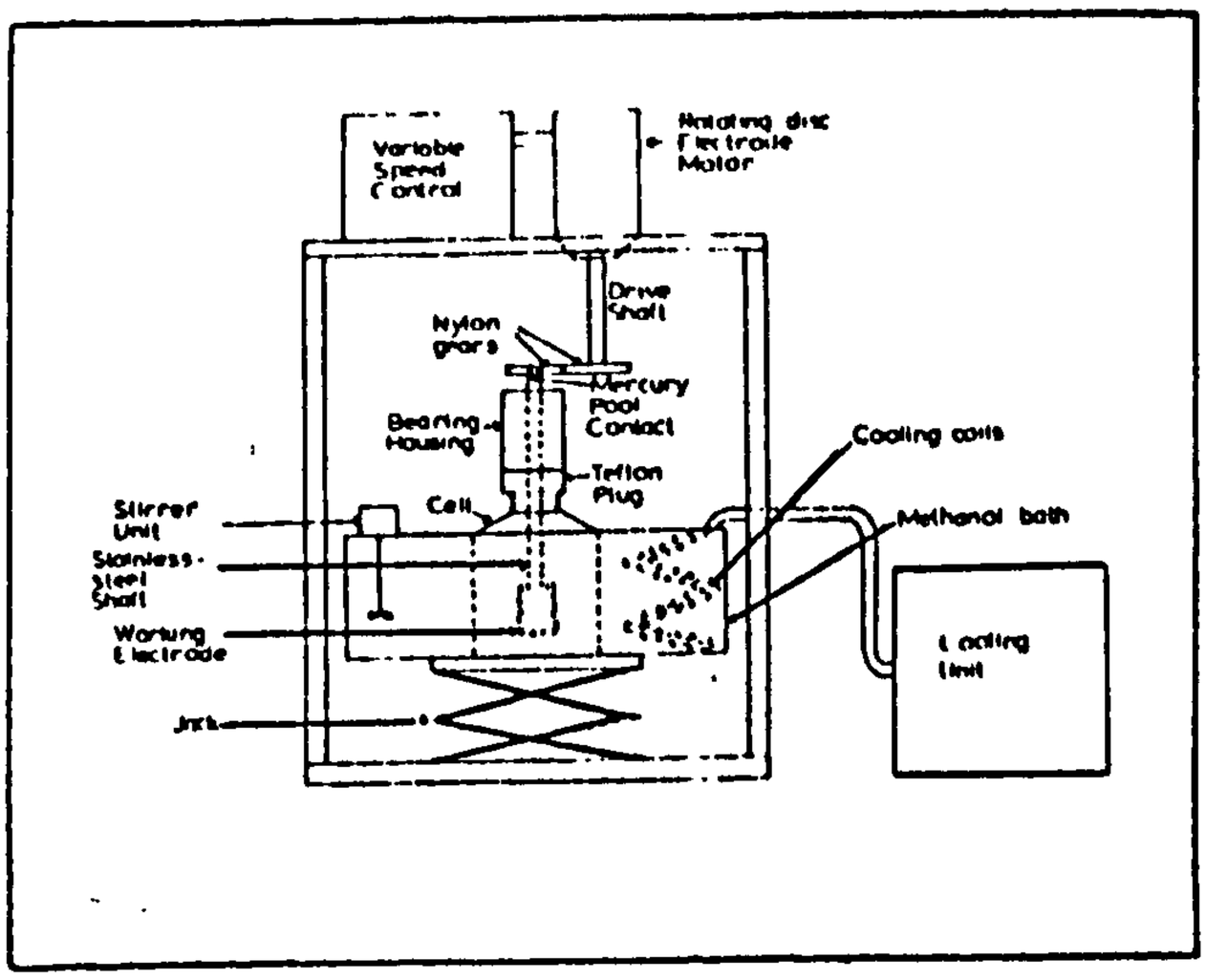
Variable Speed Control
Rotating disc Electrode Motor
Drive Shaft
Nylon gears
Mercury Pool Contact
Bearing Housing
Teflon Plug
Cell
Cooling coils
Methanol bath
Stirrer Unit
Stainless-steel Shaft
Working Electrode
Junk
Cooling Unit

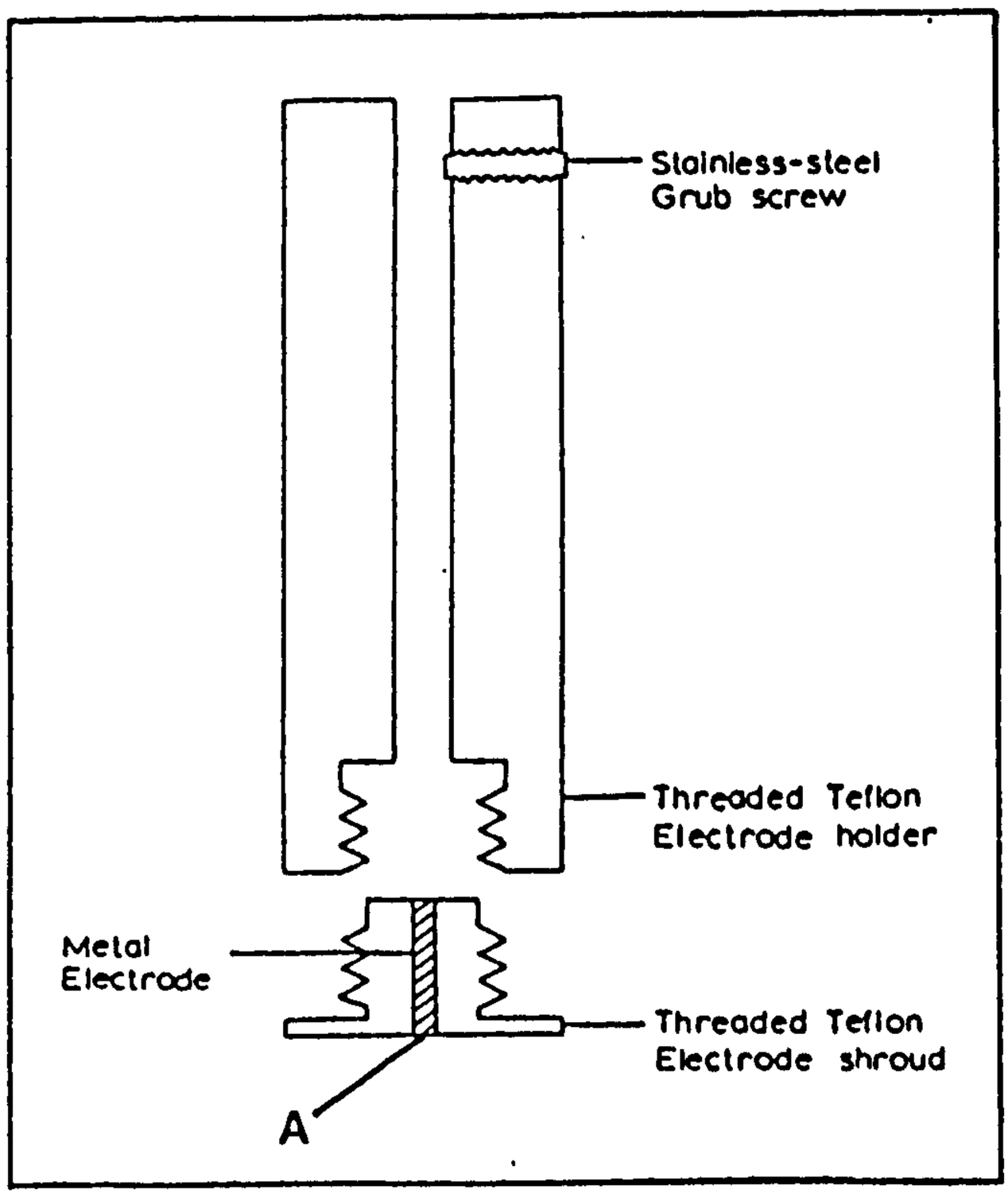
Stainless-steel Grub screw
Threaded Teflon Electrode holder
Metal Electrode
Threaded Teflon Electrode shroud
A

circuit. The preparation and pre-treatment of planar electrodes is as described in Chapters 6 and 7.

Porous electrodes were made from 'leady' oxide as supplied by Joseph Lucas Ltd. This was free from all additives other than inert terylene binder. Expander materials were added as necessary. The electrode was prepared by pasting a recess formed by Shrouding lead rod (diameter 0.3 cm, 99.999%), sectioned at right angles to the long axis, with Teflon so that the end of the shroud (diameter 1.6 cm) projected 0.076 cm below the lead. The end of the shroud was perpendicular to the long axis and polished flat. The leady oxide (and expander if necessary) was allowed to condition in 100% humidity and then dried at 70°F before electroreduction. The porous electrode was subsequently formed in an inverted position, by reduction at 18 mA cm^{-2} for a period of 72 hours in 0.5M H_2SO_4 after which period hydrogen was freely evolving from the electrode. The resulting electrodes had a nominal density of 3.35 g cm^{-3} ($\sim$ 70% voids) and a theoretical recoverable capacity of 16.8 C.

5.3.2 Reference Electrodes

Potentials were measured with reference to a Hg/Hg_2SO_4 electrode in the same concentration H_2SO_4 as the working electrode. The construction of the wick-type reference electrode is shown in Figure 5.5.

5.3.3 Counter Electrodes

The counter electrodes for galvanostatic charging were solid lead rod of purity 99.999%.

Figure 5.5

Wick type Hg/Hg_2SO_4 reference electrode.

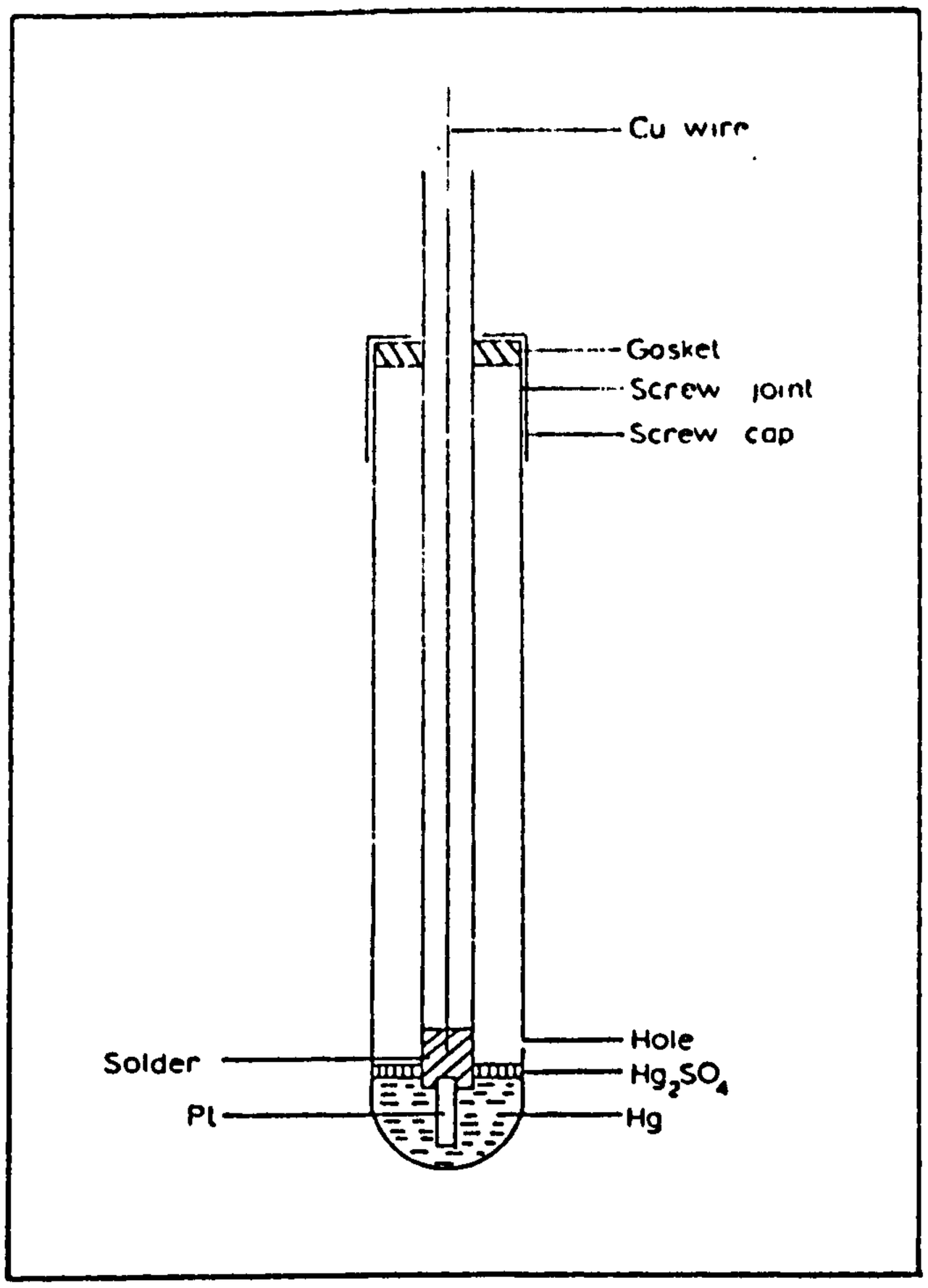
Cu wire
Gasket
Screw joint
Screw cap
Hole
Solder
Hg_2SO_4
Pt
Hg

The counter electrode for potentiostatic experiments was glassy carbon rod (Morganite) of diameter 0.5 cm.

5.4 Electrolyte

Electrolyte solutions were produced from AnalaR grade H_2SO_4 and tridistilled water. Electrolytes were normally purged with oxygen free nitrogen before experimental use.

5.5 Electronic Equipment

Galvanostatic charging was carried out by use of a constant current power source monitored by an AVO meter in series. The potential was measured using a digital voltmeter (Gould DMM7A).

Potentiostatic experiments were carried out using a machine the same or of similar design to that given in Chapter 4. All perturbing signals were produced digitally. All data recording was done digitally.

The rotating disc system used in Chapter 7 was produced to be controllable by the microcomputer system of Chapter 4 (Kemitron Electronics RD1). The electrode was driven by a high precision motor-generator using a special belt drive which obviated speed fluctuations. Rotation speed was measured and adjusted using an opto-electronic shaft encoder with feedback. This provided an accuracy of ±0.02 r.p.s. The motor-generator could be either manually controlled or automatically controlled by a Z80 based microcomputer with D to A interfacing. A box girder construction in stainless steel reduced vibration and eccentric movement to an absolute minimum.

CHAPTER 6

EFFECT OF TEMPERATURE ON THE OXIDATION OF LEAD IN 1M SULPHURIC ACID, CONTAINING AND FREE OF EXPANDER

6.1 Introduction

The solid phase formation of lead sulphate is reported to occur by two completely different processes. This is outlinted in Chapter 1.

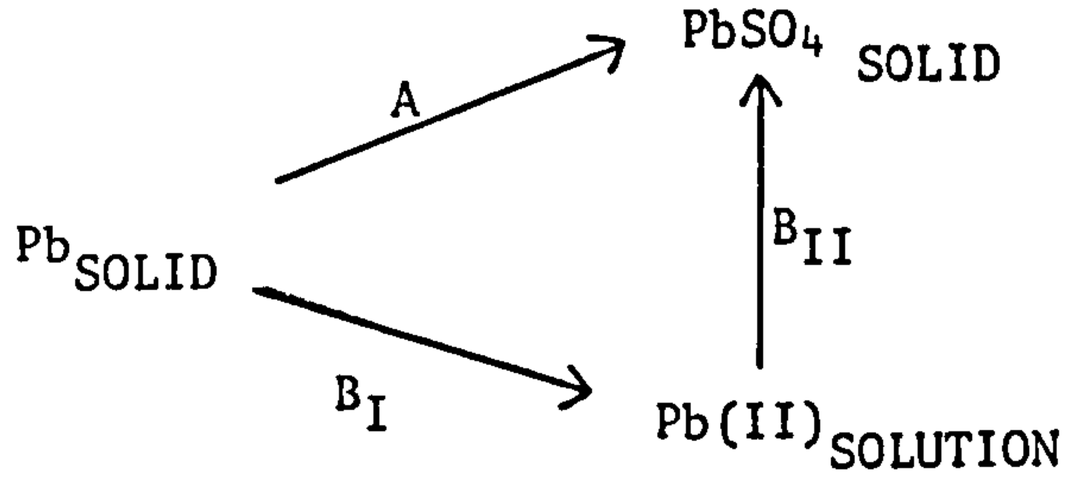

It is known that the oxidation peak of the $Pb/PbSO_4$ current potential profile is strongly influenced by cycling, all subsequent scans being very different from the first.[30,6] The charge in oxidation is always at a maximum in the initial sweep. If the sweep limit is restricted (40 mV overpotential in 1M H_2SO_4)[66] and the electrode pre-treated so as to produce a, as near as possible, defect free surface then the oxidation peak can be reproduced. The oxidation peak is only noticeably rotation speed dependent on the initial sweep all subsequent sweeps being independent. Again this is influenced by electrode pre-treatment.[18-20,144] These observations suggest that the interplay of the two mechanisms is markedly influenced by electrode surface structure. There are a number of suggestions for the role of expander at electrode surfaces in this nebulus process.[11,20,30,31,35-37]

This Chapter describes linear sweep voltammetric investigations of the effect of expander on the oxidation of solid lead electrodes in 1M sulphuric acid. At this acid concentration the solubility of lead sulphate rises to a sharp maximum (see Figure 6.1) thus any solution process should be enhanced. Experiments were carried out over a temperature range (down to the slushing point of 1M H_2SO_4) to note the action of expander in the most technologically interesting and commercially beneficial region. In addition Livshits and Rybalka[145] suggest that the diffusion of Pb(II) salts into solution decreases rapidly with temperature and consequently should influence the mechanism of $PbSO_4$ production by Pb(II) dissolution.

6.2 Procedure

Using the linear potential sweep technique, as controlled by the microcomputer system of Chapter 4, electrodes were cycled to constant response (30 cycles) before logging the i-E profile. This ensured that electrodes received the same treatment.

Experiments were carried out at a series of sweep rates in the temperature range from ambient down to $-5^{o}C$ which was found to be the effective slushing point of the electrolyte solution. The series of experiments was then repeated after saturating the electrolyte solution with Indulin C which is a lignosulphonate widely used in lead-acid battery applications.

Figure 6.1

Solubility of $PbSO_4$ in H_2SO_4 at 25°C and 0°C (Mass fractions: 5M = 0.383, 1M = 0.093).

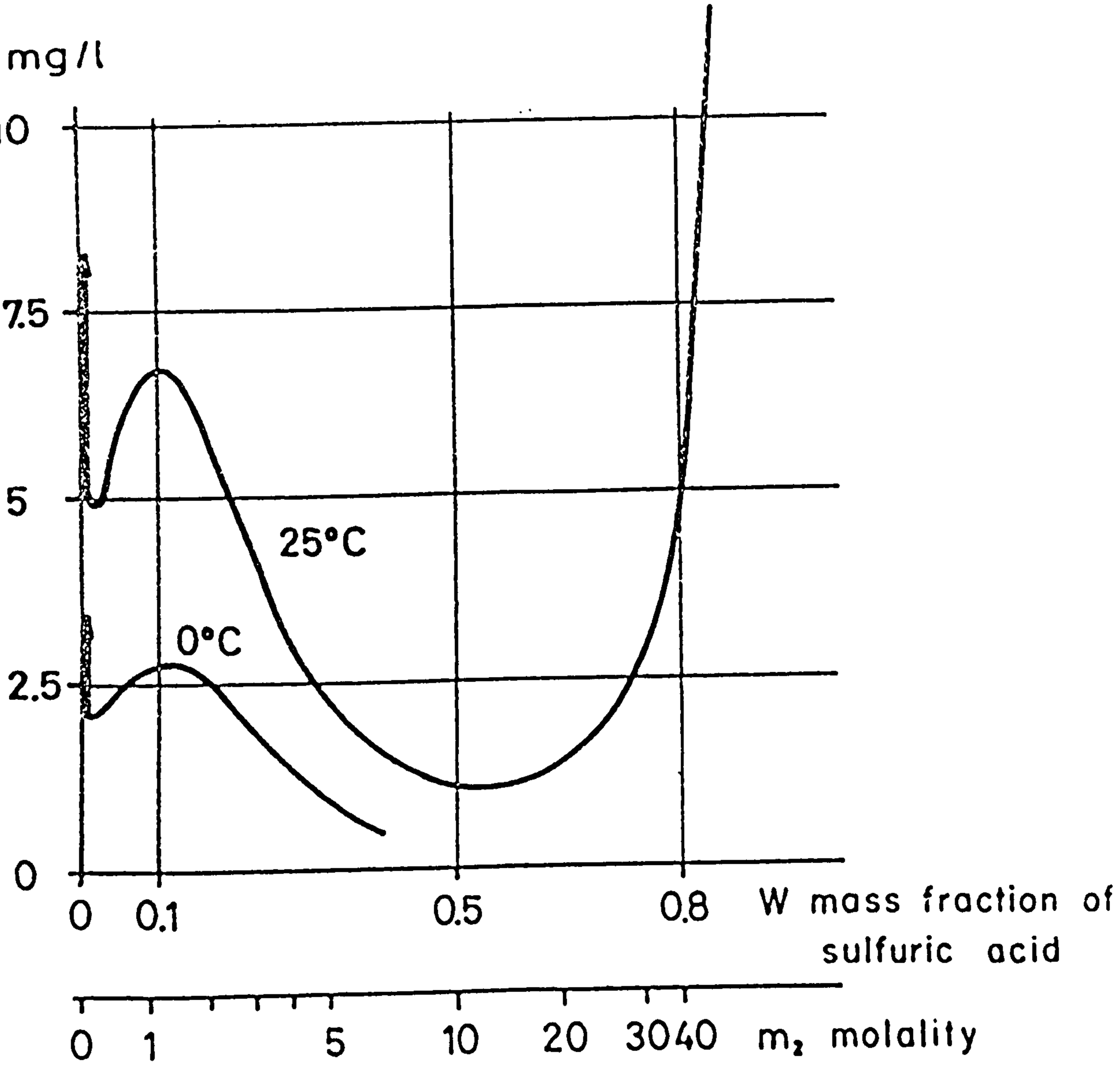
mg/l
10
7.5
5
2.5
0
25°C
0°C
0
0.1
0.5
0.8
W mass fraction of sulfuric acid
0
1
5
10
20
30
40
m₂ molality

6.3 Results

Figure 6.2 shows the results of a L.S.V. experiment at room temperature (18°C). In the potential range investigated the currents were found to be, after cycling, independent of rotation speed and consequently the reaction salts are independent of diffusion in solution. The potential range was limited so that only the Pb(II)/Pb redox reaction was observed to any great extent. The increase in current near the negative limit of the negative-going sweep is due to hydrogen evolution on the product lead; the residual current at the positive limit of the positive-going sweep is due to the residual high field conduction current through the passivating lead sulphate layer. As the temperature was lowered the current in the voltammogram everywhere reduced (Figure 6.3).

This trend continued as far as ∿ -2°C. At this point gross changes occurred on repetitive cycling of the electrode around the potential region. Figure 6.4 shows a quasi-stable voltammogram produced on prolonged cycling (∿ 30 cycles) at -2°C. This further degenerated on cycling to a linear shape with virtually no separation between the positive- and negative-going sweeps as shown in Figure 6.5. The shape is redolent of a polarisable system in spite of the clear electrochemistry exhibited in earlier sweeps. The current at the most negative potential (when the current is mainly due to the hydrogen reaction) is very small, considerably less than when the electrode is 'active' and confirms that the system is $Pb/PbSO_4(S)/H_2SO_4(1M)$ and not $Pb/H_2SO_4(1M)$ i.e. sulphate is not being reduced back to lead. This behaviour can be explained by the transformation of the lead sulphate layer at the end of the positive sweep from a relatively randomly

Figure 6.2

Linear Sweep Voltammogram of the Pb(II)/Pb System in 1M H_2SO_4 at 18°C.

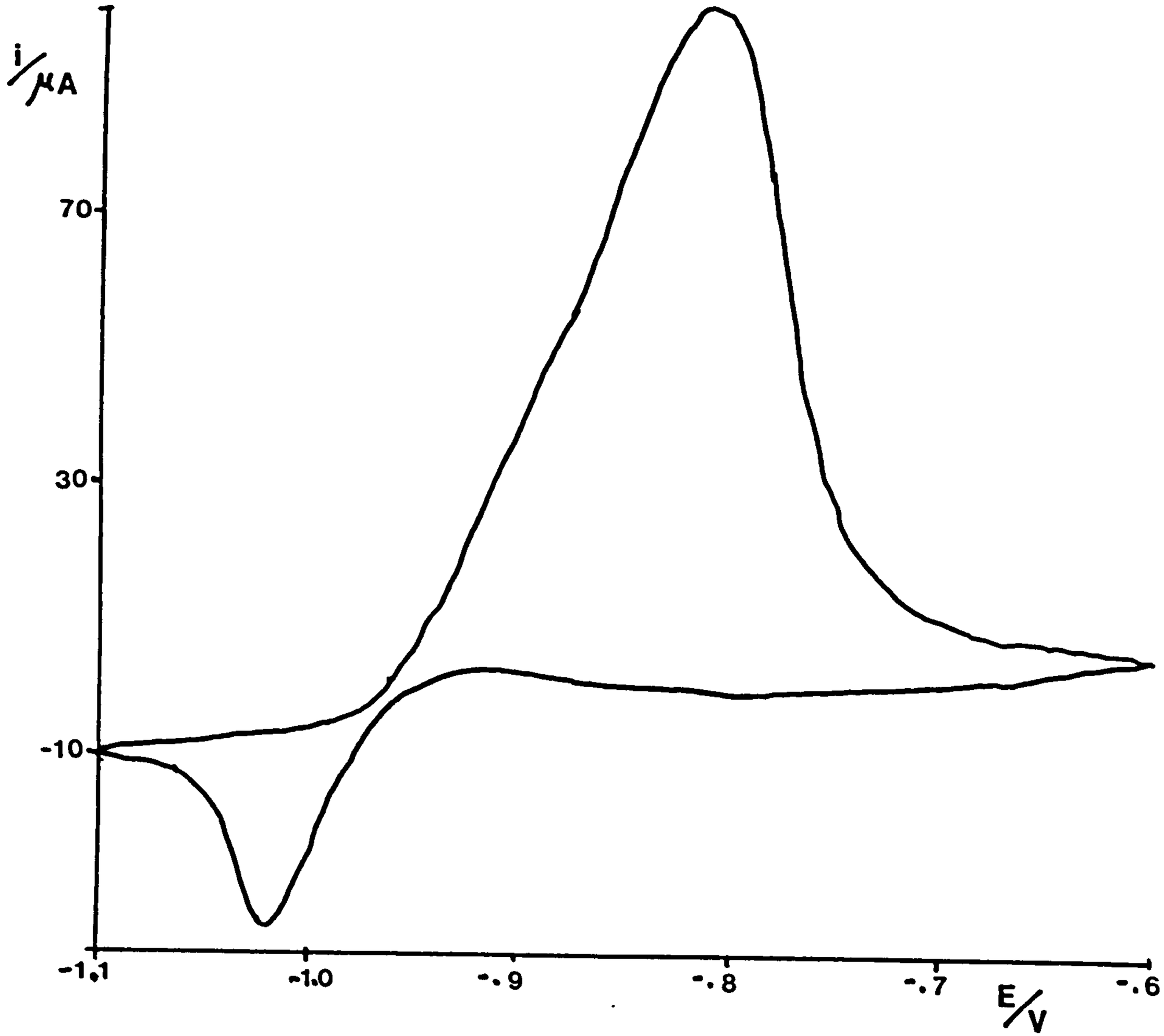
i/μA
70
30
-10
-1.1
-1.0
-.9
-.8
-.7
-.6
E/V

Figure 6.3

Linear Sweep Voltammogram of the Pb(II)/Pb System in 1M H_2SO_4 at $4^{o}C$.

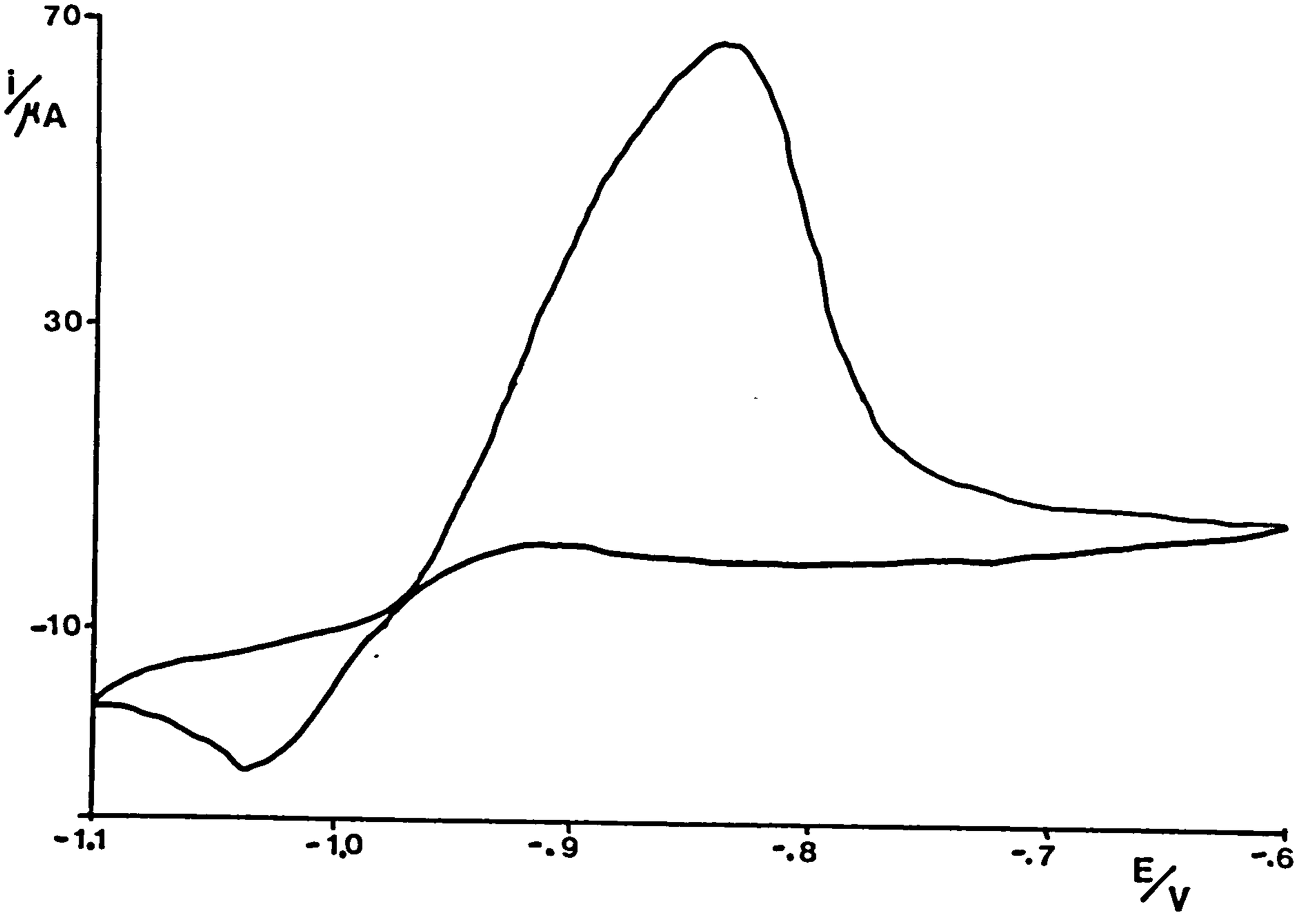
70
i/μA
30
-10
-1.1
-1.0
-.9
-.8
-.7
-.6
E/V

Figure 6.4

Linear Sweep Voltammogram of the Pb(II)/Pb System in 1M H_2SO_4 at $-2^{o}C$.

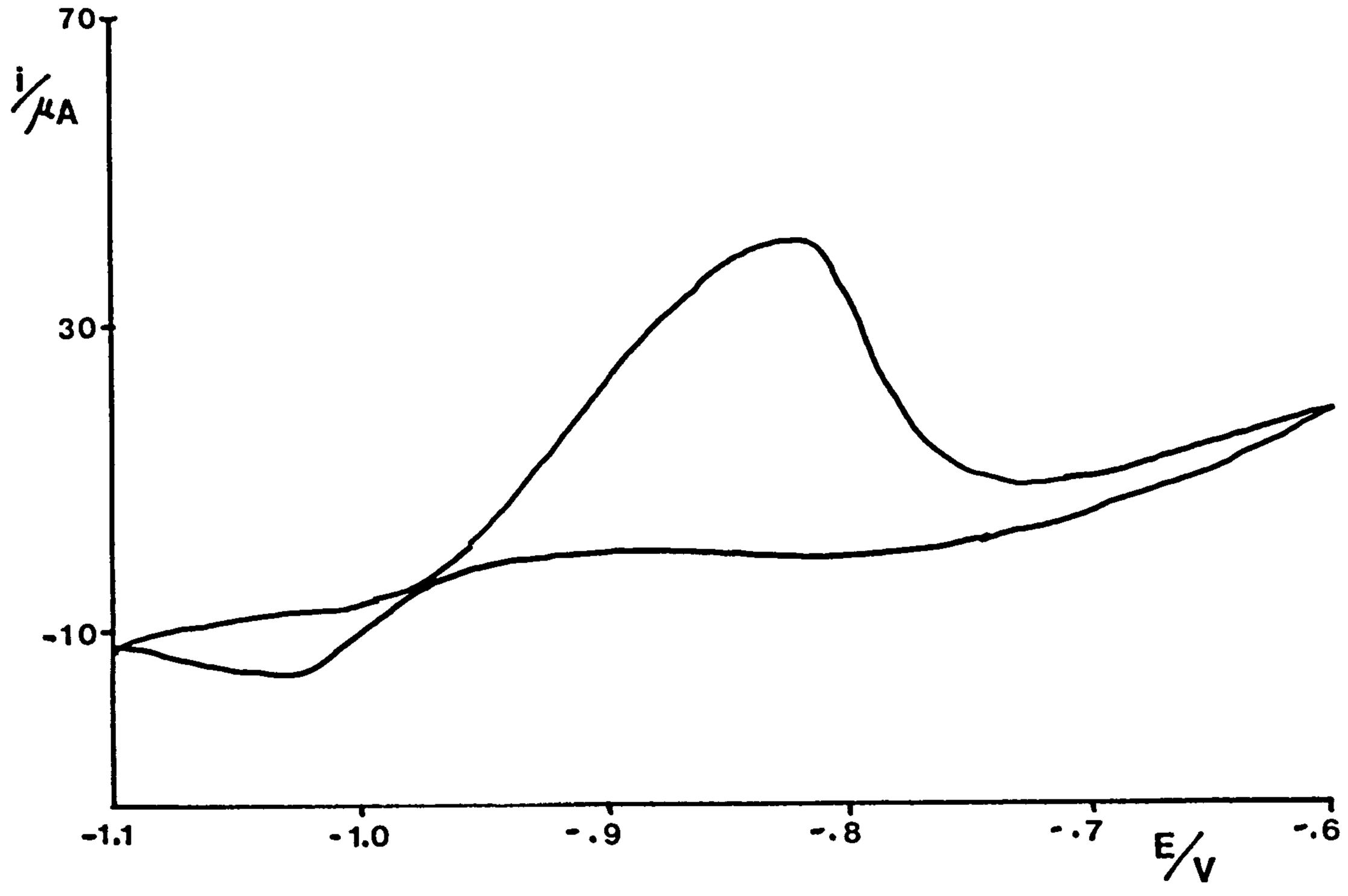
70
i/μA
30
-10
-1.1
-1.0
-.9
-.8
-.7
-.6
E/V

Figure 6.5

Linear Sweep Voltammogram of the Pb(II)/Pb System in 1M H_2SO_4 at $-2^{o}C$.

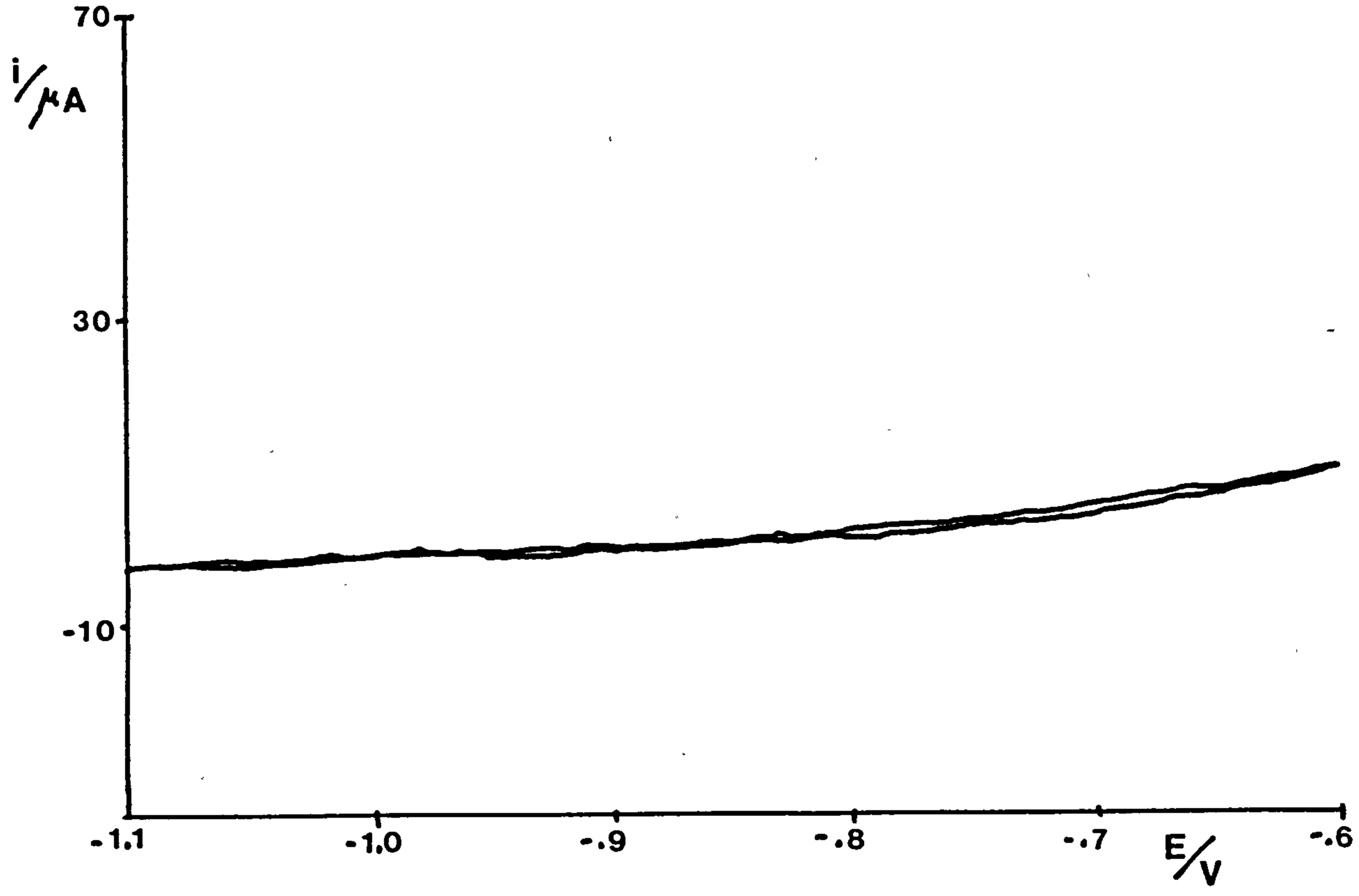
70
i/μA
30
-10
-1.1
-1.0
-.9
-.8
-.7
-.6
E/V

orientated layer through which current is readily able to pass to a much more ordered layer in which a considerable overpotential is required in order to effect the reduction of the $PbSO_4$ layer. The electrode therefore behaves in a quasi-polarisable manner over the narrow potential range.

At temperatures slightly in excess of $-2^{o}C$ the initial open voltammogram after degeneration to a single line on cycling was re-established by further prolonged cycles over the experimental region, the electrode behaviour apparently randomly switching between the two states. This indicates that the temperature could be a determining factor, possibly local slight changes due to instrumental effects determining the form of the voltammogram.

The current in the anodic peak was related to the sweep rate and Figure 6.6 shows the ip vs $\sqrt{\nu}$ relationship for current control by a diffusion process. From the treatment of linear sweep voltammetry where the oxidation peak is assumed to be limited by progressive depletion of electroactive species at the electrode (P. 29), we can use the expression relating sweep speed to peak current to allow the determination of a diffusion coefficient for the system; hence

$$i_p = (2.69 \times 10^5)\ n^{3/2}\ A\ D_o^{1/2}\ \nu^{1/2}\ C_{o,BULK} \qquad (2.86)$$

yields $D_o = 2.506 \times 10^{-8}\ cm^2\ sec^{-1}$ at $18^{o}C$.

This implies current control by diffusion of ions through a lead sulphate film which is incompletely formed and probably accounts for the observed magnitude, this is in agreement with previous work.[146] In addition the potential at the current maximum was seen to shift with sweep rate producing a linear

Figure 6.6

The ip versus $\nu^{\frac{1}{2}}$ relationship for the Pb(II)/Pb System in 1M H_2SO_4.

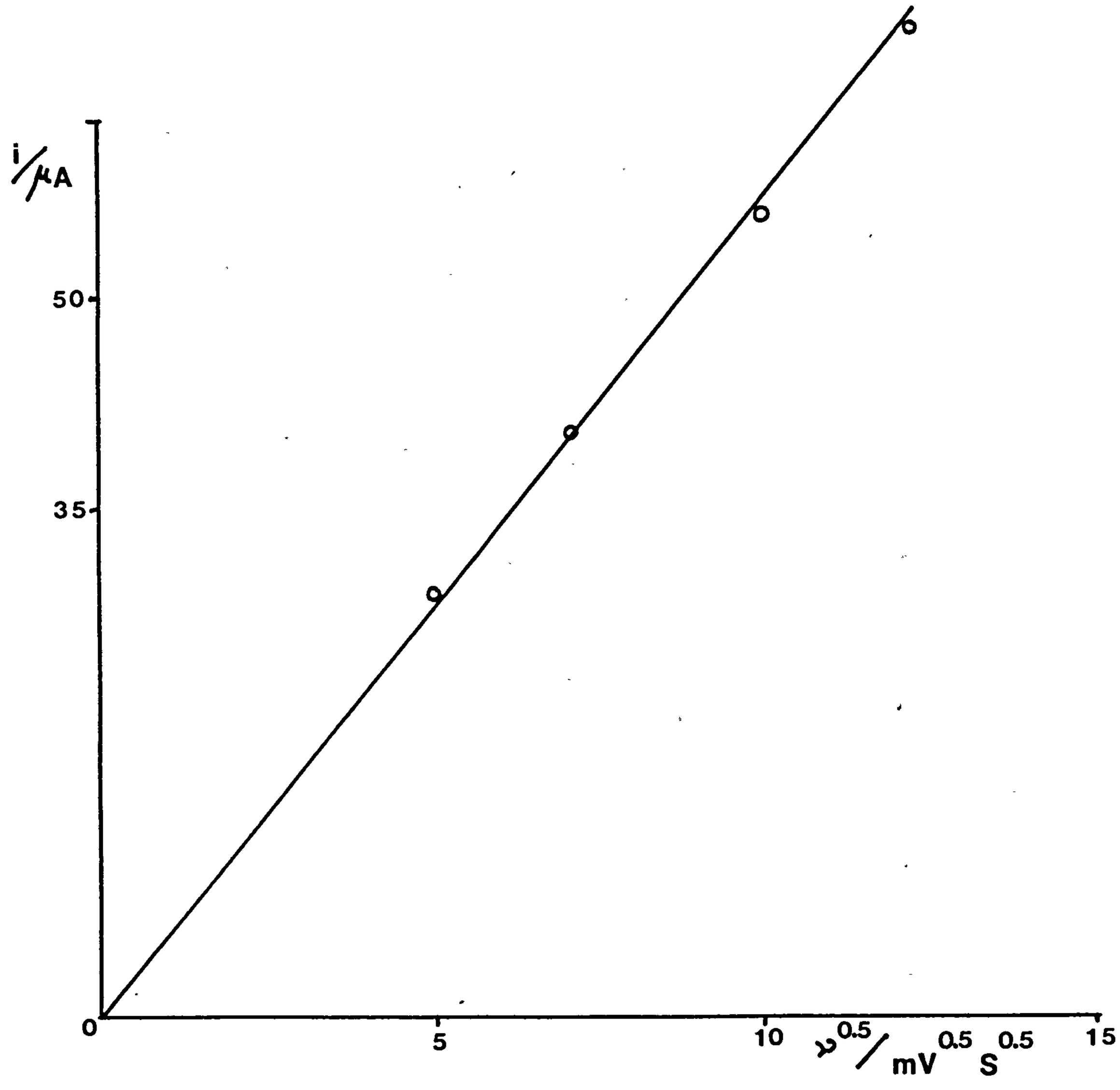
i/μA
50
35
0
5
10
15
ν^0.5/mV^0.5 S^0.5

relationship of E versus $\sqrt{\nu}$. This is in contradiction of the fact that for purely diffusive control the Ep is constant and suggests a passivation process in the sense of Müller (P. 41). The insulating lead sulphate film is formed by an electrocrystalization mechanism and limitation to total passivation and current flow is caused by the solution resistance in pores formed due to intercrystal collision and overlap. This process has been observed by others.[6,147,148] A further observation is that as sweep speed is increased although i_p increases the total charge in the peak is reduced. This suggests the deposition of a thinner film of sulphate at higher sweep rates. The value of the diffusion coefficient is found to be lower at lower temperatures as expected.

Figure 6.7 shows the data corresponding to a saturated 1M H_2SO_4 solution of Indulin C . This method of solution preparation was used due to the great insolubility of Indulin C in sulphuric acid, the saturated solution containing a barely detectable amount of the organic material although the solution was a very pale yellow colour. When the temperature was lowered the voltammogram current was everywhere reduced, however, the degeneration of the shape into a single line for a quasi-polarisable system was not observed. Even reducing the temperature to -6°C (at which the onset of electrolyte slushing was observed) did not produce the quasi-polarisability. This forces the conclusion that the presence of Indulin C in solution inhibits the formation of a highly ordered completely passivating lead sulphate film.

Throughout the experimental temperature range the current in the voltammogram increased with increasing sweep speed. However, this relationship for the Indulin C systems is for i_p

Figure 6.7

Linear Sweep Voltammogram of the Pb(II)/Pb System, in 1M H_2SO_4 saturated with Indulin 'C' expander, at $18^{o}C$.

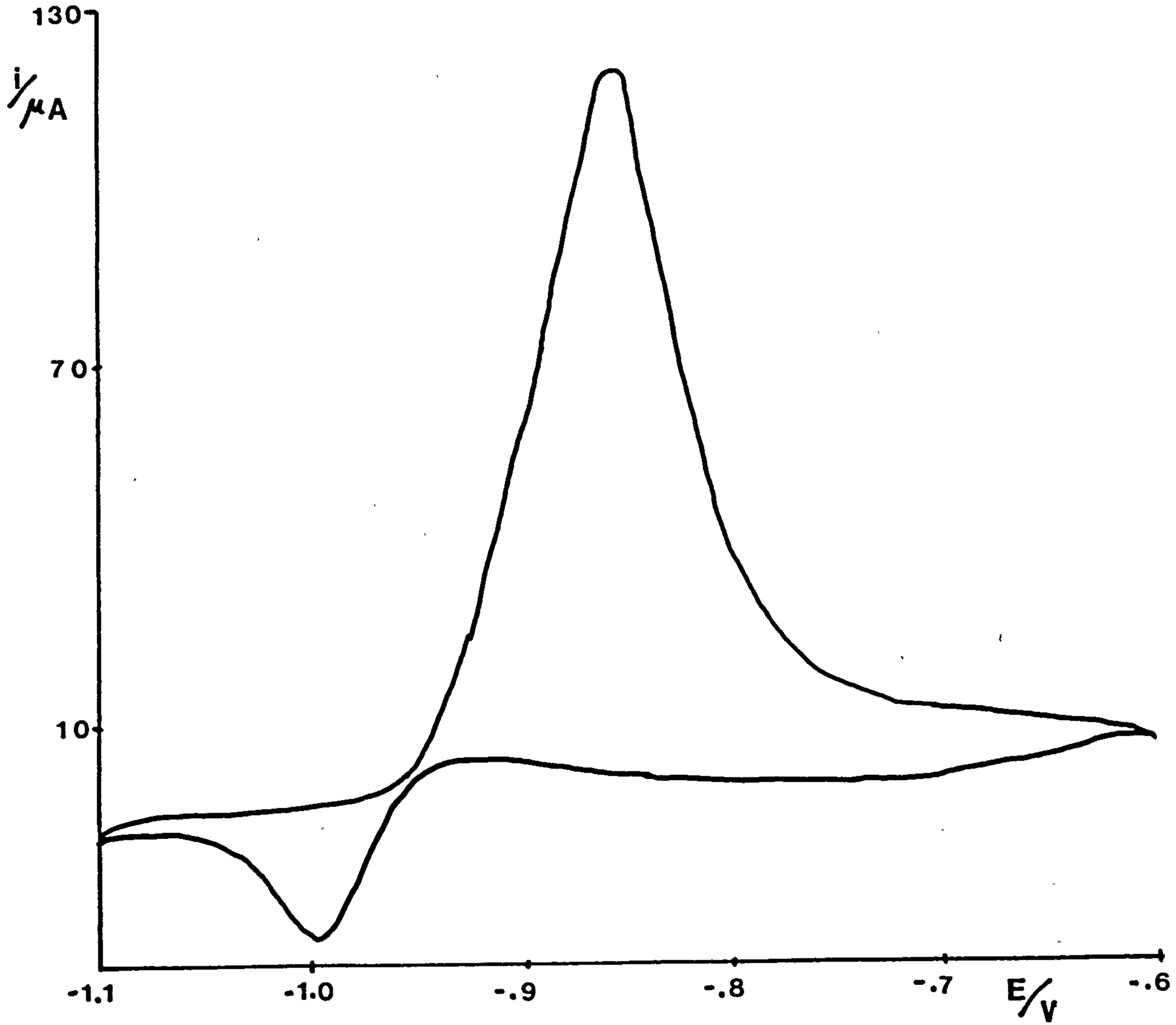
130
i/μA
70
10
-1.1
-1.0
-.9
-.8
-.7
-.6
E/V

to be rectilinear with the sweep speed. We can interpret this if the electrode passivates when a completed layer of $PbSO_4$ is formed on the surface. Since charge (q_p) in the voltammetric peak is simply the peak area (A_p) divided by the sweep rate (ν) then if the peaks remain the same shape at all sweep rates

$$i_p = C\nu \qquad (6.1)$$

where C is a constant proportional to the film thickness.

Figure 6.8 shows that equation (6.1) adequately describes the behaviour.

The value of C depends on the temperature, and the reduced slopes of the i_p and ν lines as the temperature is decreased indicate that at lower temperatures the thickness of the film required to passivate the electrode is reduced.

6.4 Discussion and Conclusions

The influence of "Indulin C" in suppressing the transformation of the electrode cycling behaviour from the active to the quasi-polarisable condition is a new aspect of expander behaviour. The specific effect may be the creation by the expander of lattice defects in the $PbSO_4$ phase which inhibit the formation of the ordered structure found in expander free systems at low temperatures. Thus in the presence of the Indulin C the current is not controlled via the passage across and through the lead sulphate film whereas in the Indulin C free system it is.

An Arrhenius plot for the temperature dependence of the process of diffusion in the $PbSO_4$ film is shown for the diffusion controlled systems in Figure 6.9. The enthalpy of activation for

Figure 6.8

The ip versus ν relationship for the Pb(II)/Pb System in 1M H_2SO_4, saturated with Indulin 'C' expander.

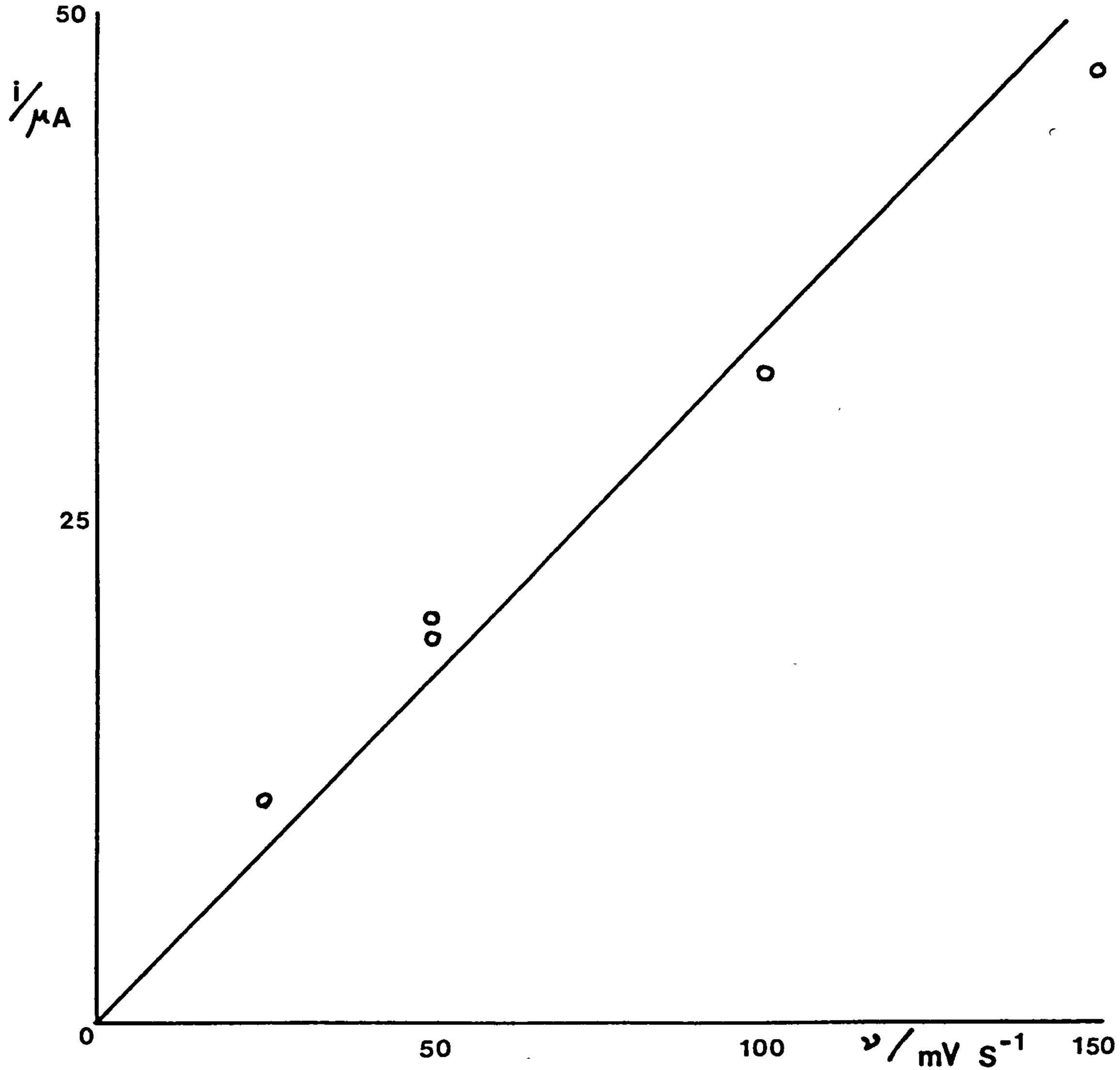
50
i/μA
25
0
50
100
ν/mV S⁻¹
150

Figure 6.9

Arrhenius Plot of ln D versus 1/T for the Pb(II)/Pb System in 1M H_2SO_4.

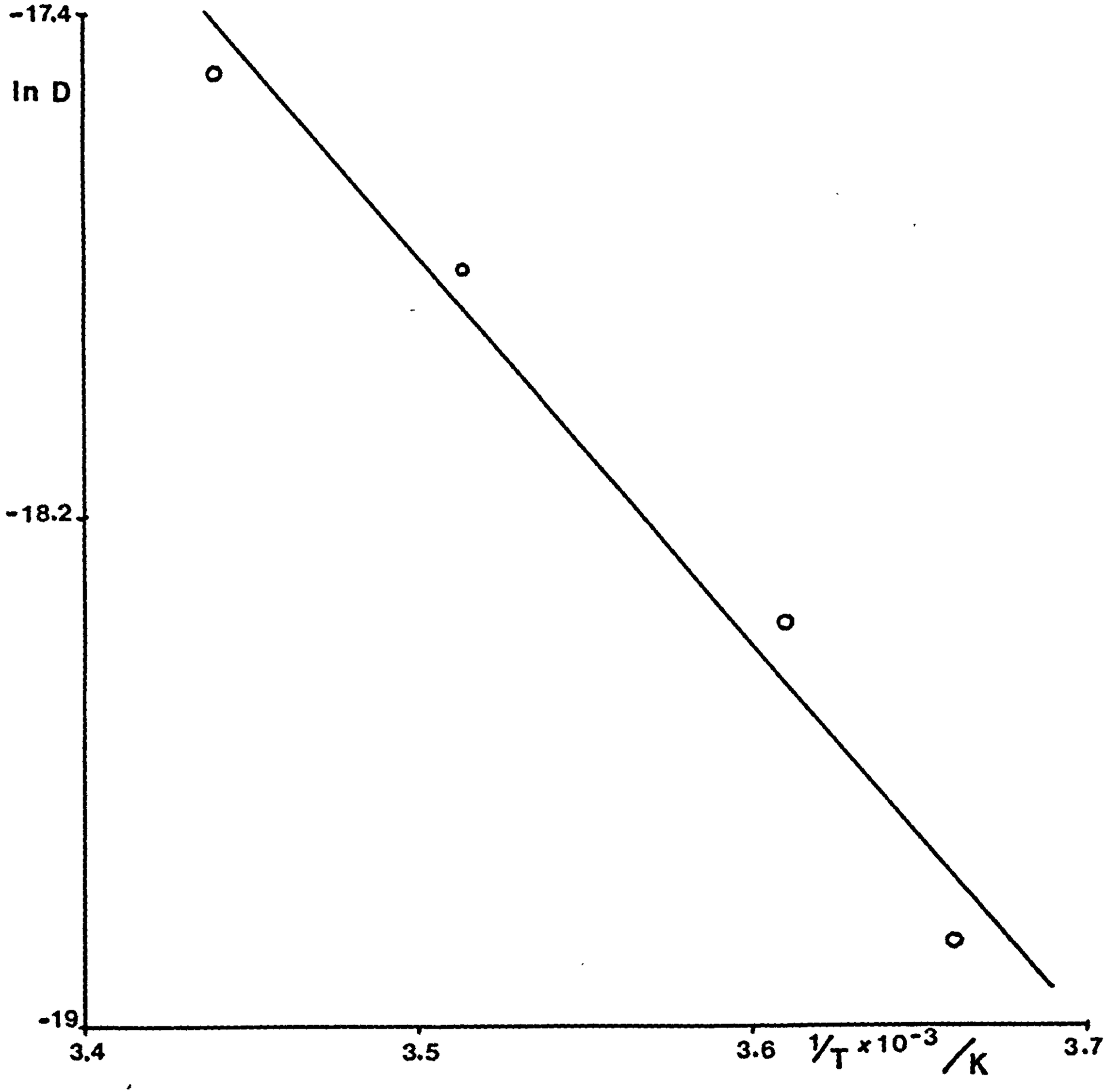
-17.4
ln D
-18.2
-19
3.4
3.5
3.6
1/T x10-3 /K
3.7

the diffusion process is 52 kJ mol^{-1}. This value is in excess of the value expected for simple diffusion in solution and supports the conclusion that the controlling diffusion is in the solid phase.

Figure 6.10 shows the Arrhenius plot for the Indulin C-containing system where lnC from equation (6.1) is plotted against 1/T. The enthalpy of activation for the formation of the passivating film is 27 kJ mol^{-1} sufficiently close to the diffusional enthalpy above to enable the Indulin C to exert a control over which mechanism solid state diffusion or film formation controls the current.

It is worth noting that in both the case of Indulin C containing and Indulin C free systems, no diffusion control in solution could be found by rotating disc examination after electrode cycling to constant i-E profile. Investigations of the polished electrode before cycling confirmed the solution species in 1M sulphuric acid, Chapter 7 extends this to 5M sulphuric acid.

Figure 6.10

Arrhenius Plot of ln C versus 1/T for the System saturated with expander.

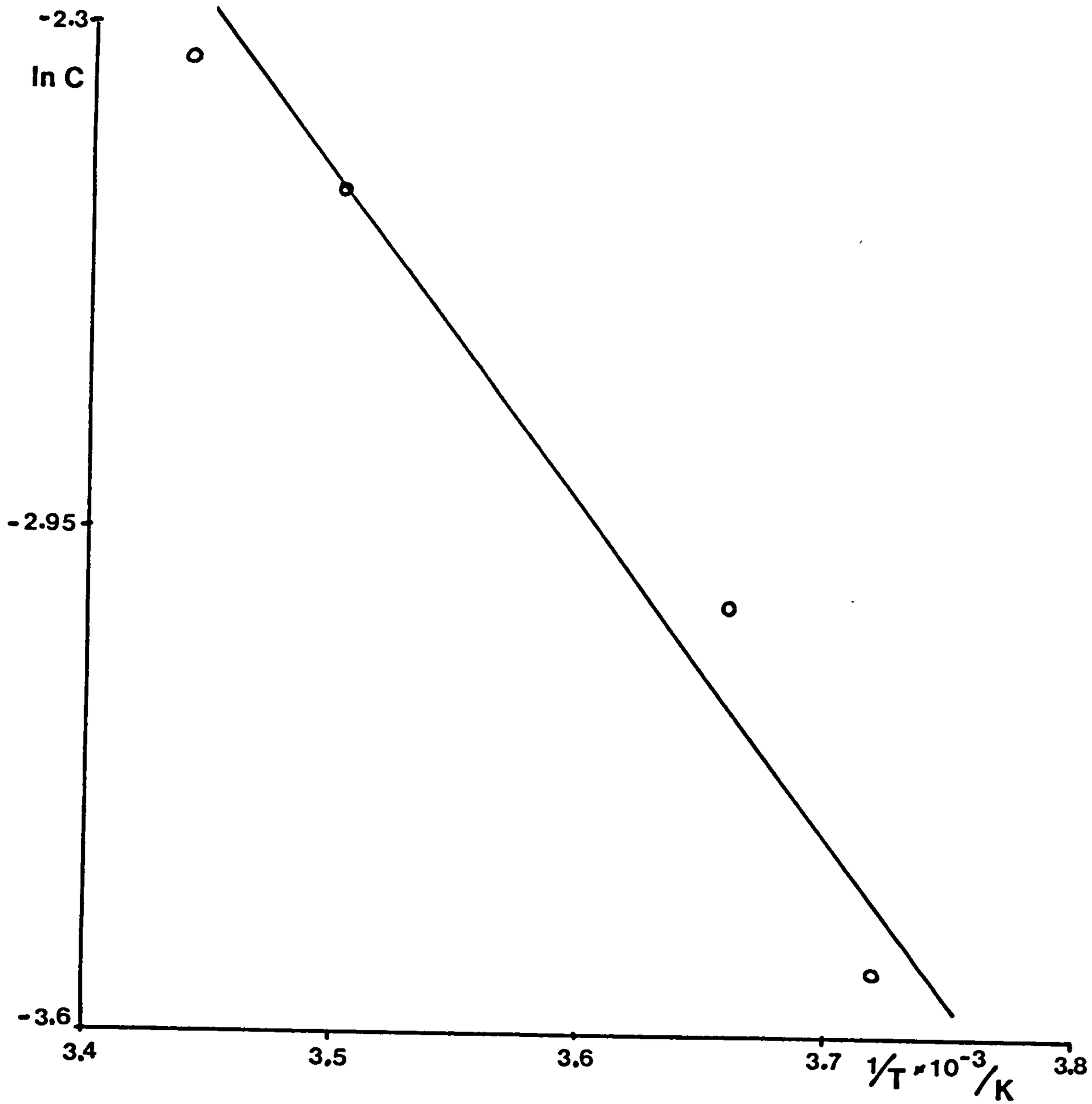
-2.3
ln C
-2.95
-3.6
3.4
3.5
3.6
3.7
3.8
1/T ×10⁻³/K

C H A P T E R 7

REACTIONS AT LEAD ELECTRODES IN 5M SULPHURIC ACID NEAR THE EQUILIBRIUM POTENTIAL

7.1 Introduction

There is no doubt that in dilute sulphuric acid solution the lead negative electrode reaction can involve solution Pb^{2+} species provided that the electrode is not driven too far positive into the potential region where solid phase $PbSO_4$ is thermodynamically stable at the electrode. Confirmation of this has been provided by a number of investigations due to Harrison et al,[17,21] Armstrong and Bladen[22] and Hampson et al.[23-26] The existence of reaction participating Pb^{2+}aq. species and the kinetic interpretation of the electrometric measurements concerned with the solution reaction has lead to the suggestion of a rather complex electrode reaction[26,28] involving a binuclear lead species.

Considerable difficulty was encountered in trying to extend the detection of Pb^{2+} species to concentrations of H_2SO_4 corresponding to the operating conditions of a lead acid cell. It has been suggested that the reasons for this include the lower solubility of $PbSO_4$ in the concentrated acid and the increased sulphate activity. There are undoubtedly complicating factors which will reduce the lead dissolution region by 30 mV for each ten-fold decrease in solubility, however, it should be possible to detect a "free dissolution" window even at very low solubilities. The possible effects of expander materials on this solution reaction are of considerable interest. This Chapter

records the results of an investigation of these effects using a rotating disc technique.

7.2 Results and Discussion

Experiments with a large number of electrode surface preparation methods indicated that the subsequent behaviour of the electrode in the vicinity of the equilibrium potential was crucially dependent upon the surface characteristics. It was apparent that an electrode system which would provide evidence of a solution reaction in which Pb^{2+} ions freely leave the electrode was difficult to prepare. Moreover once a film of $PbSO_4$ had been produced at the electrode it was not possible to demonstrate a solution Pb^{2+} reaction by any in-situ treatment that could be devised. The best method of obtaining the solution reaction was found to be electrolytic etching in a complex solution of perchloric acid, ethanol and ether ($HClO_4$ - 60%, 45 parts; C_2H_5OH, 50 parts; $(C_2H_5)_2O$, 5 parts). Most of the usual methods of electrode pretreatment, mechanical or electrolytic, did not result in evidence for a solution Pb^{2+} reaction irrespective of the in-situ treatment of the electrode following the initial electrode/electrolyte contact. Mechanical polishing with successively finer grades of carbide paper and finishing with γ alumina was the initial pretreatment. This was followed by various aqueous electrolyte etches based on nitric or perchloric acids. The organic etch given above was adopted since this was indicated to successfully produce the Pb^{2+} dissolution reaction in Archdale and Harrison's[17] investigation of the process in 1M sulphuric acid.

A simple chemical etch based on nitric acid (10%) generated an electrode free of any evidence for Pb^{2+} in the sulphuric acid electrolyte. This latter chemical treatment represented the extreme of complete solid state $PbSO_4$ formation in contrast to that of a limited solution behaviour resulting from the non-aqueous electrolytic process. These two extremes were chosen for experimental study. The aqueous etch of 40% fluoroborate, 2% sulphuric acid which produced an identical Pb^{2+} dissolution effect to the organic, in Archdale and Harrison's work,[17] was found not to be effective when transferring to 5M acid.

7.2.1 Experiments with $HClO_4$ - C_2H_5OH - $(C_2H_5)_2O$ etch

Contrary to previous experience with 1M electrolytes it was not found possible to completely eliminate the reduction current due to hydrogen ion at the rotating disc electrode. This reduction current arises due to the high hydrogen ion concentration. The presence of traces of oxygen enhances the total reduction current[22,26] and generally it was found expedient to reduce these currents to very low values by purging with nitrogen over a long period. It was not found to be possible to completely eliminate the cathodic reduction current. This complicated the electrochemistry since the hydrogen reduction intruded into the lead dissolution process.

Figure 7.1 shows the results of experiments in which lead RDE's were rotated at carefully controlled potentials close to the rest potential. From equation 2.66 the case where R is a solid metal can be derived

$$\frac{\partial i}{\partial \Omega^{\frac{1}{2}}} = \frac{0.0643\ v^{1/6}\ \ (k_b D_R^{-2/3} - k_f\ D_{ox}^{-2/3})}{nF\ (k_f\ C_{ox} - k_b C_R)} \qquad (2.66)$$

Figure 7.1

Relationship between current and rotation speed at a series of potentials. Pb electrode, 5M-H_2SO_4, 23^{o}C. Electrochemical etch

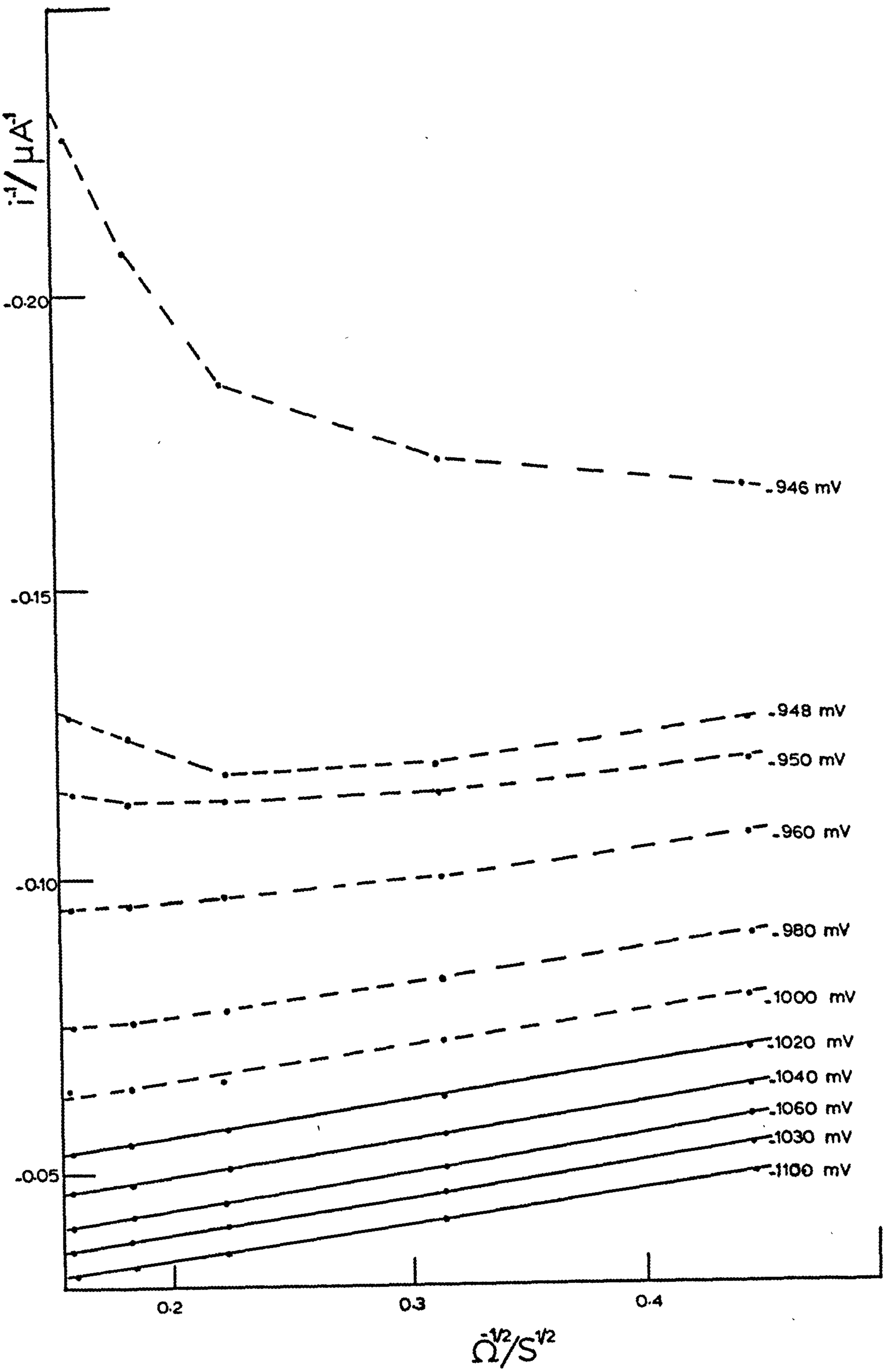
$i^{-1}/\mu A^{-1}$
-0.20
-0.15
-0.10
-0.05
-946 mV
-948 mV
-950 mV
-960 mV
-980 mV
-1000 mV
-1020 mV
-1040 mV
-1060 mV
-1030 mV
-1100 mV
0.2
0.3
0.4
$\Omega^{-1/2}/S^{1/2}$

when $C_R >> C_{ox}$ and $D_R^{-2/3} << D_{ox}^{-2/3}$

the slope becomes;

$$\frac{\partial i^{-1}}{\partial \Omega^{-\frac{1}{2}}} = \frac{0.643\ v^{1/6}}{nF} \qquad \frac{k_f\ D_{ox}^{-2/3}}{k_b\ C_R} \tag{7.1}$$

with intercept still

$$i^{-1} \text{ at } \Omega=0 = i_\infty^{-1}$$

The measurements at potentials more negative than the lead dissolution region give a series of parallel straight lines which have intercepts corresponding to infinite rotation speed currents (i_∞) which increase exponentially with potential. The change in i_∞ with potential (Figure 7.2) leads to a Tafel slope in excess of 200 mV dec^{-1} which is not uncommon for the hydrogen ion reduction reaction at an electrocatalyst of only fair activity.[6]

By extrapolation of the hydrogen reduction lines back into the lead dissolution region the net currents observed were corrected at each rotation speed in order to obtain the lead dissolution current i_{Pb} assuming that

$$i_{net} = i_{Pb} + i_{H_2} \tag{7.2}$$

where i_{H_2} is the (negative) hydrogen reduction (cathodic) current. This correction when applied to the upward curving lines of Figure 7.1 allowed the calculation of the rotation speed dependence of i_{Pb} as shown in Figure 7.3. It is clear that these lines are sufficiently rectilinear to confirm that the lead dissolution current observed in the potential region bounded by -950 mV and -946 mV corresponds to a solution controlled dissolution reaction. At more positive potentials the current increased enormously and became rotation speed independent. The Tafel line in Figure 7.4

Figure 7.2

Tafel line for the hydrogen evolution process on electrodes of Figure 7.1.

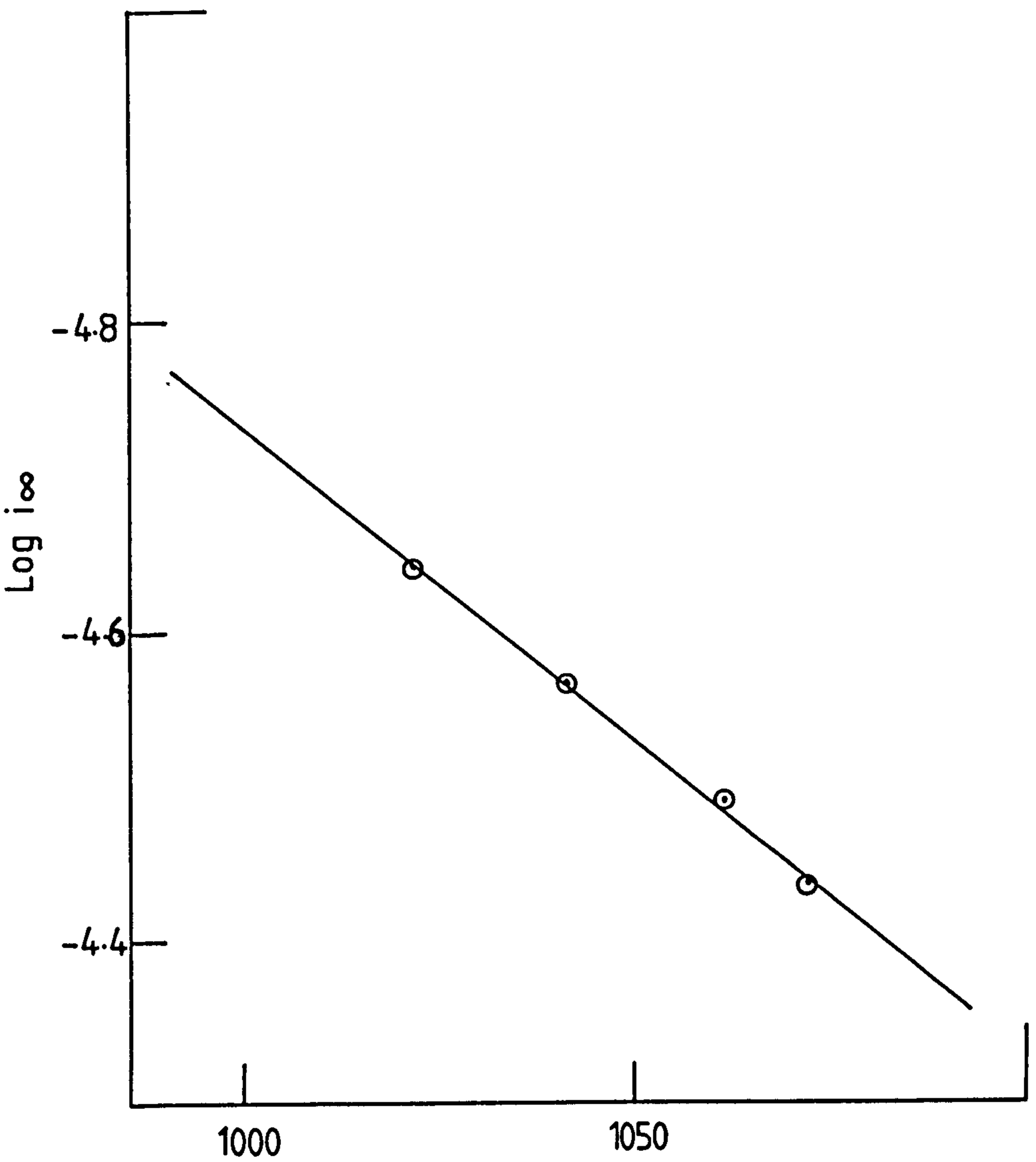
-4.8
-4.6
-4.4
Log i8
1000
1050
E/mV

Figure 7.3

Lead dissolution currents from the data of Figures 7.1 and 7.2.

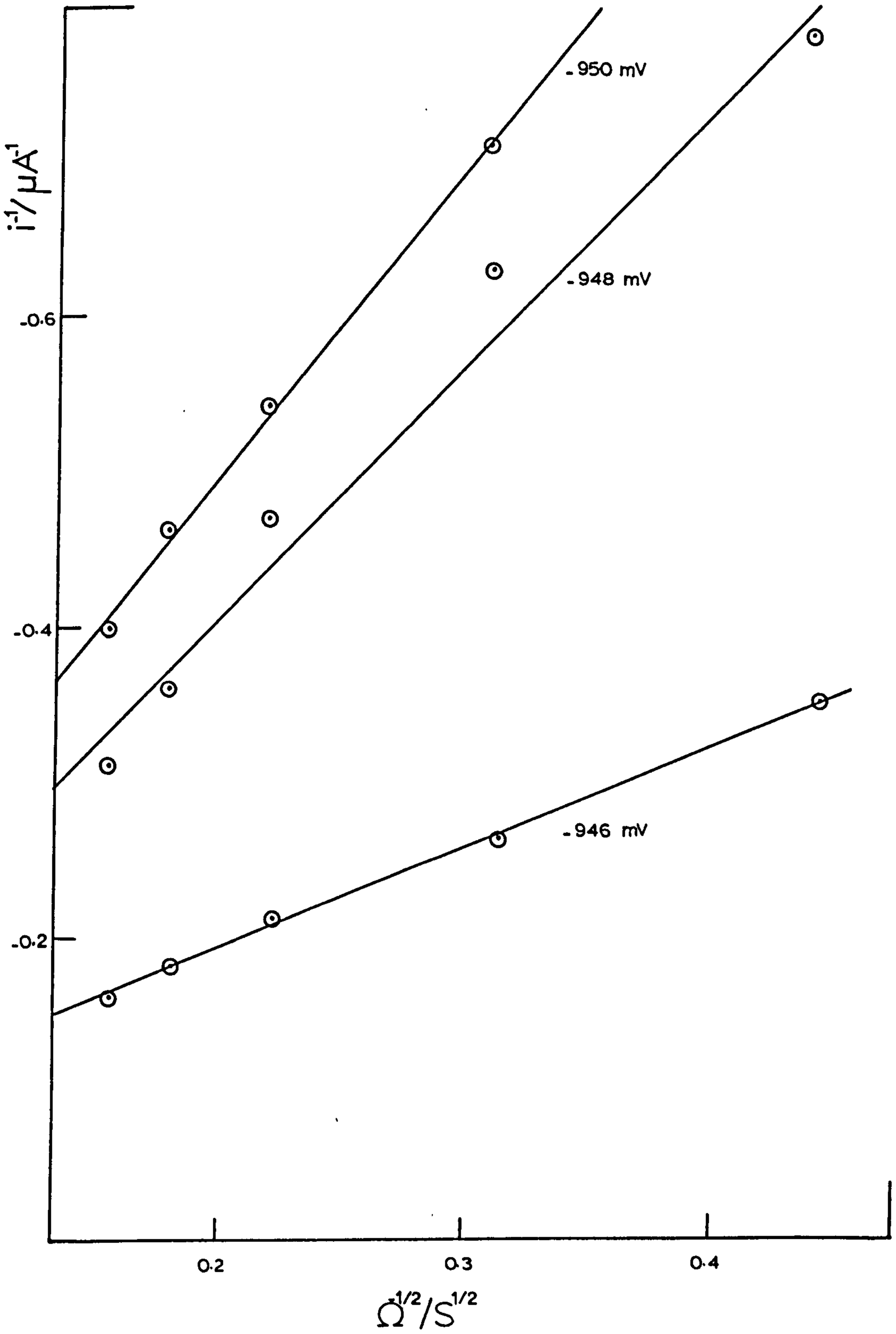
-950 mV
-948 mV
-946 mV
-0.6
-0.4
-0.2
0.2
0.3
0.4
$i^{-1}/\mu A^{-1}$
$\Omega^{1/2}/S^{1/2}$

Figure 7.4

Tafel line connecting the limited data for the lead dissolution process isolated in Figure 7.3.

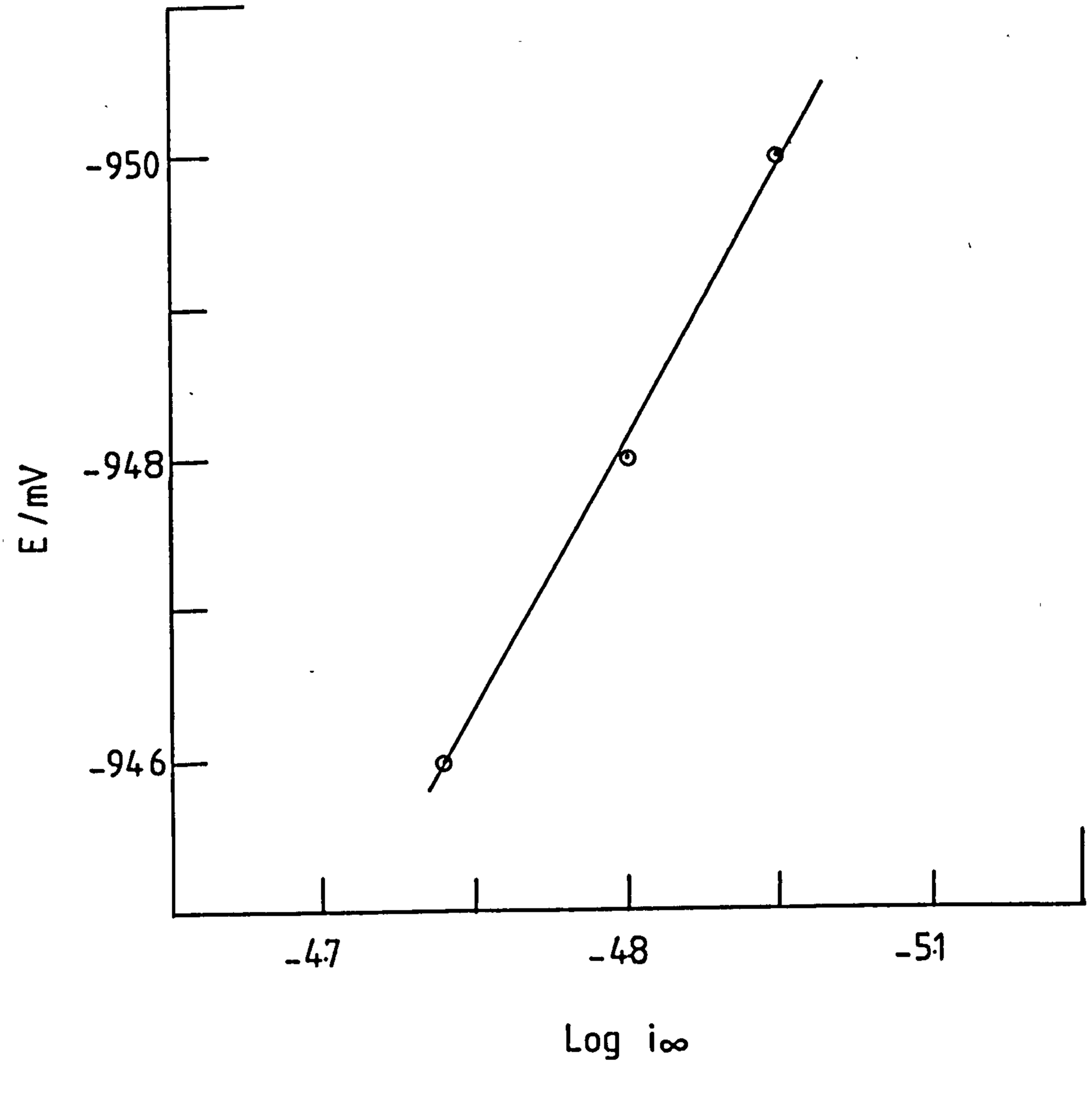
-950
-948
-946
E /mV
-4.7
-4.8
-5.1
Log i∞

represents the charge transfer controlled current i_∞, for lead dissolution (at infinite rotation speed) into 5M sulphuric acid. The Tafel slope here is rather lower $\simeq$ 20 mV than was obtained by Hampson and Lazarides[26] for 1M H_2SO_4. This is probably due to the adsorption of Pb^{2+} (or a species based on Pb^{2+}) at the electrode, at any rate the potential is such that the electrode is almost under conditions where no Pb^{2+} leaves the surface so that the reaction becomes completely solid state.

The slope dependency as calculated by the introduction of equation 2.29

$$k_f = k^\ominus \exp \{-\alpha\ nF\ (E-E^\ominus_{rev})/RT\}$$

$$k_b = k^\ominus \exp \{(1-\alpha)\ nF\ (E-E^\ominus_{rev})/RT\}$$

into (7.1) giving

$$\frac{\partial i^{-1}}{\partial \Omega^{-\frac{1}{2}}} = \frac{0.643\ v^{1/6}}{nF} \quad \frac{D_{ox}^{-2/3}}{C_R} \quad \exp \{-nF\ (E-E^\ominus_{rev})/RT\} \qquad (7.3)$$

Thus a plot of $\log \left(\frac{\partial i^{-1}}{\partial \Omega^{-\frac{1}{2}}}\right)$ versus E is linear with slope

$$\frac{\partial \log \left(\frac{\partial i^{-1}}{\partial \Omega^{-\frac{1}{2}}}\right)}{\partial E} = -2.303\ \frac{RT}{nF} \qquad (7.4)$$

and intercept

$$\log \left\{ \left(\frac{\partial i^{-1}}{\partial \Omega^{-\frac{1}{2}}}\right)_{E=E^\ominus_{rev}} \right\} = \log \{1.62\ v^{1/6}\ D_{ox}^{-2/3}/nFC_R\} \qquad (7.5)$$

gives very low values (Fig. 7.5) indicating the likelihood that conditions were on the edge of almost complete adsorption.

Figure 7.5

The dependence of $(\partial i^{-1}/\partial \omega^{-\frac{1}{2}})_E$ on potential from Figure 7.3.

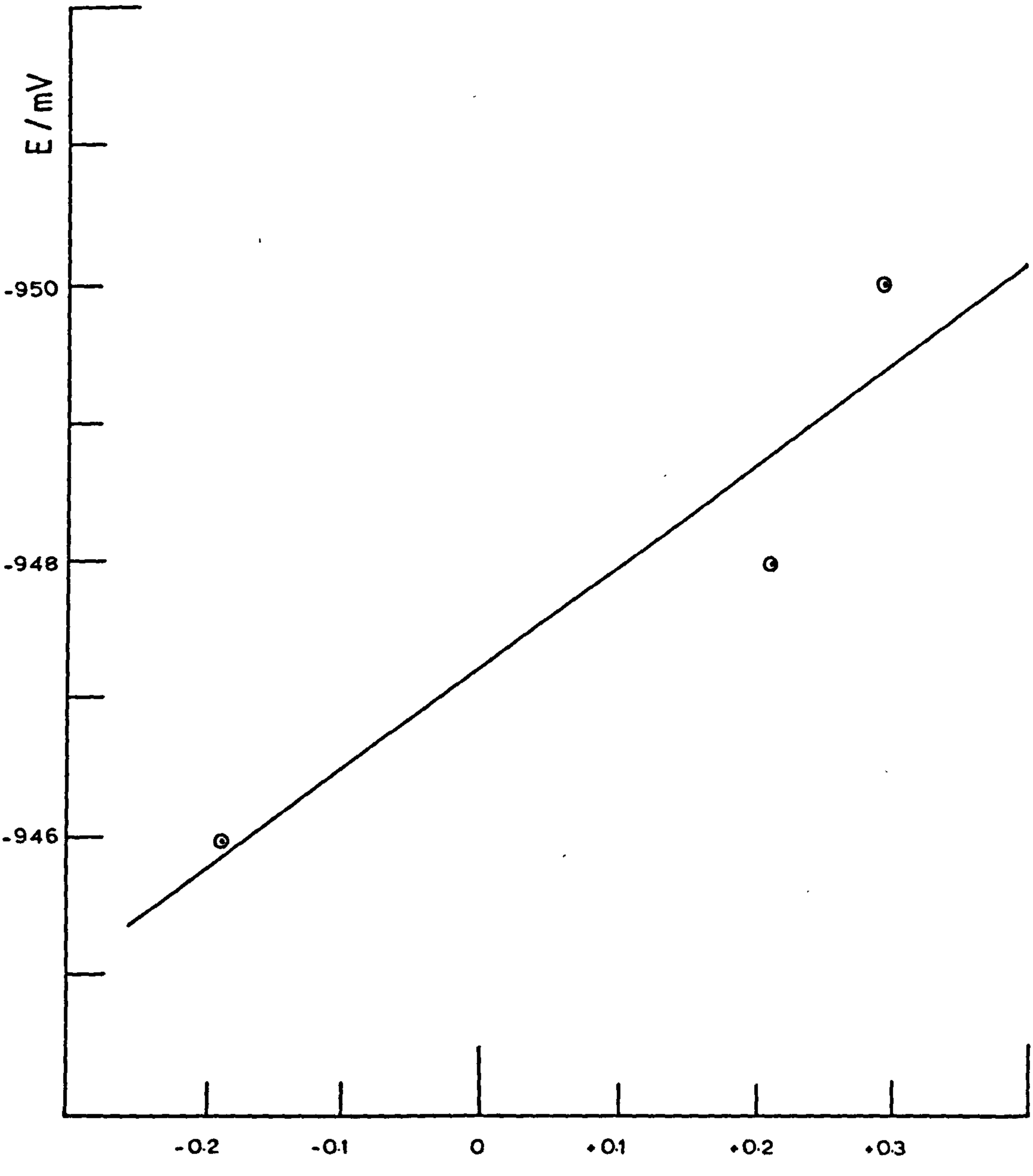
E / mV
-950
-948
-946
-0.2
-0.1
0
+0.1
+0.2
+0.3
log ∂i⁻¹ / ∂ω^-1/2

It can be concluded that there is a solution controlled lead dissolution reaction in 5M H_2SO_4 and that this occurs in a very narrow range of potential between -950 and -946 mV. Within this narrow window the reaction at the electrode under battery conditions (5M H_2SO_4) involves a simulatneous reduction of solution H^+ to form H_2 together with a lead dissolution process.

7.2.2 The effect of an expander material in the solution

An expander material (Indulin C) was introduced into the electrolyte in order to see the effect on the solution reaction. Figure 7.6 records the data from the RDE experiments. In the hydrogen region a family of straight lines similar to that observed in absence of expander was obtained. Subtraction in accordance with equation (7.2) showed that there was, within experimental limits, considerably less current due to lead dissolution at any potential in the (original) dissolution range up to the limit of the $PbSO_4$ region (Figure 7.7). Moreover as shown in Figure 7.8 the rotation speed dependence was not characteristic of a solution reaction and it is clear that the electrode was on the threshold of a solid state process. The current calculated for the case of the Indulin C saturated solution did not form well-defined i^{-1} - $\omega^{-\frac{1}{2}}$ lines, in fact the correlations exhibited an opposite gradient to that expected for a solution process. This would suggest that a cathodic solution process is occurring. This process can only be ascribed to some reducible component being present in the Indulin C. The increase in cathodic current with rotation speed appearing as an apparent reduction in anodic current. Moreover the $PbSO_4$ phase deposition initiation potential was found to be more positive by $\simeq$ 25 mV

Figure 7.6

Relationship between current and rotation speed at a series of potentials when electrolyte solution is saturated with Indulin C.

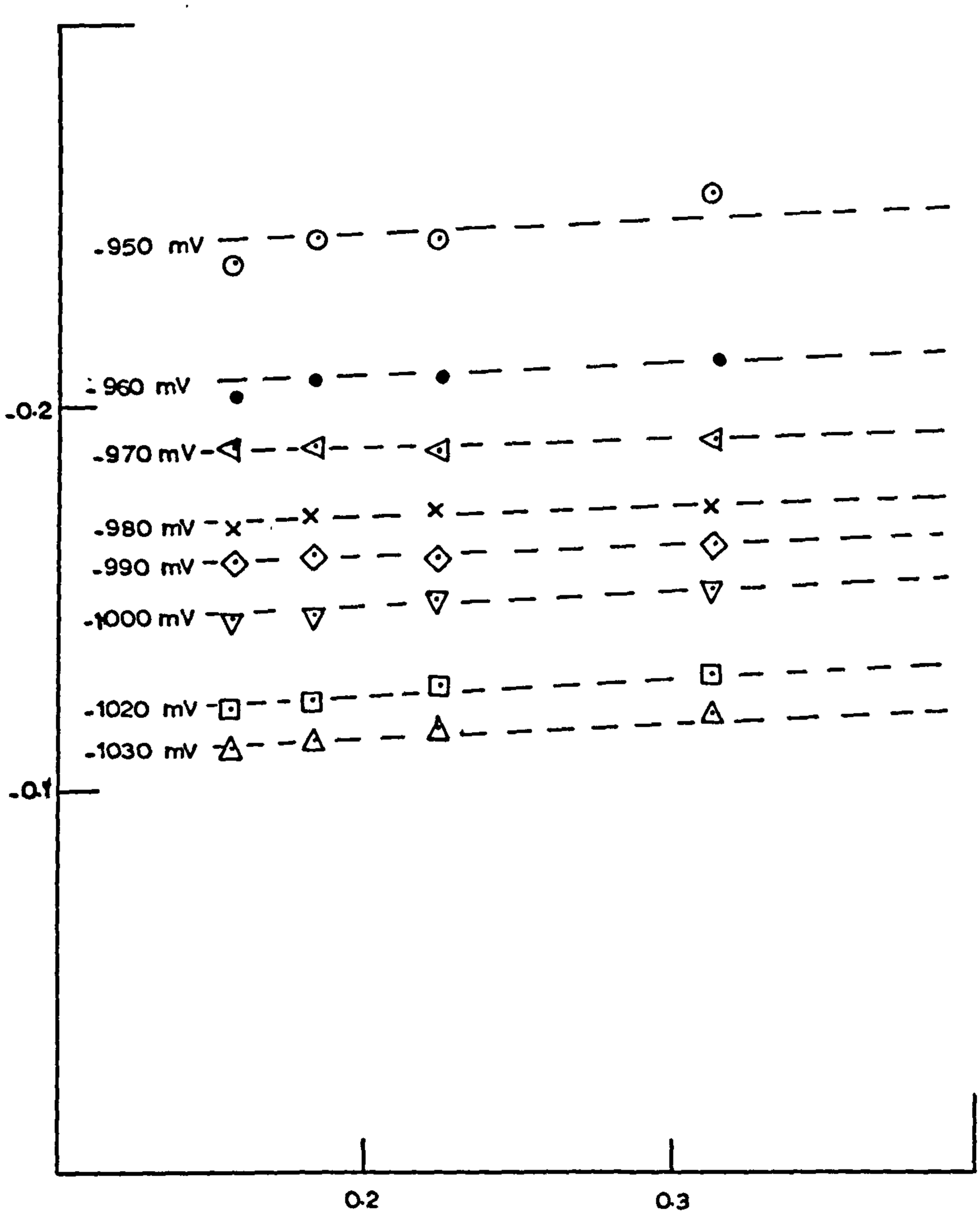
-950 mV
-960 mV
-970 mV
-980 mV
-990 mV
-1000 mV
-1020 mV
-1030 mV
-0.2
-0.1
i^{-1} / μA^{-1}
0.2
0.3
$\Omega^{1/2}$ / $Sec^{1/2}$

Figure 7.7

Tafel line for the hydrogen evolution process from the data of Figure 7.6.

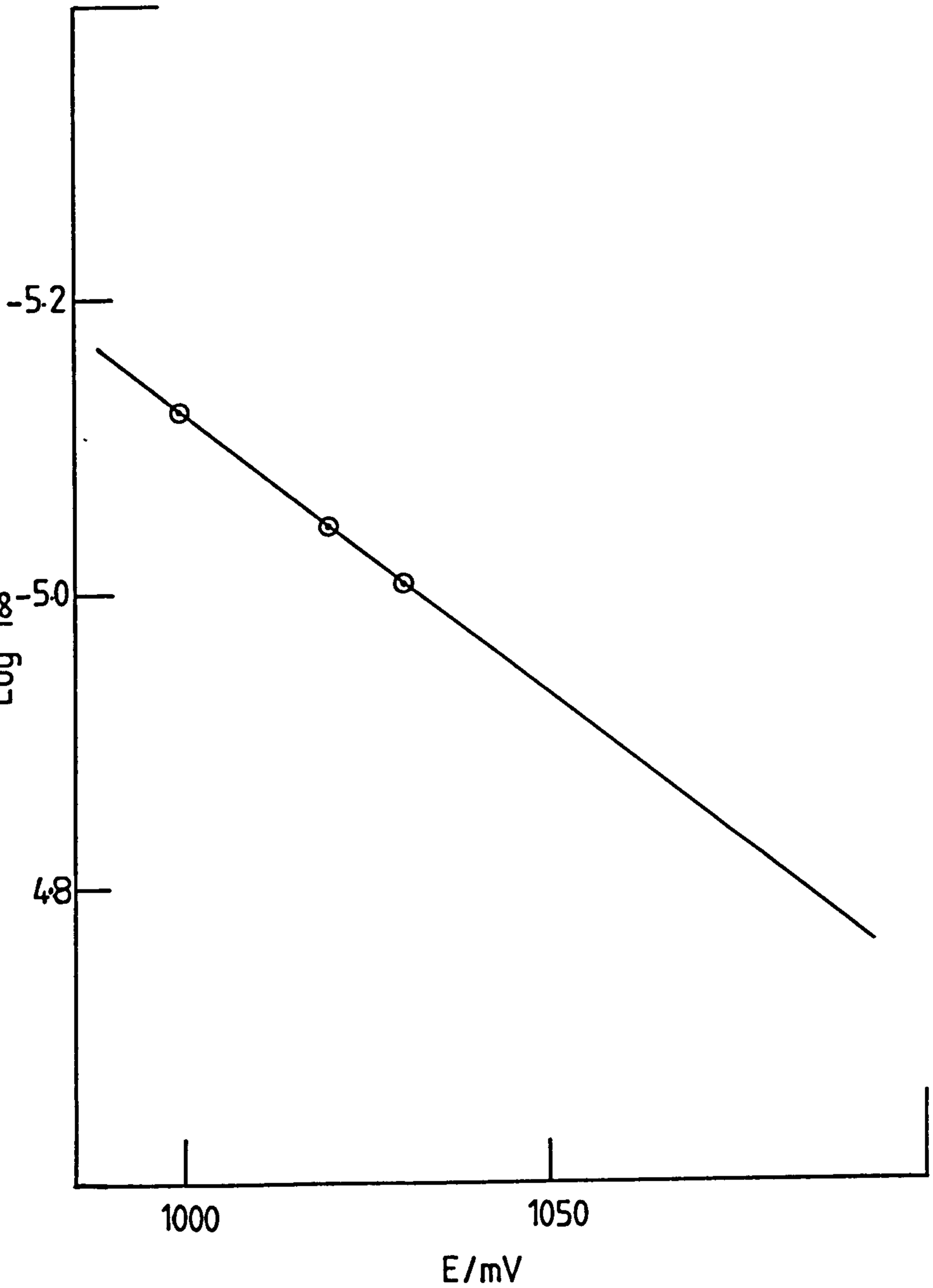
-5·2
-5·0
-4·8
Log i
1000
1050
E/mV

Figure 7.8

Residual anodic currents after the removal of the estimated hydrogen current (Figure 7.7) from the data of Figure 7.6.

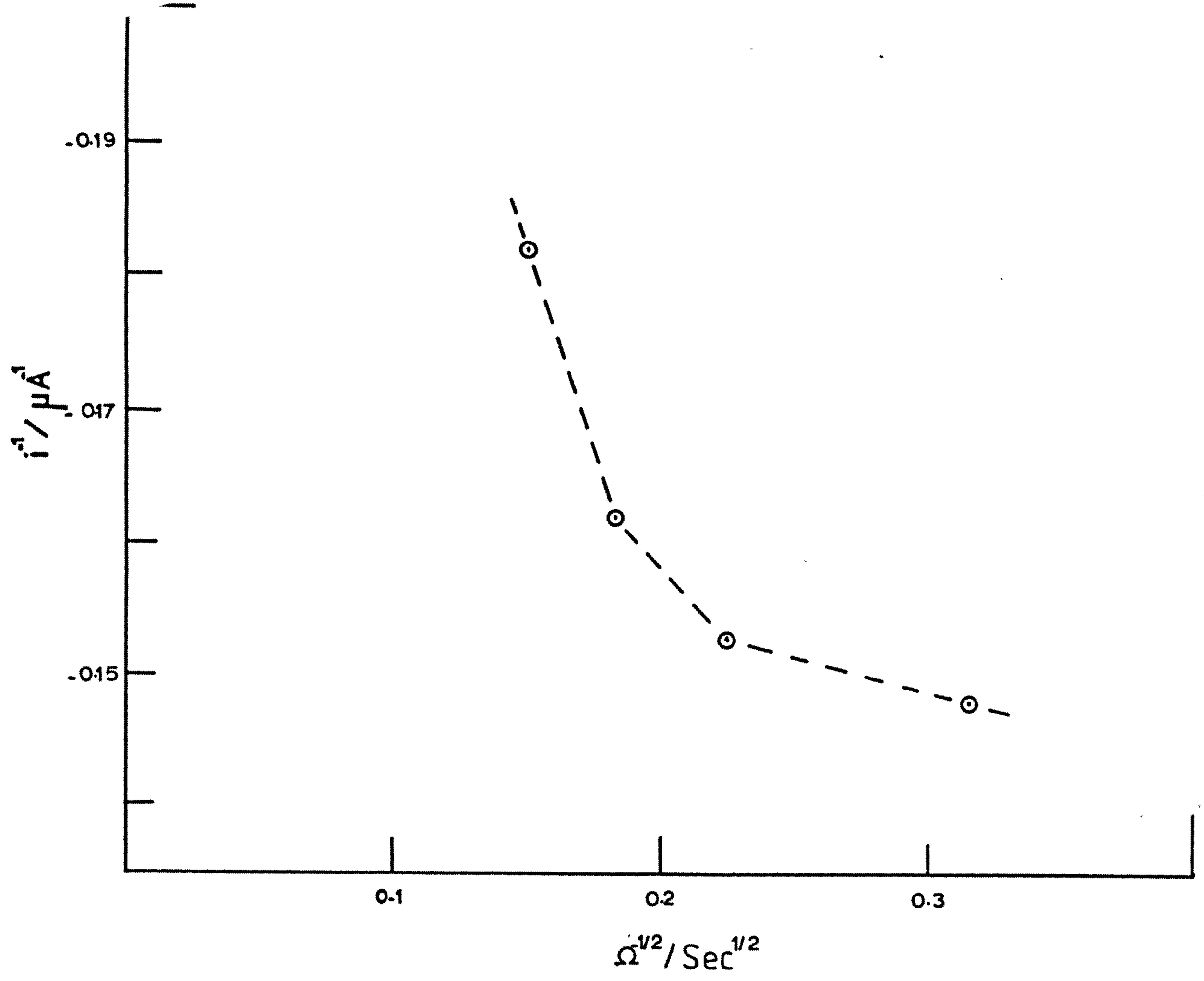
-0.19
-0.17
-0.15
$i^{-1}/\mu A^{-1}$
0.1
0.2
0.3
$\Omega^{1/2}/Sec^{1/2}$

than in the pure sulphuric acid solution. The existence of this positively shifted region in the case of the expander indicated that not only is the solution process suppressed but the solid state electrocrystallisation process is inhibited. The anodic shift is also in agreement with the findings of Archdale and Harrison in 1M H_2SO_4 at solid lead electrodes. However the shift observed in their case was 15 mV, this apparent discrepancy of 10 mV between 1M and 5M H_2SO_4 could possibly be explained by differences in the efficiency of adsorption with the degree of ionisation of Indulin C. The fact that a potential shift in nucleation point does occur suggests a reduction in crystallization rate in the presence of expander possibly due to structural hinderance of mass transfer.

These observations suggest that the expander acts via an adsorbed electrode film which both inhibits nucleation of $PbSO_4$ and hinders the progress of Pb^{2+} ion across the interphase possibly by combination of Pb^{2+} with the adsorbed film.

7.2.3 Experiments with chemically etched Pb (10% HNO_3 - 1.67 mol.l^{-1})

In order to avoid any possibility of solid phase formation due to intruding reactions the etched electrode was introduced into the cell (after washing) with the polarising circuit maintained in the hydrogen region. This avoided the production of any surface films due to the initial electrode/electrolyte contact. The current flowing on this initial contact is shown in Figure 7.9 an initially high current as the electrode is covered with H_2 species gives way to a steady-state indicating absence of films. Steady state measurements were made at a series of potentials in the range -1150 to -946 mV as shown in Figure 7.10. The strong

Figure 7.9

Chemically etched electrode (10% HNO_3). Current on electrode/electrolyte contact at -1150 mV (8.5 rps).

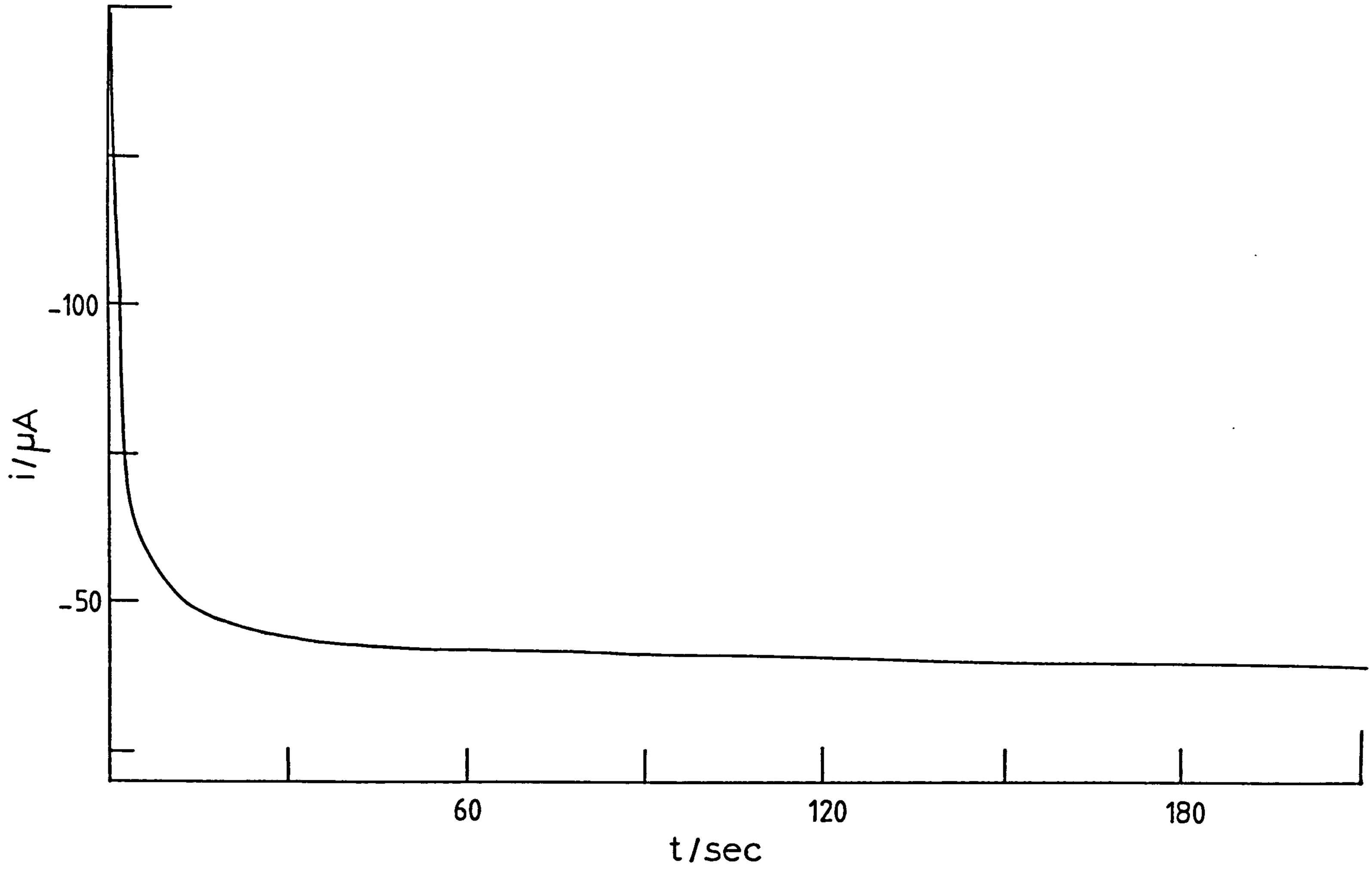
-100
-50
i/μA
60
120
180
t/sec

Figure 7.10

The dependence of current and rotation speed in the potential region -1150 mV to -946 mV. Pb electrode, 5M H_2SO_4, 23°C. Chemical etch 60 s (10% HNO_3).

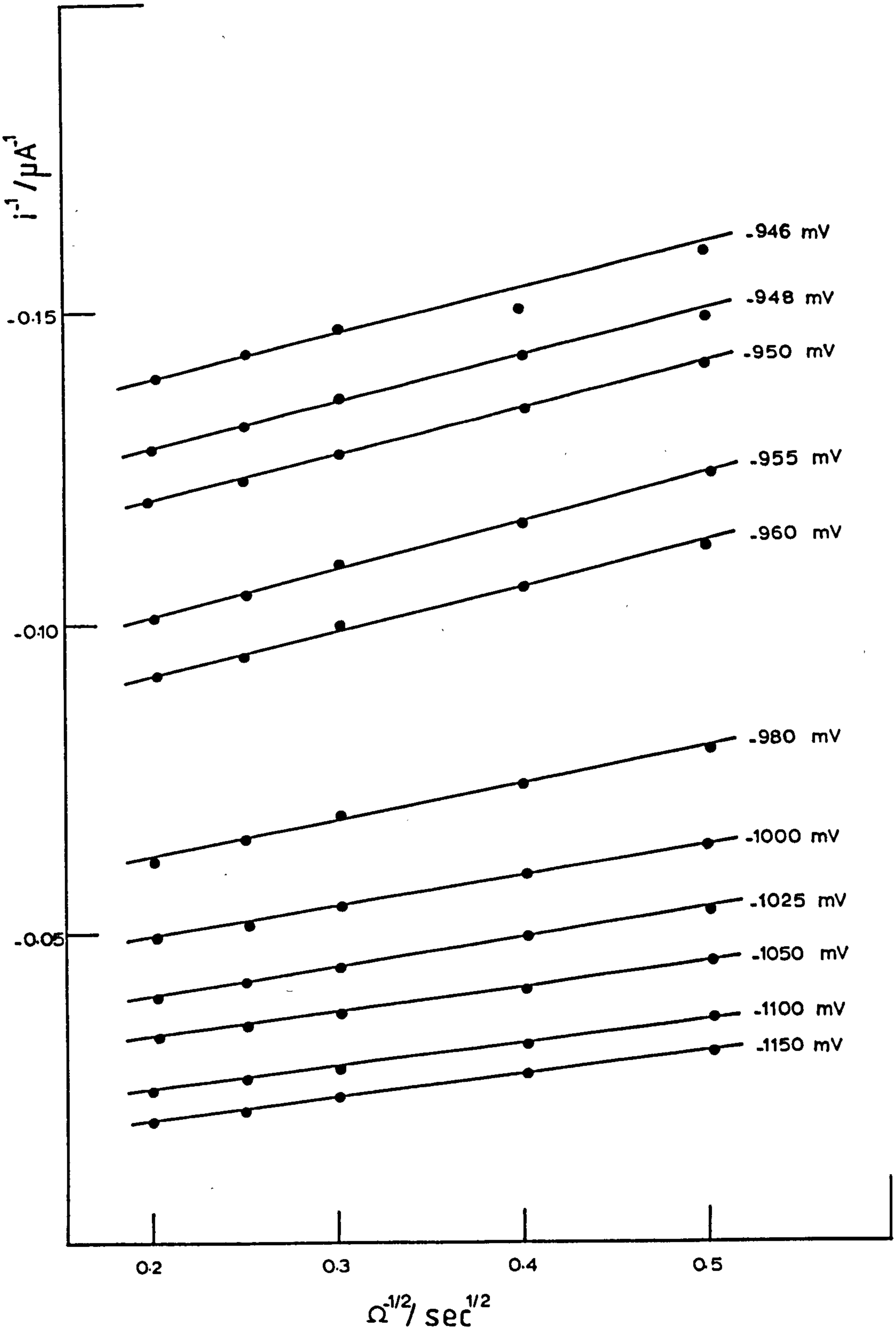
$i^{-1}/\mu A^{-1}$
-0.15
-0.10
-0.05
-946 mV
-948 mV
-950 mV
-955 mV
-960 mV
-980 mV
-1000 mV
-1025 mV
-1050 mV
-1100 mV
-1150 mV
0.2
0.3
0.4
0.5
$\Omega^{-1/2}/\ sec^{1/2}$

influence of the etching process is shown by comparison of Figures 7.10 and 7.11 where the shorter etch engenders a more reactive electrode. Tafel plots in this region obtained by extrapolating the data of Figures 7.10 and 7.11 to infinite rotation speed are shown in Figure 7.12. The Tafel slopes approximate to the 120 mV dec^{-1} region at the more anodic potentials. In general the Tafel slopes are high, these have been discussed.[6]

At potentials more positive than -946 mV it was not possible to obtain steady state currents. This is shown convincingly in the data of Figure 7.13. The curve is a well-developed crystallisation transient and although the hydrogen evolution process intrudes significantly in the early stages (-Ve currents) the form of the transient is unequivocal.[151] The deconvolution of the hydrogen and $PbSO_4$ reaction cannot be made accurately enough to decide the dimensionality of the process, but to a first approximation it seems to conform to a two-dimensional instantaneous nucleation and growth process. The shorter etch produces the higher current transient and must have given rise to the larger surface population of active centres.

It can be concluded that the etching process engenders a film (possibly oxide or hydroxide) which on contact with the electrolyte at -946 mV forms a thermodynamically stable film of $PbSO_4$ over a period of about 1 h. This film is formed by a process of growth and overlap giving rise to a rising and falling current response. The early stages are complicated by the hydrogen reaction.

The process of the post etch film is likely to arise from the high exchange current when Pb dissolves. This probably

Figure 7.11

As Figure 7.10 but 5 s etch.

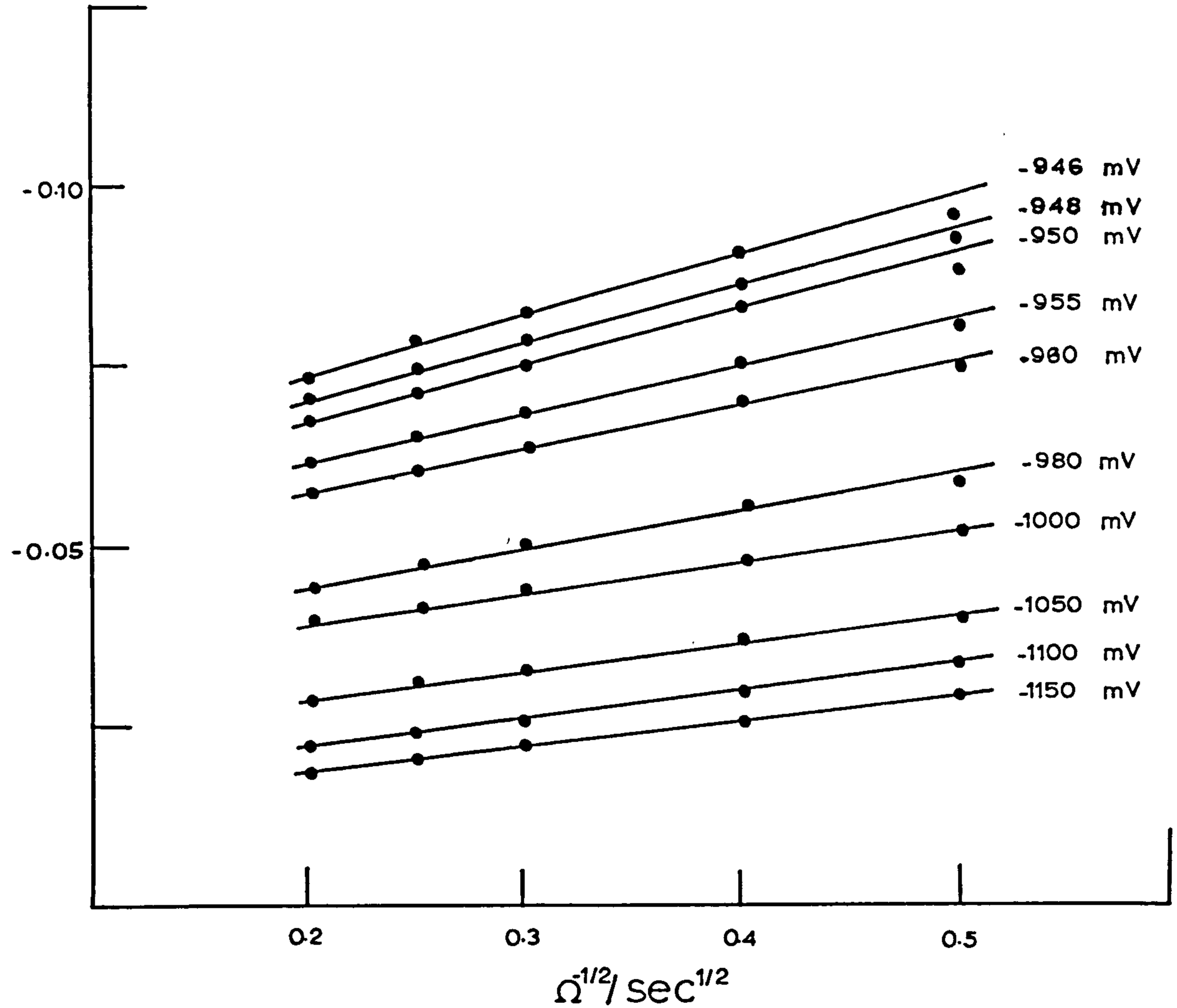
-0.10
-0.05
$i^{-1/2}/\mu A^{-1/2}$
-946 mV
-948 mV
-950 mV
-955 mV
-960 mV
-980 mV
-1000 mV
-1050 mV
-1100 mV
-1150 mV
0.2
0.3
0.4
0.5
$\Omega^{-1/2}/\sec^{1/2}$

Figure 7.12

Tafel plots corresponding to Figures 7.10 and 7.11.

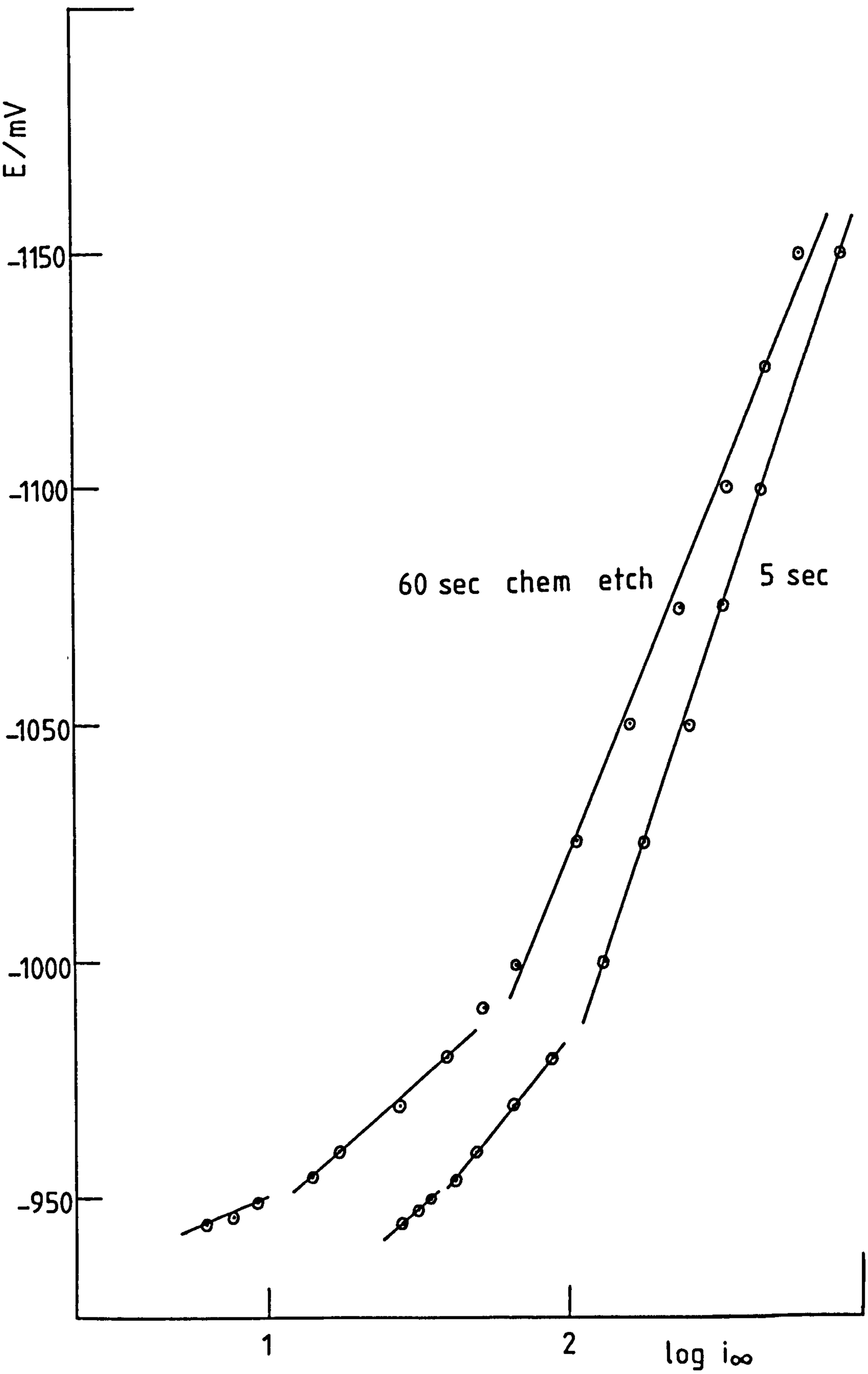
E/mV
-1150
-1100
-1050
-1000
-950
60 sec chem etch
5 sec
1
2
log i∞

Figure 7.13

Chemical etched electrode (10% HNO_3), current on electrode contact at -944 mV.

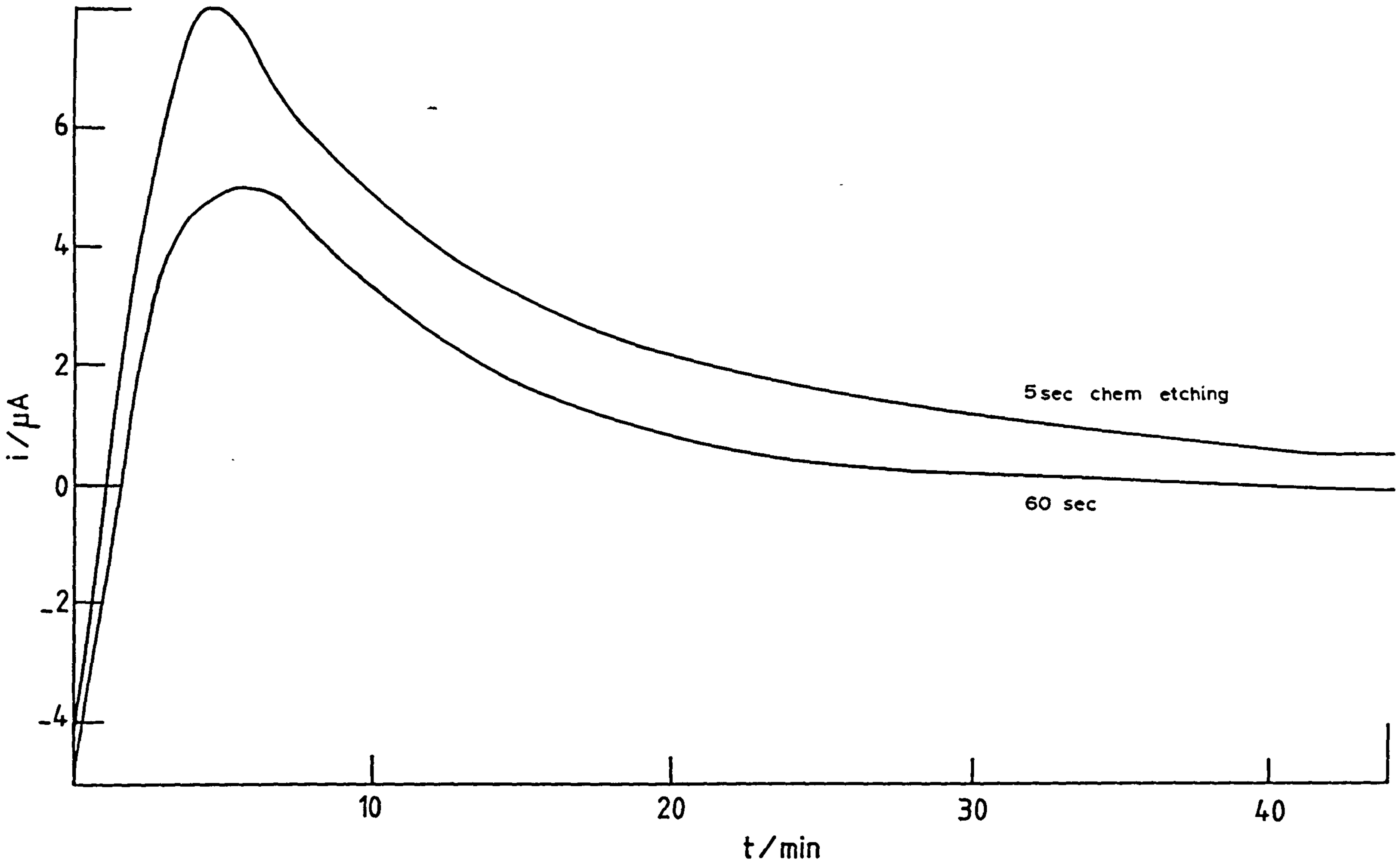
6
4
2
0
-2
-4
i/μA
5 sec chem etching
60 sec
10
20
30
40
t/min

produces pH conditions high enough to form a monolayer film of a basic salt (or hydroxide/oxide).

CHAPTER 8

THE EFFECT OF EXPANDER WHEN INCORPORATED IN AN, AS INDUSTRY, FORMED POROUS LEAD ELECTRODE

8.1 Introduction

That a Pb/Pb^{2+} solution process exists in 1M sulphuric acid, is irrefutable since the system has been adequately investigated by different laboratories[17-22 & 23-26] who ultimately draw similar conclusions. However, investigations on 'worked' lead electrodes as in Chapter 6 have failed to produce an example of Pb^{2+} free dissolution similar to that experienced with freshly prepared electrodes. The solution process can be observed in a narrow potential window in 5M sulphuric acid (Chapter 7) provided the electrode pretreatment is suitable.

Expander effects in both previously worked (1M sulphuric acid, maximum $PbSO_4$ solubility) and specially prepared solid (5M battery strength) lead electrodes have not been solution reaction promotive, but rather suppressive.

The object of the work presented in this Chapter is to extend the principles extracted from previous work to electrodes typical of form, environment and method of production to those of the lead acid battery negative.

8.2 Search for Pb^{2+}

The, 'as formed', porous lead electrodes were immersed in the 5M sulphuric acid at a potential cathodic of the reversible potential for $Pb/PbSO_4$ but sufficiently anodic to keep hydrogen

evolution to a minimum i.e. -1050 mV versus Hg/Hg_2SO_4.

The electrode potential was shifted slowly anodic, in 5 mV steps, whilst monitoring any variation in current with rotation speed. No mass transport dependent anodic reaction could be observed with either expanded or unexpanded porous lead. The only rotation speed dependent process observed was H_2 production at the more cathodic potentials. Both electrode types exhibited critical potential behaviour typical of solid state formation of lead sulphate. However no difference between the critical potential onset was observed when the expander is incorporated in the matrix, suggesting that any expander effects in porous systems are not surface effects as demonstrated at solid electrodes with expander in solution:

Linear sweep voltammetric investigations provided no evidence for a Pb^{2+} solution species. The results of linear sweep voltammetric experiments on the solid state mechanism in the porous lead system are presented in the next section.

8.3 Results and Discussion of linear sweep voltammetric investigation

Figure 8.1 shows a stable voltammogram corresponding to a solid lead electrode in 5M sulphuric acid. The addition of Indulin C to the electrolyte, to give a saturated solution, produced no visible change in the profile. This experiment was repeated with freshly prepared electrodes, introducing Indulin C either well in advance of electrode immersion or whilst the experiment was in progress, producing no observable effect.

Figure 8.1

L.S.V. Curve for the $Pb/PbSO_4$ System on a planar lead electrode in 5M H_2SO_2 (100 mV sec^{-1}, 17^{o}C, stabilised response).

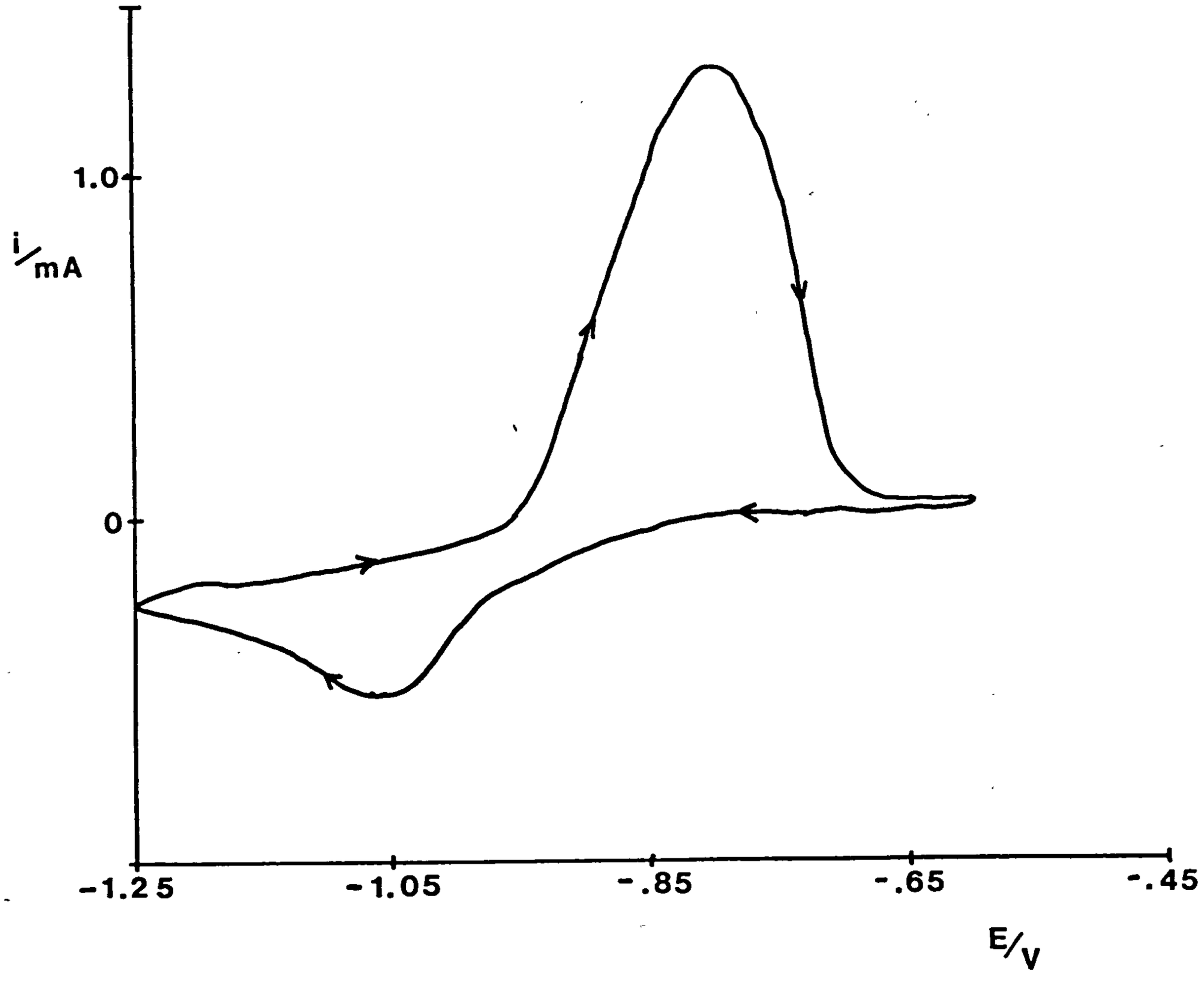
1.0
i/mA
0
-1.25
-1.05
-.85
-.65
-.45
E/V

8.3.1 Porous electrodes free from organic expander

Figure 8.2 shows a stable L.S.V. curve corresponding to a newly produced electrode immediately after formation and stabilisation in 5M H_2SO_4. The currents involved were about two orders of magnitude greater than similar experiments on solid lead in less concentrated acid and one order of magnitude greater than the experiments on solid lead in 5M. The shape of the L.S.V. is quite similar to those obtained from solid lead in both 1M and 5M sulphuric acid.

The effect of the porous structure in modifying the behaviour of electrodes is illustrated by Figure 8.3. Here, the porous electrode was withdrawn from dilute (0.5M) forming acid and immediately cycled to a constant response. The electrochemical process contains very much less charge than in the experiment with the 5M H_2SO_4 initially disposed (Figure 8.2) throughout the porous system and shows quite clearly how restricted diffusion in the porous structure results in capacity loss, presumably the dilute electrolyte solution becomes entrapped in the porous structure at stages in the oxidation to lead sulphate (discharging) when the front of the pores are blocked with electrode product. Confirmation of this explanation is obtained from Figure 8.4 which represents an intermediate case (5 minutes standing in 5M H_2SO_4 allowed for partial electrolyte replacement) showing increased charge recovery by the effective provision of additional electrolyte. With reduced sweep speed the peak heights were reduced and Figure 8.5 shows the rectilinear relationship between the peak current i_p, and the sweep speed ν. The curve within the limits of experiment passes through the origin. This behaviour is typical for a solid electrode over which a uniform insoluble insulating film is being formed by the

Figure 8.2

L.S.V. curve for the porous $Pb/PbSO_4$ system in 5M H_2SO_4. $17^{o}C$. Electrode area 0.0707 cm , depth 0.76 mm (Free of organic expander) sweep speed 100 mVs^{-1}. Stabilised sweep after ~ 100 cycles.

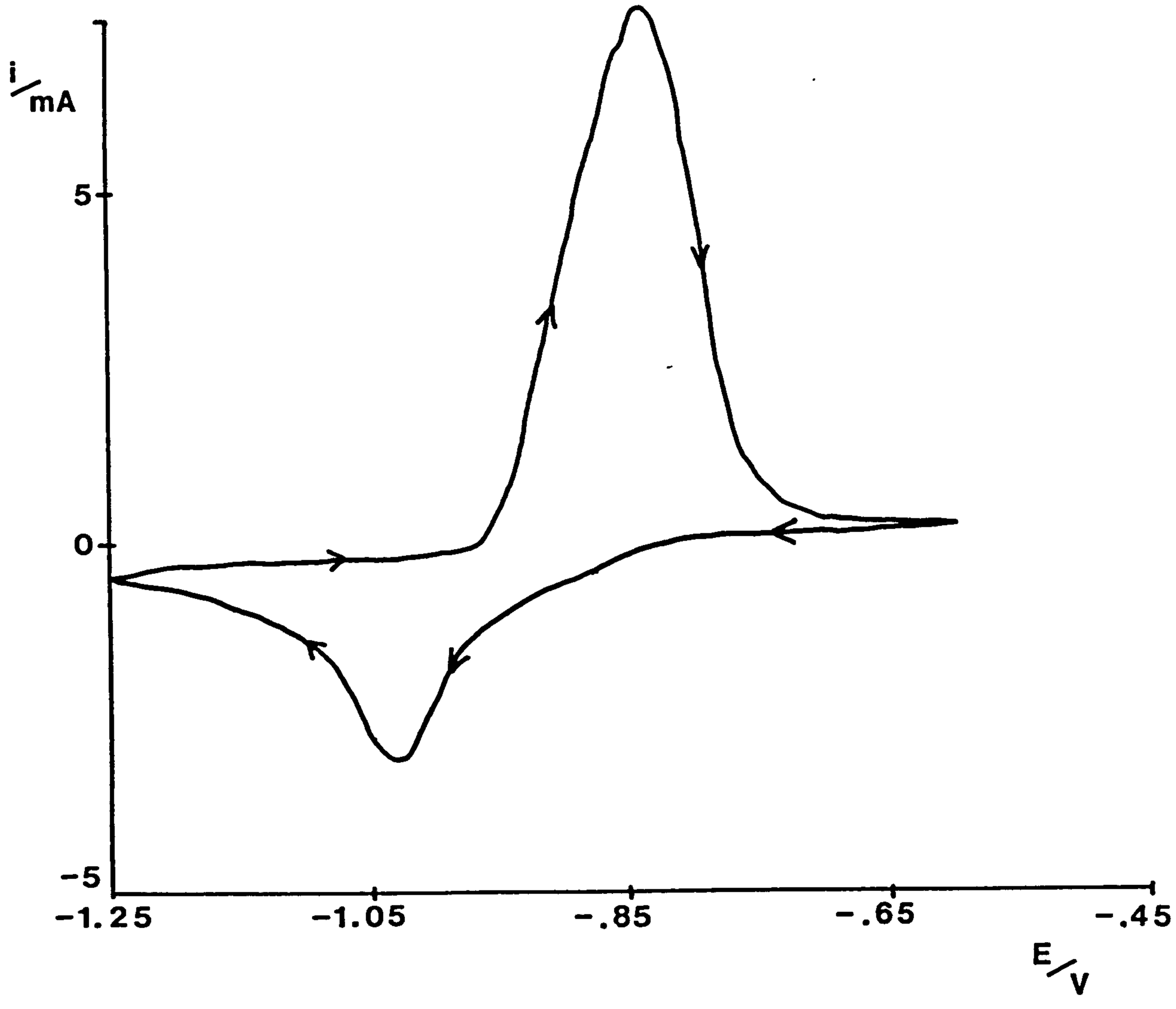
i/mA
5
0
-5
-1.25
-1.05
-.85
-.65
-.45
E/V

Figure 8.3

System immediately after withdrawing from formation circuit (0.5M H_2SO_4) and introducing into 5M H_2SO_4 solution. Other details as Figure 8.2.

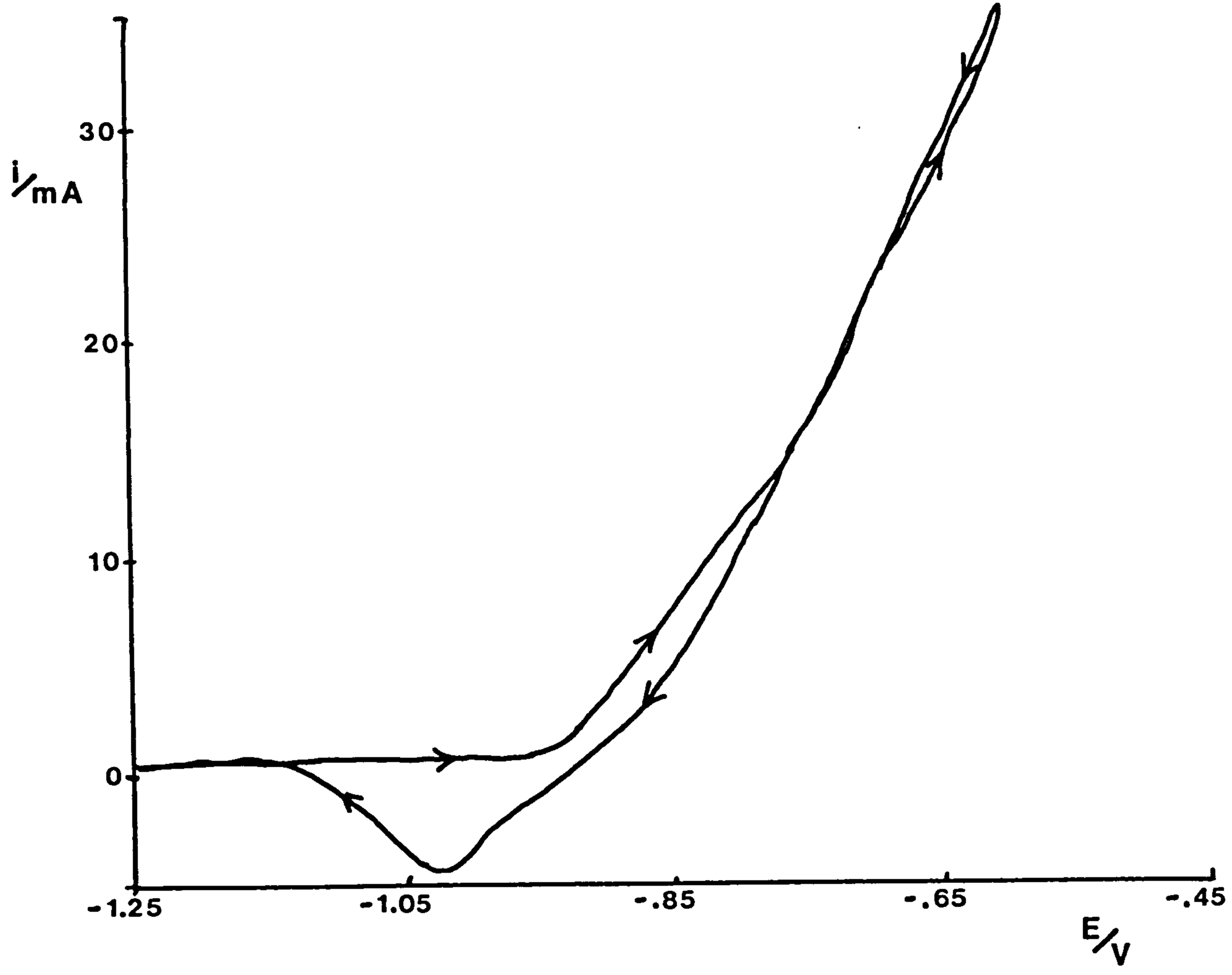
30
i/mA
20
10
0
-1.25
-1.05
-.85
-.65
-.45
E/V

Figure 8.4

As Figure 8.3 but with 5 min $^{O}/c$ period in 5M H_2SO_4 to partially replace 0.5M H_2SO_4 with 5M H_2SO_4.

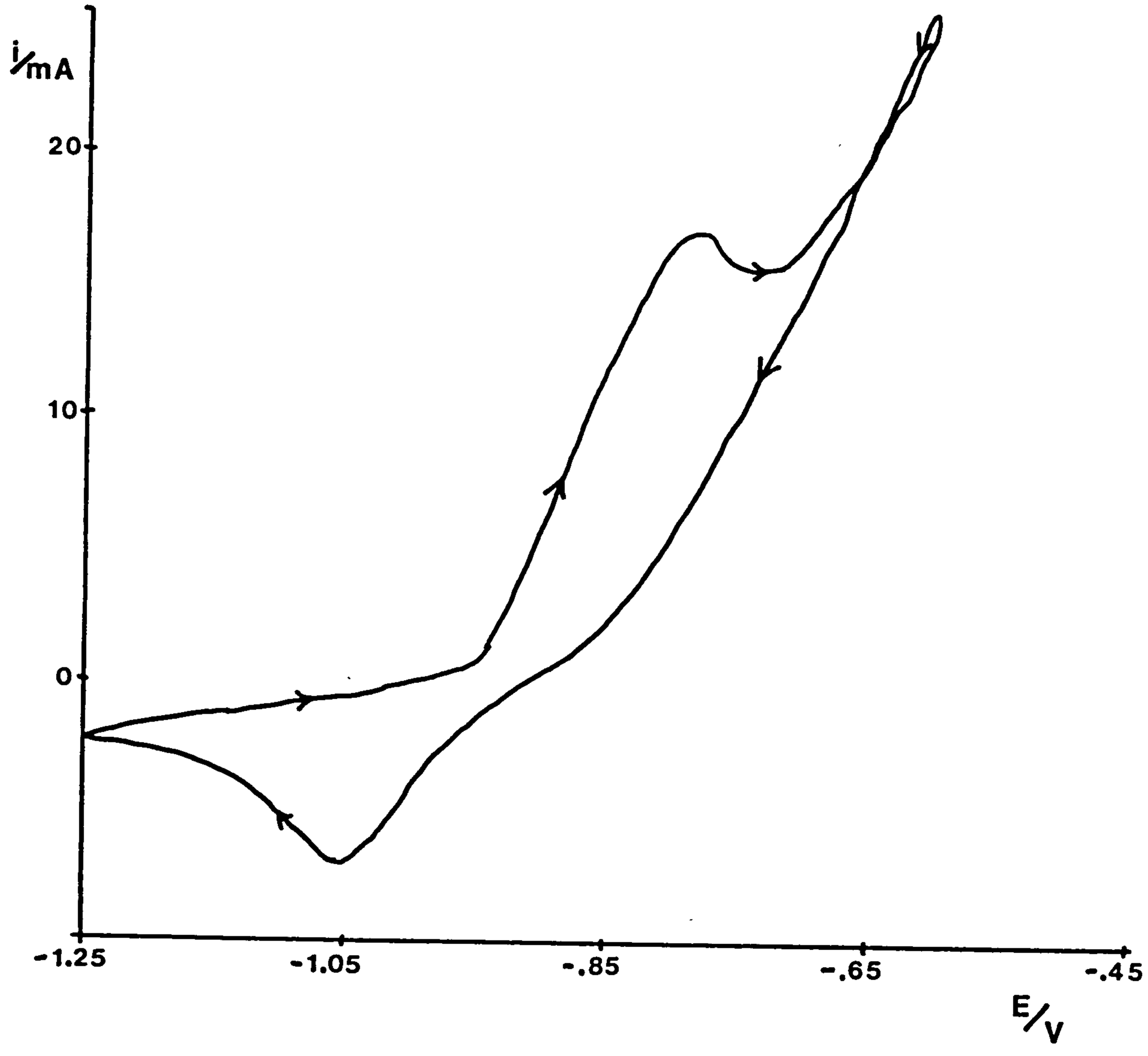
i/mA
20
10
0
-1.25
-1.05
-.85
-.65
-.45
E/V

Figure 8.5

The relationship between peak current and sweep speed. Other details as Figure 8.2.

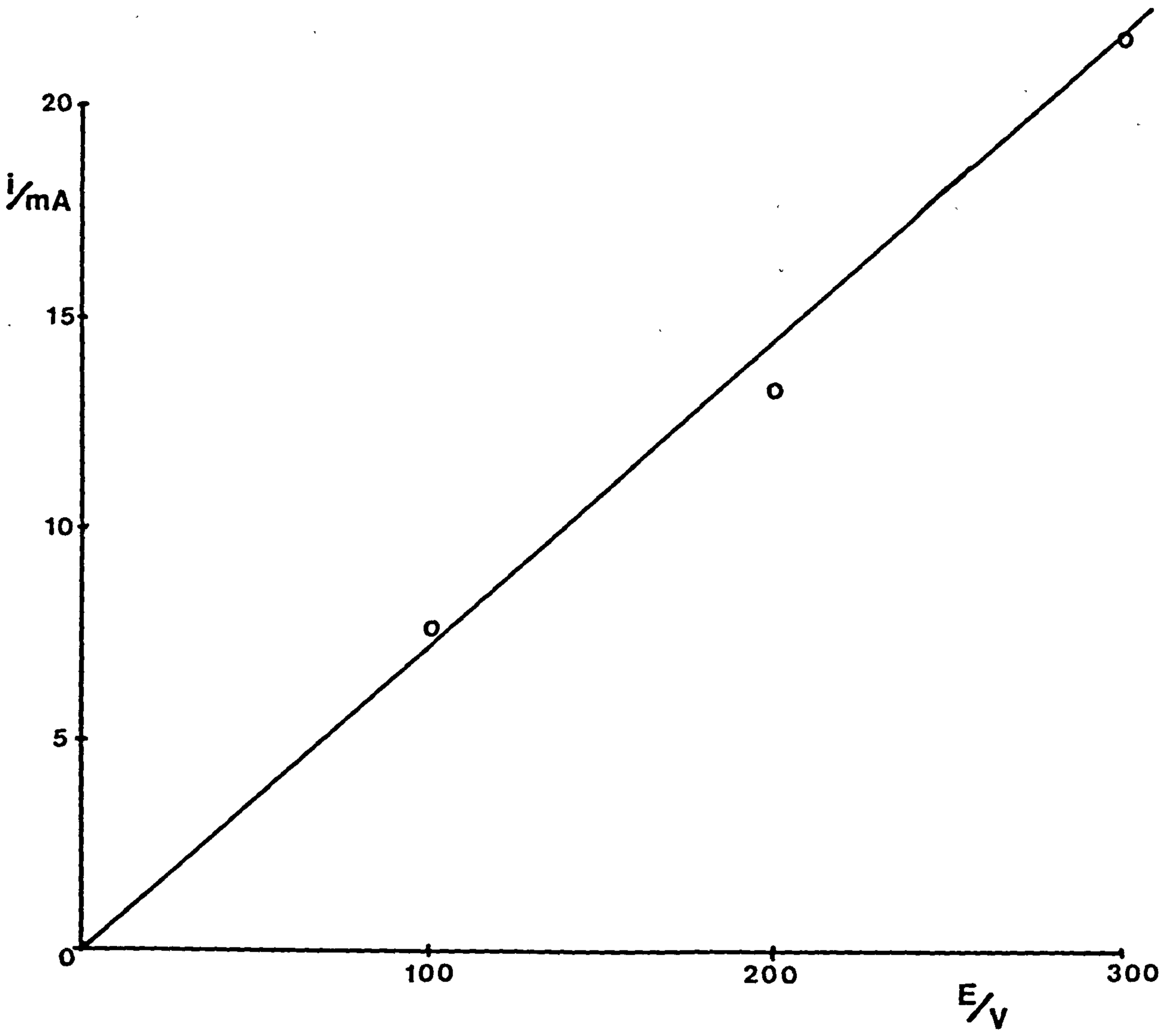
20
i/mA
15
10
5
0
100
200
300
E/V

electro-oxidation of the lattice. It could be concluded therefore that this electrode is behaving simply as one of planar characteristics and large surface area. This conclusion is neatly confirmed by the data of Table 8.1 which shows charges calculated from the L.S.V. curves (integrated area/sweep speed) to be independent of sweep speed for a fixed temperature, that is, the passivating $PbSO_4$ layer is the same for all the sweep speeds, which can only hold for a surface process.

Figure 8.6 shows a typical L.S.V. experiment at a temperature lower than ambient ($-10^{o}C$). The current in the L.S.V. curve is everywhere reduced in accordance with previous investigations using different techniques.[31,151] The shapes of the L.S.V. curves remain the same, however, as do the direct relationships between current and sweep rate. The Arrhenius plot of slope $di(max)/d\upsilon$ is shown in Figure 8.7. The slope of this line contains the enthalpy of activation for film formation in the form $\Delta H_f/_R$ which was found to be 52 kJ mol^{-1}. Strictly speaking these enthalpies are not true enthalpies of activation since the variation of equilibrium potential is not considered. This cannot be assessed since attempts at measurement fail because of the presence of an unknown thermo-liquid junction potential.

Figure 8.8 shows the Arrhenius plot of the charge in the anodic process (discharge); this too contains essentially the same information as the temperature dependence of the slope. The enthalpy for film formation from this plot was found to be 47.5 kJ mol^{-1}. In view of the uncertainties inherent in these experiments the agreement is quite reasonable. These values are very close to those observed for solid lead and strengthen the conclusion that the same passivating process is occurring; the

TABLE 8.1

Temperature/^{o}C	Sweep Rate/mV s^{-1}	Charge/C
17	300	0.00984
	200	0.01027
	100	0.00935
-18	300	1.363×10^{-3}
	200	1.336×10^{-3}
	100	1.477×10^{-3}
-31	300	1.509×10^{-4}
	200	1.585×10^{-4}
	100	1.448×10^{-4}

Figure 8.6

As Figure 8.2 but -10°C.

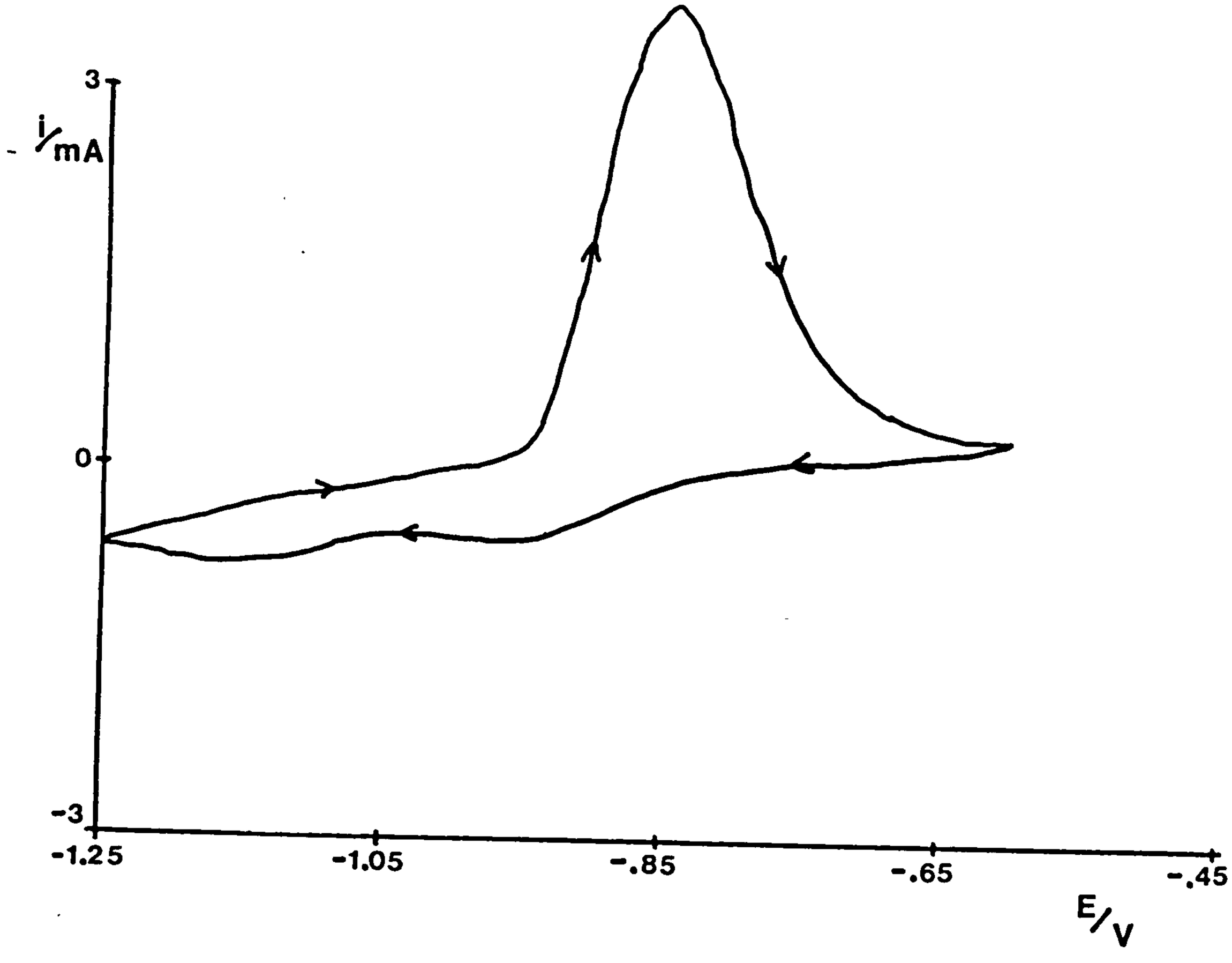
3
i/mA
0
-3
-1.25
-1.05
-.85
-.65
-.45
E/V

Figure 8.7

Arrhenius plot ($^{di}max/d\nu$) versus $^{1}/T$ for electrode systems corresponding to Figure 8.2.

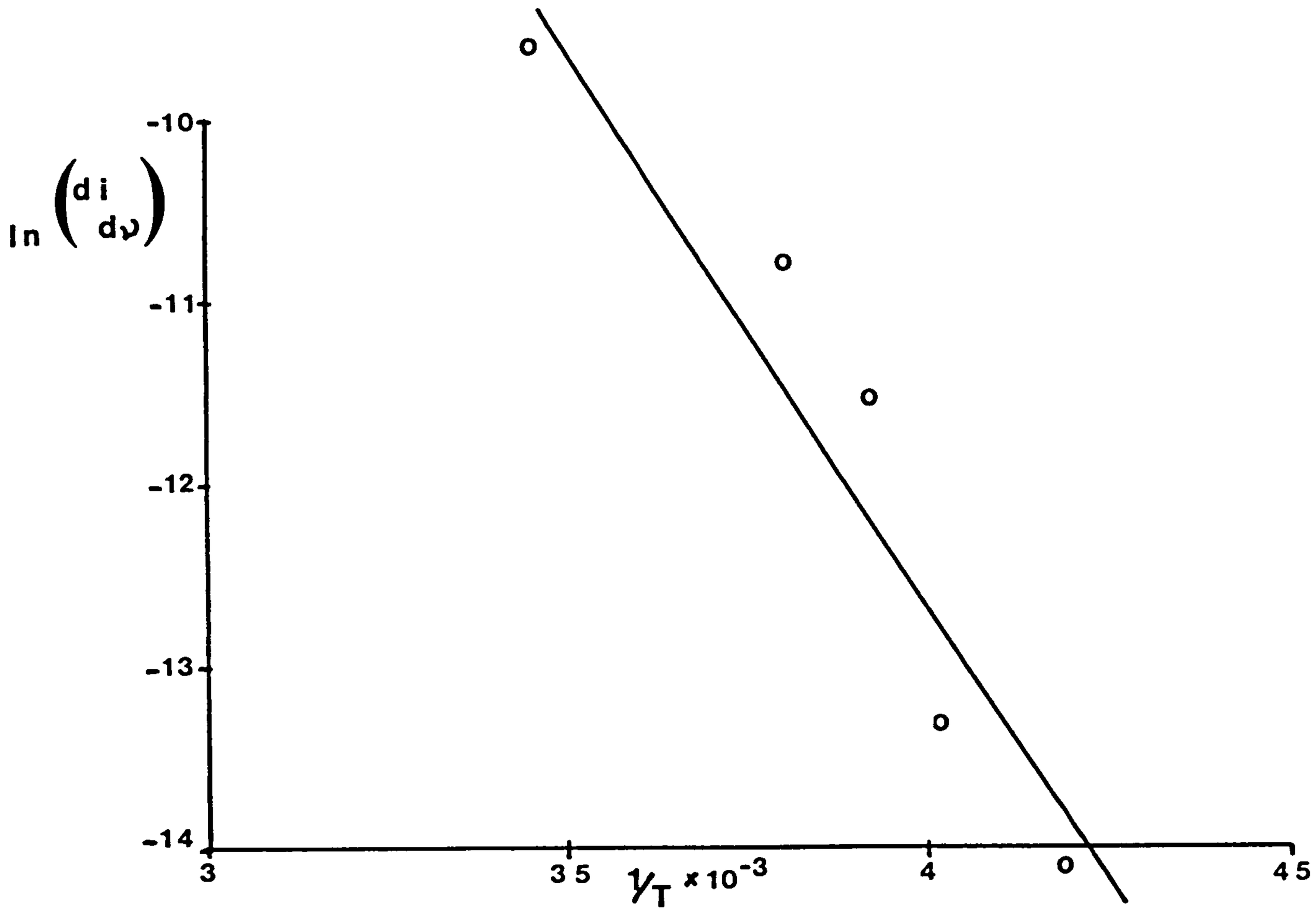
-10
-11
-12
-13
-14
ln (di/dν)
3
3 5
4
4 5
1/T x 10^-3

Figure 8.8

Arrhenius plot (passivating charge) versus $^{1}/T$ for electrode systems corresponding to Figure 8.2.

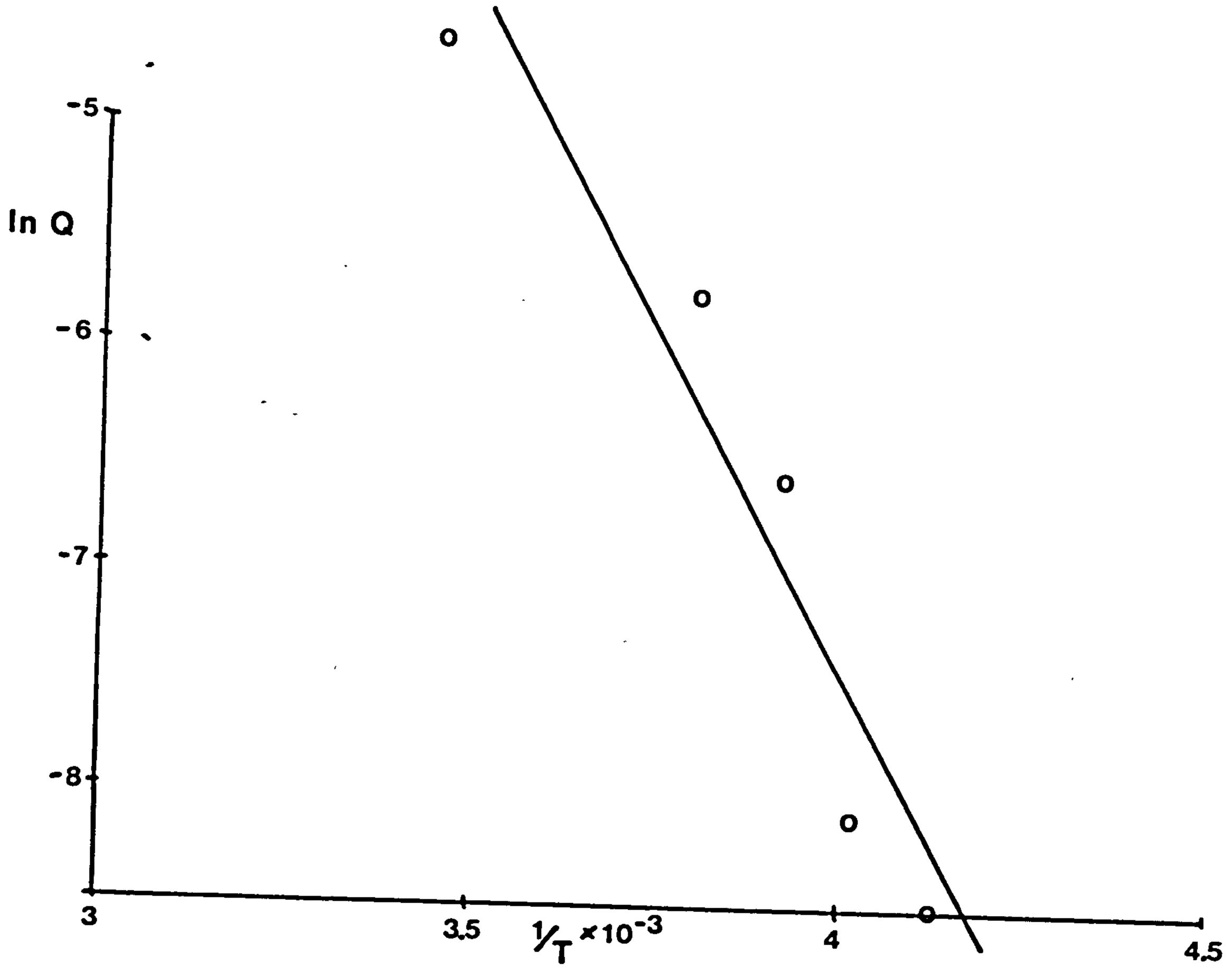
-5
ln Q
-6
-7
-8
3
3.5
1/T ×10^-3
4
4.5

effect of the porous structure is simply to provide an electrode of larger area.

8.3.2 Porous electrodes containing 0.01% organic expander (Indulin C)

Figure 8.9 shows an L.S.V. curve for a porous system containing organic expander. The effect of the expander is considerable. There is much more current in the voltammograms and the discharge (oxidation) peak is considerably broadened. The reduction peak which is quite well defined for the expander-free systems is very poorly defined here and convoluted with a continuously increasing hydrogen current. It was desirable to extend the negative limit in these sweeps beyond -1.25 V, but this was not done in view of the possibility of saturating the porous mass with gaseous product. If the limit was extended, however, there was an increase in the quantity of hydrogen evolved, whilst the lead sulphate formation peak remained unaffected. The limit of -1.25 V was chosen because the reduction peak had closed up completely by the time this limit was reached in addition to there being no evolution of hydrogen gas. If the electrode was maintained at -1.25 V gas evolution was apparent even though it was not in the sweeping experiments. This evidence was considered to be sufficient to show that at the zero current potential on the anodic sweep the electrode was completely reduced to lead.

The porous characteristics of the expander containing electrodes were demonstrated by sweeping electrodes which had been immediately withdrawn from the formation circuit (containing 0.5M H_2SO_4) and sweeping in 5M H_2SO_4. The result shown by Figure 8.10

Figure 8.9

As Figure 8.2 but containing 0.01% Indulin C incorporated in the porous structure (paste).

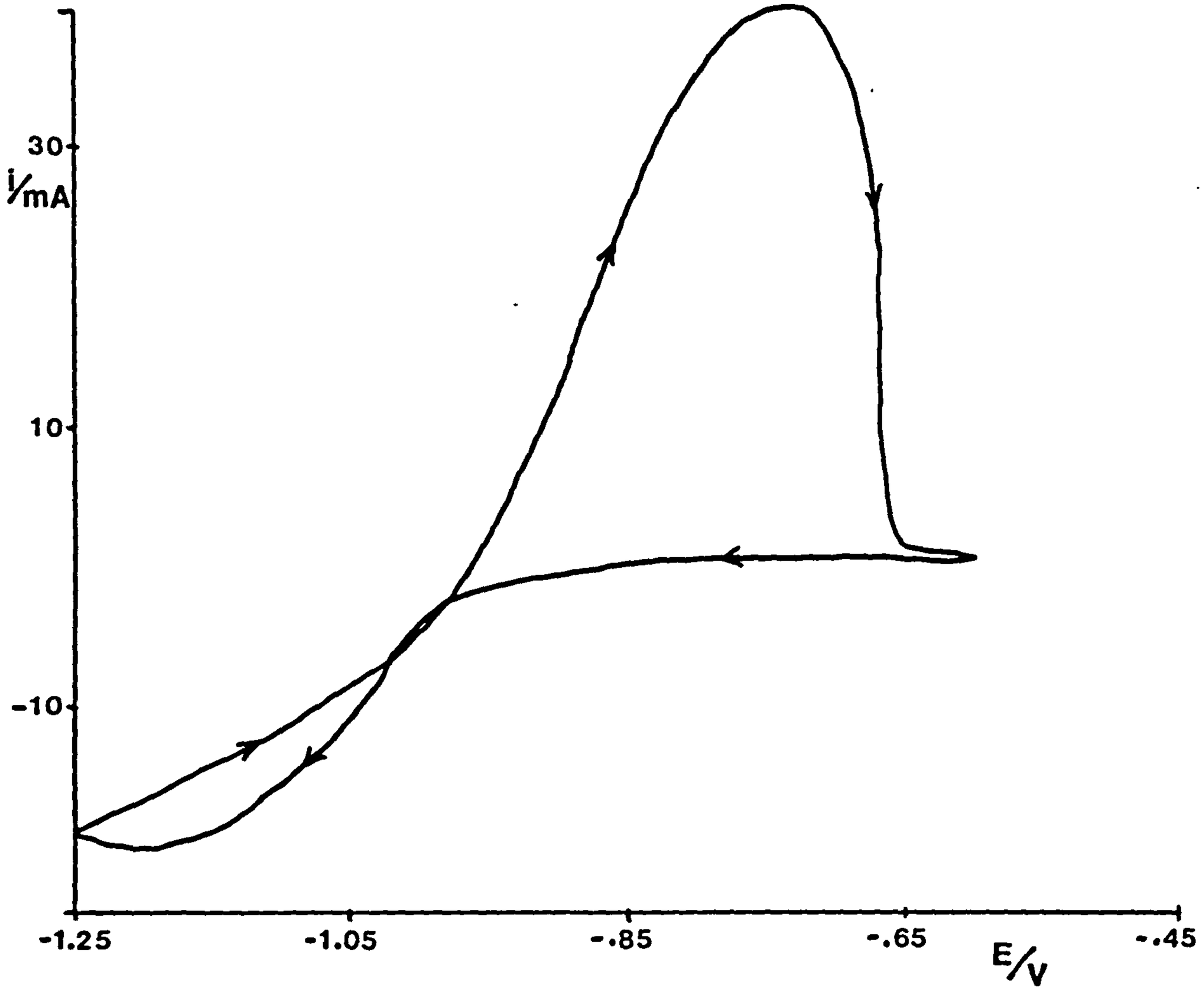
30
i/mA
10
-10
-1.25
-1.05
-.85
-.65
-.45
E/V

Figure 8.10

As Figure 8.3 but with electrode containing 0.01% Indulin. Sweep speed 300 mVs^{-1}.

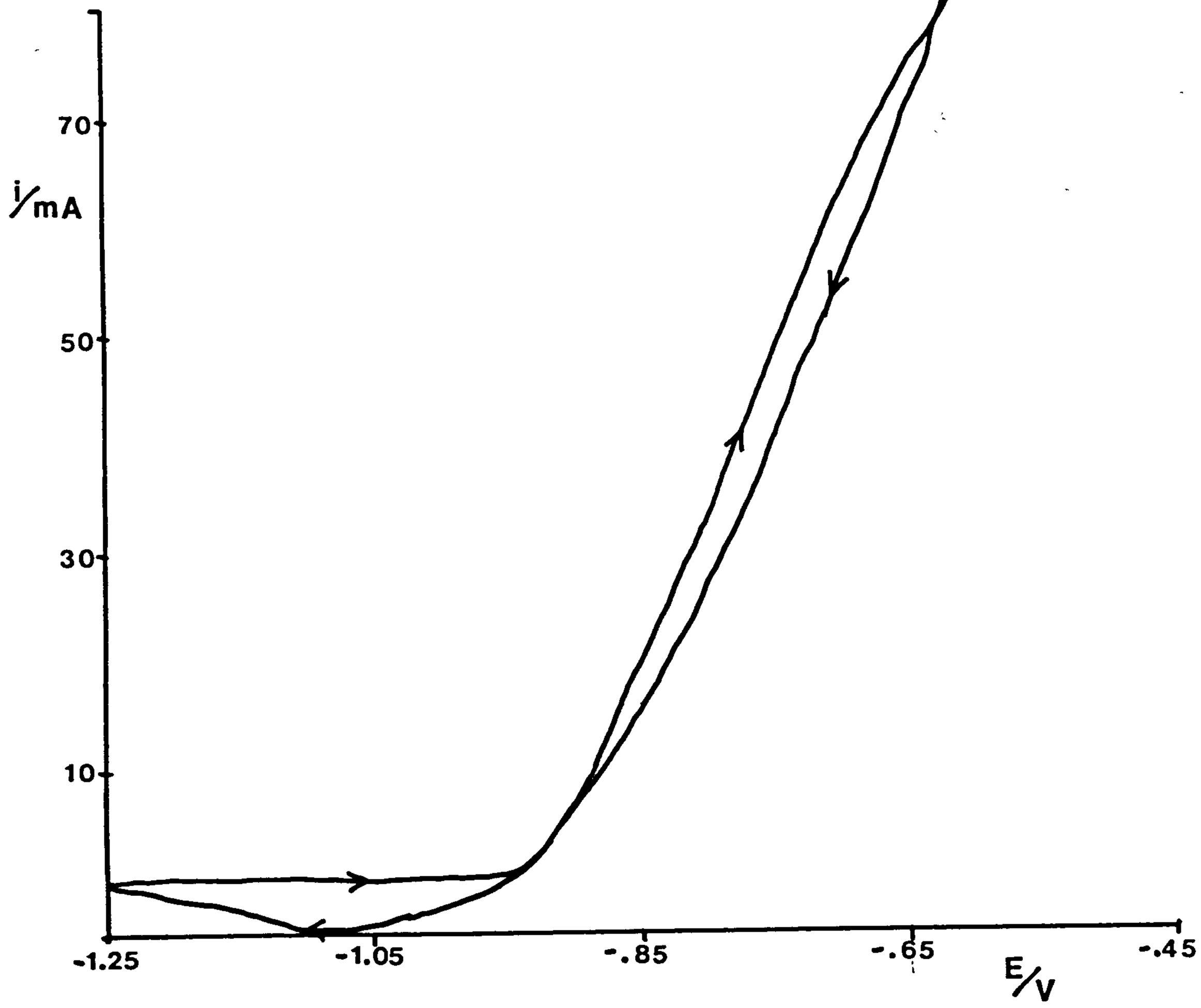
70
i/mA
50
30
10
-1.25
-1.05
-.85
-.65
-.45
E/V

confirms that similar porous characteristics in the sense of diffusion apply to both expander-containing and expander-free electrodes. The intermediate condition illustrated in Figure 8.11 is markedly different from Figure 8.4 and indicates that the expander-characteristics of a broad oxidation peak and poorly defined reduction peak begin to develop as soon as the more concentrated sulphuric acid begins to diffuse into the porous mass. This implies that expander action is not simply the provision of a more open porous structure.

The effect of temperature on the L.S.V. curve is shown in Figure 8.12. The current (and charge) in the anodic peak decreased as the temperature was lowered and the shape of the L.S.V. curve changed somewhat to become more redolent of the expander-free electrode.

The typical relationships between peak current and sweep speed are shown in Figure 8.13. At each temperature the same behaviour was observed, a fairly horizontal line. This behaviour is mirrored in the data of Table 8.2 which shows the charges obtained to be very dependent upon sweep speed. This behaviour is what would be expected from an ideal porous electrode[94] as the sweep speed becomes slower the reaction is driven ever more deeply into the porous electrode. At very high sweep speed the front of the electrode accounts for the majority of the electro-chemical reaction, penetration depth in the sense of Frumkin[152] increasing as the sweep speed is reduced (analagous to the greater penetration of a porous electrode by a low frequency A.C. signal). In spite of this pronounced dependence of passivating charge on sweep rate the expander-containing electrode provides in all cases more charge than the expander-free electrode.

TABLE 8.2

Temperature/^{o}C	Sweep Rate/mV s^{-1}	Charge/C
17	300	0.0296
	200	0.0435
	100	0.0814
0	300	8.97×10^{-3}
	200	0.0122
	100	0.0237
-10	300	4.135×10^{-3}
	200	6.1696×10^{-3}
	100	0.0121
-20	300	1.522×10^{-3}
	200	1.726×10^{-3}
	100	2.871×10^{-3}
-30	300	7.298×10^{-4}
	200	9.901×10^{-4}

Figure 8.11

As Figure 8.4 but with electrode containing 0.01% Indulin. Sweep speed 300 mVs^{-1}.

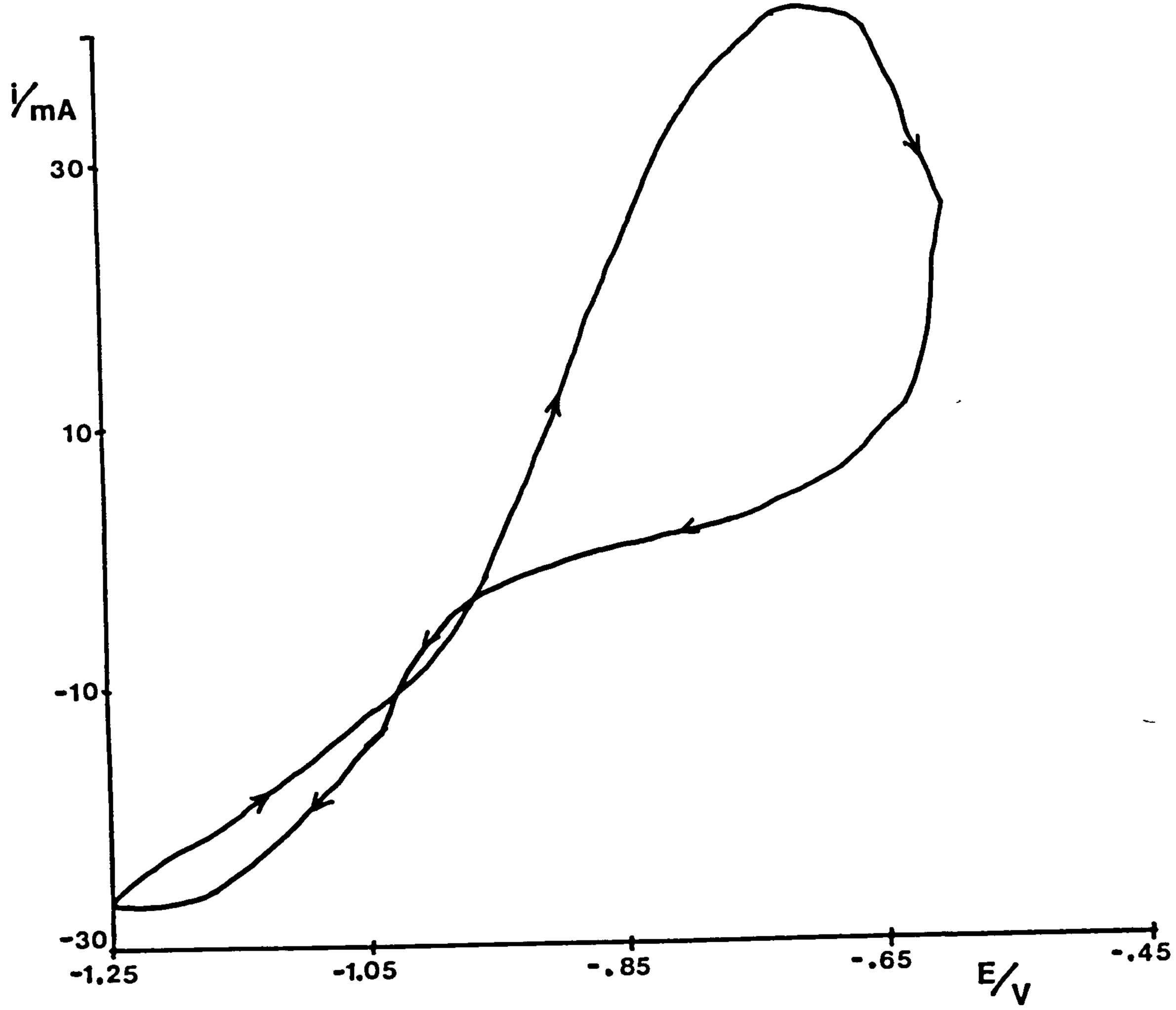
i/mA
30
10
-10
-30
-1.25
-1.05
-.85
-.65
-.45
E/V

Figure 8.12

As Figure 8.9 but -30^{o}C.

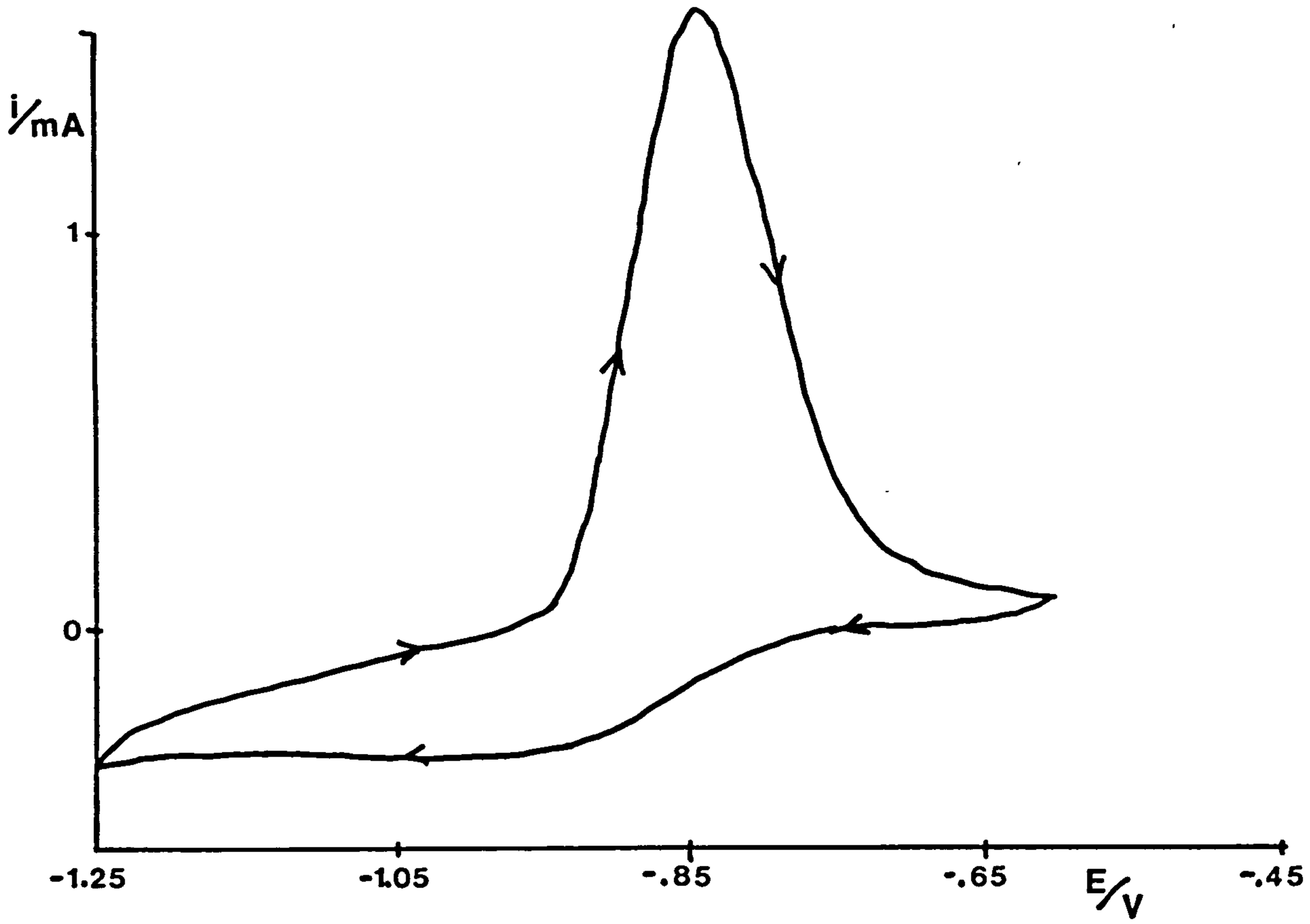
i/mA
1
0
-1.25
-1.05
-.85
-.65
-.45
E/V

Figure 8.13

The relationships between peak current and sweep speed at ~ $0^{o}C$ for electrodes as Figure 8.9.

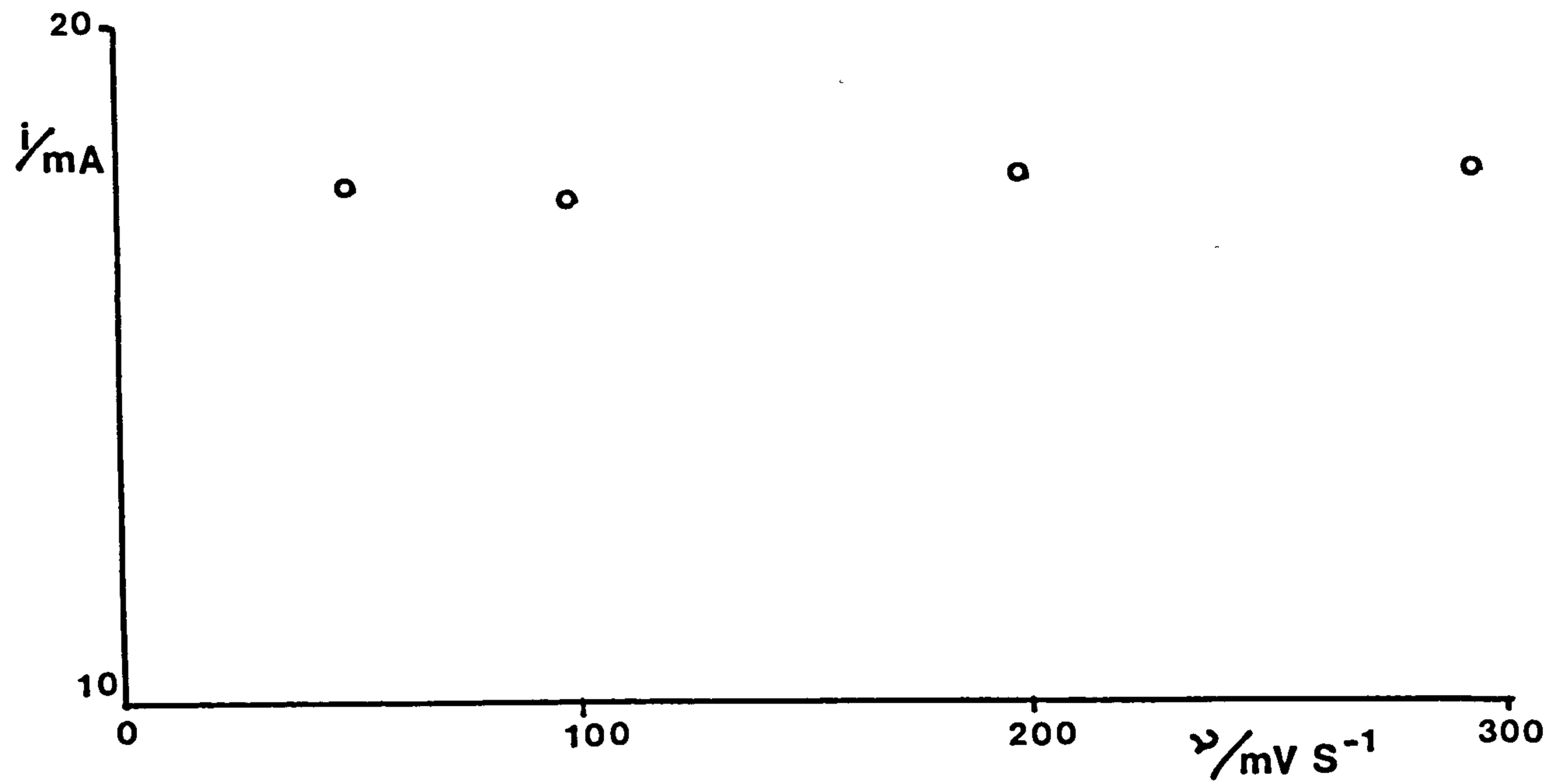
20
i/mA
10
0
100
200
300
ν/mV S-1

The enthalpy of activation for the passivation processes can be measured only at constant sweep speed as a consequence of the above observations. This data is obtained from the passivating charges at each sweep speed. The results of the inverse temperature plots are shown in Figure 8.14. The enthalpies of activation for the passivation process are 48.6, 50.5 and 50.2 kJ mol^{-1} respectively for the sweep speeds 100, 200 and 300 mV s^{-1}. The magnitudes of the enthalpies are similar to the values for the expander-free systems. When the effect of dissolved expander in the electrolyte on the passivation process on solid lead in dilute sulphuric acid was investigated, it was found that the presence of dissolved expander effectively changed the rate control from a simple cover passivity to diffusion through a thickening layer of $PbSO_4$. In the cases of the porous electrodes a difference in mechanism is quite clear from the electrochemical behaviours (from a large planar electrode-unexpanded, to a 'truly porous' electrode-expanded). From the energetics the passivation process is apparently the same in both the expander-free and expander-containing matrices and this reaction-limiting process is apparently (from the magnitude of the enthalpy) a cover passivity within the porous matrix. This is also supported by the fact that the critical crystallization potential is not shifted in expander containing electrodes.

8.3.3 Expander additions to the electrolyte

For the case of expander-free electrodes the 5M sulphuric acid solution was saturated with Indulin C. This did not produce the characteristic pale straw coloured solution observed with the dilute electrolyte solution (Chapter 6); rather a crude suspension

Figure 8.14

a, b and c Arrhenius plots (passivating charge, Q) versus $^{1}/T$ for electrode systems corresponding to Figure 8.9. a - 100 mVs^{-1}, b - 200 mVs^{-1}, c - 300 mVs^{-1}.

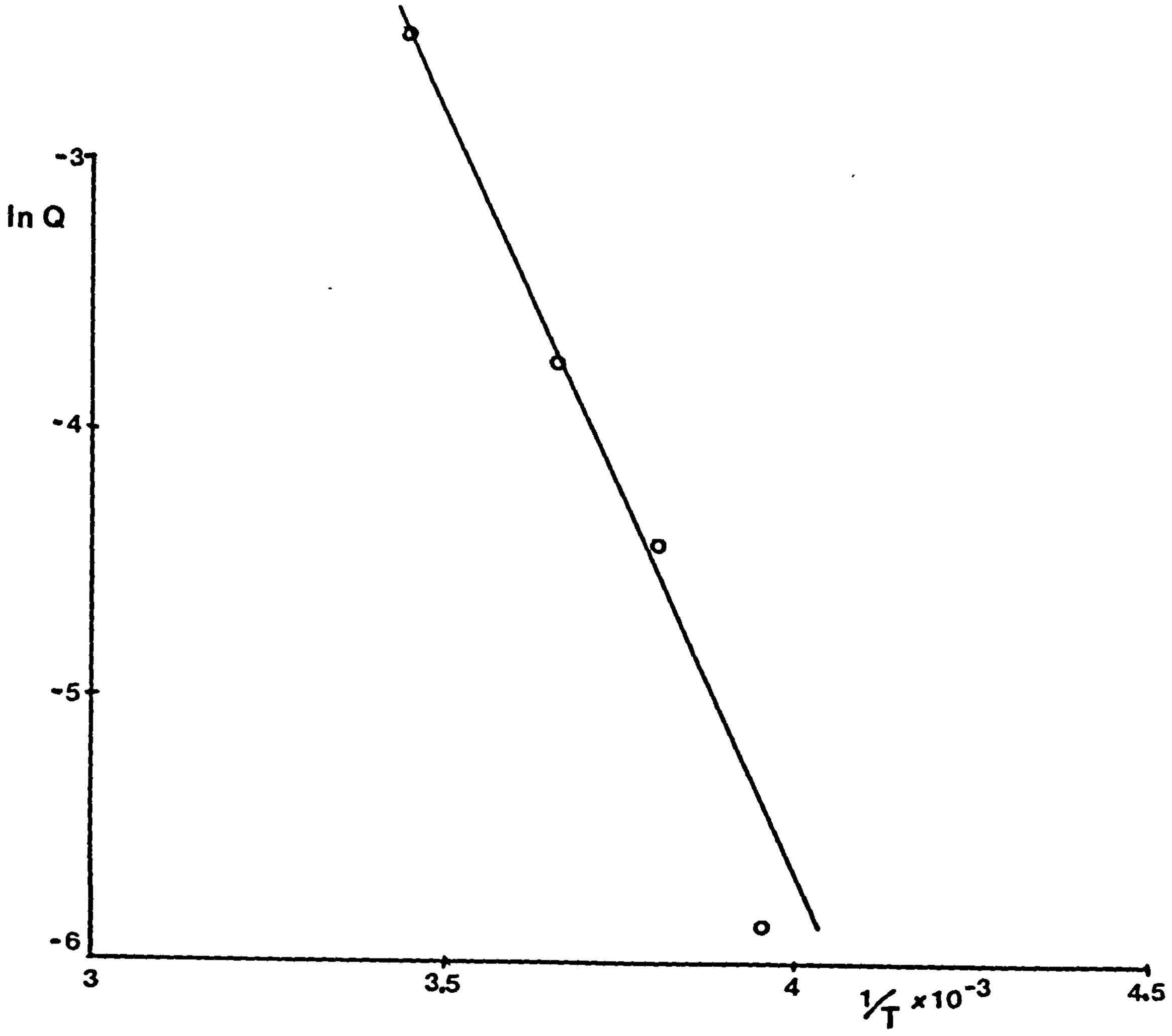
-3
ln Q
-4
-5
-6
3
3.5
4
4.5
1/T x10^-3

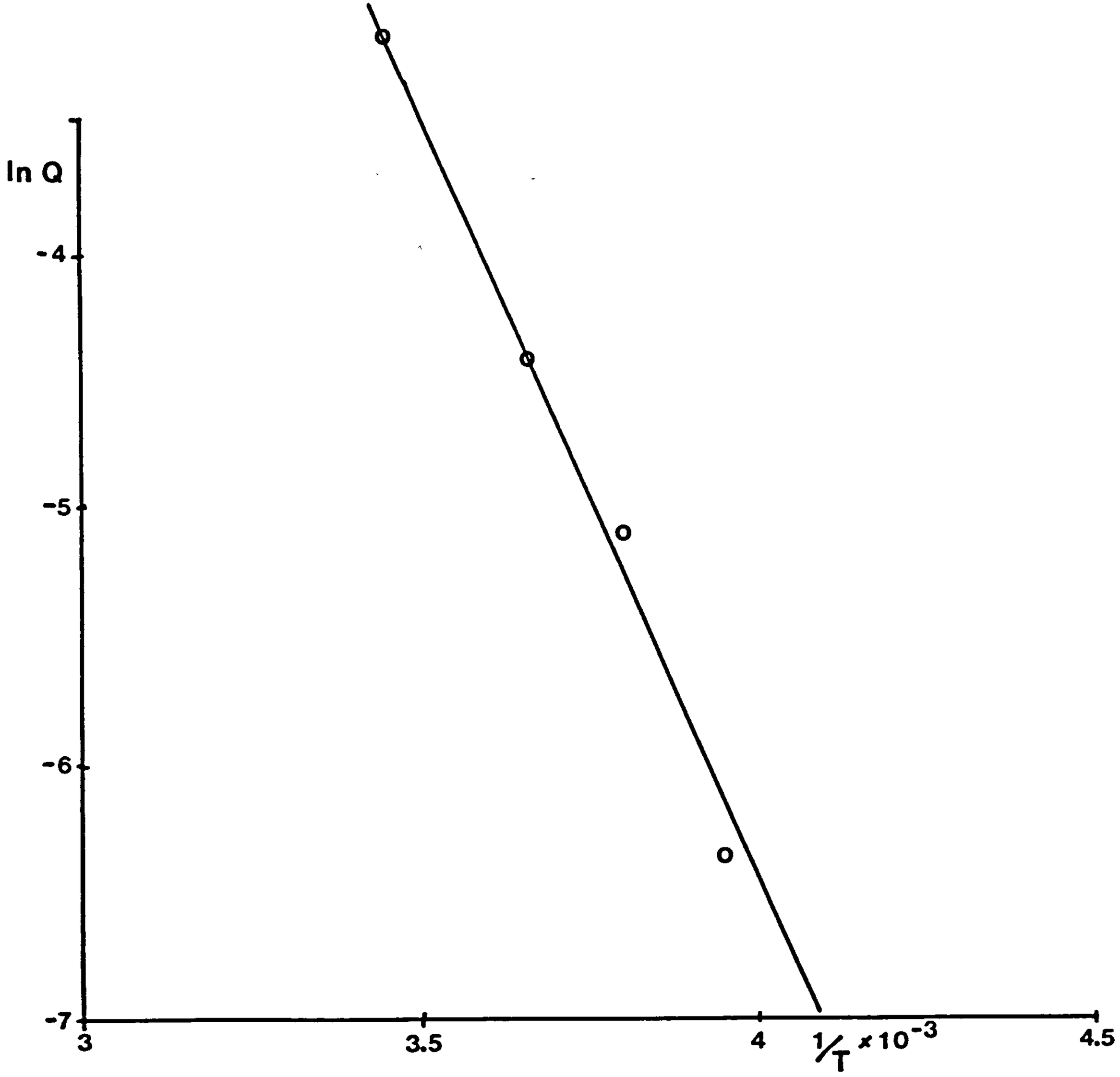
ln Q
-4
-5
-6
-7
3
3.5
4
4.5
1/T x10^-3

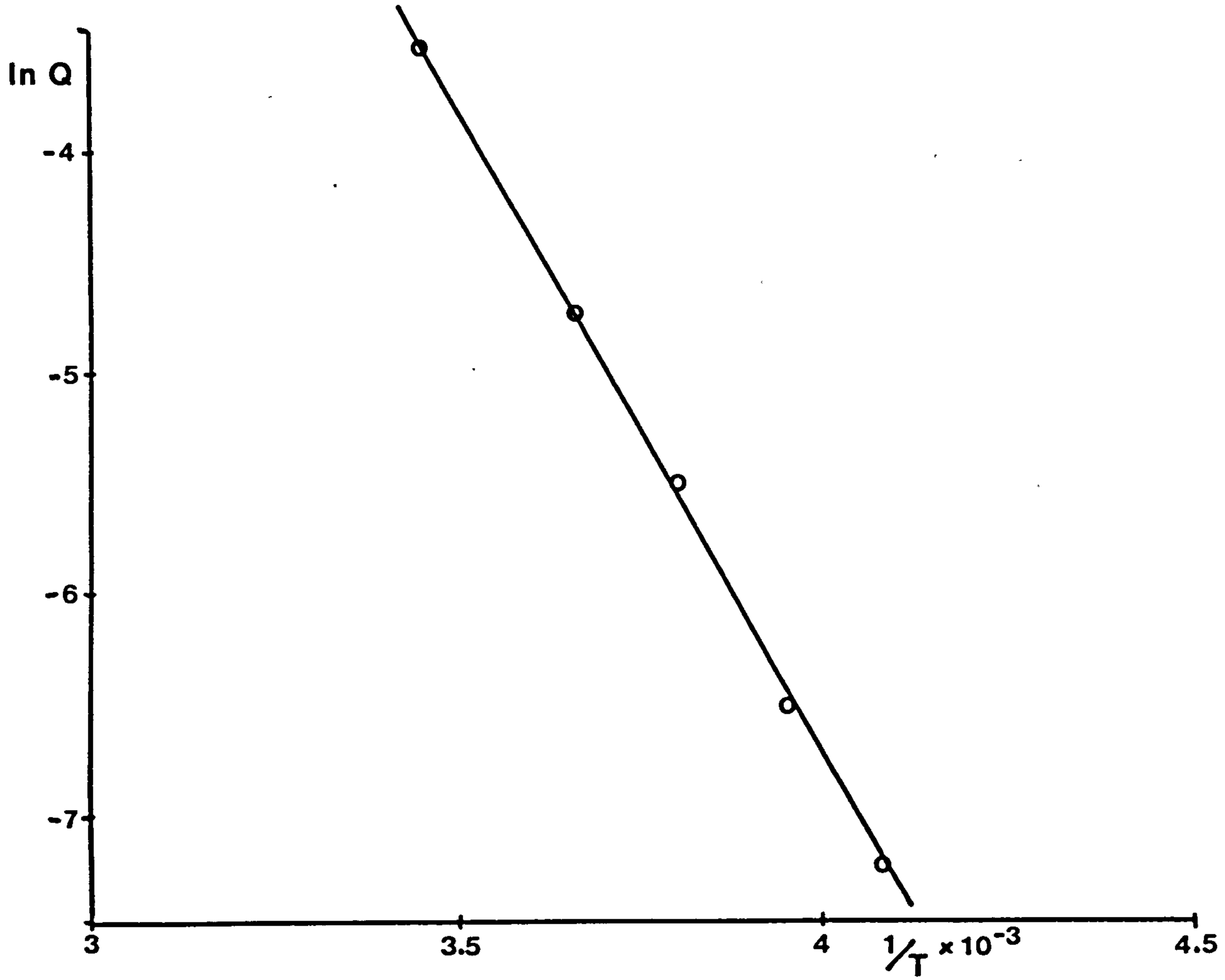
ln Q
-4
-5
-6
-7
3
3.5
4
4.5
1/T x 10^-3

was produced. The electrolyte solution could therefore be assumed to contain a negligible amount of dissolved organic. Investigation into the solubility of Indulin C in 5M sulphuric acid by other workers[153] suggest that a saturated solution can only provide up to 50 ppm ±20. This figure is temperature dependent and not reproducible due to variations in moisture content from batch to batch. Consequently the solution was agitated for 24 hours before experiments and then continuously stirred whilst L.S.V. experiments were carried out. Figure 8.15 shows the results of a typical experiment; there is no observable effect due to the dissolved expander.

8.4 Conclusions

The incorporation of Indulin C into a porous electrode fundamentally changes its electrochemical behaviour. The anodic reaction is able to more deeply penetrate the expander-containing porous electrode (as would be expected of an ideal porous electrode) as the sweep speed (reaction rate) is decreased. The expander-free electrode behaves as a simple electrode of large area.

The reasons for the behaviour are not clear. In the absence of expander the penetration into the porous electrode is limited, possibly due to a reduced porosity vis-a-vis expander-containing electrodes. Certainly the results shown in Figures 8.3, 8.4 and 8.10, 8.11 leave no room for doubt that there is restricted solution movement in the porous matrices. What is not so certain is the shape of the pores. A possible explanation of the observed behaviour would be if the pores in the expander-

Figure 8.15

As Figure 8.2. Indulin-C saturated solution.

300 mVs^{-1}.

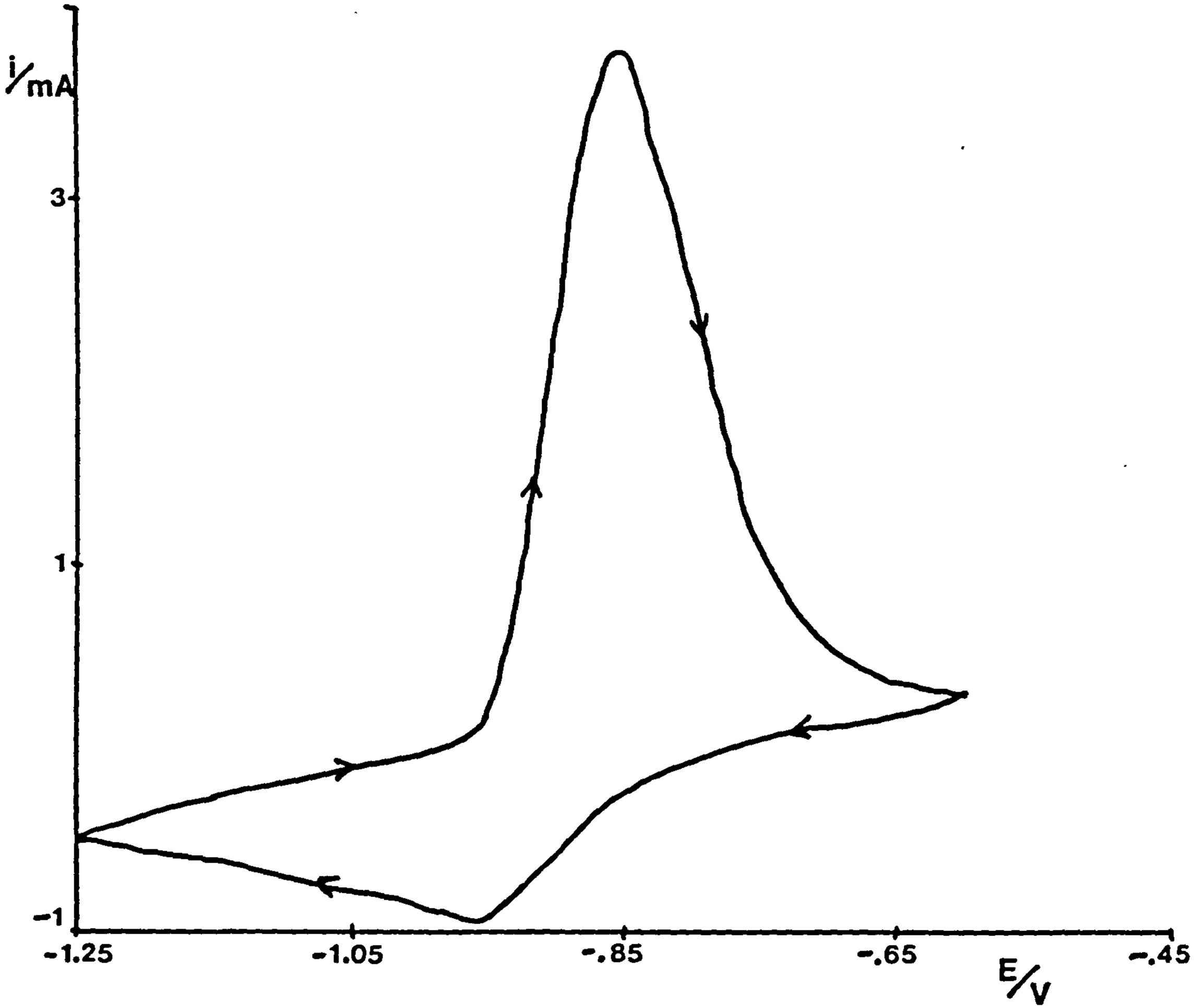
i/mA
3
1
-1
-1.25
-1.05
-.85
-.65
-.45
E/V

free electrodes were mainly of the "ink-bottle" form with restricted openings near the front of the pore, whereas in the presence of expander a more uniform pore structure is engendered.

It should be noted that these conclusions apply to very high rates of reaction and low temperatures. It is to improve performance under these conditions that organic expanders are added to negative electrodes. The conclusions may be different under different conditions.

C H A P T E R 9

CONCLUSIONS AND FURTHER WORK

9.1 Digital equipment for electrochemical experimentation

Conclusions are drawn and presented in Chapter 4. One point in particular, however, is worth stressing here, that is, the modus operandi. The microcomputer has been found to be excellent in its flexibility for data recording and equipment/ experimental monitoring. It is also highly suitable for control purposes, hence its ability to organise and execute steady state experiments. Unfortunately the usefulness of the microcomputer as a perturbing signal source for electrochemical experimentation is limited by the state-of-the-art development of digital to analogue integrated circuitry. When using digital to analogue circuitry, particularly for the investigation of transient phenomena, the experimenter must be aware of the restrictions placed on the technique by the same.

9.2 Electrochemistry

The work presented in the previous chapters has centred mainly on considerations of the dissolution/precipitation versus solid state mechanisms for lead sulphate production and the effects of expander in solution or dispersed within the porous matrix. Conclusions drawn from this project can be reviewed in point format.

(i) 'Worked' planar electrodes do not exhibit a solution species reaction even in concentrations of acid (1M) which provide conditions for maximum lead sulphate solubility.

(ii) At reduced temperatures a quasi-polarizable condition is apparent at the planar lead surface due to the production of a near perfect insulating film of lead sulphate. The mechanism of this passivation is transformed when 'Indulin C' is present in solution.

Current control in the expander-free situation switches from insulation by a film to restriction by solution resistance through pores within the lead sulphate film. The expander appears to inhibit the formation of the passivating ordered structure necessary for polarizability.

(iii) A solution species for the anodic dissolution of lead does exist in 5M (battery strength) sulphuric acid but is only apparent in a very narrow potential band. Solution species production is also highly sensitive to electrode pretreatment and appears to be greatest when surface films and nucleation centres for the solid state reaction can be avoided. Expander material in solution inhibits the production of solution species.

(iv) There is also an anodic shift in solid state nucleation potential possibly due to structural hinderance of mass transport to the electrode.

(v) No lead solution species could be found with rotating disc or linear sweep voltammetric investigations of porous lead both with and without expander.

(vi) The unexpanded porous matrix provides charge of an order of magnitude greater than that obtainable from planar electrodes. Expanded porous electrode provide more charge than unexpanded; again approximately an order of magnitude.

(vii) The inferences from (vi) are that the porous electrodes present a larger surface area to the electrolyte for reaction. The mechanism of the passivation process is apparently the same (from energetic considerations) in both expander free and expander-containing electrodes. This reaction limiting process is the formation of an insulating film within the porous matrix.

Unexpanded electrodes exhibit charge delivery sweep speed behaviour characteristic of a planar electrode of large surface area. Expanded electrodes, however, yield charges which are very dependent on sweep speed. More charge is provided at lower sweep speeds, suggesting that the expanded electrode is behaving as a truly porous electrode exhibiting penetration depth characteristics as in the sense of Frumkin.[152]

The preceding points suggest that a lead solution species would be unlikely to play a significant role in the normal operation of the lead-acid battery. This is however contradictory to evidence presented in support of the solution precipitation model of Vetter.[154] It is commonly expressed in the lead-acid battery industry that the current that can be extracted from the lead-acid cell would not be available if the solution species were not present. Yet this is not based on thorough quantitative investigations. Dendritic crystal structures do occur within the porous lead electrode suggesting solution/precipitation, but these are usually filamentous lead. Therefore Vetter's mechanism

could possibly occur in the recharge stage, when lead diffuses from lead-sulphate to the growth sites.

The method of production, the presence of impurities and the inconsistencies which are inherent in the lead-acid manufacturing industry make the presence of a lead solution species, on the basis of the present investigation, highly unlikely within a commercial pasted lead electrode.

9.3 Further Work

The rotating disc technique has been used to supply information as to the dependence of the $Pb/PbSO_4$ reaction on solution active species. Linear sweep voltammetry has provided an initial insight into the solid state mechanisms occurring at planar and porous lead electrodes, and their dependencies on expander materials.

(i) The potential step technique could now be adopted to provide information as to the exact form of nucleation and the dimensionality of the $PbSO_4$ crystal growth within a porous electrode.

(ii) Numerous different expander materials are employed by competing battery manufacturers, therefore an investigation of specific or common effects is timely.

(This project has been initiated and i-t responses have been recovered from porous electrodes with differing expanders, as yet models for their growth pattern have not been established. For examples see Figures 9.1-3.)

Figures 9.1-3

Response to a potential step (-1050 → -900 mV) of as industry formed porous lead electrodes with and without expander.

9.1 Newly formed electrodes at 23°C;

9.2 Same electrodes after 25 charge/discharge cycles at -10°C;

9.3 Electrodes returned to 23°C to record the loss in capacity or change in mechanism.

EXP A = 'Indulin C',

EXP B = Associated Lead Inc. 'KX'.

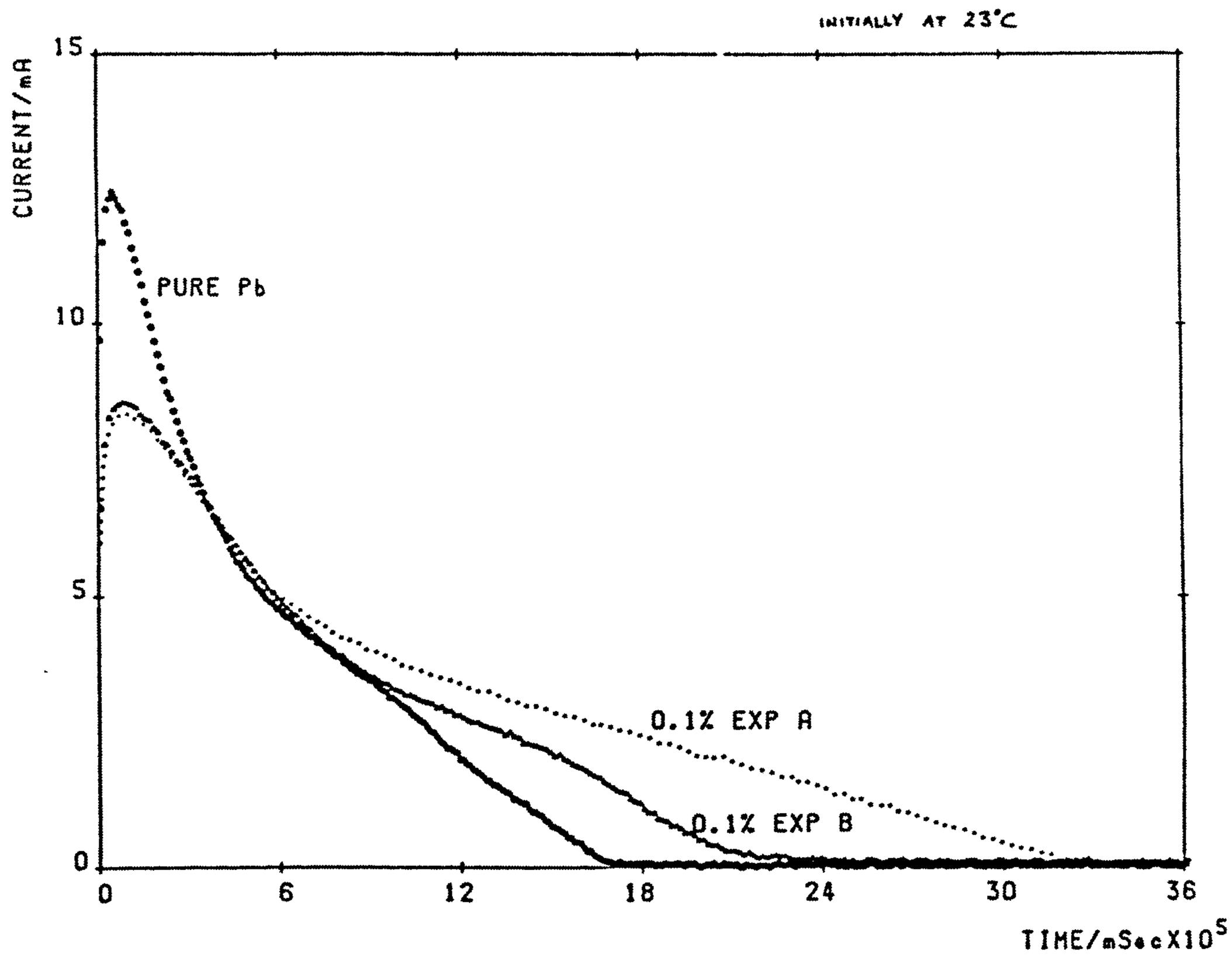
-1050 TO -900 mV
INITIALLY AT 23°C
CURRENT/mA
15
10
5
0
PURE Pb
0.1% EXP A
0.1% EXP B
0
6
12
18
24
30
36
TIME/mSecX10^5

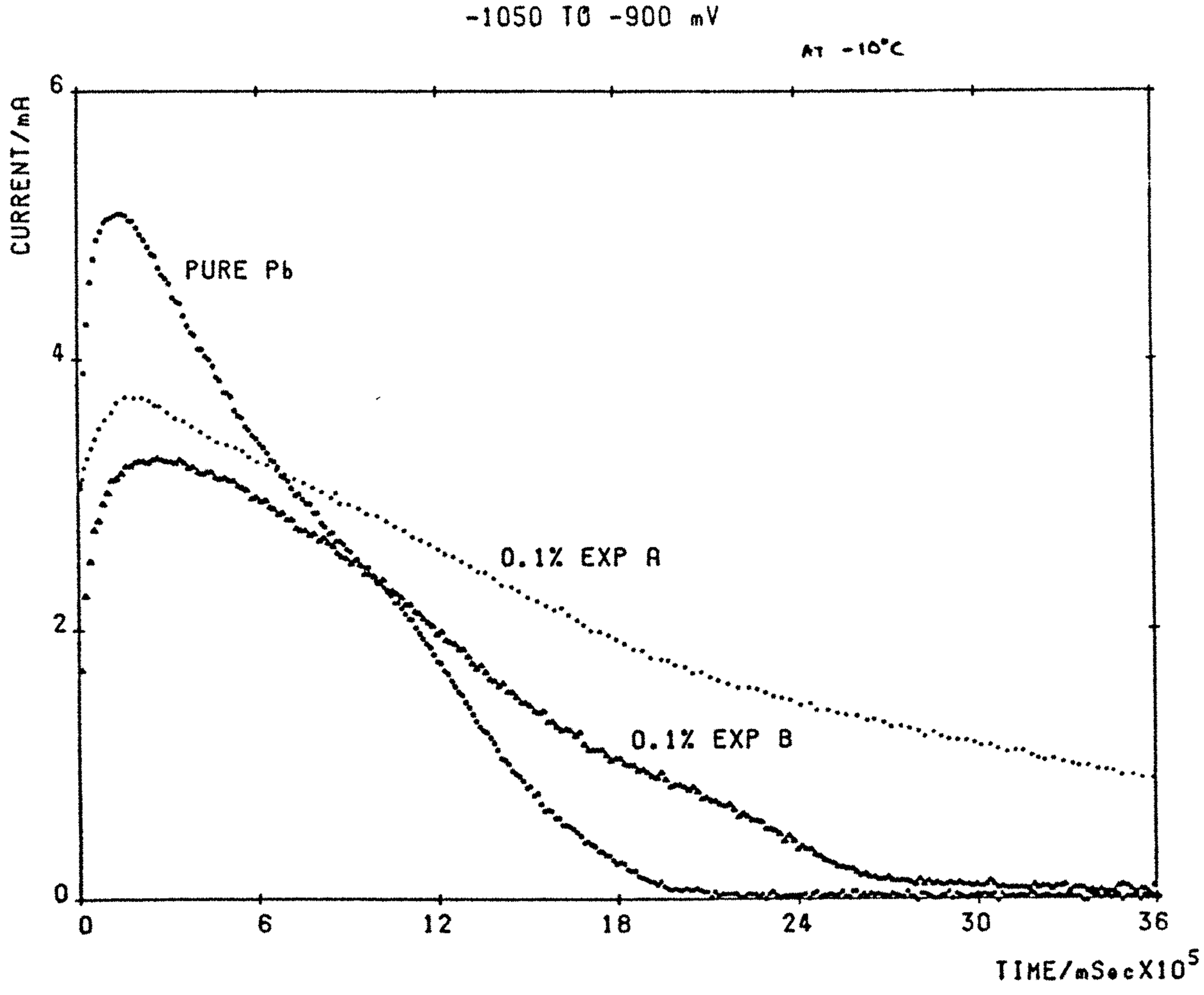
-1050 TO -900 mV
AT -10°C
CURRENT/mA
6
4
2
0
PURE Pb
0.1% EXP A
0.1% EXP B
0
6
12
18
24
30
36
TIME/mSecX10^5

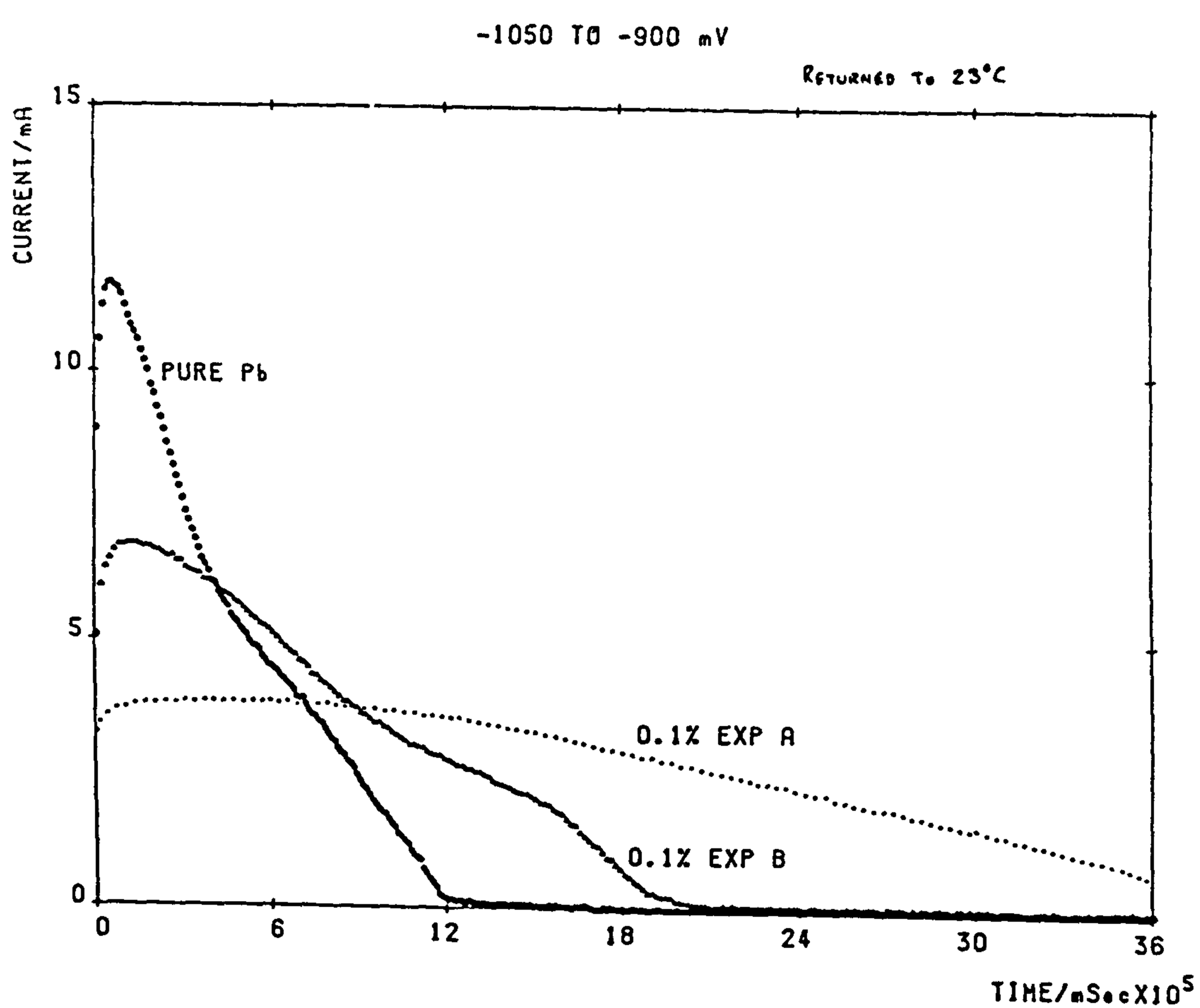
-1050 TO -900 mV
RETURNED TO 23°C
CURRENT/mA
15
10
5
0
PURE Pb
0.1% EXP A
0.1% EXP B
0
6
12
18
24
30
36
TIME/mSecX10^5

(iii) The development of a porous electrode theory to explain the behaviour of electrodes undergoing progressive phase change is recommended. This should not necessarily be confined to lead since other materials are of considerable industrial importance.

(iv) Further low-temperature studies are required to improve performance in this technologically important region. Changes in mechanism may become more apparent at reduced temperature.

APPENDIX 1 - Activated Complex Theory

From the general expression due to Arrhenius,

$$k = Ae^{-E/RT}$$

the rate of reaction is the number of activated complexes passing over the potential energy barrier per second. This rate is a function of the concentration of activated complexes and the frequency with which a complex decays into product.

Consider that the standard free energy change in going from the reactants to the complex is $\Delta G_f^{\ddagger}$ and the difference in energy between the complex and the products is $\Delta G_b^{\ddagger}$.

Consider the system below,

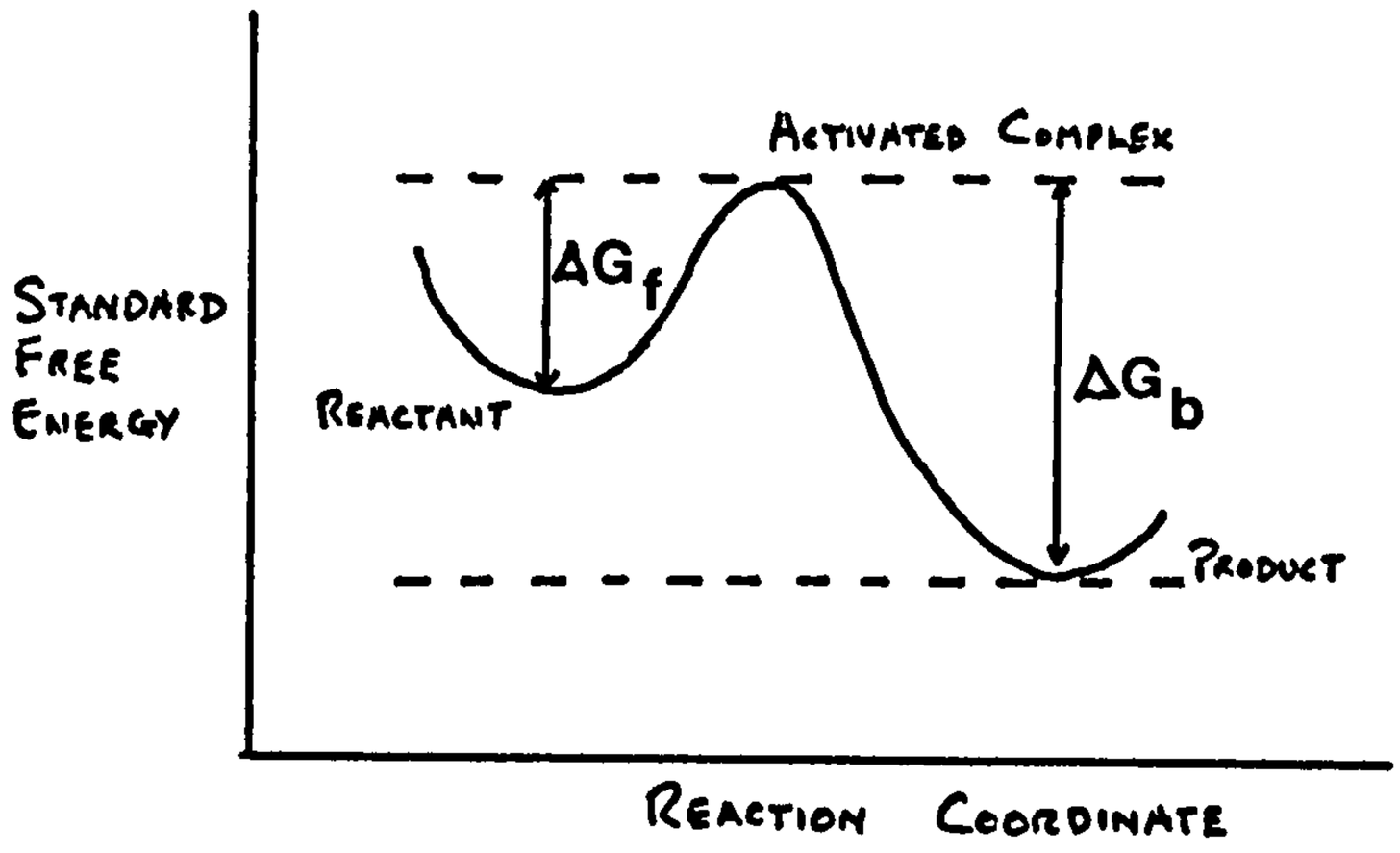

$$\frac{[Complex]}{[A]} = e^{-\Delta G_f^{\ddagger}/RT} \qquad (1)$$

$$\frac{[Complex]}{[B]} = e^{-\Delta G_b^{\ddagger}/RT} \qquad (2)$$

These complexes decay into either A or B with a combined rate constant k', and can be divided into four fractions:

(a) Those created from A and reverting back to A, f_{AA}.

(b) Those arising from A and decaying to B, f_{AB}.

(c) Those created from B and decaying to A, f_{BA}.

(d) Those arising from B and reverting back to B, f_{BB}.

Thus, the net rate of A to B is

$$k_f\ [A] = f_{AB}\ k'\ [Complex] \qquad (3)$$

and B to A is

$$k_b\ [B] = f_{BA}\ k'\ [Complex] \qquad (4)$$

At equilibrium, $k_f\ [A] = k_b\ [B]$. Therefore, f_{AB} and f_{BA} must be equal. This implies f_{AA} is equal to f_{BB} is approximately zero, if f_{AB} and f_{AB} are taken as ½. This is the simplest assumption. A more flexible treatment equates f_{AB} to $\kappa/2$ (κ = Kappa), where κ is the transmission coefficient and can take a value from 0 to 1.

Substitution of (1) and (2) into (3) and (4) respectively, gives

$$k_f = \frac{\kappa k'}{2}\ e^{-\Delta G_f^{\ddagger}/RT} \qquad (5) \text{ and}$$

$$k_b = \frac{\kappa k'}{2}\ e^{-\Delta G_b^{\ddagger}/RT} \qquad (6)$$

k' can be predicted from statistical thermodynamics, and can be shown to be $2k_BT/h$ where k_B and h are Boltzmann and Planck constants.

Thus, the rate constants in (5) and (6) can both be expressed in the form

$$k = \kappa\frac{k_BT}{h}\ e^{-\Delta G^{\ddagger}/RT} \qquad (7)$$

Since $G = H - TS$, equation (7) can be written as

$$k = \kappa \frac{k_B T}{h} e^{\Delta S^{\ddagger}/R} e^{-\Delta H^{\ddagger}/RT}$$

Marcus has formulated activated complex theory in both a quantal and classical manner.[48]

APPENDIX 2 - Electrochemical Potential

Charge transfer reactions take place for the same reason that all other rate processes take place i.e. as the result of a gradient of free energy. Electrochemical potential, $\bar{\mu}$, is a property of each species and the phase in which it exists, according to the relationship

$$\bar{\mu}_i = \mu_i^{\ominus} + RT \ln. A_i + z_i F\phi^{\alpha}$$

where $\mu_i^{\ominus}$ is the standard chemical potential, the absolute value of which is not known, but determines the relative activity A_i. ϕ^{α} is the inner potential of the phase α (Galvani potential, the absolute value of which is also unknown). In spite of its limitations this expression is valuable because we are always concerned with known differences in $\mu_i^{\ominus}$ and ϕ^{α}.

Furthermore it reminds us that electrochemical reactions, which result from gradients of $\bar{\mu}$, will be sensitive to both gradients of activity and electrical potential.

APPENDIX 3 - Ionic Mobility

Ions in solution undergo continual motion due to their thermal energy. However, in an electric field, they are subjected to an electrostatic force which accelerates them in a particular direction. Successive collisions with other species in solution and the viscosity of the medium have the effect of producing a mean or terminal velocity.

Under an applied potential gradient, E, the ion migrates at a velocity, v, which is proportional to E, i.e.

$$|v| = uE$$

The proportionality constant, u, is the "mobility" of the ion, and is the ionic velocity under unit potential gradient, (298K/ 1 atm and given concentration).

APPENDIX 4 - Nucleation Rate

The essential difference between the deposition of a phase at a conducting electrode in electrolyte and that from the vapour phase is the existance of the double layer. Theories of phase nucleation have developed from interpretations of the free energy of formation of clusters from supersaturated vapour.

For homogeneous nucleation the reaction occurs within the supersaturated parent phase by the growth of 'embryos' beyond a critical size. The net formation rate of embryos is determined by the impingement of the monomers on the embryos. This can be represented by

$$iA = A_i \qquad (1)$$

which is the overall result of a series of reactions of the type

$$A_{i-1} + A = A_i \qquad (2)$$

The dependence of the free energy of formation $\Delta G(i)$ of embryos can to a first approximation be expressed for a spherical embryo of size i as

$$\Delta G(i) = i\Delta G_\infty + i^{2/3}\ \sigma\ v^{2/3}\ (36\pi)^{1/3} \qquad (3)$$

or for an embryo of radius r, as

$$\Delta G(r) = {}^{4}/_{3}\ \pi r^3\ \frac{\Delta G_\infty}{v} + 4\pi\ r^2\ \sigma \qquad (4)$$

where σ = surface free energy

v = condensed phase volume per monomer

and ΔG_∞ = free energy change for the transformation of the bulk parent phase to the bulk nucleating phase per monomer.

The first term in equations 3 and 4 represent the free energy of formation of the embryo volume from the supersaturated parent phase and is negative. The second term represents the free energy of formation of the embryo surface and is a positive quantity.

$\Delta G(r)$ versus r is shown below.

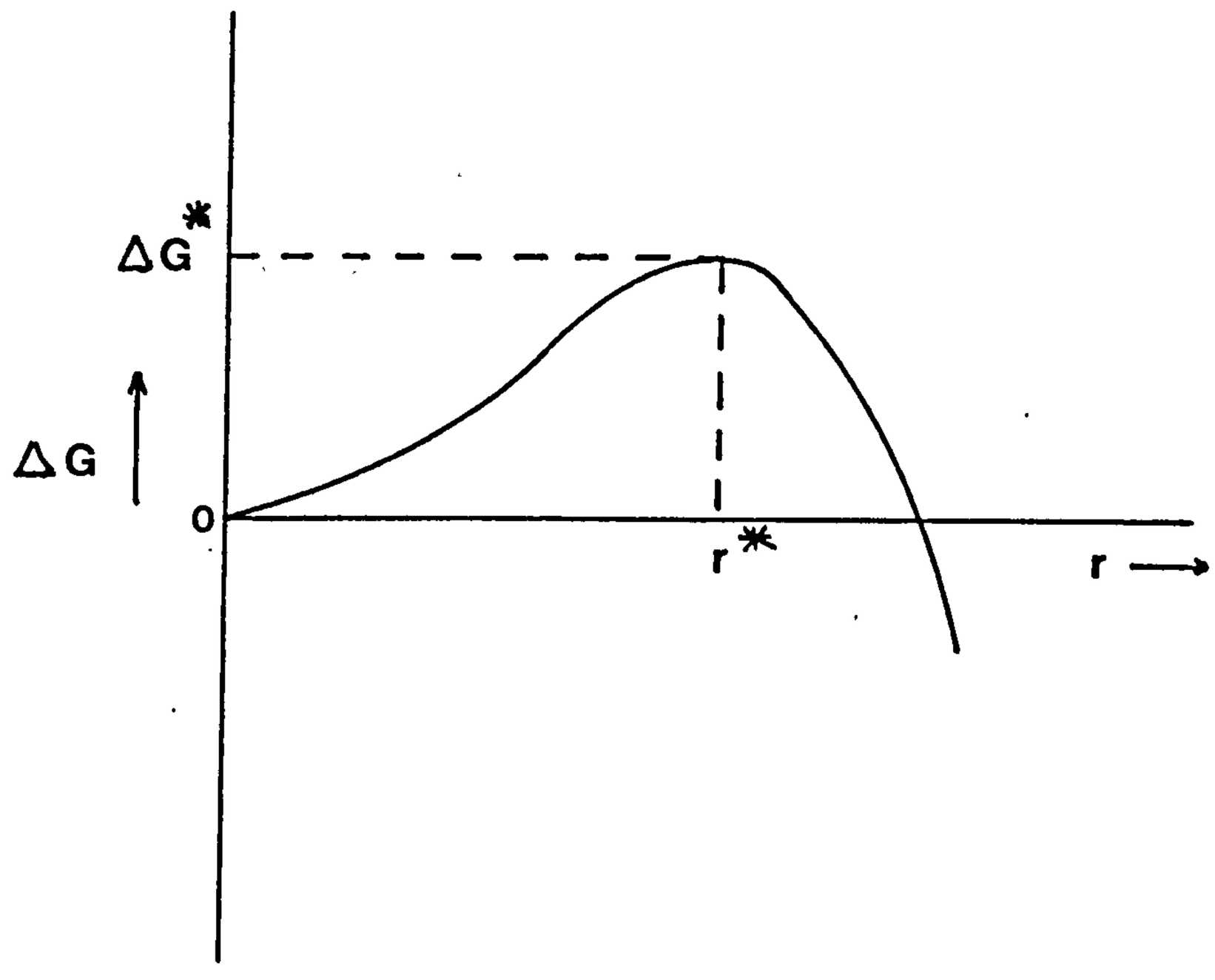

A maximum in ΔG occurs at the critical radius r^*.

$$\frac{\partial \Delta G}{\partial r} = 0, \quad r = \frac{-2\sigma}{\Delta G_V} \qquad (5)$$

where ΔG_V is $\Delta G_\infty / v$.

The free energy of formation of the critical nucleus is given by

$$\Delta G^* = \frac{16}{3} \pi \frac{\sigma^3}{(\Delta G_V)^2} \qquad (6)$$

Equation 5 can be rearranged to give

$$\Delta G_\infty = \frac{-2\sigma_V}{r^*} \qquad (7)$$

Returning to the formation rate for the reaction $iA = A_i$, the impingement rate, w, of monomer on an equilibrium concentration $n(i^*)$ of embryos of critical size i^* gives a nucleation rate I of

$$I(i^*) = wn(i^*) \qquad (8)$$

The impingement rate w can be expressed as a critical impingement rate w^* and related to the monomer flux, J, over a spherical embryo, thus:

$$w^* = 4\pi r^{*2} J = 4\pi r^{*2} P (2\pi m k_B T)^{-\frac{1}{2}} \qquad (9)$$

and the resulting nucleation rate is

$$I(i^*) = w^* n(i^*) \exp(-\Delta G^*/k_B T) \qquad (10)$$

ΔG_∞ as in equations 4 and 10 can be related to overpotential by the expression

$$\Delta G_\infty = -nF\eta \qquad (11)$$

This can be then substituted in all subsequent equations to provide

$$\eta = \frac{2\sigma v}{nFr^*} \qquad (12) \text{ from } (7)$$

and a nucleation rate which is dependent on applied overpotential.

A comprehensive review of nucleation (thermodynamics, statistical mechanics and kinetics) is provided by Zettlemoyer.[155]

1) J. H. Gladstone & A. Tribe, Nature, 25, 221 & 461; 26, 251, 342 & 602; 27, 583 (1882-1883).

2) D. N. Craig & G. W. Vinal, J. Res. Nat. Bur. Stand., 24 (1940) 475.

3) G. W. Vinal, 'Storage batteries 4th Ed.', John Wiley, 1955.

4) P. D. Gibbons, Joseph Lucas Batteries Ltd. (Foremans Road, Birmingham), Private Communication.

5) J. Perkins, J. L. Pokorny and M. T. Coyle, 'A review of materials and mechanisms which affect the performance of lead-acid storage batteries', Naval Post-graduate School, Monterey, California, 1976.

6) M. A. Dasoyan & I. A. Aguf, 'Current Theory of Lead-Acid Batteries', Technicopy, 1979.

7) H. Bode, 'Lead-Acid Batteries', John Wiley & Sons, 1977.

8) E. J. Ritchie, Trans. Electrochem. Soc., 92 (1947) 229.

9) J. R. Pierson, P. J. Gurlusky, A. C. Simon & S. M. Caulder, J. Electrochem. Soc., 117 (1970) 1463.

10) A. C. Simon, S. M. Caulder, P. J. Gurlusky & J. R. Pierson, J. Electrochem. Soc., 121 (1974) 463.

11) B. K. Mahato, J. Electrochem. Soc., 124 (1977) 1663.

12) E. J. Wade, 'Secondary Batteries', Electrician Printing & Publishing Co., 1902.

13) M. Barak, C. J. Bushrod & N. A. Hampson, Unpublished results, Chloride Batteries, 1955.

14) E. Adler, Sven. Kem. Tidskr., 80 (1968) 279.

15) K. V. Sarkanen & C. H. Ludwig (Editors), 'Lignins: Occurence, Formation, Structure and Reactions', Wiley-Interscience, 1971.

16) R. Pointelli, Z. Elektrochem., 55 (1951) 128.

17) G. Archdale & J. A. Harrison, J. Electroanal. Chem., 34 (1972) 21.

18) G. Archdale & J. A. Harrison, J. Electroanal. Chem., 39 (1972) 357.

19) G. Archdale & J. A. Harrison, J. Electroanal. Chem., 43 (1973) 321.

20) G. Archdale & J. A. Harrison, J. Electroanal. Chem., 47 (1973) 93.

21) A. N. Fleming & J. A. Harrison in A. T. Kuhn (Editor), 'The Electrochemistry of Lead', Academic Press, 1979.

22) R. D. Armstrong & K. L. Bladen, J. Appl. Electrochem., 7 (1977) 345.

23) N. A. Hampson & J. B. Lakeman, Surf. Technol., 9 (1979) 97.

24) N. A. Hampson & J. B. Lakeman, J. Power Sources, 4 (1979) 21.

25) C. Lazarides, N. A. Hampson, G. M. Bulman & C. Knowles in J. Thompson (Editor), Power Sources Symp., Brighton, Sept. 1980, Academic Press, (1981).

26) N. A. Hampson & C. Lazarides, Surf. Technol., 14 (1981) 301.

27) J. Heyrovski, Disc. Faraday Soc., 1 (1947) 212.

28) T. Hurlen, Acta Chem. Scand., 16 (1962) 1337.

29) A. N. Fleming & J. A. Harrison, Electrochim. Acta, 21 (1976) 905.

30) M. P. J. Brennan & N. A. Hampson, J. Electroanal. Chem., 48 (1973) 465.

31) N. A. Hampson & J. B. Lakeman, J. Electroanal. Chem., 119 (1981) 3.

32) D. Berndt in D. H. Collins (Editor), 'Power Sources 2', Pergamon, 1970.

33) N. A. Hampson & J. B. Lakeman, J. App. Electrochem., 11 (1981) 361.

34) E. Willihnganz, Trans. Electrochem. Soc., 92 (1947) 281.

35) T. F. Sharpe, Electrochim. Acta, 14 (1969) 635.

36) T. F. Sharpe, J. Electrochem. Soc., 116 (1969) 1639.

37) W. Simon, Bosch. Tech. Ber., 1 (1966) 234.

38) A. C. Simon, S. M. Caulder, P. J. Gurlusky & J. R. Pierson, Electrochim. Acta, 19 (1974) 739.

39) N. A. Hampson, J. B. Lakeman, J. G. Smith & K. S. Sodhi, Surf. Tech., 11 (1980) 377.

40) T. J. Hugel & R. H. Hammer in D. H. Collins (Editor), 'Power Sources 3', Oriel Press, 1971.

41) E. G. Yampol'Skaya, M. I. Ershova, V. V. Surikov, I. I. Astalkov & B. N. Kabanov, Elektrokhimiya, 8 (1972) 1236.

42) G. N. Lewis & M. Randall, (Revised by K. S. Pitzer & L. Brewer), 'Thermodyanmics', McGraw-Hill, 1961.

43) A. Sanfeld, 'Thermodynamics of Charged and Polarized Layers', Wiley-Interscience, 1968.

44) J. Koryta, J. Dvorak & V. Bohackova, 'Electrochemistry', Methuen & Co. Ltd., 1970.

45) J. Tafel, Z. Physik. Chem., 50A (1905) 641.

46) W. J. Moore,
'Physical Chemistry', Longman, 1972.

47) K. J. Laidler,
'Theories of Chemical Reaction Rates',
Robert E. Krieger Publishing Co., New York, 1979.

48) R. A. Marcus,
(a) J. Chem. Phys., 41 (1964) 2614;
(b) J. Chem. Phys., 41 (1964) 2624.

49) H. H. Bauer, J. Electroanal. Chem., 16 (1968) 419.

50) K. J. Vetter,
'Electrochemical Kinetics, theoretical aspects',
Academic Press, 1967.

51) A. J. Bard & L. R. Faulkner,
'Electrochemical Methods, fundamentals and applications',
John Wiley, 1980.

52) J. Newman,
'Electrochemical Systems', Prentice-Hall, 1973.

53) T. Von Karman, Z. Angew. Math. Mech., 1 (1921) 244.

54) W. G. Cochran, Proc. Cambridge Phil. Soc., 30 (1934) 365.

55) V. G. Levich,
'Physicochemical Hydrodynamics', Prentice-Hall, 1962.

56) W. J. Albery,
'Electrode Kinetics', Oxford University Press, 1975.

57) D. Pletcher (Editor), Lecture notes for the course:-
'Advanced Instrumental Methods in Electrode Kinetics',
Dept. of Chemistry, University of Southampton, 1975.

58) D. D. Macdonald,
'Transient Techniques in Electrochemistry', Plenum Press,
1977.

59) I. N. Stranski, Z. Physik, Chem., A136 (1928) 259.

60) T. Erdey-Gruz & M. Volmer, Z. Physik. Chem., A157 (1931) 165.

61) W. K. Burton, N. Cabrera & F. C. Frank, Phil. Trans., A243 (1951) 299.

62) A. Steinberg, Nature, 170 (1952) 1119.

63) D. A. Vermilyea, J. Chem. Phys., 25 (1956) 1254.

64) J. O'M. Bockris & G. A. Razumney, 'Fundamental Aspects of Electrocrystallization', Plenum Press, 1967.

65) J. A. Harrison & H. R. Thirsk in A. J. Bard (Editor), 'Electroanalytical Chemistry', Vol. 5, 1971.

66) J. B. Lakeman, Ph.D. Thesis, Loughborough University of Technology, 1980.

67) M. Avrami, J. Chem. Phys., 9 (1941) 177.

68) R. D. Armstrong & J. A. Harrison, J. Electrochem. Soc., 116 (1969) 328.

69) W. Davison & J. A. Harrison, J. Electroanal. Chem., 44 (1973) 213.

70) S. Fletcher & D. B. Matthews,

(a) J. App. Electrochem., 11 (1981) 1;

(b) J. App. Electrochem., 11 (1981) 7;

(c) J. App. Electrochem., 11 (1981) 23.

71) B. E. Conway & J. O'M. Bockris, Proc. Royal Soc., A248 (1958) 394.

72) A. R. Despic & J. O'M. Bockris, J. Chem. Phys., 32 (1959) 389.

73) M. Fleisdimann & H. R. Thirsk, Electrochim. Acta, 2 (1960) 22.

74) N. F. Mott & R. J. Watts-Tobin, Electrochim. Acta, 4 (1961) 79.

75) B. E. Conway & J. O'M. Bockris, Electrochim. Acta, 3 (1961) 340.

76) W. J. Müller, Trans. Faraday Soc., 27 (1931) 737.

77) U. R. Evans, 'The Corrosion and Oxidation of Metals', Edward-Arnold, 1960.

78) D. Grahame, Chem. Rev., 41 (1947) 441.

79) A. Gouy, J. Phys., 9 (1910) 457.

80) D. L. Chapman, Phil. Mag., 25 (1913) 475.

81) O. Stern, Zeit. Elektrochem., 30 (1924) 508.

82) A. N. Frumkin, Z. Physik. Chem., 164A (1933) 121.

83) W. L. Reynolds & R. W. Lumry, 'Mechanisms of Electron Transfer', The Ronald Press Co., 1966.

84) R. D. Cannon, 'Electron Transfer Reactions', Butterworth & Co. Ltd., 1980.

85) L. Pauling & E. B. Wilson, 'Introduction to Quantum Mechanics', McGraw-Hill, 1935.

86) P. W. Atkins, 'Molecular Quantum Mechanics', Oxford University Press, 1978.

87) R. A. Marcus, J. Chem. Phys., 24 (1956) 966.

88) R. A. Marcus, Disc. Farad. Soc., 29 (1960) 21.

89) R. A. Marcus, J. Chem. Phys., 43 (1965) 679.

90) R. R. Dogonadze in N. S. Hush (Editor), 'Reactions of Molecules at Electrodes', Wiley-Interscience, 1971.

91) J. O'M. Bockris & A. K. N. Reddy,
'Modern Electrochemistry' Vol. 2, Macdonald & Co. Ltd., 1970.

92) R. F. Amlie, J. B. Ockerman & P. Ruetschi, J. Electrochem. Soc., 108 (1961) 377.

93) E. Willihnganz, J. Electrochem. Soc., 102 (1955) 99.

94) R. de Levie in P. Delahay (Editor),
Adv. Electrochem. Electrochem. Eng., 6 (1967) 329.

95) E. A. Grens, Electrochim. Acta, 15 (1970) 1047.

96) J. Newman & W. Tiedmann, Am. Inst. Chem. Eng. J., 21 (1975) 25.

97) N. A. Hampson & A. J. S. McNeil in D. Pletcher (Senior Reporter), Specialist Periodical Reports, Royal Society of Chemistry, Vol. 8, 1983.

98) L. G. Austin, Trans. Faraday. Soc., 60 (1964) 1319.

99) J. Burbank, A. C. Simon & E. Willihnganz in P. Delahay & C. W. Tobias (Editors), Adv. Electrochem. Electrochemical Eng., Vol. 8, 1971.

100) V. S. Daniel-Bek, Zh. Fiz. Khim., 22 (1948) 697.

101) L. G. Austin & H. Lerner, Electrochim. Acta, 9 (1964) 1469.

102) J. A. Bialacki, N. A. Hampson & K. Julian, Surf. Tech., 19 (1983) 347.

103) A. Winsal, U. Hullmeine & E. Voss, J. Power Sources, 2 (1978) 369.

104) J. S. Newman & C. W. Tobias, J. Electrochem. Soc., 109 (1962) 1183.

105) J. S. Newman & W. Tiedemann, A. I. Ch. Eng. J., 21 (1978) 25.

106) J. S. Dunning, D. N. Bennion & J. S. Newman, J. Electrochem. Soc., 118 (1971) 1251.

107) J. S. Dunning, D. N. Bennion & J. S. Newman, J. Electrochem. Soc., 120 (1973) 906.

108) H. Gu, D. N. Bennion & J. S. Newman, J. Electrochem. Soc., 123 (1976) 1364.

109) R. C. Alkire, E. A. Grens & C. W. Tobias, J. Electrochem. Soc., 116 (1969) 1328.

110) K. Micka & I. Rousar, Electrochim. Acta, 19 (1974) 499.

111) K. Micka & I. Rousar, Electrochim. Acta, 18 (1973) 629.

112) K. Micka & I. Rousar, Electrochim. Acta, 21 (1976) 599.

113) A. D. Turner, A.E.R.E. (Harwell), R 8931/2, 1978.

114) D. Simonsson, J. Electrochem. Soc., 120 (1973) 151.

115) D. Simonsson, J. App. Electrochem., 3 (1973) 261.

116) D. Simonsson, J. App. Electrochem., 4 (1974) 109.

117) D. Simonsson, Kungl. Tekniska. Högskolan, Inst. Kemisk. Tek., KTR 73-34.

118) N. A. Hampson & J. B. Lakeman, J. Power Sources, 6 (1981) 101.

119) J. S. Mattson, H. B. Mark & M. C. MacDonald, 'Computers in Chemistry and Instrumentation - Vol. 2. Electrochemistry: Calculations, Simulation and Instrumentation', Marcel Dekker, 1972.

120) Kemitron K3000E Data Sheet, Kemitron Industrial and Scientific Computers, 21-23 Charles St., Hoole, Chester, CH2 3AY.

121) S. P. Perone & D. O. Jones, 'Digital Computers in Scientific Instrumentation', McGraw-Hill, 1973.

122) R. E. Dessy, P. J. van Vauren & J. A. Titus, Anal. Chem., 46 (1974) 917A, 1055A.

123) D. Betteridge & T. B. Goad, Analyst, 106 (1981) 257.

124) M. W. Breiter, J. Electrochem. Soc., 112 (1965) 845.

125) J. A. Harrison, Electrochim. Acta, 27 (1982) 1113, 1123.

126) J. A. Harrison, J. Power Sources, 8 (1982) 99.

127) M. I. Cohen & P. A. Heimann, J. Res. Nat. Bur. Standards, 83 (1978) 429.

128) O. R. Brown, Electrochim. Acta, 27 (1982) 83.

129) E. T. Gray & H. J. Workman in P. Lykos (Editor), 'Personal Computers in Chemistry', Wiley-Interscience, 1981.

130) N. A. Hampson & M. J. Willars, Surf. Tech., 7 (1978) 247.

131) J. B. Peatman, 'Microcomputer-based Design', McGraw-Hill, 1977.

132) Microcomputer components, Data book, 1980, Zilog, Inc., 10460 Bubb Road, Cupertino, California 95014.

133) H. Garland, 'Introduction to Microprocessor System Design', McGraw-Hill-Kogakusha, 1979.

134) A. R. Miller, '8080/Z80 Assembly Language', John Wiley, 1981.

135) T. Hogan, 'Osborne CP/M User Guide', OSBORNE/McGraw-Hill, 1981.

136) N. Goddard, Microprocessor Applications Group - Imperial College of Science and Technology, London, Private Communication.

137) R. S. Components Ltd., Data Sheet, R/4642.

138) R. S. Components Ltd., Data Sheet, R/4399.

139) R. S. Components Ltd., Data Sheet,R/4052.

140) R. S. Components Ltd., Data Sheet, R/4383.

141) National Semiconductor, Pub. No. 426305326-001A.

142) A. J. S. McNeil & N. A. Hampson, Surf. Tech., 19 (1983) 335.

143) A. J. S. McNeil & P. J. Mitchell, to be published.

144) V. Danel & V. Plichon, Electrochim. Acta, 28 (1983) 781.

145) E. S. Livshits & K. V. Rybalka, Elektrokhimiya, 14 (1978) 1431.

146) J. P. Carr, N. A. Hampson & R. Taylor, J. Electroanal. Chem., 33 (1971) 109.

147) A. J. Calandra, N. R. de Tacconi, R. Pereiro & A. J. Arvia, Electrochim. Acta, 19 (1974) 901.

148) J. Ambrose, R. G. Barradas, K. Belinko & D. W. Shoesmith, J. Colloid. Interface. Sci., 47 (1974) 441.

149) J. A. Bialacki, N. A. Hampson & K. Peters, J. App. Electrochem., 12 (1982) 627.

150) J. A. Bialaki, N. A. Hampson & K. Peters, J. App. Electrochem., 13 (1983) 103.

151) N. A. Hampson & J. B. Lakeman, J. Electroanal. Chem., 107 (1980) 177.

152) A. N. Frumkin, Zh. Fiz. Khim., 29 (1949) 1477.

153) K. Burdon, Lucas Research Centre, Solihull, W. Midlands, Private Communication.

154) K. J. Vetter, Chem. Ing. Techn., 45 (1973) 213.

155) A. C. Zettlemoyer (Editor), 'Nucleation', Marcel Dekker, Inc., 1969.